A MORPHOMETRIC STUDY OF VOLCANOES
IN
GUATEMALA, ICELAND, THE SNAKE RIVER PLAIN,
AND THE SOUTH PACIFIC

BY KAREN G. BEMIS

A dissertation submitted to the

Graduate School - New Brunswick

Rutgers, The State University of New Jersey

in partial fulfillment of the requirements

for the degree of

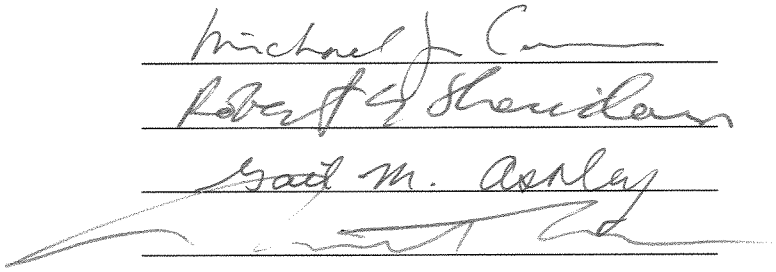
Doctor of Philosophy

Graduate Program in Geological Sciences

Written under the direction of

Professor Michael J. Carr

and approved by



New Brunswick, New Jersey

October, 1995

ABSTRACT OF THE DISSERTATION

A Morphometric Study of Volcanoes

in Guatemala, Iceland, the Snake River Plain, and the South Pacific

by KAREN G. BEMIS

Dissertation Director:

Professor Michael J. Carr

An accurate determination of the dependence of volcano morphology on eruption style requires a quantitative study of the morphology of genetically related volcanoes. This study acquired a database of geomorphic measurements of volcanoes from volcanic fields in four tectonically distinct regions. The identification and measurement criteria are based on a right-circular model of volcano shape.

The right-circular cone model, used in this and previous studies, has significant limitations. Common morphologic features of many volcanoes are ignored by the model; including the curved flanks of composite volcanoes, the breached craters of some cinder cones, and the elongation possible in many volcanic types. In addition, the basic model uses three measurements (height, basal diameter and top diameter) so that size-independent morphology is described by only two parameters. Morphological separation of volcanic types is not fully achieved in this study. The most obvious additional measurements (crater depth and cone circularity) do not improve separation.

In spite of the above limitations, four firm conclusions are demonstrated. First, different volcanic processes can produce similar volcano morphologies. The morphologic spaces of cinder cones and domes overlap almost completely. Varying degrees of overlap are observed among other combinations of volcanic types. Second, volcanoes with the same type labels, based on geologic classification, have distinct morphologies and different developmental trends in different regions. The volcanoes of the Snake River Plain

(especially cinder cones and shield volcanoes) are shallower sloped than their geologic counterparts in Guatemala and Iceland. The shield volcanoes appear to evolve into composite volcanoes in Guatemala, but not in Iceland or the Snake River Plain. Third, in Guatemala cinder cone volume is correlated with the Ba/La ratio, a tracer of subduction influence, of associated lava flows. Fourth, cinder cone shape is determined by the dependence of basal diameter on eruption energy as shown by a numerical simulation.

Large volcanoes are also modeled using topographic profiles: shield volcanoes have shallow, linear flanks; table mountains and domes have steep, linear flanks; and composite volcanoes have parabolic flanks. Numerical simulations of lava piles suggest that shield volcanoes may be piles of wedge-shaped lava flows of varying length.

Acknowledgments

This dissertation evolved out of observations made during my graduate studies at Woods Hole Oceanographic Institution, when I became involved in a project to investigate the relationship, if any, between thermal and depth anomalies in the South Pacific (Superswell region, [McNutt and Fischer, 1987]) and small-scale intraplate volcanism. Joe Cann, Debbie Smith and I noticed that many of the small submarine volcanoes in the South Pacific had shapes unlike the pointy-to-flat-topped cones of other regions of the Pacific. The "new" cone shape is characterized by a rounded top with no discernible break in slope, much like the characteristic shield volcano shape. Submarine volcanoes form through the effusion of lava. Why should there be different shapes of edifices? What controls the shape of a volcanic edifice?

This dissertation attempts to answer these two questions by investigating the variability of shape in continental volcanoes where supplementary evidence as to the eruption mechanism is more readily attained. The initial exploration of these questions was not, however, as systematic as the presentation of this dissertation. A visit to Iceland in 1990 brought the potential relevance of hyaloclastite and pillow breccia formation to my attention. I investigated the use of wax models to study the effects of lava flows piling up, but my first attempts proved unwieldy; computer simulations proved more manageable. On moving to Rutgers, I became interested in Central American volcanism. A systematic comparison of the volcanoes of Guatemala, Iceland, the Snake River Plain and the South Pacific emerged from the initial jumble of ideas, observation and data.

I would like to thank the myriad of people who helped and encouraged me as I strove to develop and write my dissertation: my husband, Doug, who put up with my many moods; my fellow students, who always seem to think better of me and my ideas than I do; my masters' advisor, Dick Von Herzen, who encouraged me to explore my initial questions about volcanoes; my advisor, Mike Carr, who was already interested in the same questions; my committee, who willingly read what I wrote and who wrote far

too many reference letters; the department secretary, who was always supportive and willing to listen to my woes and who always knew how to get the paperwork and other details processed; the volcanology group at the Smithsonian, who assisted my exploration of the world's volcanoes and maps; my family, who only want me to do well at what I want to do; my officemate, who put up with my tendency to talk all day; Debbie Smith, who introduced me to morphometrics and statistics; and, finally, my assorted friends, who forgive me for never finding the time to keep in touch.

Parts of this dissertation were supported by grants from the Natural Science Foundation including NSF EAR9316350 and NSF EAR9205053 and from the Geological Society of America. I thank Lee Siebert for assistance during my short field session in Guatemala. Mark Feigenson and James Walker made constructive comments and corrections on Chapter III.

Table of Contents

Abstract ii

Acknowledgments iv

Table of Contents vi

List of Tables ix

List of Figures xi

Chapter I. Introduction 1

Dissertation goals 2

Chapter II. Morphometric description of volcanoes 5

Introduction 5

Summary of previous studies 7

Methodology 9

Right-circular cone measurements 9

Delineation of volcanic types 12

Data 19

Volcano population studies 19

Volcanoes of Guatemala 19

Volcanoes of northern and west-central Iceland 32

Small submarine volcanoes in the South Pacific 39

Volcanoes of the Snake River Plain 46

Discussion 52

Summary of observations 52

Comparison to previous studies 52

Separating volcanic types 53

Limitations of the right-circular cone model 66

Results of chapter II 68

References cited 71

Chapter III. Cinder cone size related to subduction signature in the Ipala Graben, southeast Guatemala 74
Background 74
Data 78
Results 79
Discussion 89
Tectonic implications 94
Results of chapter III 94
References cited 96
Chapter IV. Modeling cinder cone growth and degradation 98
Introduction 98
Geomorphology of Guatemalan cinder cones 99
McGetchin model 111
Wood model of cinder cone degradation 119
Discussion 122
Results of chapter IV 126
Implications 127
References cited 129
Chapter V. Growth models for large volcanoes 131
Introduction 131
Predictions of existing models 132
Limitation of height 132
Lava armor 134
Hydraulic resistance 138
Basal deformation 140
Data 142
Morphologic parameters 142

Topographic profiles 146
Results of data analysis 155
Comparison to existing models 155
Differentiation of volcanic types using topographic profiles and slope profiles 164
Comparison of shield and composite volcanoes 170
Shield volcanoes in different tectonic settings 170
Along arc variations in composite volcano shape 173
Presentation of two new models 180
Quadratic model of composite volcano shape 180
Model of shield morphology by summing typical lava flow shapes 190
Results of chapter V 202
References cited 205
Chapter VI. Conclusions 207
Suggestions for future research 211
Appendix A. Morphologic plots 213
Appendix B. Grain size analysis 218
Appendix C. Field notes, southeast Guatemala, November 1993. 221
Appendix D Computer simulation based on the McGetchin model 225
Appendix E. Morphological descriptions of individual volcanoes 235
Appendix F. Program listing for shield simulation 237
Appendix G. Data disk 244
Bibliography 245
Vita 254

List of Tables

Table II-1. Distinguishing features of various volcanic landforms. 18

Table II-2. Summary of morphologic parameters for Guatemalan volcanoes..... 28

Table II-3. Correlations in Population Parameters for Guatemalan volcanoes by type. 29

Table II-4. Summary of morphologic parameters for Icelandic Volcanoes 37

Table II-5. Correlations between morphologic parameters for Icelandic volcanoes by type..... 38

Table II-6. Morphologic division South Pacific volcanoes. 44

Table II-7. Correlations in morphologic parameters for the South Pacific volcanoes..... 45

Table II-8. Summary of morphologic parameters for Snake River Plain volcanoes..... 50

Table II-9. Correlations between morphologic parameters for the Snake River Plain volcanoes by type. 51

Table II-10. Observations of circularity and volume. 54

Table II-11. Size distribution of volcanoes by type and region. 65

Table III-1. Geochemical and morphological data for cinder cones with MgO >= 5 Wt%..... 81

Table III-2. Regression coefficients and their significance..... 82

Table III-3. Results of particle size analysis*. 86

Table III-4. Comparison of grain size data with cone volume and Ba/La ratios. 88

Table IV-1. Summary of morphologic measurements. 105

Table IV-2. Summary of cinder cone morphology reported by previous studies. 106

Table IV-3. Correlations between morphologic variables..... 107

Table IV-4. Vent widths to reproduce observed cinder cone top diameters..... 119

Table V-1. Analysis of average upper and lower flank slopes of composite volcanoes..... 163

Table V-2. Analysis of slope profiles for Type II and Type III volcano profiles 167

Table V-3. Analysis of slope profiles for Type I volcano profiles. 168

Table V-4. Variations in shield morphology between three regions. 175

Table V-5. Variations in composite volcanoes along the arc front. 179

Table V-6. Multiple regression for the quadratic coefficients of topographic profiles. 183

Table V-7. Comparison of linear, quadratic and cubic multiple regressions for Agua. 185

Table V-8. Input parameters for the simulated shields. 196

Table V-9. Morphological parameters for the simulated shields. 197

Table V-10. Slope analysis of profiles of simulated shields. 197

Table B-1. Particle size distribution (as wt %) for basaltic scoria in selected cinder cones of southeastern Guatemala. 219

Table B-2. Standard values picked for statistical calculations. 220

Table C-1. Characteristics of cinder cones sampled for scoria. 222

Table D-1. Input parameters. 226

Table E-1. Morphologic parameter descriptions of the example volcanoes in Figure V-8. 235

Table E-2. Morphologic parameter descriptions of the composite volcanoes. 236

List of Figures

Figure I-1. Index map of regions studied. 4

Figure II-1. Flat-topped cone model of volcanic shape. 10

Figure II-2. Volcanic types graphically presented on the shape parameter plane..... 14

Figure II-3. Study location in Guatemala and El Salvador. 20

Figure II-4. Morphologic parameters of shape and size for Guatemalan volcanoes. 23

Figure II-5. Study location in Iceland. 33

Figure II-6. Morphologic parameters of shape and size for Icelandic volcanoes. 34

Figure II-7. Table mountain growth. 36

Figure II-8. Study location in the South Pacific. 40

Figure II-9. Ship track density..... 41

Figure II-10. Morphologic parameters of shape and size for submarine volcanoes in the South Pacific. 43

Figure II-11. Study location in the Snake River Plain, Idaho..... 47

Figure II-12. Morphologic parameters of shape and size for the volcanoes of the Snake River Plain..... 48

Figure II-13. Comparison with the results of Wood [1979] for monogenetic volcanoes: t/r vs. basal diameter. 55

Figure II-14. Shield volcano classes and size scale from Whitford-Stark [1975]..... 57

Figure II-15. Separation of volcanic types by h/r vs. t/r. 58

Figure II-16. Separation of volcanic types by t/r vs. 2r. 60

Figure II-17. Relationship between shape and size: h/r vs. t/r. 61

Figure II-18. Relationship between shape and size: 2r vs. h/(h+t). 64

Figure II-19. Volcano profiles as a function of h/r and t/r ratios. 67

Figure III-1. Location map for cinder cones included in this chapter. 75

Figure III-2. La/Yb vs. cinder cone volume. 83

Figure III-3. Ba/La vs. cinder cone volume. 84
Figure III-4. Ba/La vs. La/Yb. 85
Figure III-5. Mdf vs. sf plot. 87
Figure III-6. Histograms of particle size distributions for scoria samples..... 90
Figure III-7. Probability plot of scoria particle size distribution. 91
Figure III-8. Melt generation and rise in the asthenosphere beneath the back-arc region. 95
Figure IV-1. Location map for Guatemalan volcanoes..... 100
Figure IV-2. Morphometric model of cinder cone as right-circular cone. 103
Figure IV-3. Morphologic plots of Guatemalan cinder cones..... 108
Figure IV-4. Shape parameters compared with erosion number. 109
Figure IV-5. Shape parameters compared with the number of gullies per 90°. 110
Figure IV-6. McGetchin model. 113
Figure IV-7. Profiles of simulated cinder cone in different stages of development. 114
Figure IV-8. Example of simulation output. 116
Figure IV-9. Morphologic plots of the results of cinder cone simulations based on the McGetchin model..... 117
Figure IV-10. Morphologic plots of the results of applying the Wood model of cinder cone degradation. 121
Figure IV-11. Erosion patterns in morphologic space for Guatemalan cinder cones. 124
Figure V-1. The geologic units of a volcanic edifice. 135
Figure V-2. Topographic and slope profiles of the Borgia and Linneman model volcano..... 137
Figure V-3. Topographic and slope profiles of the hydraulic resistance model volcano..... 139

Figure V-4. Topographic and slope profiles of the cone deformation model volcano. 141
Figure V-5. Morphologic plots for Guatemalan shield and composite volcanoes. 143
Figure V-6. Morphologic plots for Icelandic shield volcanoes. 144
Figure V-7. Morphologic plots for Snake River Plains shield volcanoes. 145
Figure V-8. Topographic and slope profiles of examples volcanoes of various types and regions. 147
Figure V-9. Volcano height vs. summit elevation for Guatemalan volcanoes. 156
Figure V-10. Variation of volcano height along the Guatemalan arc. 157
Figure V-11. Volcano height vs. summit elevation for Icelandic volcanoes. 158
Figure V-12. Volcano height compared to summit and base elevation in the Snake River Plain. 159
Figure V-13. Volcano height compared to seafloor and summit depths in the South Pacific. 160
Figure V-14. Classes of volcanic shape based on topographic profiles. 165
Figure V-15. Location map of composite volcanoes in Guatemala. 169
Figure V-16. Shape and size relationships between composite and shield volcanoes. 171
Figure V-17. Comparison of the steepness of shield volcanoes in different regions. 174
Figure V-18. Morphologic variations in composite volcanoes along the Guatemalan arc front. 176
Figure V-19. Slope vs. crustal thickness for composite volcanoes in Guatemala. 178
Figure V-20. Diagrammatic model of topographic and slope profiles of composite volcanoes. 182
Figure V-21. Comparison of predicted and observed profiles for Volcán de Agua. 184
Figure V-22. Normalized topographic profiles. 187
Figure V-23. Examples of the output of the shield simulation program. 192

Figure V-24. Lava flow shape models. 195
Figure V-25. Shield simulation results. 198
Figure A-1. Morphologic plots for Guatemalan volcanoes. 214
Figure A-2. Morphologic plots for Icelandic volcanoes. 215
Figure A-3. Morphologic plots for South Pacific volcanoes. 216
Figure A-4. Morphologic plots for Snake River Plains volcanoes. 217
Figure C-1. Location map for scoria samples. 224

Chapter I. Introduction

Previous studies [Smith, 1988; Smith and Cann, 1992; Bemis and Smith, 1993] have noticed that submarine volcanoes are typically right-circular cones with pointy or flat summits, but may also be characterized by a rounded summit with no discernible break in slope. Careful investigation has shown that there are three basic shapes -- (1) smooth, rounded shield shapes, (2) pointy cones, and (3) flat-topped cones -- which differ somewhat in steepness and relative summit width, but not at all in size. No spatial variation was discerned. Submarine volcanoes form through the effusion of lava. Why should there be different shapes of edifices? What controls the shape of a volcanic edifice? Are these controls related to larger-scale tectonic processes?

This dissertation attempts to answer these two questions by investigating the variability of shape in continental volcanoes where supplementary evidence as to the eruption mechanism is more readily attained. The question of why submarine volcanoes vary in shape focused my studies on the growth processes of shield volcanoes. However, volcanic population studies indicate that it is important to study whole populations. Therefore, all volcanoes, regardless of volcanic type, found in each area were incorporated into this study.

The regions included in this study (in addition to the original South Pacific area) were chosen mostly for their relevance to the initial question of why all submarine volcanoes are not shaped similarly (Figure I-1). Because submarine volcanoes are formed by effusion of lava, the presence of many shield volcanoes was the primary criteria for selecting regions to study. The availability of maps and field studies was also important. The Guatemalan back arc region is the focus of much of this dissertation because more field information and geochemical data are available to test hypotheses; also, the range of volcanic eruption styles is large compared to that observed in many other regions. Iceland was chosen next, because it is the type locality of shield volcanism. In addition, table mountains (found predominately in Iceland) may illustrate some of the expected changes

in process between lava effusion into air and lava effusion into water. The Snake River Plain was included because it contains mostly shield-like volcanoes, that are known to differ from the typical shield volcano [Greeley, 1982].

DISSERTATION GOALS

The **long range intent** of the studies undertaken in this dissertation is to understand the growth of volcanoes in order to (a) **predict** the future growth and behavior of currently "active" volcanoes and (b) **interpret** the past growth history and behavior of existing volcanic edifices (including those long inactive) from topographic information. Characterization and interpretation of the range of morphologies observed in volcanic fields on Earth is the first necessary step in achieving this goal. Additional steps include correlating geochemical tracers, tectonic parameters, and physical data (from field studies) with morphologic features (on an empirical basis, but hoping to identify the underlying cause of such correlations) and numerical modeling of the growth of edifices.

In the **short range** (that is, within the scope of this dissertation), I focused on several specific projects designed to address the above issues. Beyond the acquisition of regionally compete databases of volcanic morphologic measurements, this dissertation attempted to develop models that could be used to interpret process from volcanic morphology and to verify and quantify conventional hypotheses concerning volcanic processes and morphologies. The following describes how each chapter addresses the overall intent.

Chapter II attempts **to characterize shield volcanoes in the context of volcanic populations.** To this end, the morphologic characterization of the total population of volcanoes in each of Guatemala, Iceland, and the Snake River Plains was undertaken. The data from a previously completed morphological characterization of small submarine volcanoes in the South Pacific were also included [Bemis and Smith, 1993]. Quantitative

characterization tests existing hypotheses about shield volcanoes in each of the four regions and indicates the overall variation in volcanic form within and between the four regions.

Chapter III is intended **to understand the connection between cinder cones and tectonic setting**. A detailed study of Guatemalan cinder cones and their geochemistry has been conducted. Geochemical indicators of magmatic processes are related to variations in cinder cone size.

Chapter IV was designed in order **to understand how growth and degradation processes affect subtle variations in cinder cone morphology**. A pre-existing computer program is modified to simulate the effects of eruption conditions on cinder cone shape.

Chapter V attempts **to understand how large volcanoes grow**. Predictions from published models of volcanic growth are compared with morphologic data and preliminary numeric models. A method of quantitative assessment of topographic profiles of volcanoes is presented.

Three assumptions are common to all chapters as they are inherent in the identification and measurement procedures adopted. First, in all cases, a volcano is assumed to be the aggradational result of a point-source eruption of magma. Non-volcanic topographic features were ignored. Non-aggradational and markedly elongated features were also ignored. Second, each volcanic edifice is assumed to have resulted from the processes occurring during and immediately after eruption. Thus volcano shape is assumed to reflect eruption style. Large volcanoes are assumed to be the cumulative results of many (similar) eruptions. Third, erosion is assumed to be unimportant, although the effects of lahars and crater-forming explosions are considered "volcanic". Where erosional processes had obviously altered a volcanic edifice, the feature was included in the database but eliminated from the statistical analysis. Finally, it is initially assumed that a right-circular cone model adequately describes volcanic shape.

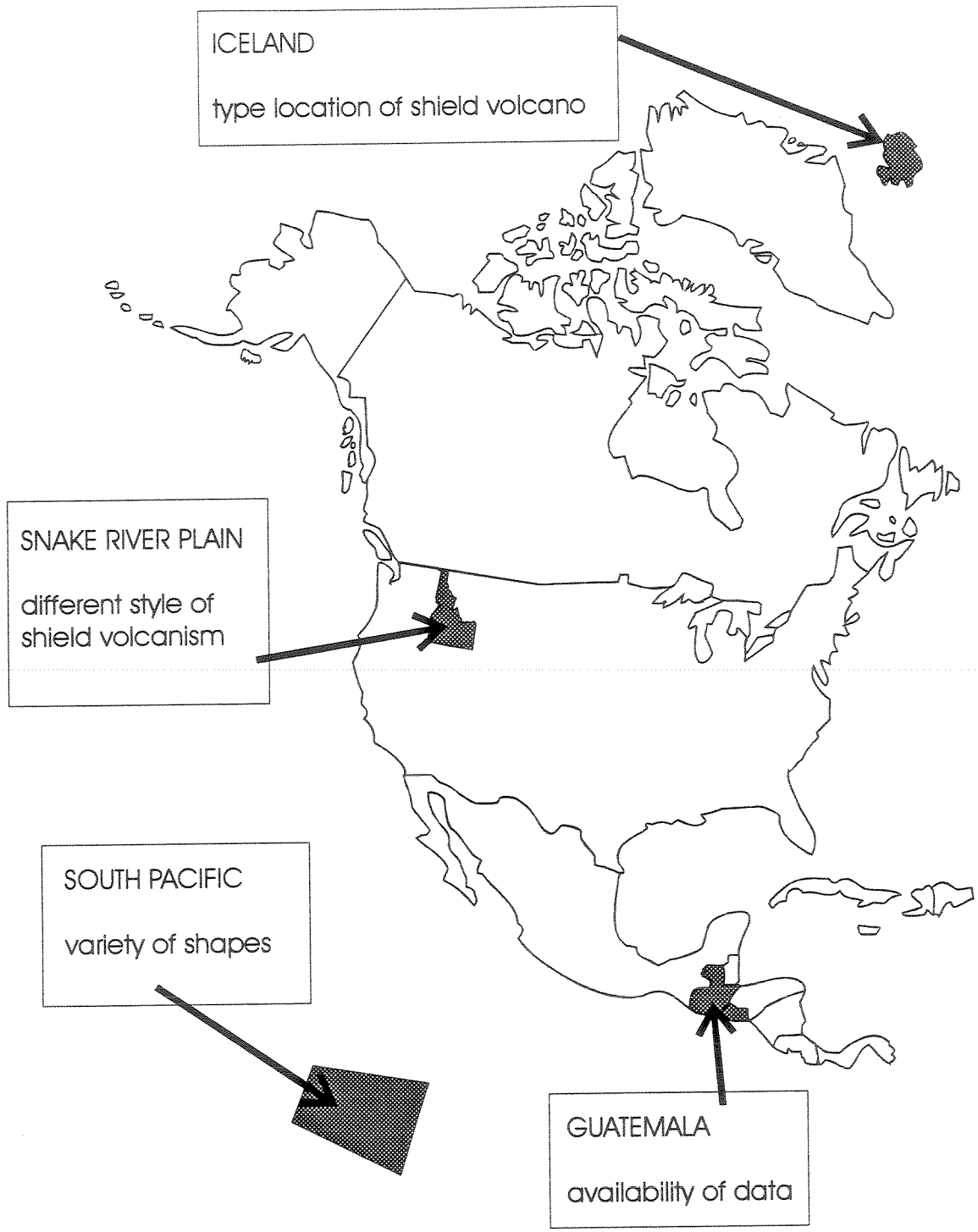


Figure I-1. Index map shows location of the four regions studied in this dissertation. Labels include the name of the region and the primary reason for its inclusion in this dissertation. The Snake River Plain is in Idaho, U.S.A. The South Pacific region is somewhat further south than indicated - at 5°S to 20°S.

Chapter II. Morphometric description of volcanoes

INTRODUCTION

Volcanic form is assumed to reflect eruption history. Wood [1979] has shown that the morphologic form of monogenetic volcanoes reflects the nature of the eruptive processes creating the volcano: effusive eruptions produce small shields and lava cones; pyroclastic eruptions produce cinder cones and maars [Wood, 1979]. The two manners of classifying volcanoes (geomorphology and eruption characterization) are related, because the form of a volcano reflects the processes operating to create it. Ideally, a distinct volcano type should be the result of the time integration of a large number of similar eruptions, or a continuum of eruptions that vary slightly with the growth of the volcano. However, a real volcano population includes many forms that are far from ideal, having resulted from more than one processes or spectrum of processes. This study attempts to quantify and interpret the real variety of forms and distinctions among volcanic types.

Few studies have systematically considered the morphologic variations among the total population of volcanoes within geologically or tectonically restricted regions. Most previous workers have studied populations with a single eruptive style (e.g., Porter's [1972] study of cinder cones on Mauna Kea Volcano, Hawaii) or have not studied geologically coherent populations (e.g., Wood's [1979] study of selected terrestrial volcanoes). While the total population of terrestrial volcanoes is a coherent population, the effects of a wide variation in tectonic and magmatic processes between volcanic regions serve to obscure the controlling factors on morphology in individual volcanoes. Therefore this study was designed to include the total population of volcanoes in four separate regions that are tectonically distinct.

A volcanic population can be defined as a group of volcanoes in a definable geologic region. Tectonic features or boundaries can generally be used to delineate the extent of a volcanic region. This study uses tectonic boundaries to delineate volcanic

fields and arbitrary boundaries (within a field) to limit the size of the sampled area. The total volcanic population of the sample area is measured. A given volcanic population (e.g., a set of volcanoes forming a volcanic field) may contain one or all of the following volcanic types, differentiated mainly by eruptive processes: cinder cones (ballistic ejecta), shield volcanoes (lava flows), domes (extruded lava, viscous flows), composite cones or stratovolcanoes (pyroclastic falls, pyroclastic flows, lava flows), table mountains (hyaloclastites), maars (ballistic ejecta, lava interaction with water). In addition, there are pseudocones, which results from the interaction of lava flows and water and are thus not true volcanoes, and buttes, which are volcanic features of unknown processes.

Of previous studies of the morphometry of volcanoes (the most relevant are summarized in the next section), only one [Smith, 1988] focuses on a single coherent population. No studies known to the author address the question of whether the morphometry of a given type of volcano can (or does) vary between localities. By applying the same classification criteria in each of four regions, I attempt to separate the variation within a region from the variation between regions.

The objective of this chapter is to make a detailed comparison of classified types and actual morphologies. To accomplish this, I look at four geologically coherent volcanic populations and characterize the range of volcanic forms within them. The methodology section discusses the measurement of volcanic morphology, based on its systematic description as a right-circular cone, and the classification of volcanoes used in this study. Although the classification scheme is based on eruption style, the explanation focuses on the resultant characteristics that can be observed on geologic and topographic maps. The tectonic setting and volcanic characteristics of each region are discussed separately. Following that, the morphologic relations in the different regions are compared and the inherent limitations of any scheme based on simple map measurements are discussed.

The results show that volcanoes with apparently similar eruption styles from different tectonic settings do not define the same morphospace. For example, shield volcanoes from Guatemala, Iceland and the Snake River Plain are geomorphologically distinct. The lack of a universal morphospace for the conventional volcanic types (e.g., shield volcanoes, composite volcanoes, domes, cinder cones) is the results from inadequacies in the right-circular cone model and from the non-uniqueness of the shapes produced by different volcanic processes. Although the textures of volcanic features produced by different eruption styles are often very different, allowing geological discrimination, the gross morphologies, as captured by the right-circular cone, can be identical. For example, cinder cones and domes have essentially the same right-circular cone shapes with similar sizes of tops and similar flank slopes. Eruption style cannot be predicted based only on simple morphological parameters. Morphological parameters (based on the right-circular cone) can be useful for quantitative investigation of growth (or size) trends of a given volcanic type, detailed differences between similar volcanic types in different regions, and morphologic variation within a population.

Summary of previous studies

As commonly used, the volcanic types, listed above, are defined by a mixture of chemical, eruption, and morphological criteria. Several attempts have been made to capture the morphospace of volcanoes and correlate morphology to chemistry or eruptive style. Pike and Clow [1981a] measured the circularity and volume of a set of volcanoes selected from around the world. Circularity is the ratio in area of a circle inscribed within the crater rim to a circumscribed circle. Major element chemistry, lava/tephra proportion, presence of crater or caldera, size and other factors were used by Pike and Clow [1981a] to define 25 classes of volcanoes. Applying principal component analysis and cluster analysis to average values for each class of the topographic variables (height/crater-depth, width/crater-diameter, height/width, volume, circularity), the classes appear distinct

morphologically [Pike and Clow, 1981b]. However, the range of values within each class may be greater than the separation between classes; in that case, a continuum would describe the morphologic variations more accurately than separate classes. Additionally, the geologic significance of the class divisions is not always clear, especially when size is a primary dividing factor. Nor is it clear why the circularity should vary between classes. While the explosive formation of maars and pseudocones predicts a high degree of circularity, there is no reason for shield volcanoes or composite cones to have particularly circular or uncircular craters. There may be other parameters that better capture the morphologic distinctions between volcanic classes and relate to the processes responsible for creating different classes.

In a similar study, Wood [1979] examined the crater and edifice diameters of selected volcanoes on the terrestrial planets. He used a previous division into volcanic types - e.g., shield volcano, cinder cone, maar, etc. - for volcanoes on Earth. Many of these types differ in their size range and in the range of the ratio crater-diameter/edifice-diameter. Cinder cones are characterized by a height/edifice-radius ratio (h/r) of 0.36 and generally have a crater-diameter/basal-diameter (t/r) ratio near 0.40 [Wood, 1980a]. Shield volcanoes differ from pyroclastic cones, in having generally larger diameters and much smaller crater-diameter-to-basal-diameter ratios ($t/r<0.10$) [Wood, 1979]. Composite cones appear to have relatively constant height-to-radius ratios ($h/r = 0.24$) and relatively constant crater-to-basal-diameter ratios ($t/r=0.03$) [Wood, 1978]. Additionally, the average slope of composite cones appears to decrease with height [Wood, 1978; Francis and Abbott, 1973]. These studies and those by Pike and Clow [1981a, 1981b] show a correlation between morphological parameters and volcanic types, defined by geologic observation and classification. However, it is not clear if these relationships hold for the entire population of a single volcanic field.

More recently, Smith [1988] used a flat-topped, right-circular cone to model the shape of submarine volcanoes. She measured basal radius r, top radius t, summit height

and cone height h_c for 70 seamounts in the Pacific Ocean. Principal component analysis on five variables (h, r, t, t/r, slope = $\arctan(h_c/(t-r))$) indicates that most of the variance is described by the height h and the top-to-base ratio t/r.

METHODOLOGY

Right-circular cone measurements

Volcanoes were identified on topographic maps using criteria developed for seamount identification on multi-beam bathymetry [Batiza, 1982], where resolvable volcanic features are approximately equant (aspect ratio > 2) edifices with heights greater than 2.5 times the contour interval (usually 50 m). As with several previous morphologic studies of volcanoes, both subaerial and submarine, the shapes of volcanoes are modeled as flat-topped cones (Figure II-1) [Porter, 1972; Wood, 1978; Pike and Clow, 1981a; Jordan et al., 1983; Smith and Jordan, 1988]. The cone height, summit height, basal diameter and top diameter were measured for each volcano using the technique of Smith and Cann [1992] in which the top and base of a volcano are identified by a closed curve drawn by hand at a break in slope near the summit and base, respectively (Figure II-1). The height of the cone is the average relief between the top and the base contours; the summit height is the average relief between the summit peak (which may be higher than the top contour) and the base. The basal and top diameters were obtained by averaging four diameters measured at 45° intervals. Latitude, longitude, summit elevation, minimum and maximum basal radius, minimum and maximum top radius, presence of crater, and other parameters were also recorded for each volcano.

In this chapter, volcano morphology is quantified using only three parameters, height, basal diameter and top diameter: the three components of the flat-topped right circular cone model. The first major assumption of this model is that each volcanic edifice is described by only 3 independent parameters - thus, there are only 3 degrees of freedom. Size is part of the information and accounts for one of the degrees of freedom, which

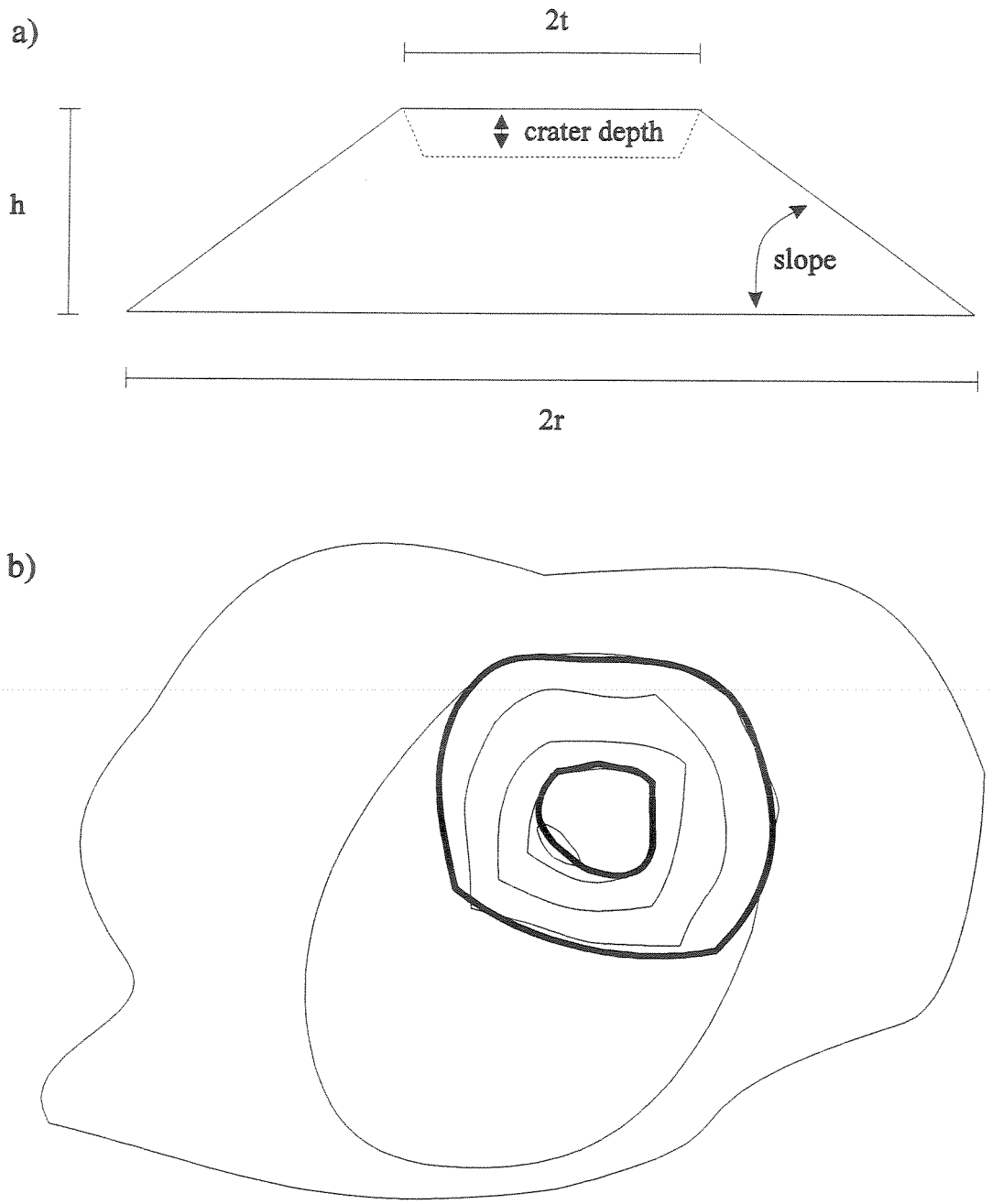


Figure II-1. Flat-topped cone model of volcano shape. (a) Measurements of h, 2r, and 2t describe the gross morphology of a conical volcano. Also shown are the physical significance of slope and crater depth. (b) The top and base contours (dark lines) are drawn for a typical volcano. Thin lines are topographic contours. Three contour lines are required to resolve a volcanic feature sufficiently to measure h, 2r and 2t.

leaves only two degrees with which to describe shape. In general, this study uses the basal diameter (2r) for size and the height-to-radius ratio (h/r) and the top-to-base ratio (t/r) to describe shape. The h/r ratio indicates the overall steepness of a feature and the t/r ratio indicates the relative size of the summit region.

The use of the right-circular cone model to describe volcanic shapes imposes a form of closure on the shape parameters. The parameters height h, basal diameter 2r, and top diameter 2t are interconnected, because the choice of the right-circular cone model constrains the relative variations of the parameters and geologic observation suggests that physical laws and rock properties impose additional constraints on form. By definition, the top diameter 2t is less than the basal diameter 2r. This constrains t/r as less than 1. Additionally, slopes greater than 45° are geologically unreasonable and talus slopes are usually even lower (~33°). Thus, the h/r ratio must be substantially less than 1 and can certainly never be greater than 1. It is important, therefore, to be aware that the following three correlations may be induced, even if the measurements are actually random: (1) positive correlation between h and 2r, (2) positive correlation between 2t and 2r, and (3) negative correlation between h/r and t/r. If these correlations are observed, they must be treated with suspicion but may still be significant for a very high correlation coefficient. In practice, this is less of a problem than might be expected as this study only occasionally observes a negative correlation between h/r and t/r.

The second major assumption of the model is that volcanoes are right-circular cones. Very few volcanoes are perfect right circular cones, especially because flank slopes are usually not linear. Minor variations include elongation, one crater rim higher than another, asymmetric placement of summit or crater, and curved flanks. Volcanoes with major variations were excluded from the study on the basis that they are too ill-formed (often because of closely spaced vents) or too eroded to provide information on the morphologic results of eruptive processes. Some older composite volcanoes with significant erosion still retained sufficient recognizable elements of their original volcanic

morphology and were included. The various types of volcanoes (described below) differ in the degree to which they depart (on average) from the right circular cone model, but no type invariably conforms. Thus, some amount of scatter is expected within the morphologic parameters for a given volcanic type.

In addition to having closure effects and problems with fit, the right-circular cone model does not capture all of the morphologic information available on topographic maps and aerial photographs. Some of this information relates to the lack of a perfect fit between model and actual shape; attempts to better model the actual shape are discussed towards the end of this chapter and in Chapter V. The remaining information comes from small-scale features that are extremely useful in identifying the eruption style of an individual volcano; the next section discusses these and other features that distinguish volcanic types. Aerial photographs and geologic maps were used, when available, to verify the origin of volcano-like topographic features and to identify small-scale features useful for determining volcanic type. A one week field check during 1993 and the prior field experience of Michael Carr was useful in classifying the volcanoes of southeast Guatemala. Volcanoes were assigned to particular classes, or types, on the basis of identification of significant features (generally unrelated to the right-circular cone measurements), supplemented by published identifications. Many volcanoes in each region were not identifiable as a specific type, because either no small-scale features were recognizable to distinguish the feature from an erosional remnant or the recognizable features indicated more than one volcanic type and a dominant type could not be identified.

Delineation of volcanic types

An extensive body of literature discusses the types of volcanic eruptions, the processes associated with them, and the nature of the deposits left by them [see Basaltic Volcanism Study Project (BVSP),1981; Cas and Wright, 1988; Wilson and Head, 1994].

In this section, I characterize the morphology of distinctive volcanic landforms, because, in general, different eruption mechanisms produce different landforms. The following discussion associates eruption processes with landform and deposit features (the discussion is summarized in Table II-1 and its predictions in terms of the shape parameters are illustrated in Figure II-2) and focuses on those landforms recognizable on topographic maps in the regions studied.

Cinder cones result from strombolian eruptions [Cas and Wright, 1988; Wood, 1980a]. They are composed of nearly 100% highly vesicular scoria [Houghton and Schmincke, 1986; Walker and Croasdale, 1972], but this feature is not determinable from a map. On a topographic map, a cinder cone is identified by the presence of a bowl-shaped crater, steep (>20°), straight flanks, and a roughly circular plan. The breaks in slope at the base and top are usually very sharp. The straight flanks of ideal cinder cones result from landsliding and avalanching of scoria ballistically deposited on steep slopes. Maars and tuff cones (discussed below in more detail) are composed of a significant fraction of wall rock; they are distinguished from cinder cones by a wider crater (relative to base diameter) and a deeper crater. Domes are composed of lava and breccia (or talus), generally lack a well-defined crater, and have less cleanly shaped flanks than cinder cones. Large domes often do not have a simple circular plan.

A hill, shaped by erosion, can be distinguished from a cinder cone because it has no crater, is more amorphously shaped, and is generally not composed of scoria. As cinder cones are degraded (eroded), they lose their well-defined outlines and their craters may infil [Wood, 1980b; Dohrenwend et al., 1986]; very old cinder cones may look like (and in a sense be) erosionally-shaped hills. Aerial photographs may be necessary to determine if a crater is present as cinder cone craters are not commonly much deeper than 20-50 m even when fresh [BVSP, 1981]. Cinder cones in early stages of erosion have a distinctive radial pattern of rills (small gullies) typical of the initiation of drainage [Kear, 1957; Hasenaka and Carmichael, 1985; Loewenherz, 1991]; this pattern is commonly visible on

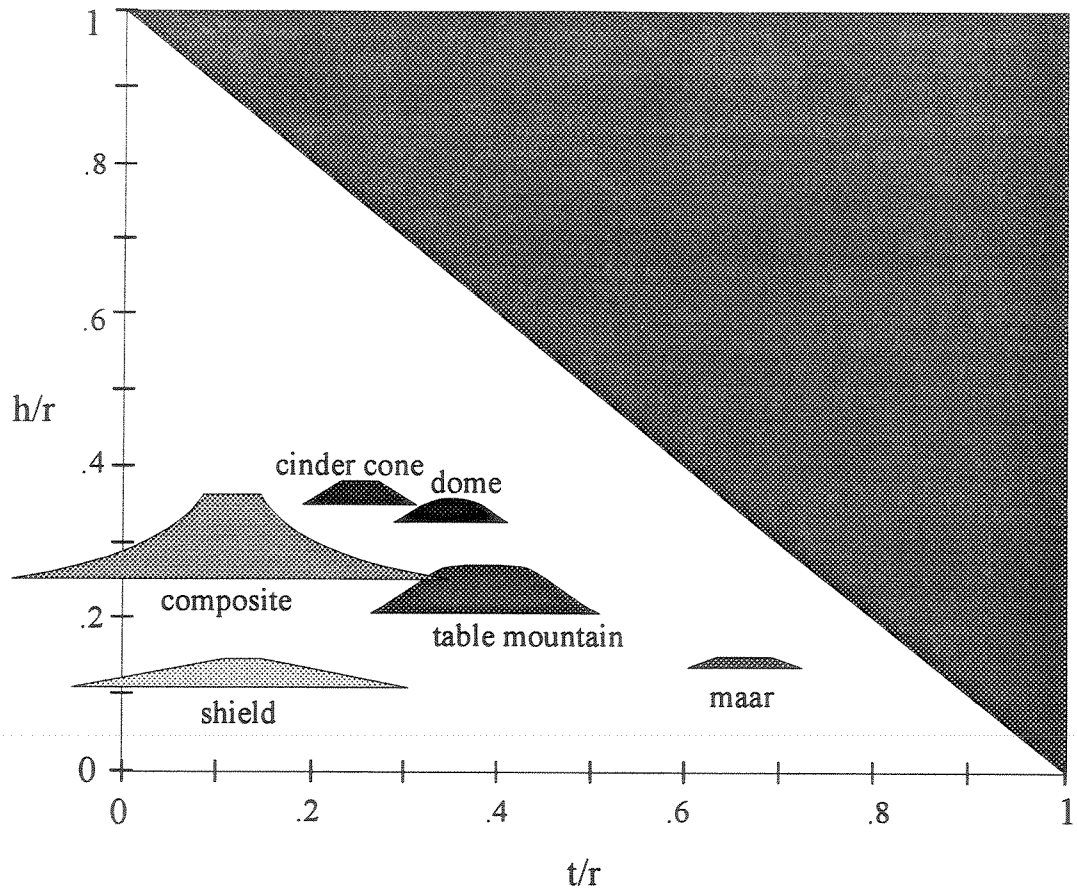


Figure II-2. The profile shapes of the major volcanic types are shown as shadow images in their approximate position on the shape parameter plane. Profile shapes correspond to those generally accepted in the literature [Cas and Wright, 1988]; this study makes no change in the shadow image. Position on the shape parameter plane is based on the average parameter values found in this study; where they differ significantly between regions, the values from Guatemala are used. Most volcanic types have a large range of parameter values. It is not physically possible for any volcanic type to have a shape occupying the darkened region of the shape parameter plane. The diagonal line forming the lower edge of the shaded region corresponds to a 45° flank slope, which cannot be exceeded based on the material properties of igneous rocks - for loose material (scoria, etc.) the limiting slope should be reduced to 33° (based on the angle of repose), which would lower the intersection of the limit line with the h/r axis.

aerial photographs. Initial morphology is usually retained for over 40 ka [in Mexico: Hasenaka and Carmichael, 1985; in Arizona: Wood, 1980b].

Maars (including tuff rings and tuff cones) are craters with or without a ring of debris and scoria formed by phreatic and phreatomagmatic eruptions [Cas and Wright, 1988]. They are shaped similarly to cinder cones, but have larger or deeper craters, are composed in part of wallrock, have a finer grain-size on average, may contain accreationary lapilli, and have gentler slopes [Cas and Wright, 1988]. Deposit structures are usually more complex than cinder cones (including breccia, base surge, airfall, and surge deposits). Most of these differences are related to the greater explosivity of phreatic and phreatomagmatic eruptions compared to strombolian eruptions; the depth of the crater is also related to the level at which the explosive process was initiated. Those with the largest amount of juvenile material (and thus greatest height and steepest slopes) (tuff cones) may be hard to distinguish from cinder cones on a topographic map. Cinder cones are sometimes 'nested' inside tuff rings.

Domes are the result of the eruption of highly viscous magma [Williams, 1932]. Exogenous domes generally are composed of only minor pyroclastics but have talus slopes on their flanks. They can be distinguished from cinder cones and maars by the lack of a crater, from shield volcanoes by a broad flat top with very steep flanks, and from erosional hills by more regular shape and flow features. Large domes may not have a simple circular plan, but may be composed of several overlapping lobes. Endogenous growth may also be important for domes. Domes are the volcanic features most difficult to reliably identify from topographic maps, because the only morphologic features useful for identification, other than overall shape, are viscous flow features which do not show up on small-scale maps and may be obscured by later ash falls or minor erosion.

Shield volcanoes are best defined as piles of lava flows resulting from Hawaiian eruptions [Wood, 1977; Cas and Wright, 1988]. The resulting landform is usually circular to elliptical in plan, convex-up, and gently sloped [Wood, 1977; Wood, 1979; Cas and

Wright, 1988]. Minor pyroclastics and breccias may be present (especially as such features as spatter cones, pit craters, etc.). Shield volcanoes are often divided into several classes: Hawaiian (large polygenetic edifices with summit calderas, major rift zones, and complicated histories), Icelandic (smaller symmetrical edifice with small central crater), Galapagos (similar to Hawaiian but smaller and more complicated shape). All share the characteristics of being composed primarily of lava and having gentle flank slopes and broad summit regions. Shield volcanoes, however, rarely have a discernible break in slope near the summit region; for this reason, in the absence of a summit crater/caldera, the actual top diameter measured may be somewhat erratic and is often smaller than the diameter of the perceived summit region.

Stratovolcanoes, or composite volcanoes, are formed by a combination of large pyroclastic eruptions, smaller explosions, and effusive activity. Epiclastic processes are more important in controlling the shape of composite volcanoes than most other volcanoes. Large pyroclastic eruptions result in the deposition of large volumes of loose ash on relatively steep slopes - consequently mass wasting processes are important in the removal and redeposition of this material on the lower slopes and surrounding Plain. The upper cone is formed primarily of lava and welded pyroclastics from smaller (or at least lower energy) eruptions [Cas and Wright, 1988; Vessel and Davies, 1981]. Composite volcanoes are also divided into several classes based on magma composition and the presence of a summit crater, collapse scar, or caldera [Pike and Clow, 1981a]. These classes can be difficult to distinguish on topographic maps, especially as the measurement techniques discussed above may not recognize the presence of a collapse scar. Morphologically, the main difference in these classes is the presence or absence of summit craters, calderas and collapse scars - the remaining cone is similarly shaped and sized in all the classes. Any composite volcano could fall in one or all three classes over the course of its history. Composite volcanoes are distinguished from shield volcanoes by the importance of pyroclastics in the edifice structure and by the importance and effect of

epiclastic processes (which result in a greater merging of the composite volcano cone with the surrounding topography by creating a large apron of volcanoclastic debris). When profiles are analyzed, composite volcanoes are observed to have convex down profiles (steepen towards summit) in contrast to the convex up profiles (flatten towards summit) of shield volcanoes (see analysis of profile shapes in chapter V; also Milne [1878] and Becker [1885]).

Table mountains are formed by a central vent erupting lava beneath a glacier [BVSP, 1981]. They are composed of interbedded hyaloclastic breccia and pillow lavas capped by a lava flow sequence which may in turn be surmounted by a cinder cone [BVSP, 1981]. As a landform, table mountains are steep-sided and flat-topped. Unlike cinder cones (which are generally much smaller features anyway), they may have an irregular plan and generally have relatively irregular flanks. They commonly have a summit crater, but it is generally much smaller than the morphologically defined top. (It is especially important in the case of table mountains to remember that the top diameter is not a crater diameter.) Table mountains differ from shield volcanoes in having steeper slopes, a more abrupt change in slope from flank to summit, and in having a summit crater smaller than the summit region.

Table II-1. Distinguishing features of various volcanic landforms.

Volcano Type	Eruption Process	Landform Features*	Deposit Features*	Confused Most With	Generally Accepted Morphology	Source
Cinder Cone ●	hawaiian strombolian	*central crater* *straight steep flanks* *circular plan* *gullies* or rills	coarse scoria associated lava flow	maar dome erosional hill	flat-topped cone h/r~0.36 t/r~0.38 < 300 m tall	Cas and Wright, 1988 Wood 1980
Maar ▲	phreatomagmatic phreatic	*crater- floor at or below ground level* *gentle sloped ring of debris/scoria*	fine scoria wallrock or lithics airfall, surge deposits ground water	cinder cone	as above, but h/r smaller t/r larger	Cas and Wright, 1988
Composite Volcano ✖	plinian to strombolian epiclastic	*concave-up* *summit crater, collapse or caldera*	short lava flows+ pyroclastic flows ashfall	large shield	h/r~.24 t/r~.05	Wood, 1979
Shield Volcano ✚	lava flows hawaiian	*convex-up* *flow features* *gentle slopes* *broad summit with crater/caldera*	lava flow fields+ minor pyroclastics and breccias	composite dome	h/r ~.04-.12 t/r ~.05-.12	Cas and Wright, 1988
Dome ■	viscous lava flows pyroclastic flows?	*rounded or flat top* viscous flow features+	viscous flow features flanks defined by talus slopes	cinder cone shield	h/r moderate t/r high	
Table Mountain □	hyaloclastites lava flows	*rounded or flat top* *steep flanks*	hyaloclastites pillow lavas glacial features lava flow cap	dome erosional hill	h/r moderate t/r high	BVSP, 1981

*features identifiable on a topographic map in italics.
+ may be distinguishable on topographic map.

DATA

Volcano population studies

In the following four sections, the tectonic boundaries and volcanic populations of each of the four study regions are discussed. The boundaries of each study area are defined in terms of the regional geology. The volcanic population within each study area is discussed in terms of the types of volcanoes observed, distribution of edifices, and the degree of morphologic separation observed between volcanic types. Morphologic separation is discussed in the context of the three parameters describing size and shape: basal diameter 2r (or height h), the height-to-base h/r, and the top-to-base ratio t/r. Statistically significant relationships between any of the morphologic parameters for a given volcanic type are discussed in the light of what they may indicate about eruptive processes and growth trends. Note that h and 2r correlate for all volcanoes. Each region is discussed separately, although comparisons between regions are included. A more complete set of morphologic plots can be found in the Appendix A; the figures in the following sections were chosen to illustrate the main points of the texts (and the dominant characteristics of each region).

Volcanoes of Guatemala

The volcanic regions of Guatemala consist of (1) part of the Central American volcanic arc, a line of large volcanoes along the Pacific coast, and (2) several isolated back-arc extensional regions. The Central American volcanic front is related to the subduction of the Cocos plate. Approximately 10 volcanic complexes lie along the volcanic front within the study region (from Boqueron, El Salvador to Santa Maria, Guatemala); these consist mainly of stratovolcanoes but also include dome complexes, a large caldera, and other volcanic features (Figure II-3). The borders of this volcanic region are composed of the arc front to the south, the transform to the north, and arbitrary lines to east and west (actually chosen based on the availability of maps).

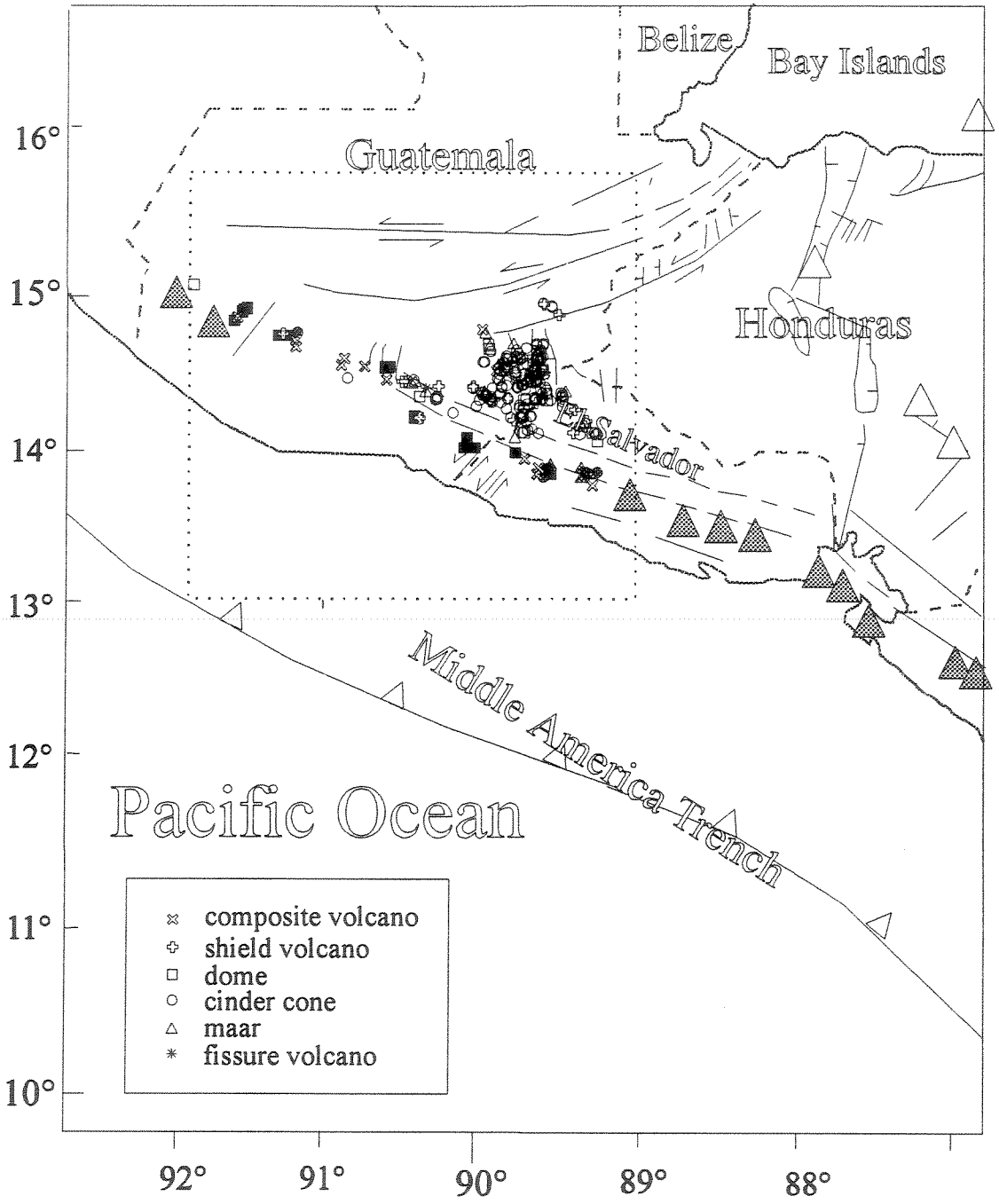


Figure II-3. (a) Location of study area is the arc front and back arc of Guatemala and El Salvador. The large triangles indicate eruption centers not included in this study. The small symbols indicate volcanic type (see inset). Solid symbols indicate which volcanoes are considered part of the arc front.

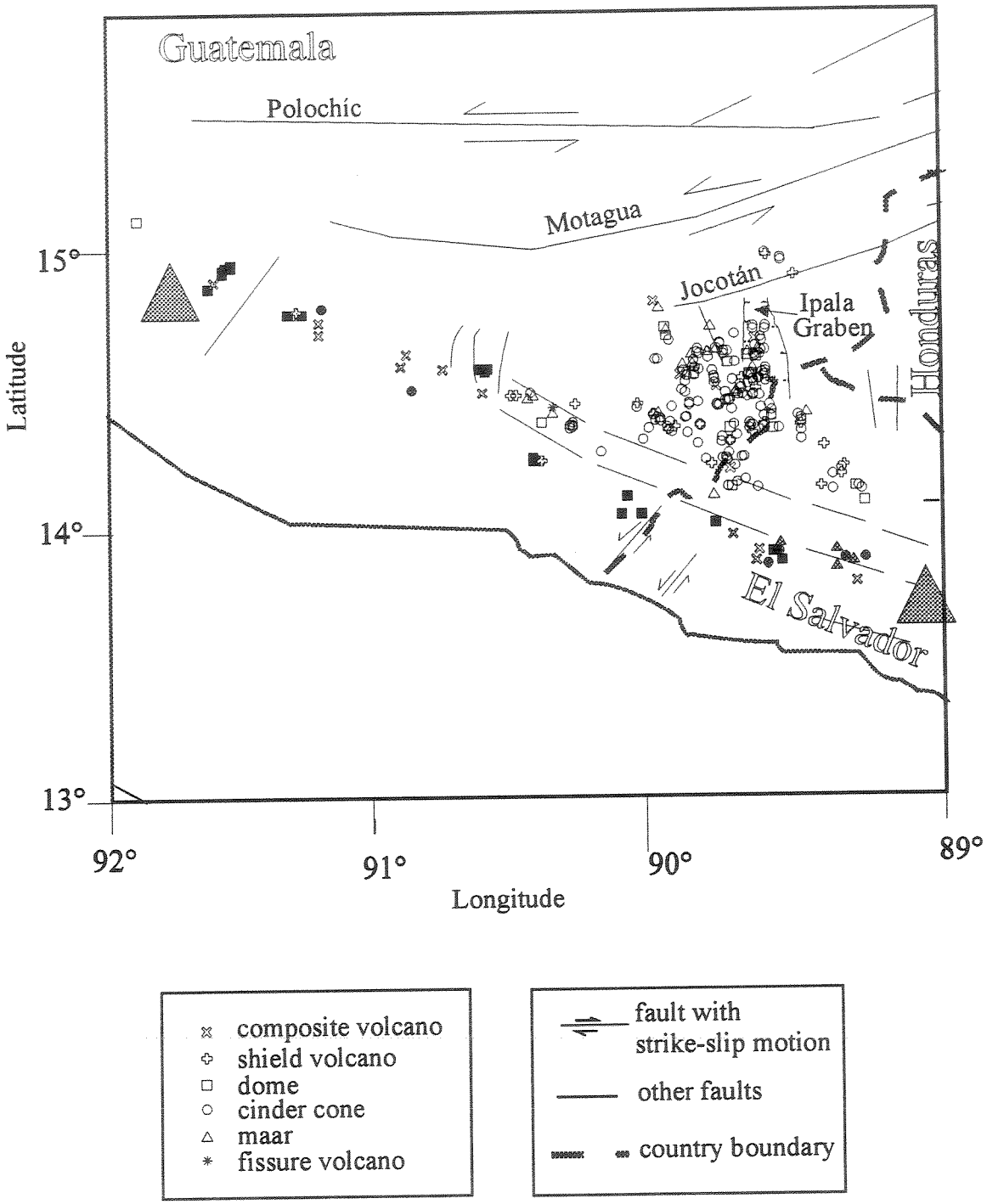


Figure II-3. (b) Enlargement of study area shows the relative locations of the individual volcanoes measured (small symbols). Most of the back arc volcanism occurs in or near the Ipala Graben, southeast Guatemala, which is bounded by normal faults.

All of the back-arc volcanism in northern Central America is related to local extensional structures that generally trend N-S, oblique to the volcanic front. The Ipala Graben in southeast Guatemala is by far the largest of several areas of behind the front volcanism in Central America. The Ipala Graben extends across the Jocotán fault, an E-W striking, left-lateral, strike-slip fault that, together with the similarly oriented Motagua and Polochíc faults to the north, comprise the Caribbean-North American plate boundary [Plafker, 1976]. Thus the tectonic setting of this volcanic region is a composite of back-arc and transform settings [Burkart and Self, 1985]. The Ipala Graben is an area of basalt-rhyolite volcanism [Williams et al., 1964; Bohnenberger, 1969] behind the volcanic front of Central America (Figure II-3). Quaternary extension is evident along the north trending Ipala Graben, within which most of the volcanism occurs. More than 95 cinder cones are associated with lava flows and small shield volcanoes (Figure II-3). Rhyolitic domes occur approximately in the center of the volcanically active region. The cones are estimated to be Holocene or slightly older; some cones and associated flows have little vegetative cover and appear to be comparable in age to the older historic flows along the volcanic front.

The volcanic fields Guatemala contains 369 volcanoes of which 121 cinder cones, 14 shield volcanoes, 16 composite volcanoes, 19 domes and 13 maars have been identified by eruption style (Table II-2). The other 186 volcanoes could not be classified according to volcanic type, but most are cinder cones that are malformed for a variety of reasons. Generally, the shield volcanoes, cinder cones and maars lie behind the volcanic front, while the stratovolcanoes lie along the front. Exceptions do occur. Domes are equally common in both volcanic fields. These two volcanic fields are treated as one for convenience and because the volcanic types tend to separate by location (see Figure II-1). In cases where the distinction between front and back arc locations may be important, it will be discussed.

Shape and size parameters separate most of the volcanic types with little overlap. The exception is cinder cones and domes which overlap completely. Separation of shape

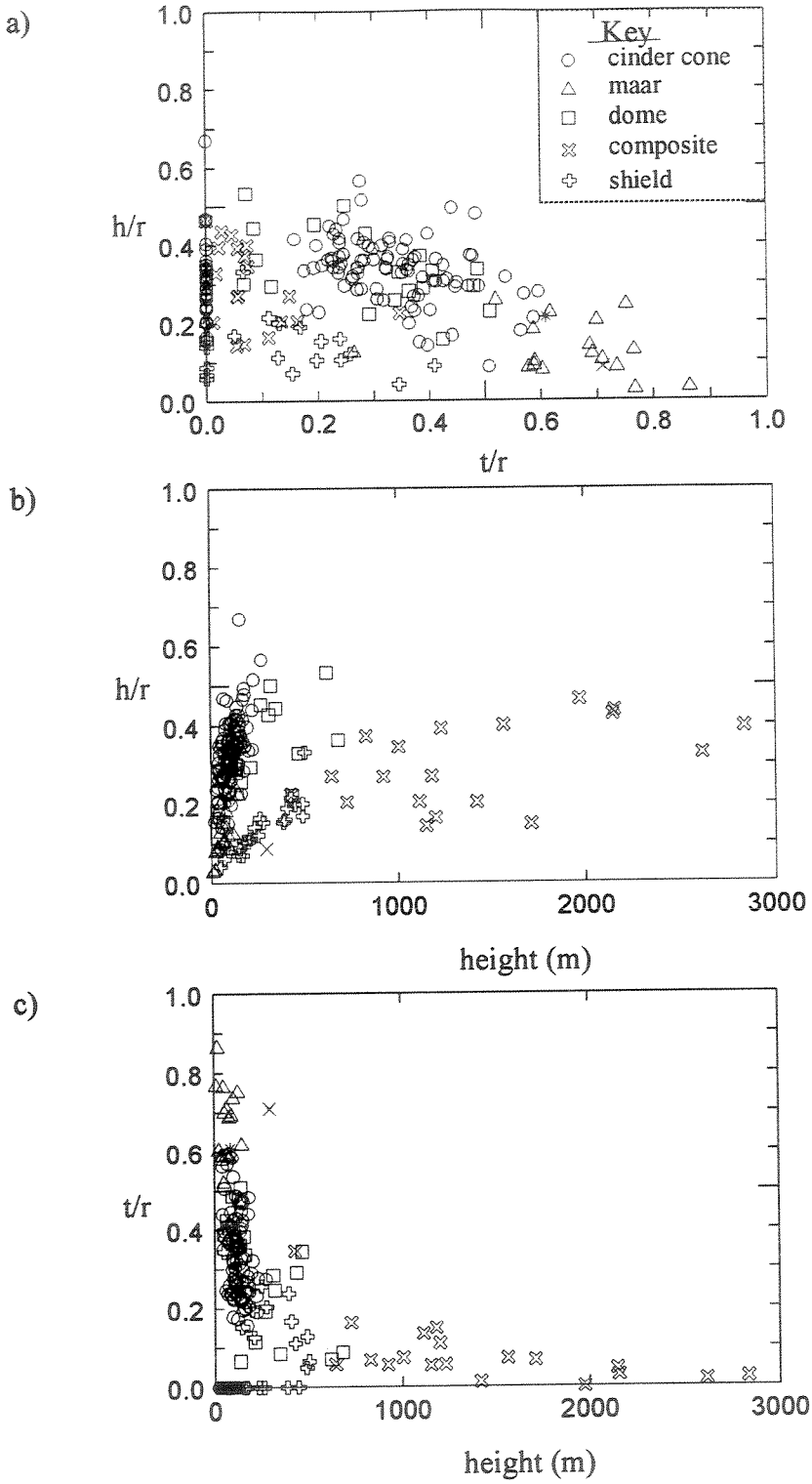


Figure II-4. The parameters describing volcano shape and size are plotted against each other for Guatemalan volcanoes. Symbols indicate volcanic type as in Figure 2. (a) The h/r ratio vs. the t/r ratio show the different shapes of most volcanic types. (b) The volcanic types differ greatly in size. (c) Differences in the range of t/r ratios result in a L shaped separation.

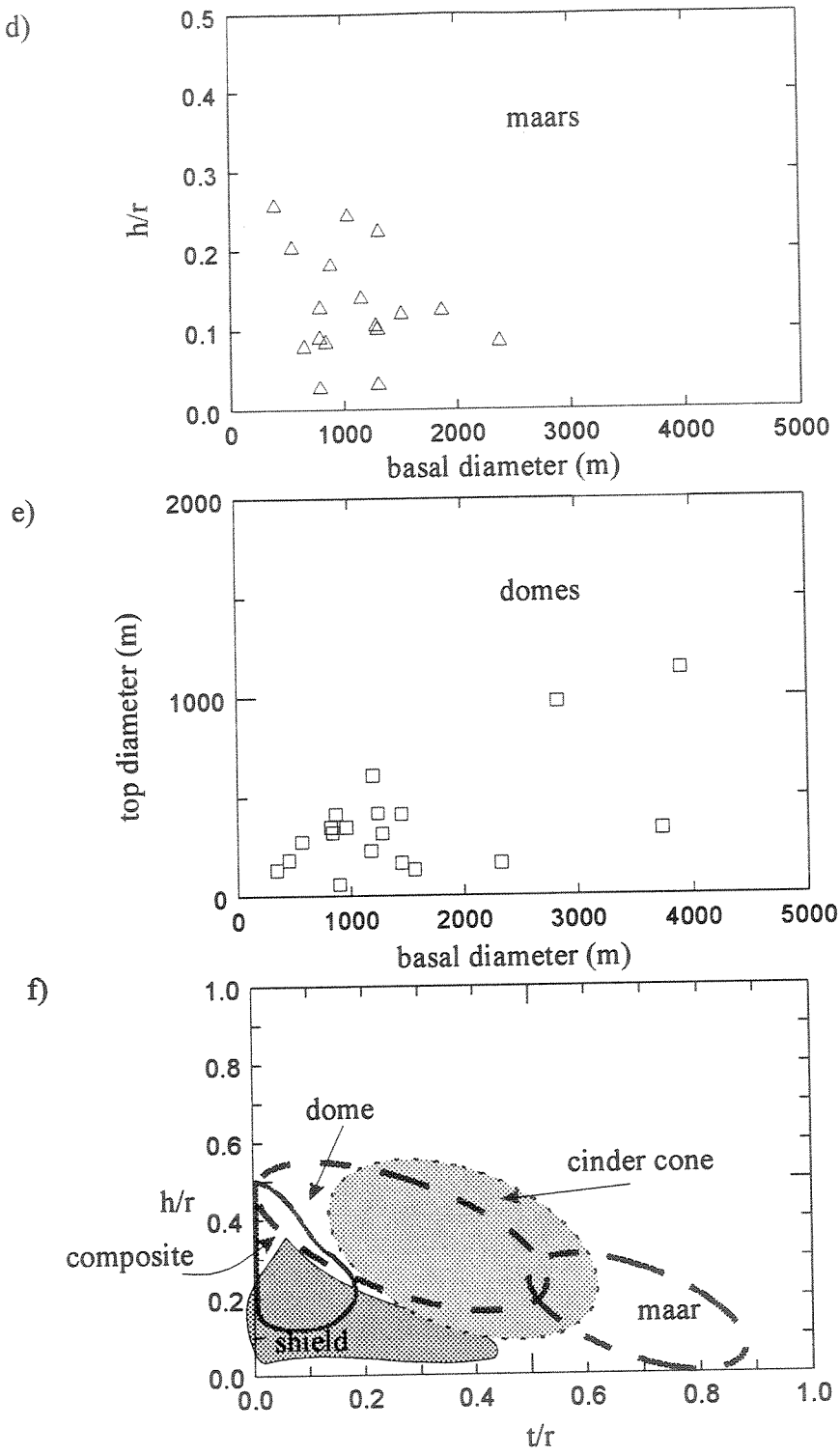


Figure II-4. (d) The h/r ratio decreases with increasing height for maars. (e) The top diameter 2t increases consistently with basal diameter 2r for domes. (f) Summary of overlap between the morphospace of different volcanic types. Notice that the dome field and the cinder cone field are almost coincident.

by volcanic type is seen best, for Guatemalan volcanoes, in plots of h/r vs. t/r (Figure II-4a), h/r vs. h (Figure II-4b) and t/r vs. h (Figure II-4c). Generally, the various volcanic types differ in steepness (h/r) and flatness (t/r); some also differ in size. The average height-to-radius ratios for each volcanic type decreased in the following order: uneroded cinder cones, composite volcanoes, maars = shield volcanoes (Table II-2, Figure II-4a). The average top-to-base ratios decreased in the following order: maars, cinder cones, shield volcanoes, composite volcanoes (Table II-2, Figure II-4a). Domes overlap completely with cinder cones on a h/r vs. t/r plot (Figure II-4a, Table II-2). If size is considered (Figure II-4 (b-c)), domes are sometimes, but not always, much larger than cinder cones. Cinder cones, maars and about half the domes are much smaller than shield and composite volcanoes and generally have larger t/r (notice the L shaped separation in Figure II-4c).

Compared to monogenetic shields measured by Wood [1979], the shield volcanoes of Guatemala have slightly steeper, but still shallow, slopes (8° ± 3°) and a wider range in flatness (t/r=0.00 to 0.35); the Guatemalan shields may not all be monogenetic. The height-to-radius ratios increase with increasing height h (R=0.96) (crosses in Figure II-4b) and basal diameter 2r (R=0.55) while the flatness (t/r=0.12±0.12) remains constant with increasing h or r (Figure II-4c). Flatness is controlled primarily by the top diameter (for t/r vs. 2t, R=0.95), which is apparently independent of volcano size. Shield volcanoes in Guatemala appear to grow by adding height as predicted by Borgia and Linneman's [1990] model of the growth of Arenal (this is actually a composite volcano, but the edifice consists solely of lava flows).

Composite volcanoes in Guatemala are steeper than shield volcanoes (slope = 17° ± 6°) with similar flatness (t/r = 0.00 to 0.35). The steeper cone probably reflects the addition of pyroclastic material in the near vent region as well as more viscous (so shorter) lava flows. The crater sizes are probably similar except where calderas or collapse scars are present. The average height-to-radius ratio (h/r = 0.29±0.11) and average flatness (t/r

= 0.08±0.09) are reasonably close to Wood's (1979) results. Linear regression of h with 2r and 2t with 2r do not particularly reflect Wood's results because of the relatively short volcanoes in the southeastern section of the arc front volcanic field (in El Salvador), the relatively large craters (Ipala, Pacaya) of some volcanoes, and the high degree of erosion (Tahual, Suchitan) of some back arc volcanoes. Overall, both slope and height-to-radius ratio h/r do not vary with increasing height h and basal diameter 2r (x's in Figure II-4b), although they may decrease slightly in the very largest composite volcanoes. There appears to be two separate paths of growth: the volcanoes in Figure II-4b with lower h/r ratios are mostly from southeast Guatemala and El Salvador whereas those with higher h/r ratios are mostly from southwest Guatemala. However, Chapter V observes that the slope and h/r change smoothly along the arc front. Thus, there may simply be a single broad growth trend in Figure II-4b; progressive changes in eruption conditions along arc and differences in volcano lifespan are both likely factors in determining the growth pattern observed. Eruptive processes apparently change along the arc front. The h/r ratio correlates negatively with the top diameter 2t (R=-0.72), suggesting that composite volcanoes with exceptionally large craters appear less steep because the steep summit region has been removed by the crater forming eruption. Flatness t/r and crater size 2t are independent of volcano size (Figure II-4c). Composite volcanoes appear to grow more evenly in height h and basal diameter 2r than shield volcanoes do.

Cinder cones have steep slopes and wide craters on average but exhibit high variability in all parameters (Table II-2). The morphologies observed here are consistent with models of cinder cone growth [McGetchin et al., 1974 ; Wood, 1980a] and degradation [Wood, 1980b], but show much more complexity in the interrelationships of the morphologic parameters than previously discussed. The morphologic parameters reported in this chapter are for all volcanoes identified as cinder cones (with heights over 50 m), which are assumed to be relatively uneroded based on their inferred young age (see above) and on morphological criteria [Hasenaka and Carmichael, 1985; Dohrenwend et

al., 1986] (see Chapter IV for a more detailed analysis). Flank slopes vary from 10° to 43° (those over 33° are due to underestimation of the basal diameter on cones sitting against or on larger features or measurement error on small cones). The height-to-radius ratio h/r increases with height h (Figure II-4b) and decreases slightly with basal diameter 2r and top diameter 2t as predicted by the McGetchin model (see Chapter IV). The flatness t/r depends almost entirely on the top diameter 2t (as is observed in numerical simulations of the McGetchin model). The top diameter 2t increases significantly with basal diameter 2r, which is not predicted by the McGetchin model, but may reflect an increase in volatile content with increasing magma supply (see Chapter III). Large cinder cones may form from more explosive eruptions, which would naturally result in a larger vent diameter [Head and Wilson, 1987].

Maars have generally high flatness and low h/r (Table II-2), which decreases with r. Maars, formed by the explosive contact of erupting lava with water, are distinct from cinder cones by being much flatter and shallower sloped; the decreasing h/r with increasing r (R=-0.66) suggests the amount of material ejected increases slower than the area in which it is deposited. Strong correlation between 2r and 2t (R=0.81) suggests both are controlled by the strength of the explosion; a possible correlation between t/r and 2t (R=0.43) suggests 2t may be more sensitive to the explosivity than 2r.

Domes are superficially similar to cinder cones, but exhibit a narrower range of shape parameters (Table II-2). Correlation coefficients between parameters suggest that growth trends reflect the viscous flow process of growth: the top diameter increases as the basal diameter increases (R=0.60); the height-to-radius ratio increases with height (R=0.50) while the flatness decreases with height (R=-0.61); the flatness is only vaguely correlated with the top diameter (R=0.37). However, the visual patterns (see Figure II-4 and Appendix A, Figure A-1) are very erratic, suggesting that more than one growth pattern is involved.

Table II-2. Summary of morphologic parameters for Guatemalan volcanoes.

		Average[1]			Range				
Type	N	H/R	Slope	T/R	H (m)	2R (m)	H/R	Slope	T/R
Cinder Cone	115	0.34±0.08	25°± 6°	0.26±0.17	41- 270 m	263- 1400 m	0.09-0.67	10-43°	0.00-0.60
Shield	14	0.12±0.05	8°± 3°	0.12±0.12	50- 490 m	2328- 4880 m	0.04-0.20	3-13°	0.00-0.35
Composite	16	0.29±0.11	17°± 6°	0.08±0.09	426-2835 m	3778-23120 m	0.14-0.47	9-25°	0.00-0.35
Dome	19	0.34±0.10	26°± 6°	0.29±0.15	49- 679 m	340- 3905 m	0.16-0.53	15-34°	0.07-0.51
Maar	13	0.15±0.06	24°± 9°	0.64±0.13	50- 295 m	390- 6855 m	0.08-0.26	10-45°	0.26-0.77

[1]average values are reported with standard deviation.

Table II-3. Correlations in Population Parameters for Guatemalan volcanoes by type.

Volcano Type	Correlation between:	R	t	n	Confidence
Cinder Cone[1]	h & 2r	0.65	8.79	111	>99.8%
	h & 2t	0.35	3.96	111	>99.8%
	2t & 2r	0.67	9.51	111	>99.8%
	h/r & h	**0.54**	6.77	111	>99.8%
	h/r & 2r	-0.24	-2.61	111	99%
	h/r & 2t	-0.25	-2.64	111	99%
	t/r & h	0.19	2.00	111	95%
	t/r & 2r	0.35	3.86	111	>99.8%
	t/r & 2t	**0.89**	20.95	111	>>99.8%
	h/r & t/r	-0.16	-1.67	111	90%
Maars[1]	h & 2r	0.53	1.97	12	90%
	h & 2t	0.35	1.17	12	n.c.
	2t & 2r	**0.81**	4.39	12	>99.8%
	h/r & h	0.18	0.57	12	n.c.
	h/r & 2r	**-0.66**	-2.80	12	98%
	h/r & 2t	**-0.58**	-2.27	12	95%
	t/r & h	-0.18	-0.57	12	n.c.
	t/r & 2r	-0.14	-0.46	12	n.c.
	t/r & 2t	**0.43**	1.52	12	80%
	h/r & t/r	-0.04	-0.13	12	n.c.

[1]Heights restricted to greater than 50 m as contour interval on topographic maps is 20 m.
Correlation coefficients in boldface are of particular interest and discussed in the text.
n.c. = no confidence.

Table II-3. continued

Volcano Type	Correlation between:	R	t	n	Confidence
Shield Volcano	h & 2r	0.72	3.62	14	99%
	h & 2t	0.03	0.11	14	n.c.
	2t & 2r	0.09	0.30	14	n.c.
	h/r & h	**0.96**	11.65	14	>99.8%
	h/r & 2r	**0.55**	2.30	14	95%
	h/r & 2t	-0.05	-0.16	14	n.c.
	t/r & h	-0.16	-0.58	14	n.c.
	t/r & 2r	-0.14	-0.48	14	n.c.
	t/r & 2t	**0.95**	10.03	14	>99.8%
	h/r & t/r	-0.22	-0.79	14	n.c.
Composite Volcano	h & 2r	0.54	2.67	19	98%
	h & 2t	-0.36	-1.60	19	80%
	2t & 2r	0.30	1.29	19	n.c.
	h/r & h	0.50	2.36	19	95%
	h/r & 2r	-0.40	-1.81	19	90%
	h/r & 2t	**-0.72**	-4.26	19	>99.8%
	t/r & h	-0.61	-3.19	19	99%
	t/r & 2r	-0.35	-1.53	19	80%
	t/r & 2t	**0.66**	3.64	19	99.8%
	h/r & t/r	-0.41	-1.86	19	90%

Correlation coefficients in boldface are of particular interest and discussed in the text.
n.c. = no confidence.

Table II-3. continued

Domes[1]	h & 2r	**0.87**	6.97	18	>99.8%
	h & 2t	0.25	1.03	18	n.c.
	2t & 2r	**0.60**	2.97	18	99%
	h/r & h	**0.50**	2.30	18	95%
	h/r & 2r	0.06	0.23	18	n.c.
	h/r & 2t	-0.40	-1.73	18	80%
	t/r & h	**-0.61**	-3.09	18	99%
	t/r & 2r	-0.41	-1.79	18	90%
	t/r & 2t	0.37	1.61	18	80%
	h/r & t/r	-0.52	-2.44	18	95%

[1]Heights restricted to greater than 50 m as contour interval on topographic maps is 20 m.
Correlation coefficients in boldface are of particular interest and discussed in the text.
n.c. = no confidence.

Volcanoes of northern and west-central Iceland

Iceland lies on the Mid-Atlantic rift and much of the volcanism and tectonic activity relates to spreading processes [Sæmundsson, 1979]. Iceland is also inferred to sit over a hot spot [Sæmundsson, 1979]. Volcanologically, Iceland has a variety of magma types reflecting ridge and hot spot origins [Schilling, 1973; Sæmundsson, 1979]. Both fissure eruptions and central volcanoes are important [Williams et al., 1983].

The volcanic population of the northern rift zone from approximately 64°45' N to the northern coast of Iceland (Figure II-5) was measured. The north-south boundaries are the edge of the neovolcanic zone. A small area in the middle rift zone was also included (Figure II-5). Volcanic features with extreme elongation (that is, fissure volcanoes) were not included in this study.

The 130 volcanoes identified in the northern and central rifts of Iceland (Figure II-5) consist of only shield volcanoes (25), table mountains (27), maars (3) and a composite volcano. The other 74 volcanoes could not be classified according to volcanic type. The lack of more explosive types of volcanoes in Iceland probably can be attributed to the relatively low volatile content of Icelandic magmas (MORB type) compared to arc and continental magmas. Note, however, that more composite volcanoes exist outside the study area in Iceland - many in the south-central rift area [Thorarinsson and Sæmundsson, 1979]. Table mountains are well separated from shield volcanoes on almost all morphologic plots (Figure II-6; see also Figure A-2 in Appendix A) reflecting that table mountains are taller, steeper and more flat-topped than shield volcanoes (Table II-4).

Icelandic shield volcanoes have low height/radius ratios ($h/r=0.08\pm0.04$) which correspond to gentle slopes (slope = 6 ± 5) and moderately sized summits ($t/r=0.16\pm0.15$) like the Guatemalan shields. However, the relationships between morphologic parameters differ greatly. The height-to-radius ratio is independent of height and basal diameter (Figure II-6b), indicating that Icelandic shields maintain a constant slope as they grow.

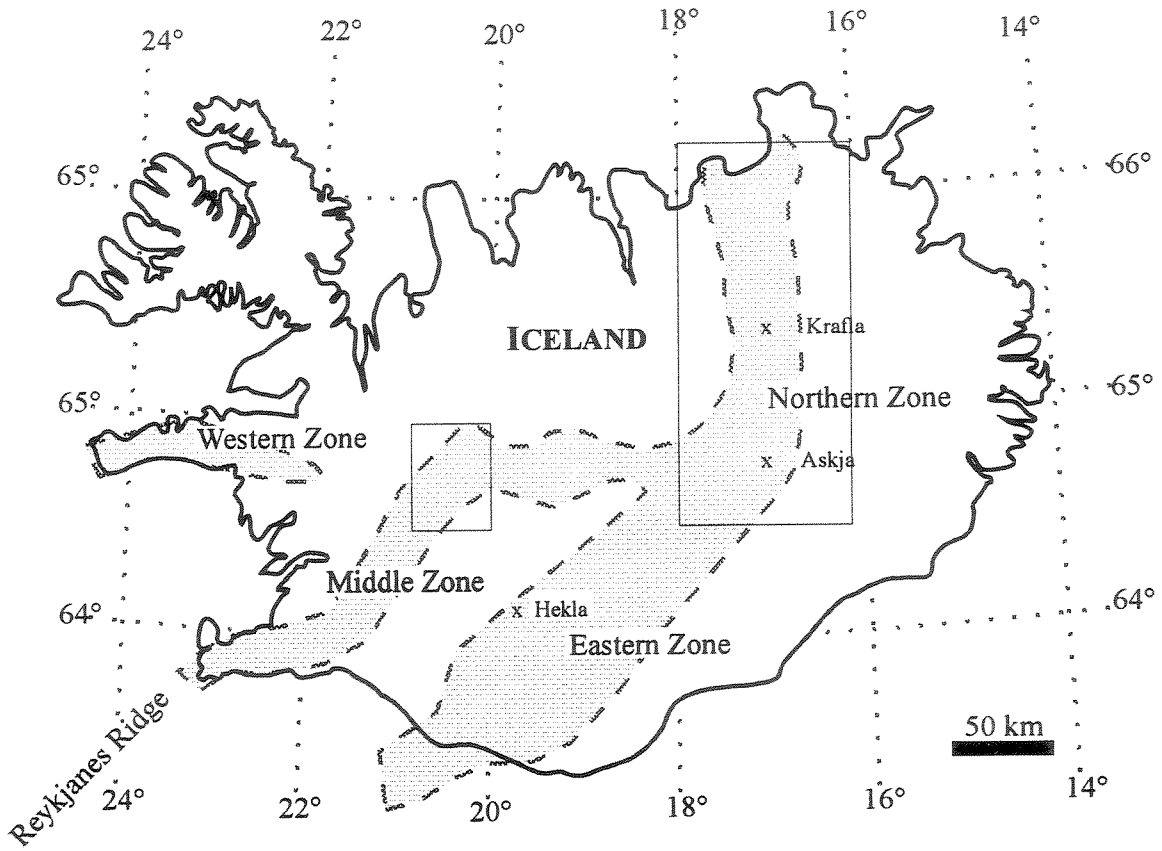


Figure II-5. The study areas (boxes) for the volcanic population of Iceland are in the northern rift zone and middle rift zone. The stippled regions represent the approximate extent of the neo-volcanic zones.

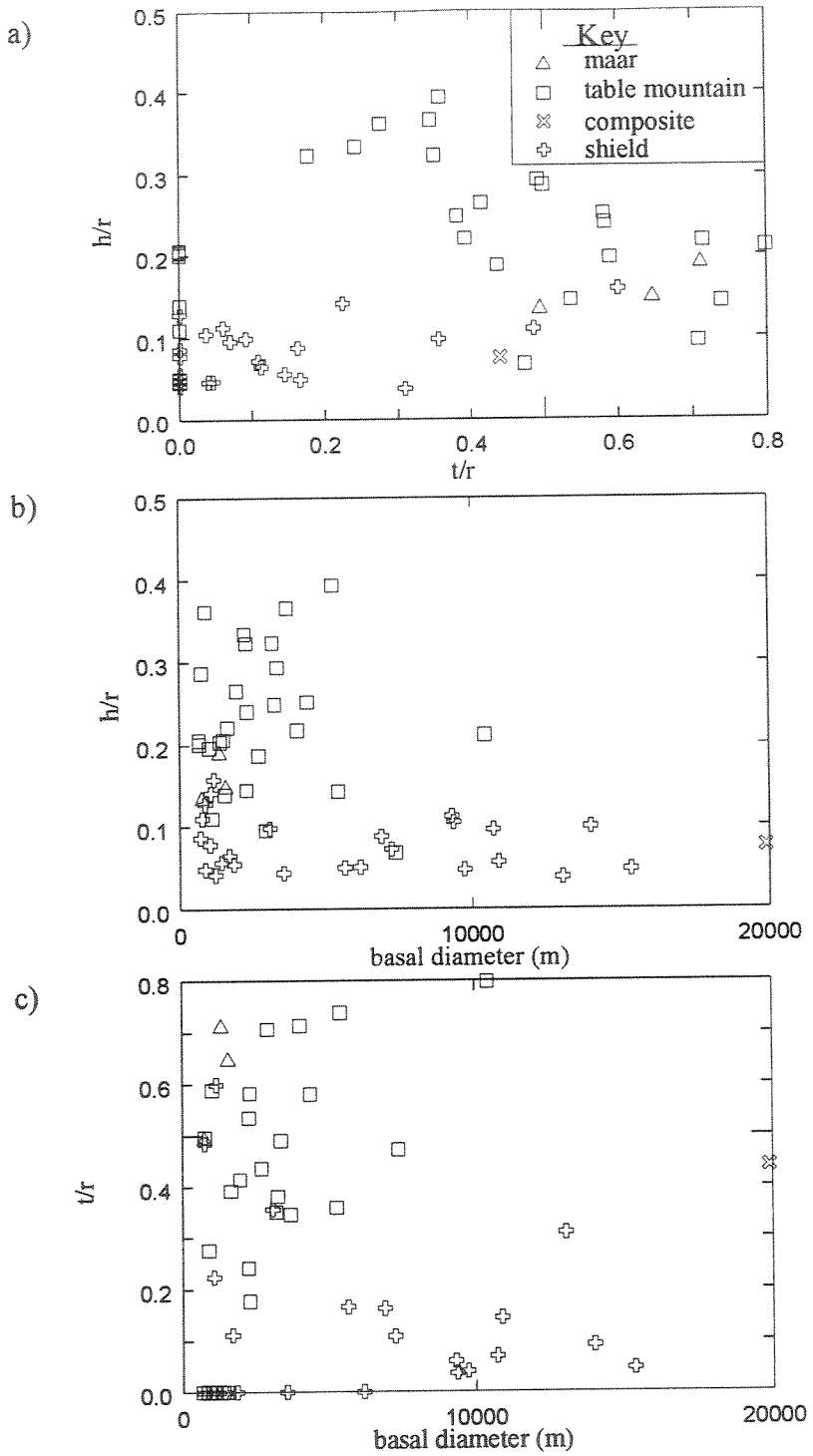
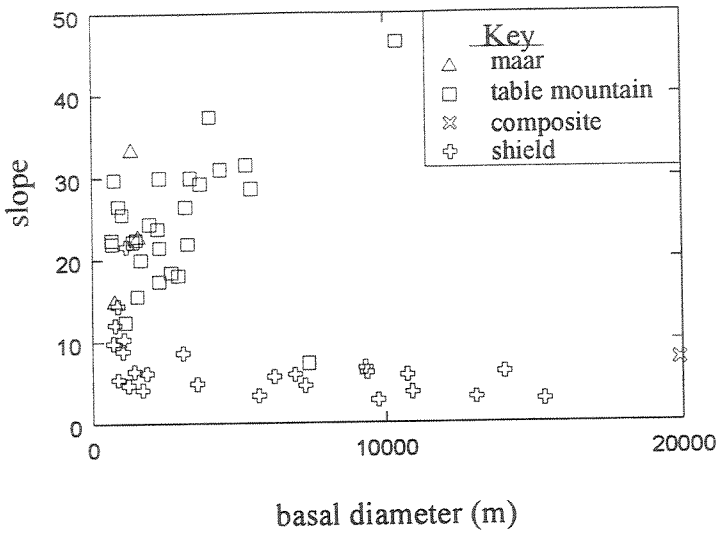


Figure II-6. The parameters describing volcano shape and size are plotted against each other for Icelandic volcanoes. Symbols indicate volcanic type (crosses are shield volcanoes; boxes are table mountains; triangles are maars). (a) The h/r ratio vs. the t/r ratio show the different shapes of shield volcanoes and table mountains. (b) Shield volcanoes and table mountains are similar in size, but table mountains are steeper. (c) Table mountains have wider flat-tops than shield volcanoes.

d)



e)

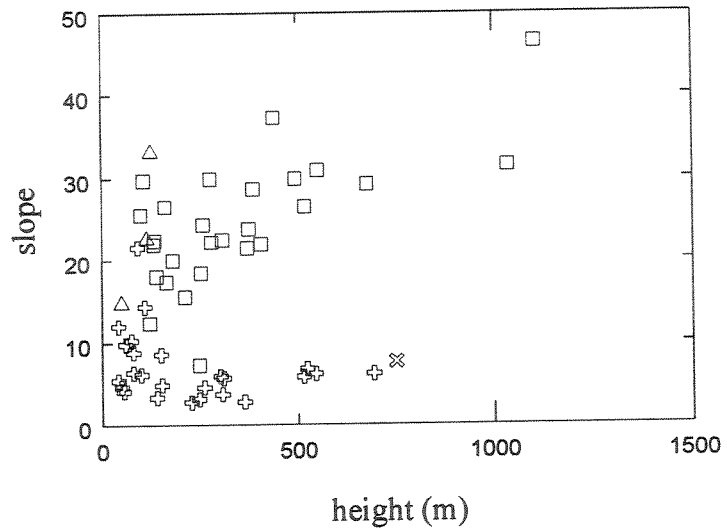


Figure II-6. The slope of table mountain flanks increases with height (e) and basal diameter (d). Shield volcanoes have constant slope.

The t/r ratio and the top diameter change little with volcano size (Figure II-6c); the size of the summit region may be related to processes of magma supply and withdrawal.

Table mountains have steep flanks (h/r=0.25±0.09; slope = 25 ±8) and wide flat tops (t/r=0.49±0.17). Strong correlations between the height h, basal diameter 2r and top diameter 2t (Table II-5) suggest that table mountains grow equally in all dimensions. Flatness t/r increases with basal diameter (R=0.59), reflecting a faster increase in top diameter than basal diameter. The h/r ratio increases only slightly with height (R=0.46) (Figure II-6e), but the slope increases steadily with both height (R=0.67) and basal diameter (R=0.42) (Figure II-6d). Table mountains get flatter and steeper as they grow (Figure II-7), which probably reflects pillow lava and hyaloclastite formation and the resultant rubble added to the flanks.

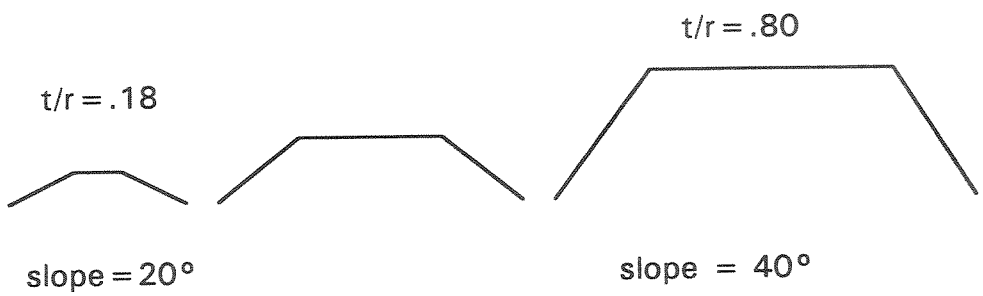


Figure II-7. As table mountains grow, their flanks become steeper and their flat-tops get wider.

Table II-4. Summary of morphologic parameters for Icelandic Volcanoes

		Average			Range				
Type	N	H/R	Slope	T/R	H (m)	2R (m)	H/R	Slope	T/R
Shield	25	0.08±0.03	7° ± 4°	0.13±0.16	41- 694	693-15,355	0.04-0.16	3 - 22°	0.00-0.60
Table Mt	27	0.23±0.09	25° ± 8°	0.37±0.25	100-1105	655-10,433	0.07-0.39	7°- 46°	0.00-0.80
Maar	3	0.18±0.10	25° ± 8°	0.60±0.10	50-191	750- 1563	0.13-0.27	14°-46°	0.49-0.71
Composite	1	0.08	8°	0.44	751	19,880			

Table II-5. Correlations between morphologic parameters for Icelandic volcanoes by type.

Volcano Type	Correlation between:	R	t	n	Confidence
Shield Volcano	h & 2r	0.83	7.24	25	>99.8%
	h & 2t	0.31	1.59	25	80%
	2t & 2r	0.60	3.61	25	>99.8%
	h/r & h	0.10	0.50	25	n.c.
	h/r & 2r	-0.22	-1.10	25	n.c.
	h/r & 2t	-0.12	-0.63	25	n.c.
	t/r & h	-0.16	-0.79	25	n.c.
	t/r & 2r	-0.08	-0.39	25	n.c.
	t/r & 2t	0.42	2.24	25	95%
	h/r & t/r	0.49	2.76	25	98%
Table Mountains	h & 2r	**0.76**	5.82	27	>99.8%
	h & 2t	**0.66**	4.36	27	>99.8%
	2t & 2r	**0.94**	13.95	27	>99.8%
	h/r & h	**0.46**	2.56	27	98%
	h/r & 2r	-0.08	-0.40	27	n.c.
	h/r & 2t	-0.16	-0.84	27	n.c.
	t/r & h	0.31	1.66	27	80%
	t/r & 2r	**0.59**	3.68	27	>99.8%
	t/r & 2t	0.72	5.11	27	>99.8%
	h/r & t/r	-0.08	-0.38	27	n.c.

n.c. = no confidence.

Boldface regression coefficients are of particular interest and discussed in the text.

Small submarine volcanoes in the South Pacific

The French Polynesian region of the South Pacific (Figure II-8) has several unique topographic characteristics. It is noted for its many hot spot chains, which include the Cook, Austral, Tuamotu and Society Islands [Calmant and Cazenave, 1987]. It is also noted for its anomalously shallow bathymetry: seafloor depths are typically 250-750 m shallower than predicted by thermal subsidence models [McNutt and Fischer, 1987; McNutt and Judge, 1990; Parsons and Sclater, 1977]. In addition, the adjacent section of the east Pacific Rise between 9°S and 22°S, an ultrafast spreading segment, has lower than predicted subsidence rates on the Pacific Plate side [Cochran, 1986]. The anomalous region of seafloor in French Polynesia, south of the Marquesas fracture zone on crust greater than 20 My old, has been named the Superswell by McNutt and Fischer [1987] (Figure II-8).

Bemis and Smith [1993] investigated the production of small (50-700 m high) volcanoes in the region of the Superswell and found that seamount abundance's increase three-fold going southward across the Marquesas fracture zone, the inferred northern boundary of the Superswell. No difference in seamount abundance between young crust (0-18 my) and older crust (20-60 my) was observed leading to an uncertainty in where and why the seamounts were produced [Bemis and Smith, 1993].

Shape statistics were compiled for 556 volcanoes in 3 study regions in the South Pacific from Sea Beam bathymetry data (Figure II-9). The sample mean of the height-to-radius ratio for all 556 volcanoes is $h/r=0.18\pm0.08$. Flatness varies from $t/r=0.0$ (pointy cone) to $t/r=0.8$ (flat-topped cone) and shows a great range in values for all heights. No significant variations in the mean shape parameters were observed across the Marquesas fracture zone or between young and old crust [Bemis and Smith, 1993]. This study looks at a subset of the entire data set containing 289 small submarine volcanoes in an effort to relate their observed variation in shape to the shapes of subaerial volcanoes.

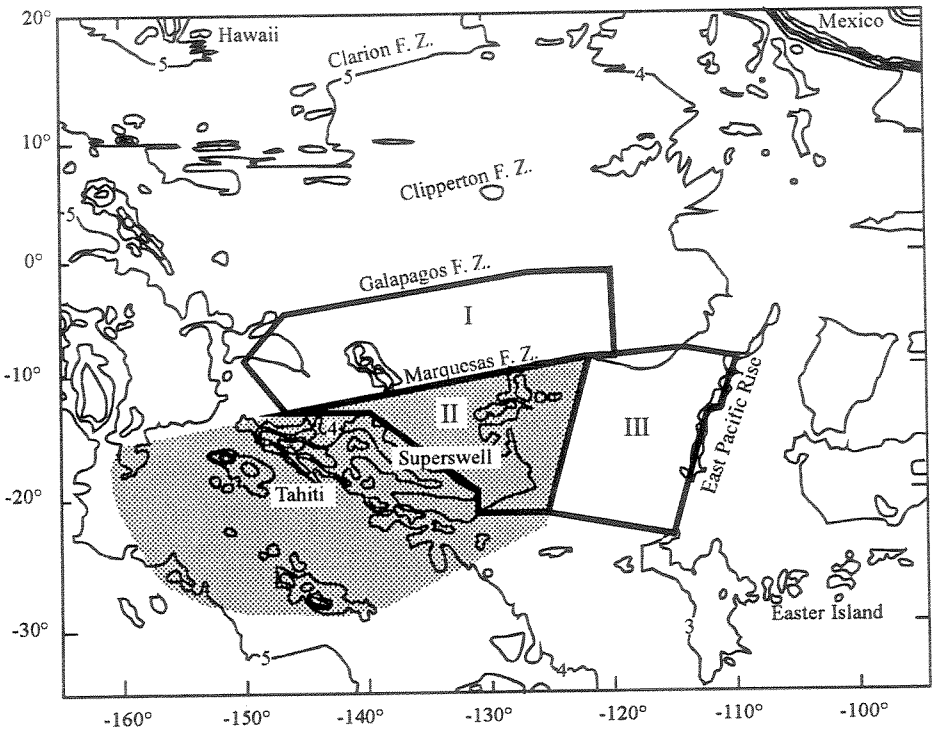


Figure II-8. Location map of the French Polynesia region of the South Pacific. The thick line outlines the regions sampled. Most of the data in this study comes from region III. Bathymetric contours are labeled in 1 km intervals. The approximate area of the Superswell is shown shaded.

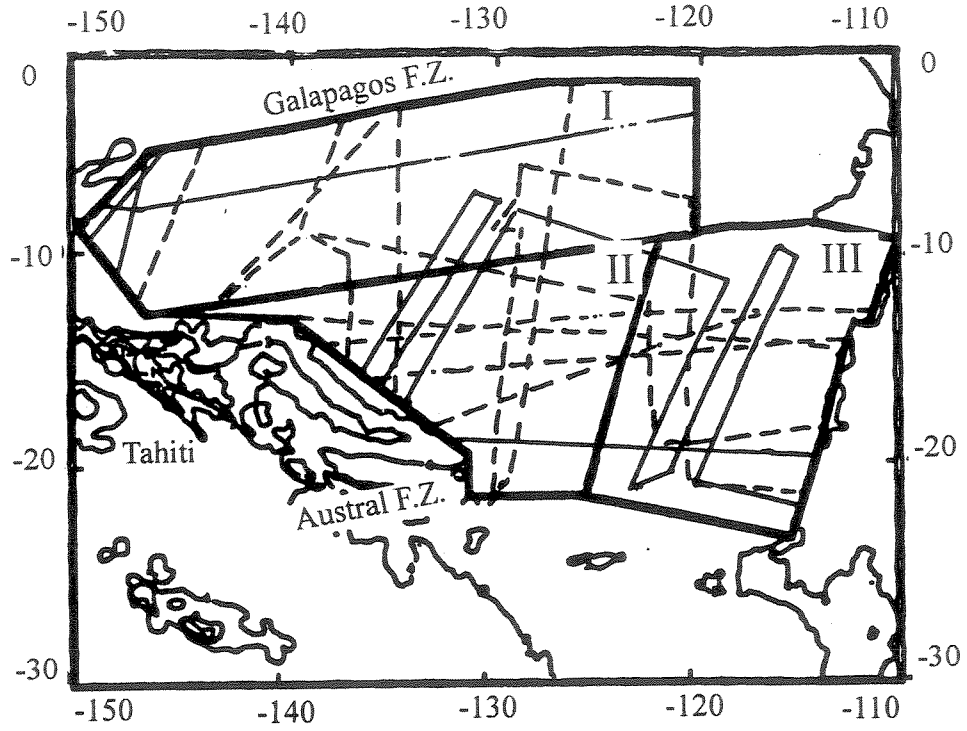


Figure II-9. The ship track lines are shown for the regions outlined in Figure II-8.

All volcanoes in this study have been under at least 2000 m of seawater since their formation. They can be presumed to have grown in a manner similar to shield volcanoes (i.e., piling of lava flows), although dome processes (viscous flow), hyaloclastite formation and pillow lava piles are also possible. Overall, the small submarine volcanoes of the South Pacific (h/r = 0.05 to 0.36) are steeper than subaerial shield volcanoes (h = 0.04 to 0.20) and have an very large range in flatness (t/r = 0 to 0.8). Both the height h and the top diameter 2t increase with increasing basal diameter (Table II-6; Appendix A). The height-to-radius ratio may increase with increasing height (R=0.39) (Figure II-10b). The flatness t/r is primarily dependent on the top diameter. Note that these volcanoes cover almost all of the possible morphologic space with the exception of the higher values of h/r ratios (Figure II-10a).

Visual observation suggested that the South Pacific volcanoes are not uniform in style - confirmed by the wide rage of the shape parameters. It was noted, in particular, that a significant number of the volcanoes had rounded (shield-shaped) tops, while others were more ideal flat-topped cones and still others were extremely pointy (t~0.0). So a visual search was attempted to identify those volcanoes that exemplify a particular shape as well as those that are more moderate. To this end, an attempt was made to assign each volcano to one of the categories in Table 6 based on three visually perceived aspects: (1) closeness of contour spacing (steepness), (2) width of flat-top, (3) presence of a rounded, rather than flat, top. The seven groups so defined do fall in different parts of the shape plots (Figure II-10; see Figure A-3 in Appendix A), but do not show the dramatic separation observed in Guatemalan volcanoes or even as strong a separation as seen in Iceland.

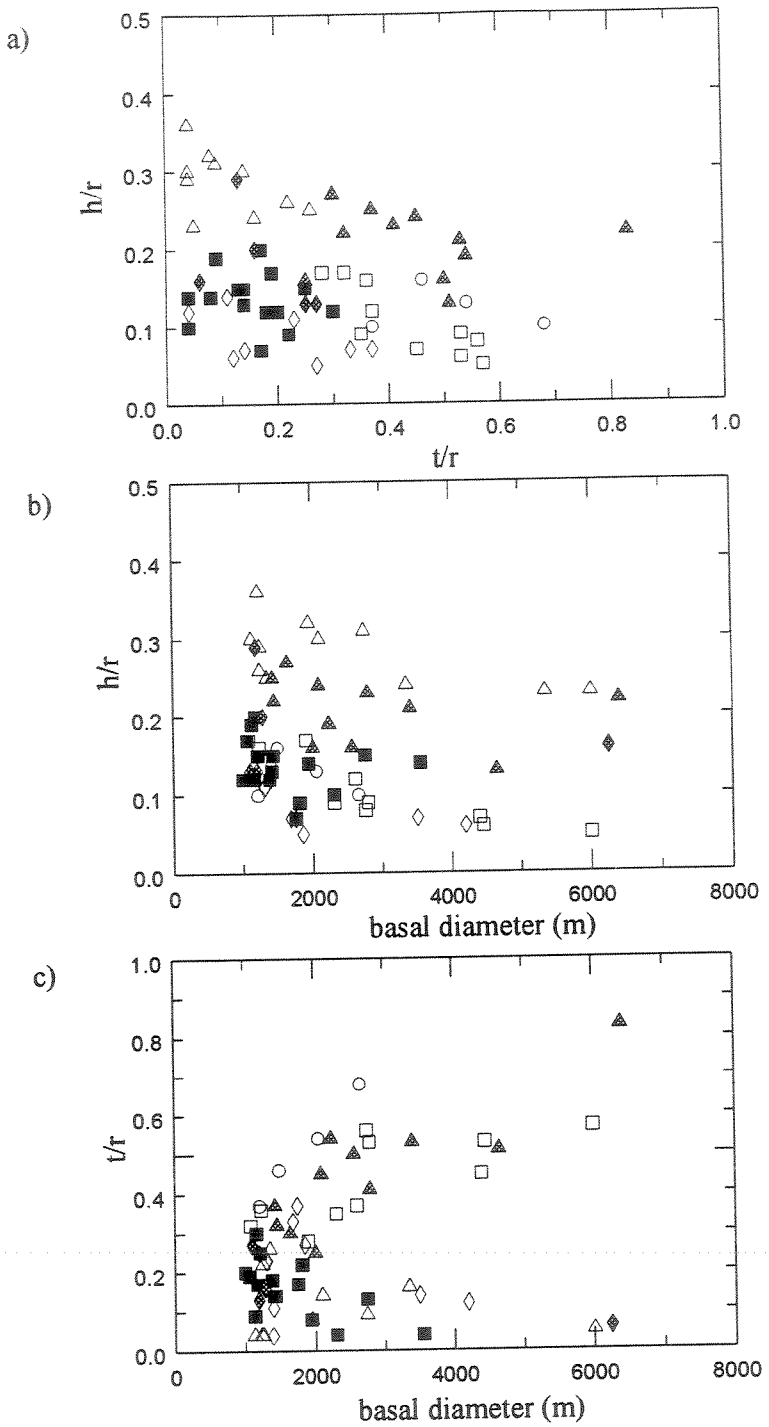


Figure II-10. The parameters describing volcano shape and size are plotted against each other for the South Pacific submarine volcanoes. Symbols indicate an attempt to define different styles (open triangles = steep, pointy; filled triangles = steep, flat-topped; open boxes = shallow, flat-topped; filled boxes = shallow, pointy; open diamonds = shallow, rounded; closed diamonds = moderate slope, rounded top; open circles = moderate slope, flat-top). (a) Submarine volcanoes fill most of the h/r vs. t/r plane. (b) Little variation in h/r is observed with size. (c) Little variation in t/r is observed with size.

Table II-6. Morphologic division South Pacific volcanoes.

			Average			RANGE				
Type	Description[1]	N	H/R	Slope	T/R	H (m)	2R (m)	H/R	Slope	T/R
1 △	steep, point	11	0.28±0.04	17°± 2°	0.07±0.10	160-680	1130-6000	0.23-0.36	13-20°	0.00-0.26
2 ▲	steep, flat[2]	11	0.21±0.04	22°±10°	0.46±0.16	160-690	1430-6400	0.13-0.27	12-51°	0.25-0.83
3 □	shallow, flat[2]	10	0.11±0.05	10°± 3°	0.43±0.11	90-160	1080-6000	0.05-0.17	6-14°	0.28-0.57
4 ■	shallow, point	15	0.14±0.04	8°± 2°	0.02±0.05	60-240	3200-4200	0.07-0.20	5-12°	0.00-0.17
5 ◇	shallow, round	9	0.09±0.03	5°± 2°	0.00±0.00	50-120	1300-4200	0.05-9.14	3- 8°	0.00-0.00
6 ◆	moderate, point	5	0.18±0.07	10°± 4°	0.01±0.03	70-490	1100-6250	0.13-0.29	7-16°	0.00-0.06
7 ○	moderate, flat[2]	4	0.12±0.03	15°± 4°	0.51±0.13	60-130	1210-2650	0.10-0.16	9-17°	0.37-0.68
All	All	289	0.18±0.07	13°± 6°	0.23±0.16	50-690	1080-6400	0.05-0.43	3°-51°	0.00-0.83

[1] First word describes slope; second describes shape and size of summit.

[2] Flat indicates a flat topped cone.

Table II-7. Correlations in morphologic parameters for the South Pacific volcanoes.

Volcano Type	Correlation between:	R	t	n	Confidence
Total Data Set	h & 2r	**0.73**	18.2	289	>99.8%
	h & 2t	0.43	7.9	281	>99.8%
	2t & 2r	**0.75**	19.2	281	>99.8%
	h/r & h	**0.39**	7.13	289	>99.8%
	h/r & 2r	-0.22	-3.83	289	>99.8%
	h/r & 2t	-0.25	-4.39	281	>99.8%
	t/r & h	0.09	1.45	276	80%
	t/r & 2r	0.34	5.9	273	>99.8%
	t/r & 2t	**0.74**	18.3	276	>99.8%
	h/r & t/r	-0.27	-4.72	276	>99.8%

Boldface regression coefficients are of particular interest and discussed in the text.

Volcanoes of the Snake River Plain

The Snake River Plain is a broad, flat lava plain that forms an arcuate trough across Idaho [Kuntz et al., 1990]. Pleistocene and Holocene basaltic lava flows (with minimal sediment cover) are exposed in the eastern Snake River Plain (Figure II-11), which is bounded on the north by folded Mesozoic through Precambrian rocks that were uplifted by Tertiary and Quaternary normal faults (Basin and Range) [Kuntz et al., 1990]. Large calderas are the remnants of Neogene rhyolitic volcanism [Kuntz et al., 1990]. The volcanism in this region has been generally attributed to hot spot volcanism (with the hot spot now in the Yellowstone vicinity) [Geist and Richards, 1993].

This study has focused on the volcanic population of an area in the eastern Snake River Plain. The study area is bounded by the latitudes 43°30' N and 44°07'30" N and the longitudes 113°W and 112°W (Figure II-11).

84 volcanoes were measured in the eastern Snake River Plain; of these 16 are cinder cones, 29 are pseudocones, 1 is a maar, 20 are shield volcanoes, and 2 are table mountain-like buttes. The other 16 volcanoes could not be classified according to volcanic type. No composite volcanoes exist within the study region. Overall, the volcanoes of the study area are much smaller (especially much shorter; the tallest shield volcano is only 141 m tall) and have extremely gentle slopes (the steepest volcanoes have slopes of 10-20°) compared to the other regions discussed in this study (Figure II-12). This observation is consistent with the observations of Greeley [1982] on "Plain"-style volcanism. Separation of volcanic types (shield volcanoes and explosive volcanoes) is seen best on a t/r vs. 2r plot (Figure II-12c). Shield volcanoes have wider bases and lower average t/r (0.08±0.05) compared to the explosive volcanoes (t/r=0.20±0.25). All volcanoes in this area of the Snake River Plain (SRP) have very low heights (h<=141) and h/r ratios (h/r <= 0.38); shield volcanoes have slightly lower h/r ratios (h/r=0.03±0.01) than the explosive volcanoes (h/r=0.07±0.06). Individual types of explosive volcanoes were not separable on any morphologic parameter space.

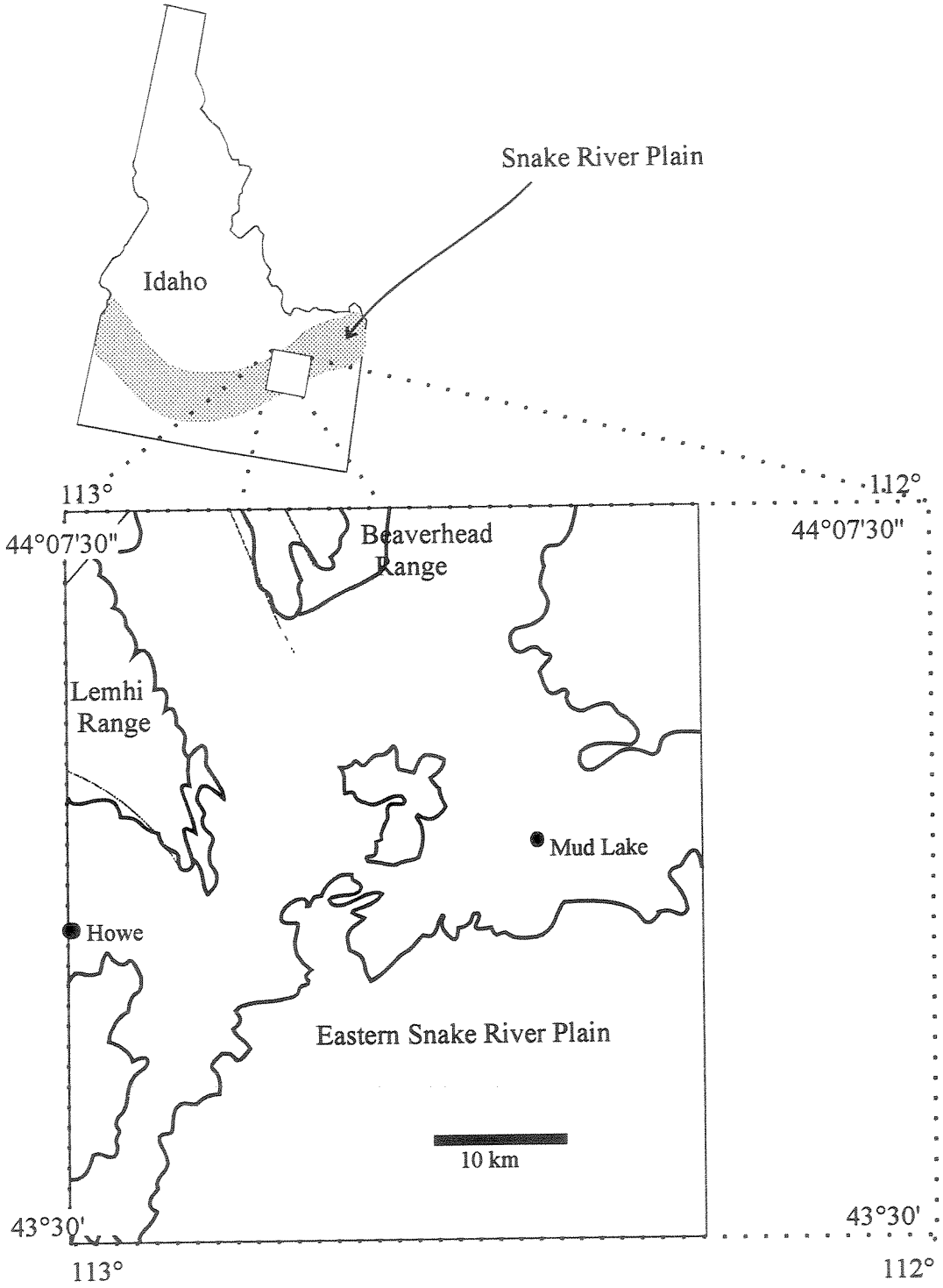


Figure II-11. Location map of the eastern Snake River Plain.

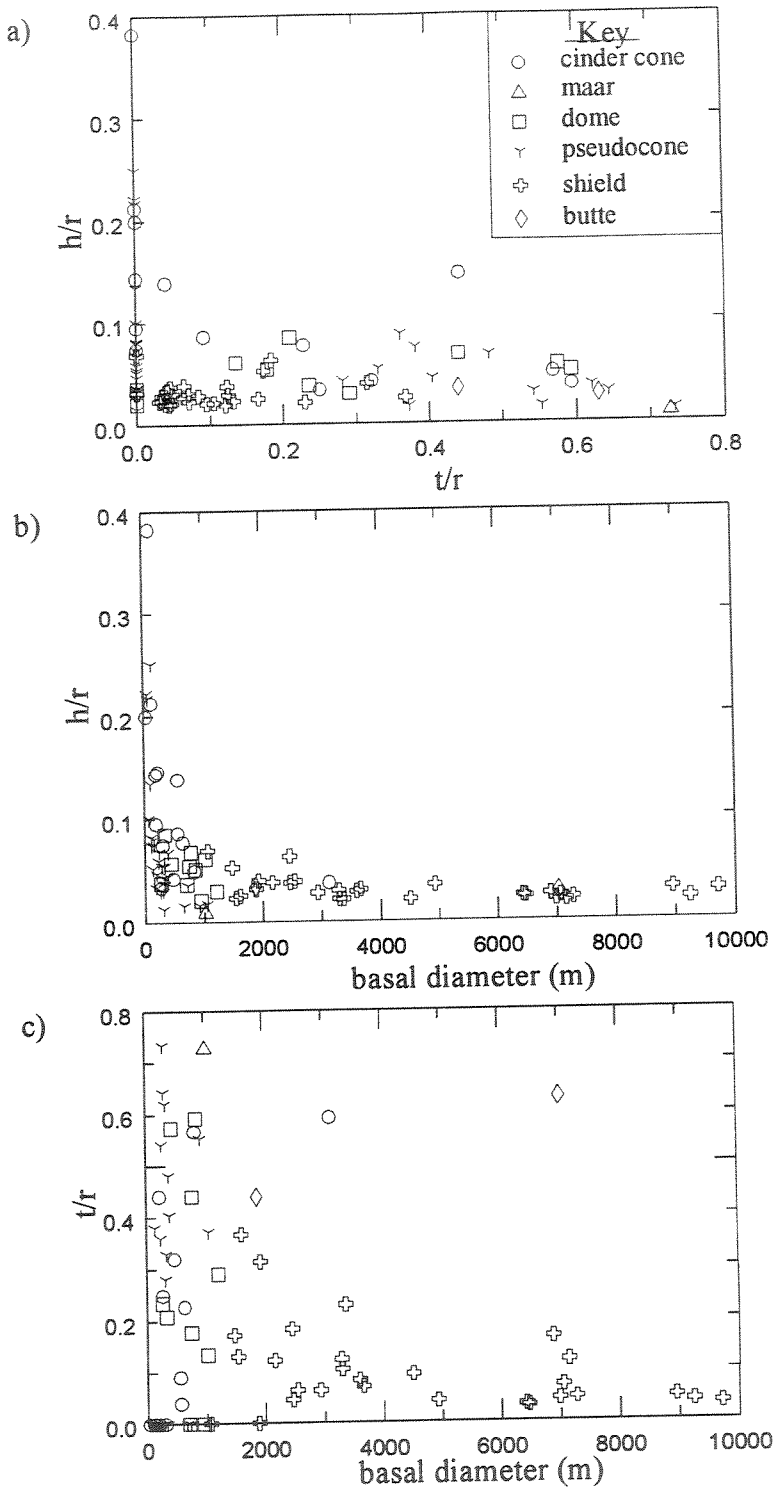


Figure II-12. The parameters describing volcano shape and size are plotted against each other for the Snake River Plains volcanoes. Symbols indicate volcanic type (see inset). (a) The h/r ratio vs. the t/r ratio show the different shapes of shield volcanoes and explosive volcanoes. (b) Shield volcanoes have much larger basal diameters but only slightly lower h/r ratios. (c) Explosive volcanoes (cinder cones, maars, and psuedocones) have a large range in t/r ratios.

The explosive volcanoes of the SRP were initially identified as cinder cones, pseudocones, and maars based on geomorphic features (e.g., size and depth of crater, proximity to river or lava flow). However, there is no statistical difference between the shape parameters of these groups. The explosive volcanoes show a wide range of t/r ratios (0.00-0.75), but generally low h/r ratios (0.01-0.38) and slopes (1°-21°) compared to the cinder cones and maars of Guatemala (h/r=0.08-0.67; slope=10°-45°). The Guatemalan cinder cones and maars (h=41-295 m) are also much taller than the Snake River Plain explosive volcanoes (h=3-59 m). (Side note: the contour interval on topographic maps is 5-10 m for the SRP and 20 m for Guatemala; so shorter volcanoes are sampled in the SRP, but this does not effect the expected incidence of taller volcanoes.) This is consistent with the prediction of the McGetchin model that smaller cinder cones will have shallower flanks. Correlation trends for the SRP explosive volcanoes indicate that h, 2r and 2t increase together (Table II-9). The h/r ratio may decrease with increasing basal diameter 2r (R=-0.34) (Figure II-12b) and the t/r ratio may increase with increasing 2r (R=0.32) (Figure II-12c); both are consistent trends with those observed for maars in Guatemala. The explosive volcanoes of the SRP probably vary from small cinder cones (with slightly higher h/r and lower t/r) to pseudocones and maars (with slightly lower h/r and higher t/r), formed by the interaction of lava flows and rising magma with the wetlands of the SRP.

The shield volcanoes of the eastern SRP have more gentle slopes (1.6°±0.7°) than even the shield volcanoes of Iceland (slope = 6 ±5). The summit region is similarly sized to that in other regions (relative to basal diameter) (t/r=0.08±0.05). The height-to-radius ratio h/r may decrease with basal diameter (R=-0.51) suggesting that the shields become more and more like lava flows as they increase in size. The top diameter 2t (generally a crater diameter) is independent of size (Table II-9), which was also observed in both Guatemala and Iceland. The SRP shield volcanoes are somewhat similar to Icelandic shield volcanoes but show a tendency to increase their basal diameters preferentially.

Table II-8. Summary of morphologic parameters for Snake River Plain volcanoes.

		Average			Range				
Type	N	H/R	Slope	T/R	H (m)	2R (m)	H/R	Slope	T/R
Cinder Cone	16	0.11±0.09	6.6°±4.8°	0.21±0.23	3-59	30-3120	0.03-0.38	2°-21°	0.00-0.59
Pseudocones	29	0.07±0.06	4.6°±3.3°	0.20±0.25	2-16	55-1052	0.01-0.25	1°-14°	0.00-0.75
Maar	1	-	-	-	5	1013	.01	1	0.73
All explosive	49	0.08±0.08	5.3°±4.0°	0.21±0.25	2-59	30-3120	0.01-0.38	1°-21°	0.00-0.73
Shield	20	0.03±0.01	1.6°±0.7°	0.08±0.05	36-141	1059-9710	0.02-0.07	1°-4°	0.00-0.23
Butte	2	-	-	-	32-97	1868-7014	0.02-0.03	2°-3°	0.44-0.63
Dome	8	0.05±0.02	3.6°±1.8°	0.23±0.21	10-31	335-1208	0.02-0.09	1°-6°	0.00-0.59

Table II-9. Correlations between morphologic parameters for the Snake River Plain volcanoes by type.

Volcano Type	Correlation between:	R	t	n	Confidence
Cinder Cones	h & 2r	0.72	6.70	44	>99.8%
Pseudocones	h & 2t	0.61	5.08	44	>99.8%
Maar	2t & 2r	0.93	17.5	44	>99.8%
	h/r & h	0.17	1.12	44	n.c.
	h/r & 2r	**-0.34**	-2.38	44	95%
	h/r & 2t	-0.29	-1.98	44	90%
	t/r & h	0.11	0.76	44	n.c.
	t/r & 2r	**0.45**	3.27	44	99%
	t/r & 2t	0.61	4.93	44	>99.8%
	h/r & t/r	-0.46	-3.31	44	>99.8%
Shield Volcano	h & 2r	0.89	8.17	20	>99.8%
	h & 2t	0.14	0.59	20	n.c.
	2t & 2r	0.31	1.38	20	80%
	h/r & h	-0.18	-0.79	20	n.c.
	h/r & 2r	**-0.51**	-2.53	20	95%
	h/r & 2t	-0.47	-2.27	20	95%
	t/r & h	-0.33	-1.50	20	80%
	t/r & 2r	-0.20	-0.87	20	n.c.
	t/r & 2t	0.79	5.37	20	>99.8%
	h/r & t/r	-0.39	-1.78	20	90%

n.c. = no confidence.

Boldface regression coefficients are of particular interest and discussed in the text.

DISCUSSION

Summary of observations

The method and extent of separation between volcanic types varies from region to region. In Guatemala, h/r vs. t/r and t/r vs. h separate the total volcanic population into 4 groups: (cinder cones, domes), (maars), (shield), and (composite). Cinder cones and domes do not separate. Cinder cones and domes are separated from maars by t/r ratios. Shield and composite volcanoes are separated in size and h/r ratio. In Iceland, shield volcanoes and table mountains are separated by h/r and t/r ratios; they do not differ in size. In the SRP, explosive volcanoes and shield volcanoes are separated by t/r vs. 2r plots. The different types of explosive volcanoes (cinder cones, pseudocones, and maars) are not separable. There is no single plot or variable which separates volcanic types in all regions. The submarine volcanoes of the South Pacific show no separation based on the roundness of the summit; they cover the full morphospace of the shape parameters.

Growth trends for individual volcanic types also vary between the regions, particularly for shield volcanoes. Shield volcanoes increase in height faster than basal diameter in Guatemala, increase consistently in height and basal diameter in Iceland and increase in basal diameter faster than in height in the SRP; these three sets of shields appear to represent a spectrum of processes of shield growth. The submarine volcanoes of the South Pacific cover the full range in size (up to the limit imposed by the width of the SeaBeam swaths) and shape that is covered by the shield volcanoes, domes and table mountains of the other three regions. The growth trends for maars, cinder cones and other related features are fairly consistent between the regions, but the exact range of morphologies and styles present in each region varies.

Comparison to previous studies

The results of the above morphologic analyses of the volcanic populations of Guatemala, Iceland, the South Pacific and the Snake River Plain are generally consistent

with the results of previous studies. Wood's [1979] study of monogenetic volcanoes found that explosive volcanoes (pyroclastic cones) are generally smaller, steeper and more flat-topped than effusive volcanoes (monogenetic shields) - I have also observed this in both Guatemala and the Snake River Plain. McGetchin et al. [1974] predicted the shapes of cinder cones from the ballistic trajectories of ejecta. The cinder cones of Guatemala fit this model (see Chapter IV for a detailed discussion); extensions of it to phreatic and phreatomagmatic volcanism (which from the perspective of the model differs mainly in velocities and angles of ejection) are consistent with the shapes of maars in Guatemala and explosive volcanoes in the SRP. Greeley's [1982] description of SRP shield volcanoes as "plains" volcanism is consistent with the results of this study.

The composite volcanoes included in this study present a very different picture of composite volcano growth trends than observed by Wood [1979]. Wood [1978] observed that the slope of composite volcanoes decreased with size and that the crater diameter increased consistently with both height and basal diameter. This study does not observe a significant change in h/r, slope, or top diameter with size. A slight decrease in slope occurs at the very largest basal diameters but it is not a consistent decrease (slope is constant for small basal diameters).

Separating volcanic types

As stated in the introduction, Pike and Clow [1981a] used top circularity and volume to separate volcanic classes. Circularity (for both base and top) is calculated in this study as the ratio of the smallest radial distance to the largest radial distance. There is little difference in the ranges of circularity between the volcanic types in this study (Table II-10). Base circularity does vary significantly between types, but the overlap in range means it is a poor predictive tool. Volume does separate some of the volcanic types (Table II-10 shows that composite volcanoes are bigger than shield volcanoes and table mountains which are in turn bigger than domes, cinder cones, and maars), but, again, there

is considerable overlap in ranges. Pike and Clow [1981b] also looked at principal component analysis of morphologic parameters in an attempt to further differentiate between volcanic types. Principal component analysis on the Guatemalan volcanic population using covariance coefficients simply returns the three measured parameters (2r, 2t, h) as accounting for most of the variance. If correlation coefficients are used (in order to remove effect of differences in the absolute magnitude of parameters), the results are difficult to interpret and the three components accounting for most of the variance (66%) separate the volcanic types no better than (and about the same as) the shape and size parameters used above (h/r, t/r and h or 2r).

Table II-10. Observations of circularity and volume.

Volcanic	Base Circularity		Top Circularity		Volume (km^3)	
Type	Average	Range	Average	Range	Average	Range
Composite (G)	0.38±0.23	0.00-0.76	0.45±0.28	0.00-0.87	68±70	2-257
Shield (G)	0.39±0.16	0.17-0.75	0.29±0.31	0.00-0.88	1.11±0.96	0.10-3.50
Shield (I)	0.48±0.12	0.29-0.75	0.32±0.27	0.00-0.91	6.3±9.7	0.01-39.2
Shield (S)	0.27±0.13	0.05-0.51	0.39±0.21	0.00-0.72	0.90±1.01	0.01-3.60
Table (I)	0.46±0.13	0.17-0.81	0.23±0.20	0.00-0.74	4.6±14.7	0.02-76.7
Dome (G)	0.51±0.20	0.12-0.83	0.44±0.22	0.00-0.86	0.46±0.82	0.00-2.72
Cinder (G)	0.58±0.15	0.00-0.92	0.41±0.29	0.00-1.00	0.03±0.03	0.0-0.117
Maar (G)	0.70±0.09	0.53-0.86	0.63±0.10	0.38-0.75	.05±0.08	0.0-0.336
Explosive (S)	0.52±0.14	0.24-0.82	0.20±0.23	0.00-0.80	0.007±0.04	0.0-0.290

G = Guatemala; I = Iceland; S = Snake River Plain. Circularity = smallest radius/largest radius.

Wood's [1979] study of monogenetic volcanoes separated explosive (pseudocones, spatter cones, cinder cones, maars) and effusive (steep shields, low shields, Icelandic

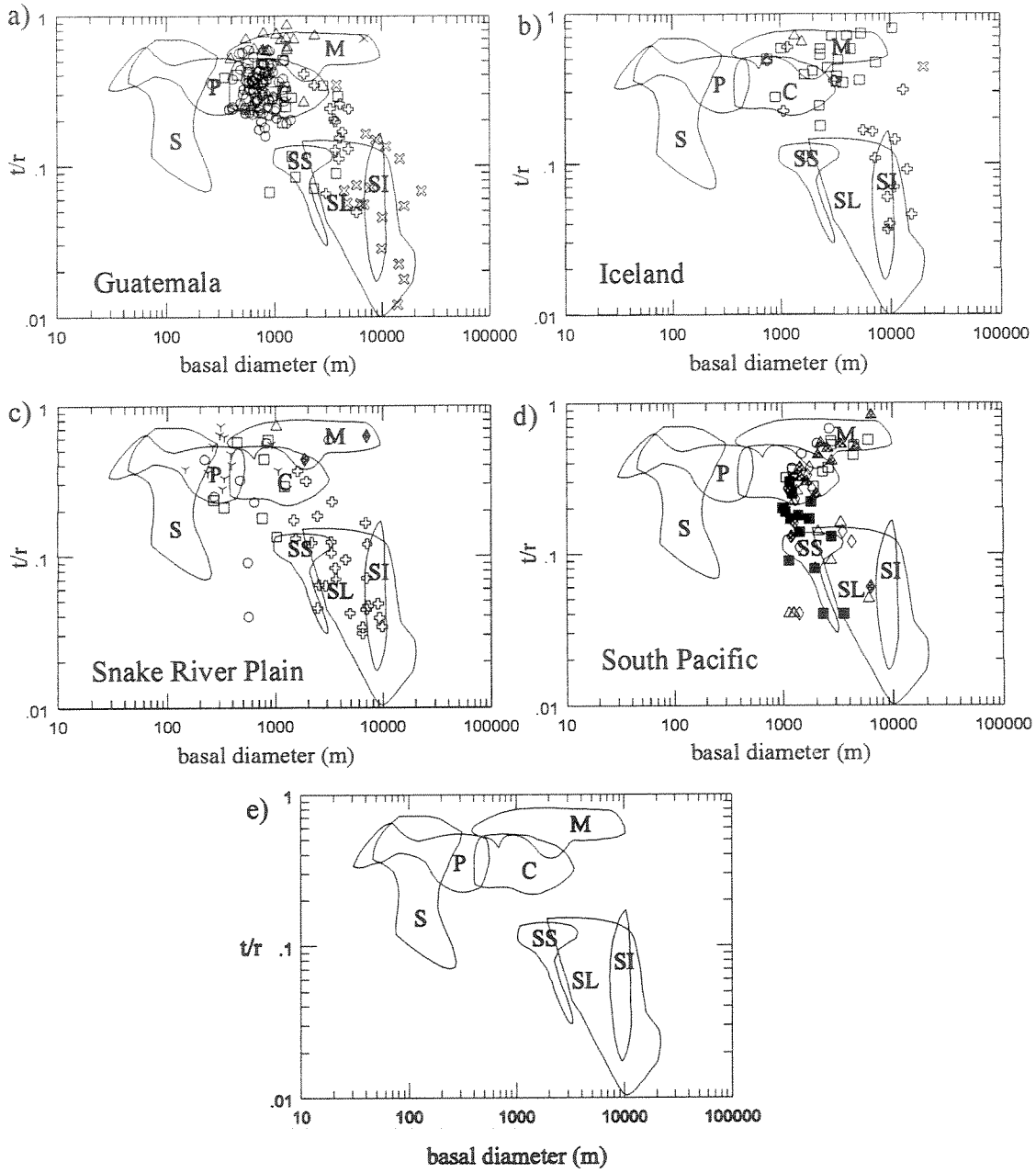


Figure II-12. Comparison of the volcanoes in this study with the results of Wood [1979] for monogenetic volcanoes. (a) Guatemala, (b) Iceland, (c) Snake River Plain and (d) South Pacific. (e) Wood's [1979] determination of terrestrial monogenetic volcano groups. P=psuedocones, S=spatter cones, C= cinder cones, M=maars, SS = steep shield volcanoes, SL = low shields, SI = Icelandic shields. The solid lines indicate the boundaries of Wood's groups in a-d. Other symbols are as in previous figures.

shields) volcanoes on a log-log plot of t/r vs. 2r. The separation achieved is similar to that on a non-log plot (compare Figure II-13 and Figure II-16). However, this study does not observe a good fit to Wood's classes or even a consistent location of volcanic types that would make a consistent definition of global classes possible (Figure II-13). The cinder cones, maars and pseudocones of this study fall in the same general location as Wood's, but exhibit a higher range in t/r ratio. The shields of this study exhibit consistently higher t/r ratios. Domes, table mountains, buttes and submarine volcanoes overlap both the pyroclastic fields and the shield fields; composite volcanoes overlap the shield fields. Many of the larger volcanoes in this study (Guatemalan shield and composite volcanoes; Icelandic table mountains) are probably polygenetic rather than monogenetic - this may explain the greater range in shapes.

A comparison of the volcanoes of this study to Whitford-Stark's [1975] classes of shield volcanoes based on type localities (Figure II-14) demonstrates that these classes indicate nothing but size. The Icelandic volcanoes of this study overlap the Icelandic class but extend into smaller and larger sizes. Guatemalan shields are generally the same size as Icelandic shields (in spite of being steeper). The Snake River Plain shields are of Scutulum size. The submarine volcanoes of the South Pacific show a greater range in size (the upper limit of which is a function of the sampling process not a limit in growth).

For all volcanoes, h increases with r. Over the full range of volcano sizes, the relative rate of increase appears to be the same regardless of type or location (Figure II-14) (except in the Snake River Plain, which has a lower overall trend). However, plots of h/r against h or r and a more detailed analysis of h vs. r plots shows that the relative rate of increase varies extensively between volcanic types. Thus, plots of h against r covering a large range of sizes are not useful in distinguishing volcanic types. They may be useful in distinguishing regional trends in style. The Snake River Plain volcanoes, considered to be of a style intermediate between plateau volcanism (e.g. Columbia River basalt) and shield

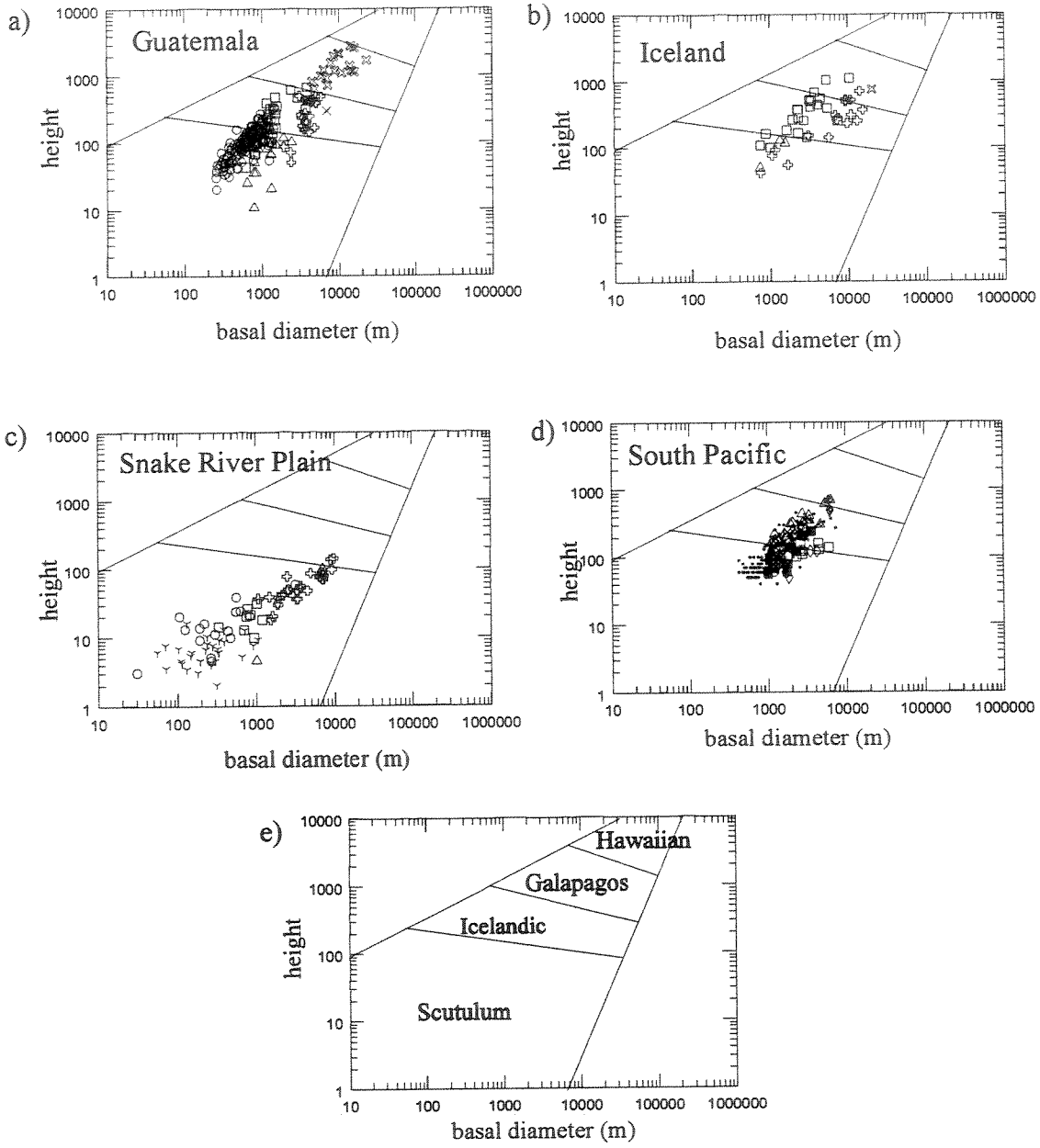


Figure II-14. Comparison of shield volcano classes (based on Pike and Clow [1981]) with size scale from Whitford-Stark [1975] and with the volcanic populations of this study. (a) Guatemala, (b) Iceland, (c) Snake River Plains and (d) South Pacific. (e) Shield volcano classes. Symbols are as in previous figures.

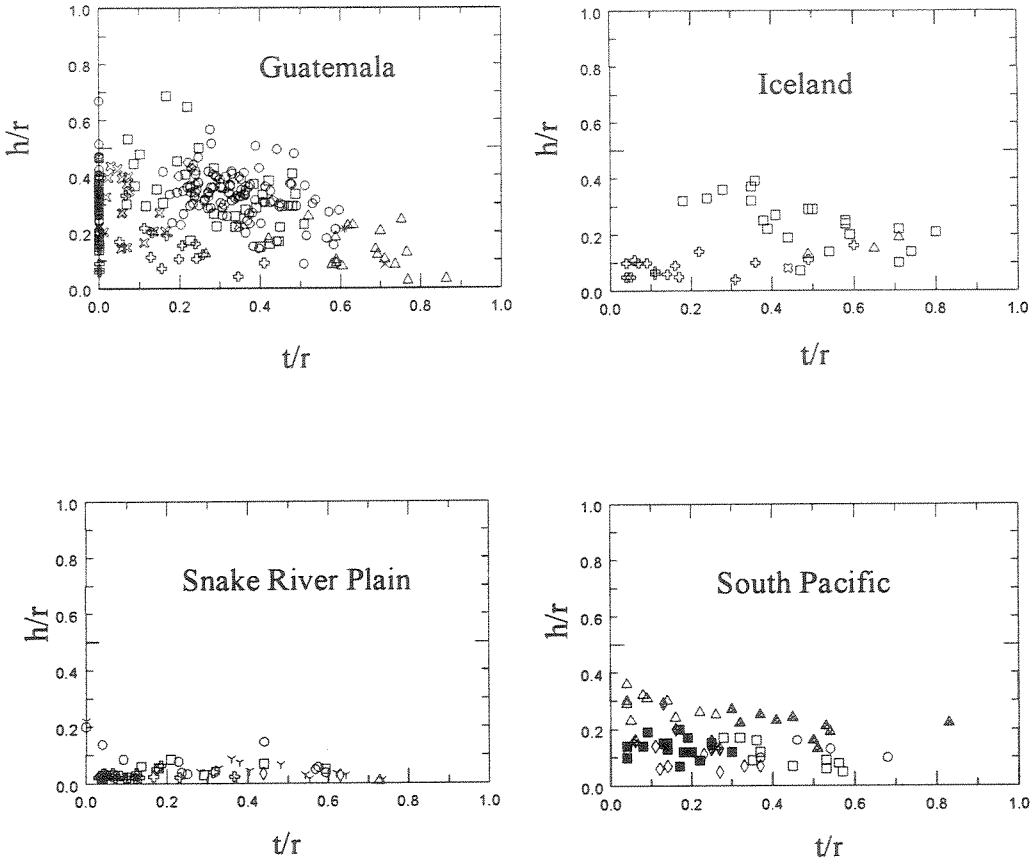


Figure II-15. Comparison of the difference in h/r and t/r ratios for volcanic types in each region. Symbols are as in previous figures.

volcanism [Greeley, 1982], form a different trend in Figure II-14 compared to the other regions.

This study considered three additional ways of separating volcanic types. Figure II-15 shows a plot of h/r vs. t/r: the different average h/r and t/r ratios of the volcanic types indicated an expected separation. The volcanic types are separated in each region (except cinder cones and domes); however, there is significant overlap and no consistent boundaries for a given type for all regions. Figure II-16 shows a plot of t/r vs. 2r. This gives a cleaner separation of shields and composite volcanoes from cinder cones and domes; maars separate from cinder cones and domes slightly less cleanly than on the h/r vs. t/r plot.

Recognizing that the volcanic types differ as much in size as in shape, the three dimensional morphologic space was sectioned into three intervals of basal diameter (0-2000 m, 2000-5000 m, >5000 m) and projected onto the h/r-t/r plane (Figure II-17). In Guatemala, this separates the volcano population into three groups with limited overlap: (1) domes, cinder cones and maars (and one shield); (2) shield volcanoes (and five domes, three composite volcanoes, and one maar); and (3) composite volcanoes (and one shield volcano). Unfortunately, table mountains and the shield volcanoes of Iceland and the Snake River Plain fall equally in all three size categories. The explosive volcanoes of the Snake River Plain (except one) fall in the smallest size category. This technique does not provide a universal separation either - although it may have useful regional application. The South Pacific volcanoes were not included in this analysis, because the data collection technique limited the maximum size resolvable.

Another way of looking at size and shape variations together is to project the shapes on to a single line and plot against size. The h/r and t/r ratios are recast as $h/(h + t)$ and plotted against basal diameter (Figure II-18). The shield and composite volcanoes of Guatemala are clearly separated from the cinder cones and maars of Guatemala, mostly because of the great difference in size. Domes fall in both groups. The volcanic types of

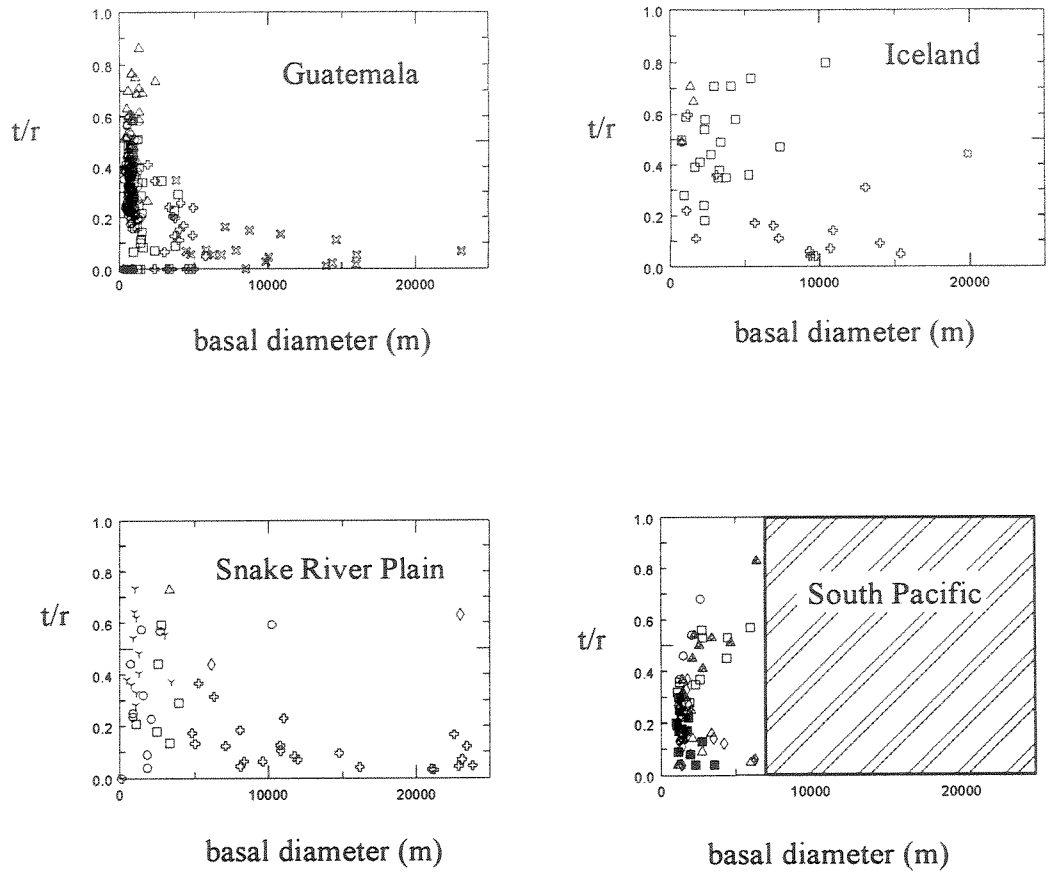


Figure II-16. Comparison of the separation produced by a t/r vs. 2r plot for each region. Note that not all volcanic types are separated using the same scales for all regions. Shaded for South Pacific plot indicates size ranges not imaged by the SeaBeam swaths.

A)

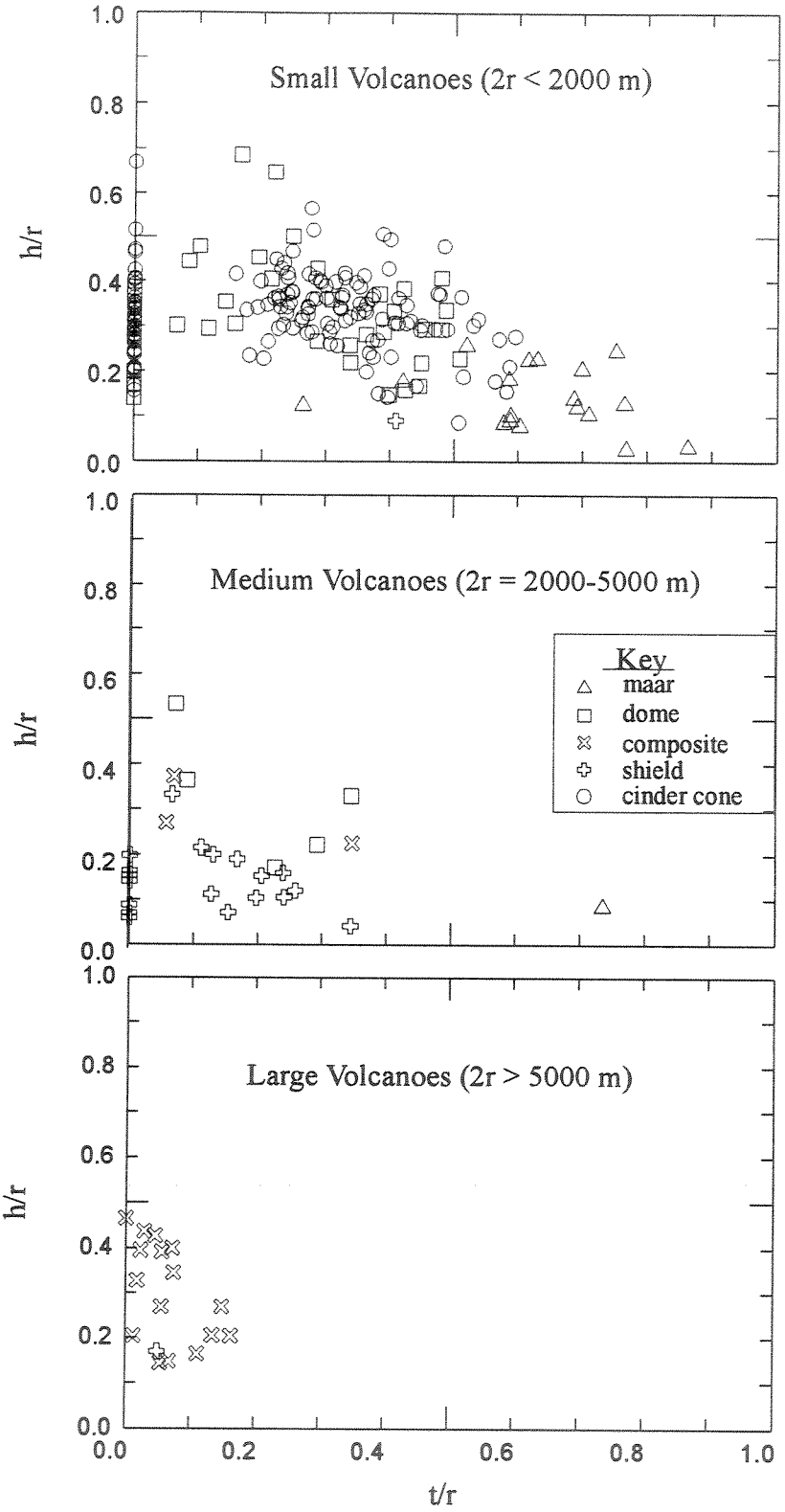


Figure II-17. Relationships between shape and size of volcanic types. (A) Guatemala.

B)

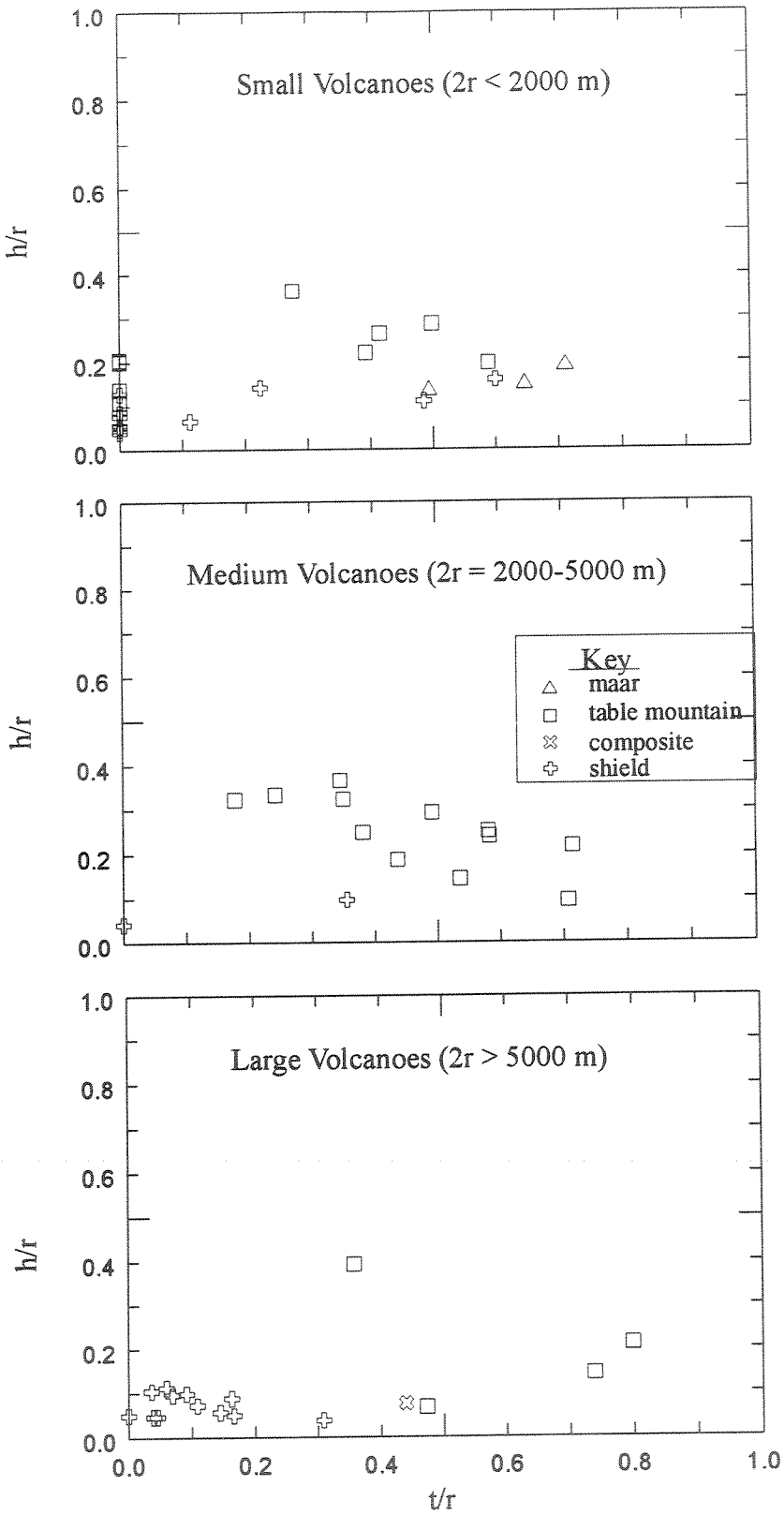


Figure II-17. Relationships between shape and size of volcanic types. (B) Iceland.

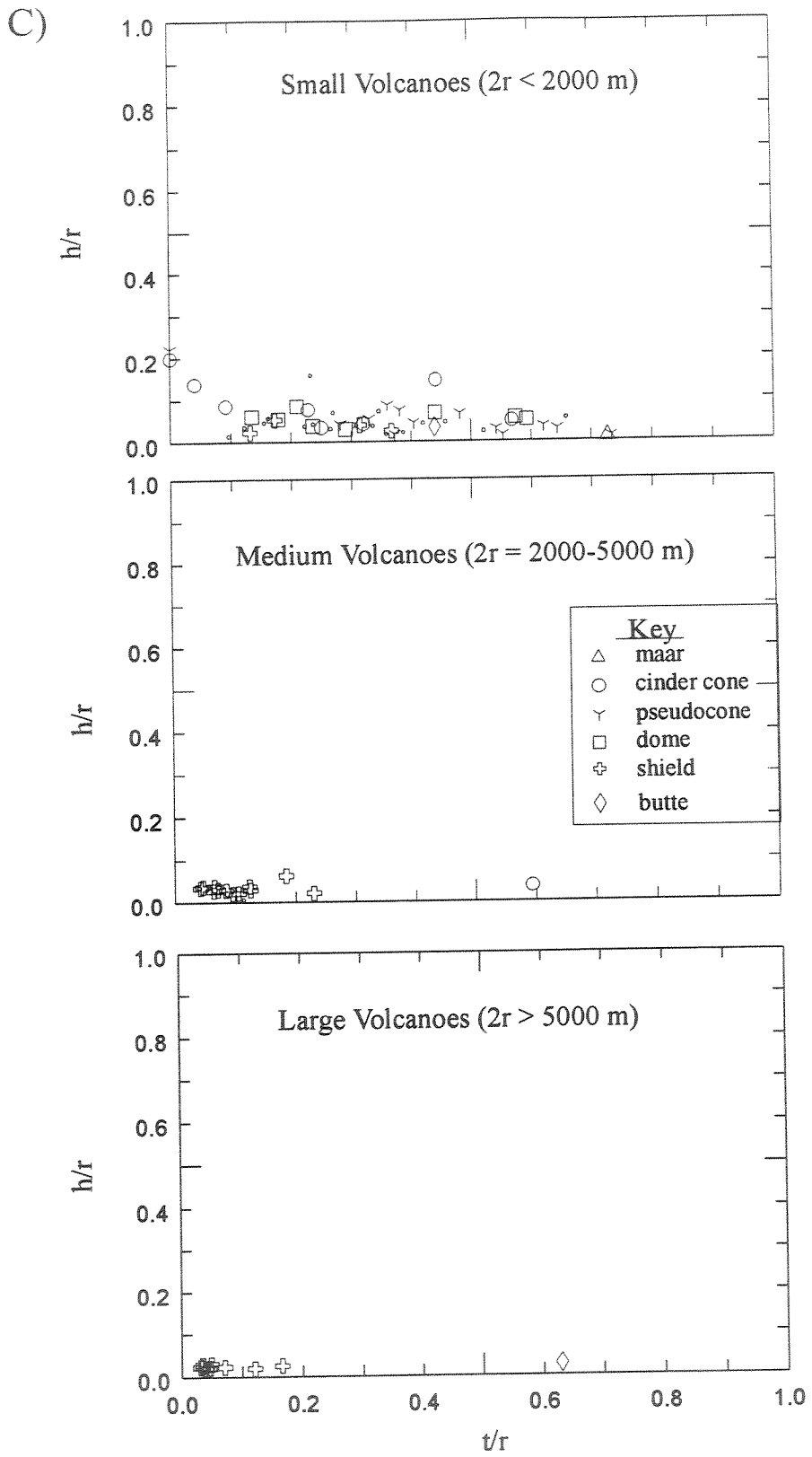


Figure II-17. Relationships between shape and size of volcanic types. (C) Snake River Plain.

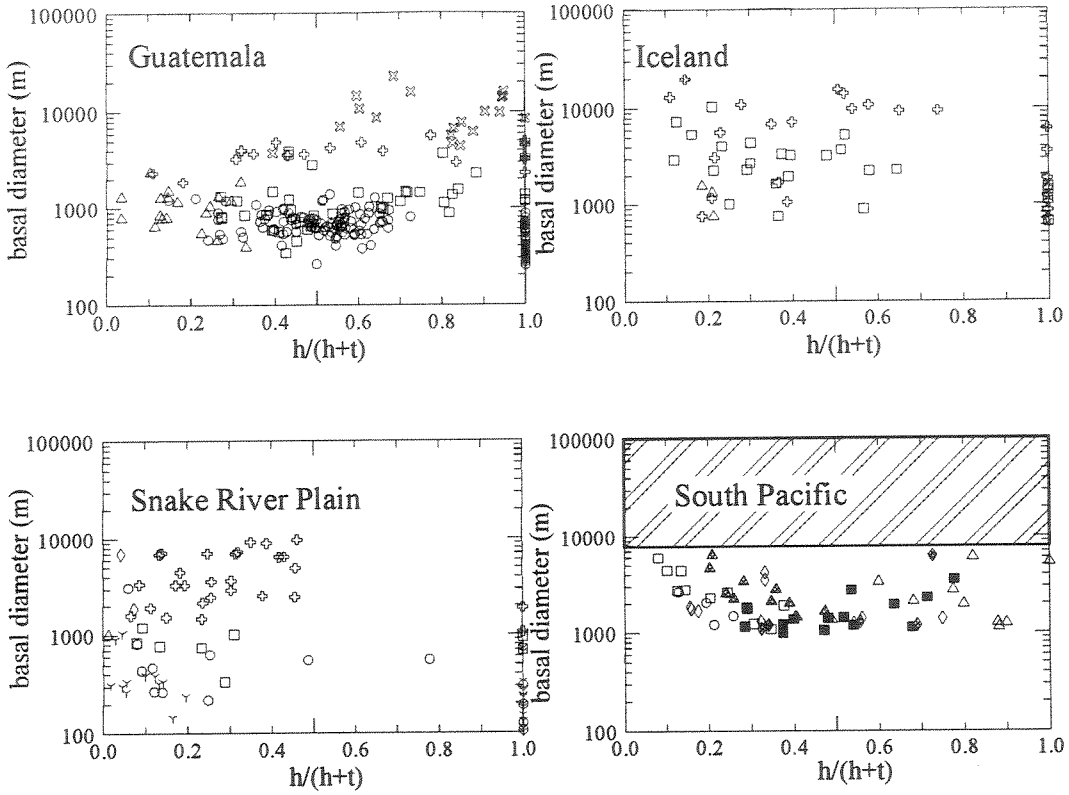


Figure 11-18. Relationships between shape and size of volcanic types. Horizontal axis is a measure of shape, ranging from flat-topped cones (h/(h+t)=0) to pointy, or rounded, cones (h/(h+t)=1). Vertical axis is a measure of size (basal diameter is highly correlated with volume). Excellent separation is achieved for Guatemalan volcanoes; little separation occurs in the other regions.

other regions are poorly, if at all, separated. This view of morphology emphasizes the importance of size. Separation is improved for Guatemalan volcanoes, but is worse for the other regions.

Table II-11. Size distribution of volcanoes by type and region.

Size	Guatemala					Iceland		SRP	
>2r (m)	Composite	Shield	Dome	Cinder	Maar	Shield	Table	Shield	Explosive
500	0	0	2	29	2	0	0	0	34
1000	0	0	16	87	7	4	4	0	7
1500	0	0	16	9	7	5	4	2	2
2000	0	1	2	0	2	2	3	4	0
3000	0	2	2	0	1	0	6	5	0
4000	1	9	3	0	0	2	4	5	1
5000	2	8	0	0	0	0	2	2	0
6000	1	1	0	0	0	1	2	0	0
7000	2	0	0	0	0	2	0	4	0
8000	2	0	0	0	0	1	1	3	0
9000	2	0	0	0	0	0	0	1	0
10000	1	0	0	0	0	3	0	2	0
>10000	7	0	0	0	0	5	1	0	0

None of the separation methods above work well for all regions: each volcanic type varies from region to region in the exact expression of its morphology and some volcanic types have inherently similar morphologies as described by the right-circular cone model (e.g. cinder cones and small domes; large domes and table mountains). Any interpretation of eruption style from morphology must be made with great caution and

based on local information. Note, also, that the use of the right-circular cone model limited the range of shapes describable. The next section discusses the limitations of the right-circular cone model and some possibilities for moving beyond them.

Limitations of the right-circular cone model

As mentioned in the measurement methods section, the right-circular cone model of volcano shape is constrained by only three measurements. The resulting data set has only three degrees of freedom - one of which must be size; the other two relate to shape. Now, this actually captures the complete range of possible shapes for a right circular cone. While two cones of differing shape might have the same h/r ratio, they will have different t/r ratios (or vice versa). Slope can be used instead of the h/r ratio. Figure II-19 shows the plane of right circular cone shapes. Since all right circular cone shapes are captured and differentiated by the h/r and t/r ratios, I would expect volcanic types to be separated on a h/r vs. t/r plot. Why doesn't this occur? There are three answers.

First, the volcanic types are not uniquely different in shape. There is inherent overlap in the range of volcanic shapes for different volcanic types. The volcanic types were differentiated on the basis of features identified on aerial photographs and topographic maps - much of this information does not pertain to overall shape. For example, cinder cones and domes were differentiated by the presence (or absence) of a crater, the smoothness (or roughness) of the flanks, the development (or lack) of gully structure, and the absence (or presence) of viscous flow features. The gross shape of cinder cones and domes is very similar; even a comparison of profiles would probably not produce a consistent separation. Growth trends do differ between cinder cones and domes, but growth trends can only be discerned after volcanic type is identified.

Second, The right circular cone model does not capture all of the variation in the shape of volcanoes. Most volcanoes deviate from a perfect right circular cone. The

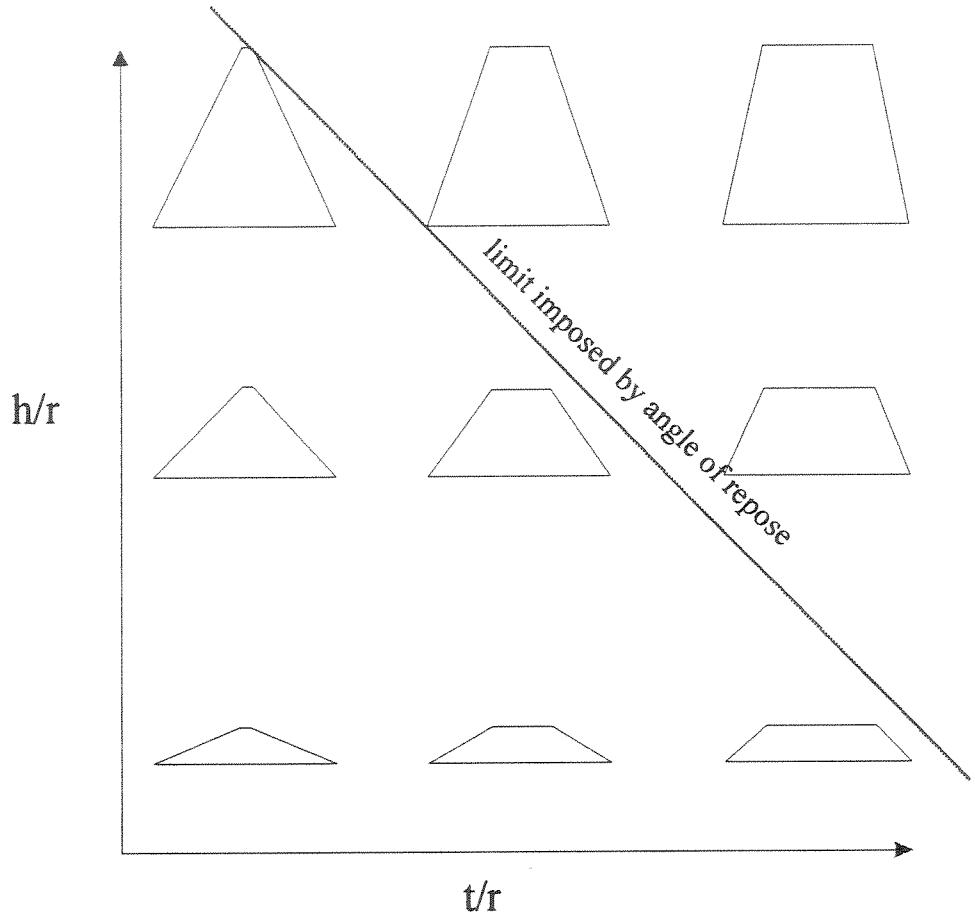


Figure II-19. Diagram shows how volcano profiles vary with the shape parameters h/r and t/r. All possible shape variations of the right circular cone are captured in this plane. However, not all possibilities are geologically reasonable - flank slopes greater than 45° are unstable. Shapes above the diagonal line will not occur in nature; the shapes below do occur in nature (but not necessarily all at all locations or in all types).

circularity (of base and top) varies greatly for all types of volcanoes (see Table II-10) from a minimum of 0 to a maximum of 1. Most types of volcanoes have a crater of discernible diameter and size. Some types of volcanoes have curved flanks. These properties can potentially be used to separate the shapes of volcanic types. Measurements of potential use include crater diameter, crater depth, minimum slope and maximum slope. The profile of a volcano can also be digitized, which preserves more information but is harder to compare quantitatively (see Chapter V for a discussion of profiles of shield and composite volcanoes).

Third, the measurements (basal diameter, height and top diameter) are defined by abstract concepts and are not directly related to process. For example, flatness t/r is highly variable in all types of volcanoes and volcanic regions. Part of the variation is related to the definition of top diameter not necessarily corresponding to the crater diameter or vent size. Cinder cones usually have well-defined tops corresponding to the central crater, but measurement errors can be significant at the smallest sizes. Shields generally exhibit a concave shape - that is, a gradual decrease in slope towards the summit rather than a coherent break in slope. In some cases, the identifiable break in slope may yield a much larger diameter than the central crater; in other cases, there may not be an identifiable break in slope even though the shape could never be described as pointy. Composite volcanoes often have multiple craters, which increases the measured top diameter. Table mountains and domes have flat-tops related to growth (non-explosive) processes. Thus, the measurement 2t and the t/r ratio do not relate to a single volcanic process. This is probably true for the other measurements and shape parameters discussed in this study.

RESULTS OF CHAPTER II

This study has characterized the morphologic variations of four geographically distinct volcanic populations. The morphology of each volcano was described using a

right-circular cone model. Classification of each volcano by volcanic type was based on geomorphic properties (other than cone shape) observed on topographic maps and aerial photographs. Detailed analysis of the morphometry of each volcanic population has shown that there is no universal method for separating volcanic types. The best separation method varies by region. Volcanic types also vary morphologically between regions. In general, for a given volcanic type, the differences between regions exceed the variation within regions. Volcanic morphology is consistent enough between regions to impose a single classification scheme (based on eruption style), but not consistent enough to predict eruption style (or volcanic type) from morphology.

Attempts to find a description of volcanic shape that will allow prediction of eruption style from volcanic shape fail because (1) different eruption processes do not produce distinctly different shapes, (2) systematic deviations from a right-circular cone are associated with some volcanic types, and (3) subtle variations in eruption style (in different regions) can produce distinctly different volcanic shapes and growth trends. The last implies that there may be other factors besides eruptive style that effect morphometry. Modification of the methodology of quantifying volcano morphology can account for many of the common deviations from a right-circular cone. However, the lack of uniqueness of the morphological results of eruptive processes places restrictions the use of morphology as a predictive tool: eruption processes may be suggested by morphologic data, but can be confirmed only by field evidence of the petrology and structure of a deposit, observation of the actual eruption, or remote sensing data indicating definitive petrologic, structural, or geomorphic characteristics. Eruption style is best predicted on the basis of geomorphic features (e.g., crater presence, flank roughness, fluvial development, flow features, flank curvatures).

Quantitative descriptions of volcanic shape are useful for discerning the growth trends of a given volcanic type, comparing similar volcanic types in different regions, and identifying the range of volcano morphologies present in a region. This thesis discusses

several examples in subsequent chapters. Measurements of cinder cone morphology from a topographic map can be compared with similar measurements of numerical simulations based on the model of cinder cone growth presented by McGetchin et al. [1974] (Chapter III). A comparison of the growth trends and morphologies of shield and composite volcanoes in Guatemala suggests that shield volcanoes may evolve into composite volcanoes (Chapter V). The shapes and growth trends of shield volcanoes are different in Guatemala, Iceland and the Snake River Plain; this may reflect a set of processes affecting shield growth with the relative importance of each process varying between regions. The total range of morphologies of submarine volcanoes in the South Pacific is comparable to the total possible range of morphologies for volcanoes.

REFERENCES CITED

Basaltic Volcanism Study Project. *Basaltic Volcanism on the Terrestrial Planets*, Pergamon Press, Inc., New York, 1981.

Batiza, R. Abundances, distribution and sizes of volcanoes in the Pacific Ocean and implications for the origin of non-hotspot volcanoes. *Earth Planet. Sci. Lett.*, vol. 60, p.195-206, 1982.

Becker, G. F. The geometrical form of volcanic cones and the elastic limit of lava. *American Journal of Science*, 30, 283-293, 1885.

Bemis, K. G., and D. K. Smith. Production of small volcanoes in the Superswell Region of the South Pacific. *Earth Planet. Sci. Lett*, 118, 251-262, 1993.

Bohnenberger, O. H. Los focos eruptivos cuaternarios de Guatemala. Trabajos Technicos Presentados en la Segunda Reunion de Geologos de America Central, Publicaciones Geológicas del Institutio Centroamericano de Investigacion y Tecnologia Industrial, Numero II, 1969.

Borgia, A. and S. R. Linneman, On the mechanisms of lava flow emplacement and volcano growth: Arenal, Costa Rica, in *Lava flows and domes*, edited by J. H. Fink, International Association of Volcanology and Chemistry of the Earth's Interior Proc. Volcanol., 2, 208-243, 1990.

Burkart, B., and Self, S. Extension and rotation of crustal blocks in northern Central America and effect on the volcanic arc: *Geology*, v. 13, p. 22-26, 1985.

Calmant, S., and A. Cazenave, Anomalous elastic thickness of the oceanic lithosphere in the south-central Pacific, *Nature*, 328, 236-238, 1987.

Cas, R. A. F., and J. V. Wright, *Volcanic Successions: Modern and Ancient*, London: Chapman and Hall, 1988.

Cochran, J. R., Variations in subsidence rates along intermediate and fast spreading mid-ocean ridges, *Geophys. J. R. Astron. Soc.*, 87, 421-454, 1986.

Dohrenwend, J. C., S. G. Wells, and B. D. Turrin. Degradation of Quaternary cinder cones in the Cima volcanic field, Mojave Desert, California. *Geol. Soc. Am. Bull.*, 97, 421-427, 1986.

Francis, P. W., and B. M. Abbot. Sizes of conical volcanoes, *Nature*, 244, 22-23, 1973.

Geist, D., and M. Richards. Origin of the Columbia Plateau and Snake River plain: deflection of the Yellowstone plume, *Geology*, 789-792, 1993.

Greeley, R., The Snake River Plain, Idaho: Representative of a new category of volcanism, *J. Geophys. Res.*, 87, 2705-2712, 1982.

Head, J. W., III, and L. Wilson. Lava fountain heights at Pu'u' O'o', Kilauea, Hawaii: indicators of amount and variations of exsolved magma volatiles., *J. Geophys. Res.*, 92, p. 13715-13719, 1987.

Hasenaka, T., and I. S. E. Carmichael. The cinder cones of Michoacán-Guanajuato, Central Mexico: their age, volume and distribution, and magma discharge rate. *J. Vol. Geotherm. Res.*, 25, p. 105-124, 1985.

Houghton, B. F., and H.-U. Schmincke. Mixed deposits of simultaneous strombolian and phreatomagmatic volcanism: Rothenberg Volcano, East Eifel Volcanic Field, *J. Vol. Geotherm. Res.*, 30, 117-140, 1986.

Jordan, T. H., H. W. Menard, and D. K. Smith. Density and size distribution of seamounts in the eastern Pacific inferred from wide-beam sounding data, *J. Geophys. Res.*, 88, 10508-10518, 1983.

Kear, D., Erosional stages of volcanic cones as indicators of age. *New Zealand Journal of Science and Technology*, 38, 671-682, 1957.

Kuntz, M. A., B. Skipp, M. A. Lanphere, W. E. Scott, K. L. Pierce, G. E. Dalrymple, L. A. Morgan, D. E. Champion, G. F. Embree, R. P. Smith, W. R. Hackett, D. W. Rodgers. Revised geologic map of the Idaho National Engineering Laboratory and adjoining areas, eastern Idaho. U.S.G.S. Open-file report 90-333, 1990.

Loewenherz, D., Stability and the initiation of channelized surface drainage: a reassessment of the short wavelength limit. *J. Geophys. Res.*, 96, 8453-8464, 1991.

McGetchin, T. R., Settle, M., and Chouet, B. A. Cinder cone growth modeled after Northeast Crater, Mount Etna, Sicily: *Journal of Geophysical Research*, v.79, p.3257-3272, 1974.

McNutt, M. K., and K. M. Fischer, The South Pacific Superswell. *Seamounts, Islands and Atolls*, AGU Geophys. Monogr. 43, 25-34, 1987.

McNutt, M. K., and A. V. Judge, The Superswell and mantle dynamics beneath the South Pacific, *Science*, 248, 969-975, 1990.

Milne, J. On the form of volcanos. The Geological Magazine, 5, 337-345, 1878.

Parsons, B., and J. G. Sclater, An analysis of the variation of ocean floor bathymetry and heat flow with age, *J. Geophys. Res.*, 82, 803-827, 1977.

Plafker, G. Tectonic aspects of the Guatemala earthquake of 4 February 1976: *Science*, v. 193, p. 1201-1208, 1976.

Pike, R. J. and G. D. Clow. Revised classification of terrestrial volcanoes and catalog of topographic dimensions, with new results on edifice volume. *U.S. Geological Survey Open-File Report* 81-1038, 1981a.

Pike, R. J. and G. D. Clow, Numerical taxometry of central volcanoes on the planets, in *NASA Tech. Memo.* 84211, Reports of Planetary Geology Program - 1981, compiled by H. E. Holt, 138-140, 1981b.

Porter, S. C. Distribution, morphology and size frequency of cinder cones on Mauna Kea Volcano, Hawaii. *Geol. Soc. Am. Bull.*, 84, p.382-483, 1972.

Sæmundsson, K., Outline of the geology of Iceland, *Jökull*, spec. issue, 29, 7-28, 1979.

Schilling, J.-G., Iceland mantle plume: geochemical evidence along Reykjanes Ridge, *Nature*, 242, 656-571, 1973.

Smith, D. K. Shape analysis of Pacific seamounts. *Earth Planet. Sci. Lett.*, vol. 90, pp. 457-466, 1988.

Smith, D. K. and J. R. Cann, The role of seamount volcanism in crustal construction at the Mid-Atlantic Ridge (24°-30°N), *J. Geophys. Res.*, 97 (B2), 1645-1658, 1992.

Smith, D. K. and T. H. Jordan. Seamount Statistics in the Pacific Ocean, *J. Geophys. Res.*, 93, 2899-2918, 1988.

Thorarinsson, S., and K. Sæmundsson, Volcanic activity in historic time. *Jokull*, 29, 29-32, 1979.

Vessel, R. K., and D. K. Davies, Non-marine sedimentation in an active fore-arc basin, In *Recent and ancient non-marine depositional environments: models for*

exploration, F. G. Ethridge and R. M. Flores (eds), 31-45, SEPM Spec. Publn 31, 1981.

Walker, G. P. L., and R. Croasdale. Characteristics of some basaltic pyroclastics, *Bull. Volcanol.*, 35, 303-317, 1972.

Whitford-Stark, J. L., Shield volcanoes, in *Volcanoes of the Earth, Moon and Mars*, eds. G. Fielder and L. Wilson, London: Paul Elek Ltd., 1975.

Williams, H., *The history and character of volcanic domes*, Univ. Calif. Publn Bull Dept. Geol. Sci., 21, 51-146, 1932.

Williams, H., McBirney, A. R., and Dengo, G., 1964, Geologic reconnaissance in southeastern Guatemala: Univ. California Publ. Geol. Sci., v.50, p.1-56

Williams, R. S., S. Porarinsson, and E. C. Morris, Geomorphic classification of Icelandic volcanoes. *Jokull*, 33, 19-24, 1983.

Wilson, L., and J. W. Head, III. Mars: review and analysis of volcanic eruption theory and relationships to observed landforms, *Rev. Geophys.*, 32, 221-263, 1994.

Wood, C. A. Cinder cones on Earth, Moon and Mars, *EOS, Trans. AGU*, 58, 425, 1977.

Wood, C. A., Morphometric evolution of composite volcanoes, *Geophysical Research Letters*, 5 (6), 437-439, 1978.

Wood, C. A., Monogenetic volcanoes of the terrestrial planets, *Proc. Lunar Sci. Conf.* 10th, 2815-2840,1979.

Wood, C. A., 1980a, Morphometric evolution of cinder cones: *J. of Vol. and Geotherm. Res.*, v.7, p.387-413.

Wood, C.A., 1980b, Morphometric analysis of cinder cone degradation: *J. of Vol. and Geotherm. Res.*, v.8, p.137-160.

Chapter III. Cinder cone size related to subduction signature in the Ipala Graben, southeast Guatemala

BACKGROUND

Most previous studies concerned with volcano morphology and geochemistry have considered the full range of volcanic types and chemical compositions [e.g., Wood and Schuver, 1981; Pike and Clow, 1981a; Carr, 1984]; this study looks at a single volcanic type (cinder cones) with a narrow range of chemical compositions. Cinder cone morphology has been extensively documented and related to eruptive processes [McGetchin et al., 1974; Blackburn et al., 1976; Wood, 1980a; Dehn, 1987; Head and Wilson, 1989] and erosion [Wood, 1980b; Hasenaka and Carmichael, 1985]. Most cinder cones are composed of basalt and basaltic andesite and formed by short-lived eruption sequences. Strombolian eruptions, which are typical cinder cone forming eruptions, are generated by degassing and decompression of the volatiles in the magma. The morphology of the cone and the grain size of the scoria should reflect the volatile content of the magma with finer-grained cones resulting from higher volatile contents [Head and Wilson, 1989]. After much of the gas has been explosively released, the bulk of the erupted magma emerges fluidly in the form of lava flows [Wood, 1980a].

The Ipala Graben region in southeast Guatemala is an area of basalt-rhyolite volcanism [Williams, et al., 1964; Bohnenberger, 1969] behind the volcanic front of Central America (Figure III-1). Quaternary, and earlier, extension has been previously documented along the north trending Ipala Graben, within which most of the volcanism occurs [Plafker, 1976; Burkart and Self, 1985]. More than 95 cinder cones are associated with lava flows and small shield volcanoes (Figure III-1). Rhyolitic domes occur approximately in the center of the volcanically active region. The cones are estimated to be Holocene or slightly older; some cones and associated flows have little vegetative cover

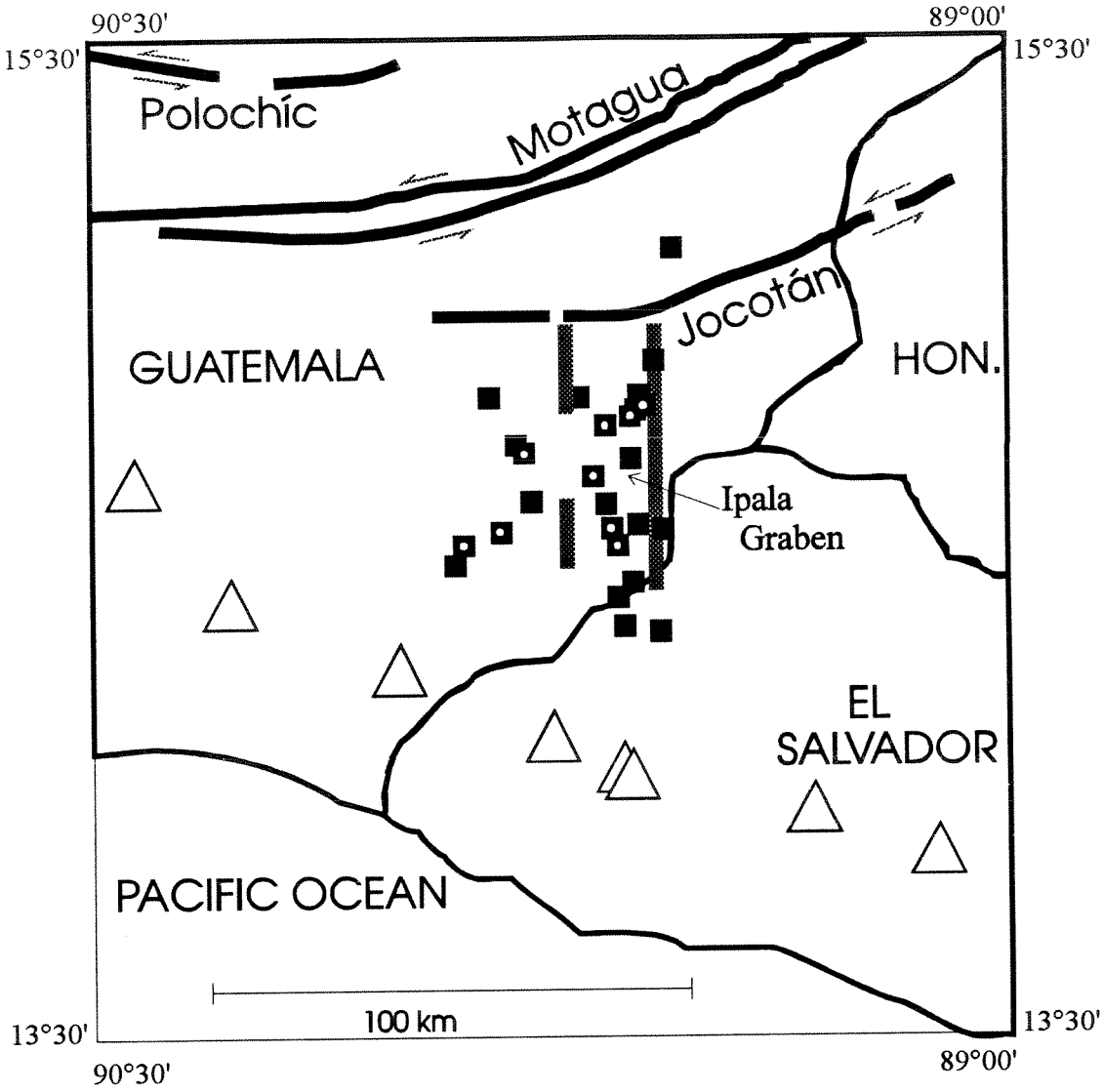


Figure III-1. The map shows the location of the cinder cones, and their associated lava flows, used in this chapter (black boxes). Small white dots indicate the location of scoria samples used in the grain size analysis. The triangles are the arc front volcanoes. The thick lines indicate faults. The Polochíc, Motagua and Jocotán faults have sinistral strike-slip motion and are the transform boundary between the Caribbean and North American plates [Plafker, 1976]. The Ipala Graben is bounded by N-S trending normal faults. Most of the cinder cones in this study lie within the Ipala Graben.

and appear to be comparable in age to the older historic flows along the volcanic front. The Ipala Graben is by far the largest of several areas of behind-the-front volcanism in Central America. All of the back-arc volcanism in northern Central America is related to local extensional structures that generally trend N-S, oblique to the volcanic front. The Ipala Graben extends across the Jocotán fault, an E-W striking, left-lateral, strike-slip fault that, together with the similarly oriented Motagua and Polochíc strike-slip faults to the north, comprise the Caribbean-North American plate boundary [Plafker, 1976]. Thus, the tectonic setting of this volcanic region is a composite of back-arc and transform settings [Burkart and Self, 1985].

Previous petrologic studies of these volcanoes have shown that major element chemistry reflects fractionation of clinopyroxene, olivine and plagioclase within or at the base of the crust, followed by rise, and subsequent crystallization of just olivine and plagioclase phenocrysts as the clinopyroxene field decreases with decreasing pressure [Walker, 1981]. Although crystal fractionation has taken place, the ranges of MgO (3.72-8.00%), Ni (8-119 ppm) and Cr (16-325 ppm) show that fractionation ranges between moderate to minor [Walker, 1981]. Sr, Nd, and Pb isotopic ratios indicate variable crustal contamination, increasing with increasing distance behind the volcanic front and especially in areas near Mesozoic intrusives [Walker et al., in press].

Studies of the volcanic front in Central America show that most lavas have a hydrous flux component that is derived from the subducted Cocos Plate [Carr et al., 1990; Leeman et al., 1994]. The least ambiguous indicator of recycling of subducted sediment is ^{10}Be and Central American lavas have some of the highest $^{10}Be/^{9}Be$ ratios in the world [Morris et al., 1990]. The incompatible element ratio, Ba/La, correlates well (R=0.87) with the $^{10}Be/^{9}Be$ ratio [Leeman et al., 1994]. This is reasonable, because the sediments being subducted in Central America have extremely high Ba contents, up to 8000 ppm (DSDP site 495 in Carr et al. [1990]). La and ^{9}Be are primarily derived from mantle peridotite, whereas ^{10}Be and Ba are wholly to predominately derived from (directly or as

a flux form) the subducted slab. Furthermore, in a worldwide comparison, Central America has the highest normalized Ba contents in arc lavas and the highest Ba concentration in subducted material [Plank and Langmuir, 1993]. Therefore, for Central America, Ba/La is a good and easily measured tracer for subducted sediment or fluids derived from it.

The importance of a subducted component for volcano morphology is the likelihood that higher subduction contents will lead to higher volatile contents. Stolper and Newman [1994] analyzed H_2O in submarine basaltic glasses from the Mariana back-arc. They found that the volatile content of the glasses correlates positively with Ba and other incompatible elements. Therefore, since the subducted material in DSDP 495, offshore Guatemala, is particularly enriched in Ba, Ba/La can be used as a proxy for volatile content.

This chapter attempts to relate the tectonic processes of a behind-the-arc subduction setting to the distribution and shape of cinder cones, by making a comparison of morphological and geochemical data from cinder cones in southeast Guatemala. This comparison reveals a positive correlation (R=0.58) between cinder cone volume and Ba/La, a tracer of subducted slab component, and a negative correlation (R=-0.55) between volume and La/Yb, a measure of the degree of melting. These correlations are interpreted as: higher hydrous flux from the subducted slab (as indicated by higher Ba/La) causes (1) higher degrees of melting (indicated by lower La/Yb) and (2) larger magma volumes. The slab tracer, Ba/La, appears to be randomly distributed in space. Furthermore, the minimum Ba/La values of about 18 are only slightly higher than the range of values found for MORB, suggesting that the hydrous flux from the slab is not the sole or dominant cause of melting in this region. Because of the obvious crustal extension in the region, it is suggested that asthenospheric decompression is an important cause of melting. Thus melt generation results from combining the effects of asthenospheric decompression, caused by tectonically generated back-arc extension along the Ipala

Graben, and minor to moderate amounts of metasomatism of the mantle by subducted material.

DATA

Air photographs and topographic maps allowed clear determination of volcano morphology, using a modification of criteria developed for submarine volcanoes [Smith 1988; Smith and Cann, 1992; Bemis and Carr, 1993]. The volume of each cinder cone was calculated from the measured height, basal diameter, and crater diameter with the assumption of a right-circular conical shape. Volumes were determined with an error of about 10%. Unfortunately, the volume of any associated lava flow is obscured by a combination of vegetative cover and variable land-use modification, which prevented most of the lava flows from being readily identified. Field mapping in the region is only at reconnaissance levels so there are no reliable lava flow volumes to associate with the cinder cone volumes.

Geochemical data including major, trace and rare earth elements and Sr, Nd, and Pb isotope ratios are available on 69 samples, most of which were collected in previous studies summarized by Walker et al. [in press]. Of these, 20 are mafic ($MgO \geq 5$ wt %) lava flows or scoriaceous bombs from well-defined cinder cones, whose volume was measured.

Samples of relatively fresh scoria were obtained from nine cinder cones spanning a wide range of volumes. These cinder cones were selected based on the presence of pre-existing quarries which made obtaining fresh samples of the scoria feasible (the tropical environment causes rapid soil development in Guatemala). Scoria samples were sieved to determine their particle size distributions and then analyzed for major, minor and rare earth elements.

RESULTS

I combined the morphological data (i.e., height, basal diameter, volume, particle size) with geochemical data that should be a proxy for degree of fractionation and/or assimilation (MgO content), for degree of melting (La/Yb) and for the amount of hydrous flux from the subducted Cocos Plate (Ba/La) (Table III-1). To minimize the effects of assimilation and fractionation, I eliminated all samples with less than 5 Wt % MgO. Cinder cone volume correlates positively with Ba/La and negatively with La/Yb (Table III-2). The negative correlation between cinder cone volume and La/Yb (R=-0.55) is weak, but it is what would be expected if a high degree of melting (low La/Yb) makes larger magma batches that lead to larger eruptive episodes (Figure III-2). Similarly, cinder cone volume correlates negatively with LREE contents (for example, volume and Ce have a correlation coefficient of R=-0.68). The positive correlation of cinder cone volume with Ba/La (R=0.56) suggests that fluxing by a slab component, and the volatiles introduced into the magma by it, are important in the generation of the magmas (Figure III-3). Ba/La and La/Yb are negatively correlated (Figure III-4) as expected if increased flux from the slab increases the degree of melting. Ba/La correlates only weakly negatively with most LREE. I carefully examined the spatial variation of La/Yb and Ba/La in southeast Guatemala, but, in agreement with Walker et al. [in press], found no changes with distance behind the front or along the axis of the Ipala Graben. There is a wider range in Ba/La and La/Yb values closer to the volcanic front, but this could be an artifact of greater sampling density. Overall, Ba/La values range from only just higher than values expected for MORB to values typical of the Guatemalan arc front.

The samples with MgO contents greater than 5 Wt % were removed from the data set in order to minimize the effects of assimilation and fractionation. Table III-2 contains the correlation coefficients for the relationships studied for both the original data set (MgO unrestricted) and the present data set (MgO > 5 Wt%). A weak correlation

between Ba/La and MgO disappears after the low MgO samples are removed. No correlation exists between volume and MgO when MgO is unrestricted (R=0.22); this suggests that the weak positive correlation between volume and MgO (R=0.39) observed when MgO is restricted to > 5 Wt% is probably coincidental (Table III-2).

Field investigation of nine Guatemalan cinder cones revealed that they are composed almost entirely of highly vesicular scoria with minor silicic pumice present in one case (these pumices are probably lithic inclusions). Large bombs are present in about half the cones; plastic deformation features are clearly visible on bombs. However, the small clasts composing the bulk of the cone are never observed to be plastically deformed, indicating a low pyroclast temperature on landing [Head and Wilson, 1989]. No obvious variation of pyroclast nature or size over cone history was observed in any of the quarries. Visual observation of the sections suggest that most beds have similar clast size and distribution and reverse grading (related to grain flows occurring during active growth). No observations are available on the stratigraphic relationships of these cinder cones and their associated flows.

Particle size analysis of scoria sampled from cinder cones yielded the expected size distributions with approximate log-normal shapes and high variability of grain size. Table III-3 reports the usual grain size distribution parameters. The median grain size (Md_ϕ) and dispersion (sorting) (σ_ϕ) of the nine scoria samples fall in the Strombolian field on Md_ϕ-σ_ϕ plots of Walker and Croasdale [1972] (Figure III-5). No significant correlation was observed between median grain size and cinder cone volume nor between Ba/La and grain size (Table III-4). Two possible correlations are noted: (1) mode of grain size and volume (R=0.74) and (2) dispersion of grain size (sorting) and volume (R=-0.81). Therefore, in general, smaller cones have less well-sorted, coarser scoria and larger cones have more well-sorted, finer scoria (Figure III-6).

Table III-1. Geochemical and morphological data for cinder cones with MgO >= 5 Wt%

Sample	SiO_2	MgO	Na_2O	Ba	La	Yb	H^+	$Base^+$	F^*	$Volume^+$
GuC30	49.6	8.00	3.20	307	12.1	2.06	145	800	0.41	0.0383
GuC702	50.0	6.44	3.56	408	15.7	2.40	120	730	0.24	0.0217
GuC707	51.8	5.32	3.83	520	18.6	2.62	107	678	0.39	0.0199
SalC203	51.4	6.42	3.63	506	16.7	2.54	55	770	0.40	0.0133
SalC202	49.5	5.94	3.58	280	13.8	2.20	110	540	0.28	0.0114
SalC7	50.0	7.06	3.23	388	10.6	2.18	220	998	0.23	0.0736
GuC201	49.8	6.88	3.30	581	13.3	2.22	270	953	0.28	0.0872
GuC405	52.6	5.77	3.24	574	18.0	2.55	170	818	0.16	0.0353
GuC710	50.2	5.59	3.52	520	17.9	2.38	152	888	0.27	0.0421
GuC202	51.2	5.88	3.45	384	21.0	2.82	74	613	0.37	0.0110
GuC309	52.8	5.09	3.54	436	11.4	2.51	130	773	0.36	0.0303
GuC403	48.6	6.73	3.30	327	10.8	2.04	138	893	0.41	0.0455
GuC404	50.9	5.52	3.31	597	20.6	3.10	73	603	0	0.0069
GuC714	50.2	6.00	3.15	361	13.7	2.12	155	760	0.33	0.0337
GuC1005	50.5	6.46	3.45	460	17.8	2.47	40	253	0	0.0069
GuC1002s	50.5	7.34	3.13	386	12.2	2.16	270	953	0.28	0.0872
GuC1005s	50.3	6.48	3.14	483	17.4	2.33	40	253	0	0.0069
GuC1007s	50.1	7.10	2.81	471	17.1	2.50	138	893	0.41	0.0455
GuC1008s	48.3	6.62	2.69	357	13.0	2.19	155	760	0.33	0.0337
GuC1009s	51.0	6.36	3.15	444	16.3	2.45	120	730	0.24	0.0217
G1**	70.8	0.14	4.66	863	23.5	3.21	-	-	-	-
G2**	59.7	3.33	2.93	512	19.3	3.27	-	-	-	-

$^+$Height (H) and Base (diameter) in m; Volume in km^3.

*Top diameter/ Base diameter.

** Crustal samples; G2 is diorite.

Table III-2. Regression coefficients and their significance.

			MgO >= 5 Wt %				MgO unrestricted			
Correlation:			R	t	n	confidence	R	t	n	confidence
Subduction tracer = Ba/La										
Volume*	&	Ba/La	0.56	2.92	21	99%	0.60	4.00	30	99.8%
Degree of melting = La/Yb, Ce										
Volume*	&	La/Yb	-0.55	-2.85	21	98%	-0.40	-2.29	30	95%
Ba/La	&	La/Yb	-0.48	-2.36	21	95%	-0.52	-3.25	30	99%
Volume*	&	Ce	-0.68	-4.05	21	99.8%	-0.76	-6.26	30	99.8%
Ba/La	&	Ce	-0.50	-2.49	21	95%	-0.56	-3.55	30	99.8%
Fractionation = MgO										
Volume*	&	MgO	.39	1.88	22	90%	0.22	1.30	37	<80%
Ba/La	&	MgO	-0.04	-0.18	21	n.c.	-0.43	-2.49	30	98%
La/Yb	&	MgO	-0.30	-1.34	21	80%	0.18	0.97	30	n.c.
Ce	&	MgO	-0.43	-2.05	21	90%	-0.05	-0.26	30	n.c.

* Volume in Log_{10} units.
n.c. = no confidence.

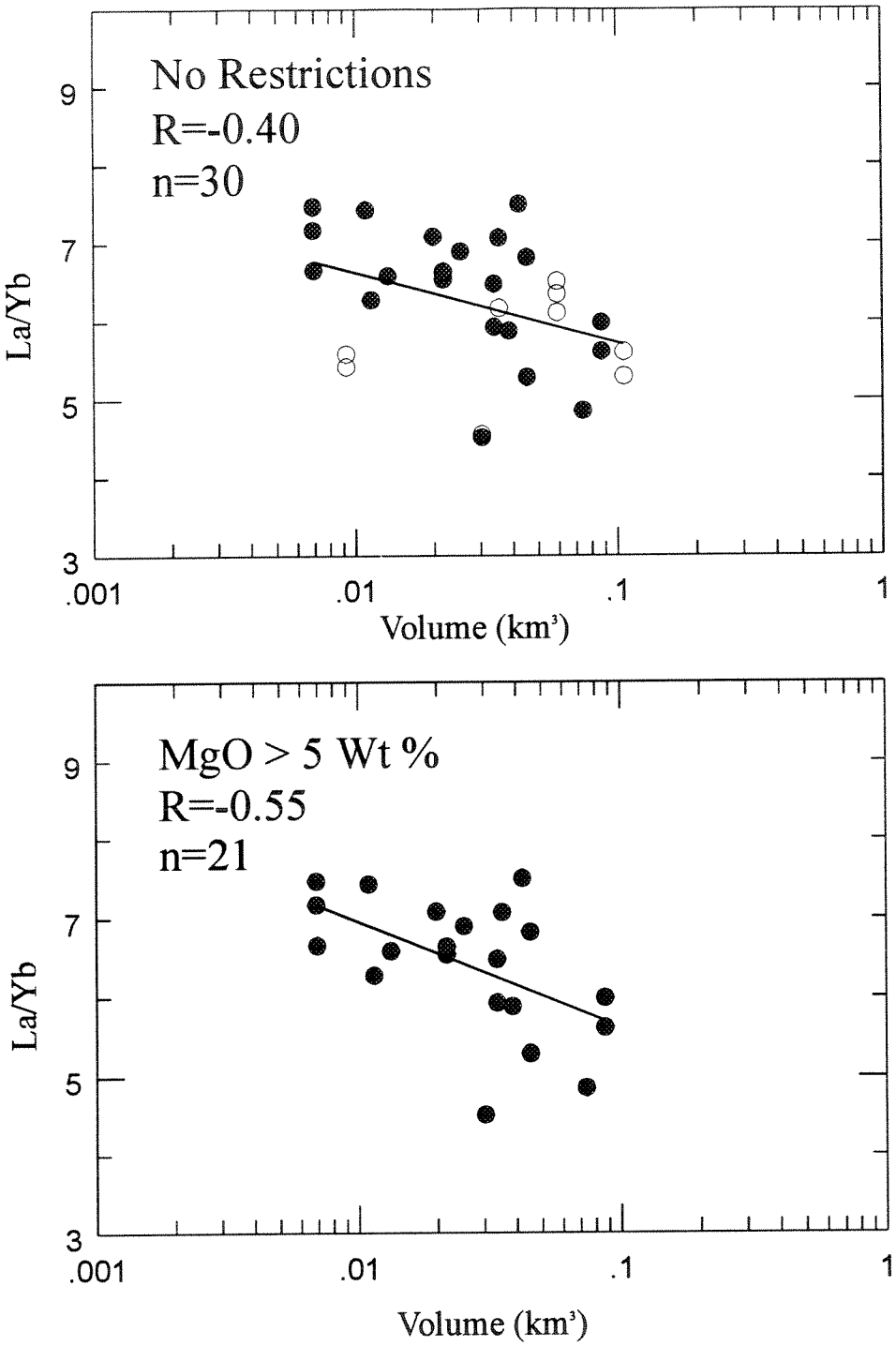


Figure III-2. La/Yb decreases with increasing cinder cone volume. Lower La/Yb indicates a higher degree of melting and, therefore, a larger batch of magma and a larger cone. See Table III-2 for statistical analysis. Closed circles have MgO greater than or equal to 5 wt%; open circles have MgO less than 5 wt%.

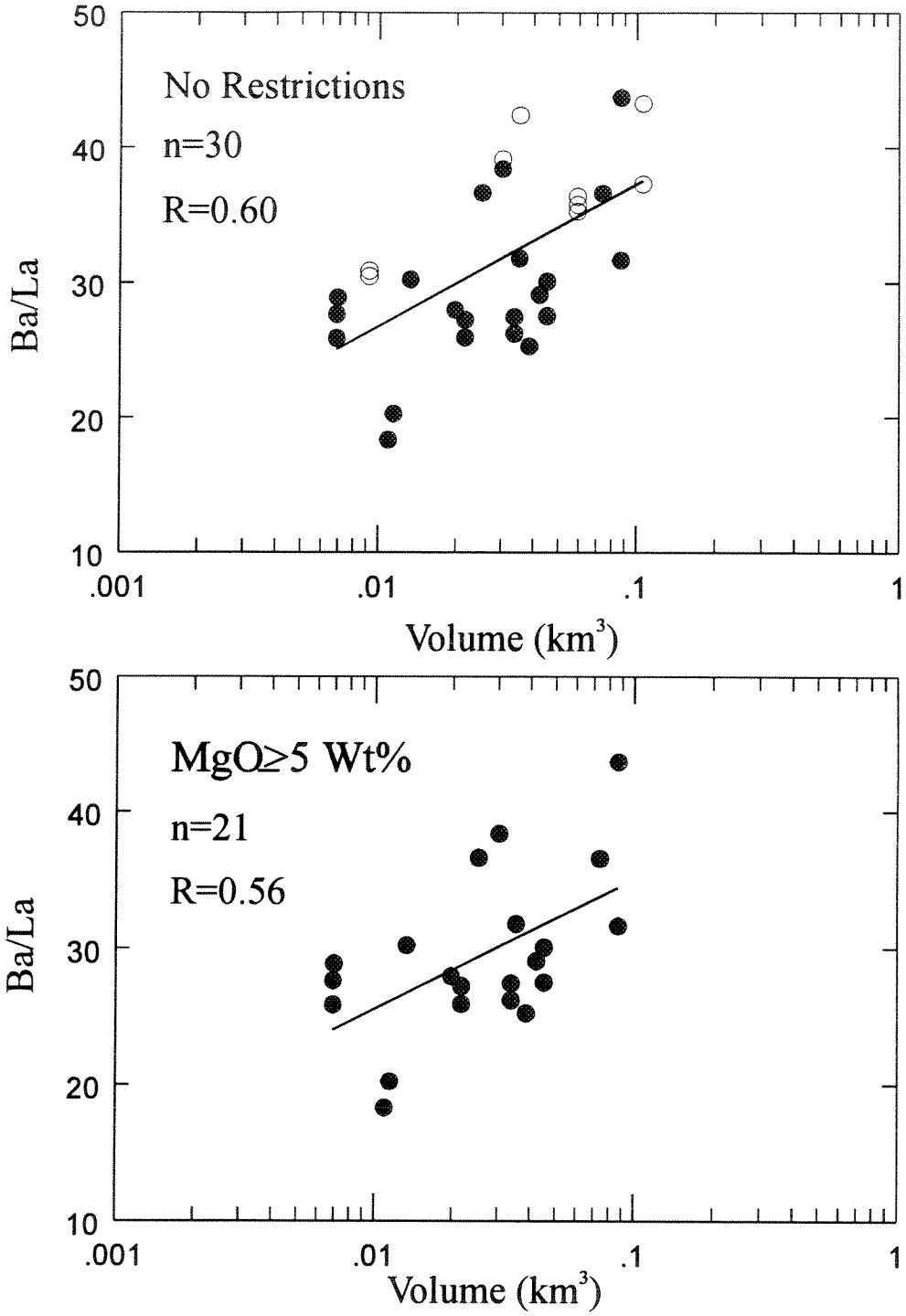


Figure III-3. Ba/La, an index of slab fluid, increases with increasing cinder cone volume. Higher hydrous flux from the subducted slab results in a higher degree of melting, thus a larger batch of magma and a larger cone. See Table III-2 for statistical analysis. Open circles have MgO contents of less than 5 wt%; closed circles have MgO contents of greater than or equal to 5 wt%.

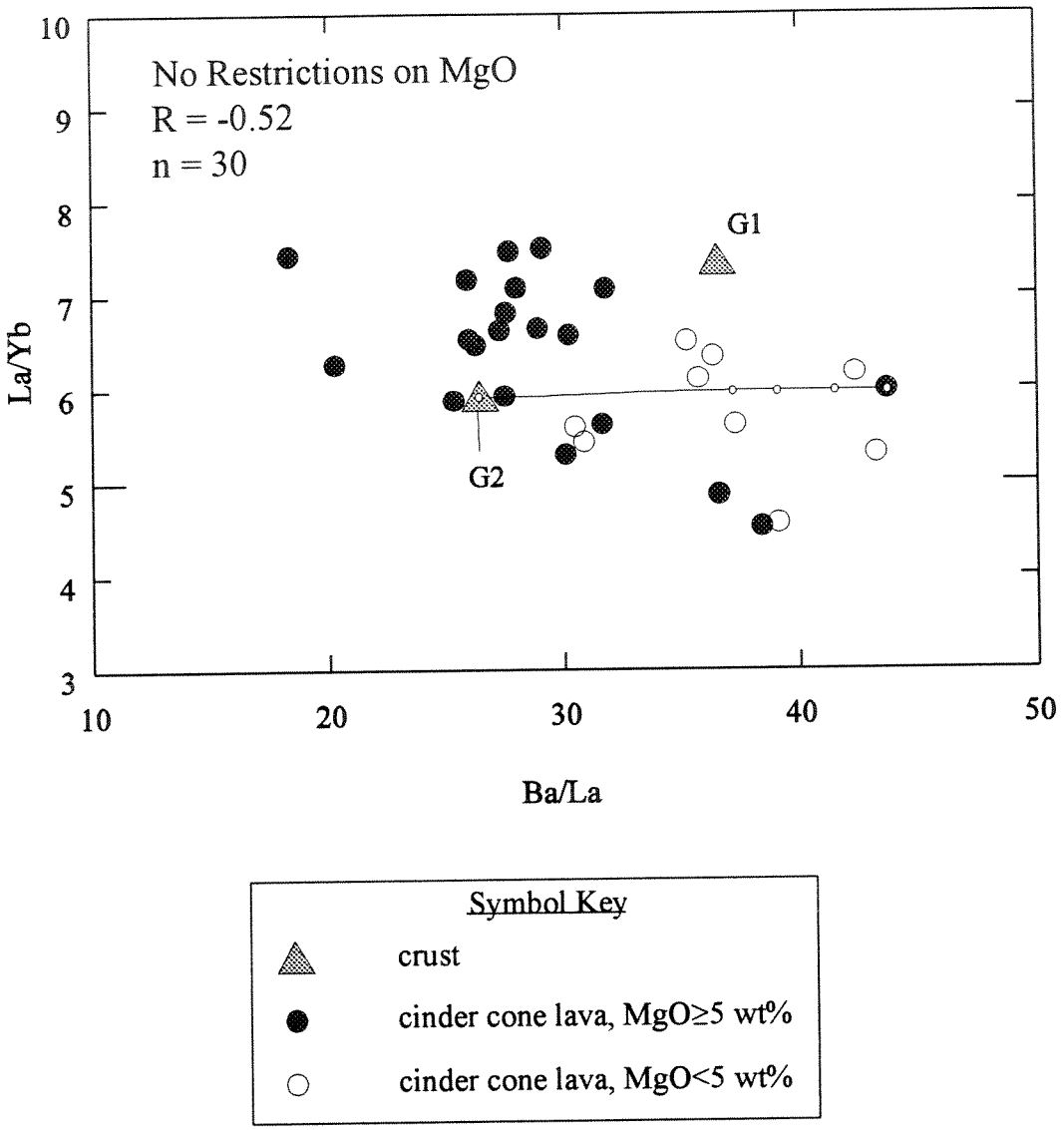


Figure III-4. A negative correlation is observed between Ba/La and La/Yb. Analysis of the mixing line show that the Ba and La contents of the crust are not different enough to account for the correlation by fractionation and assimilation. The best canidates (triangles) for crustal assimilations (based on Sr, Nd, and Pb isotopes [Walker et al., in press]) have Ba, La, and Ba/La values similar to the lavas of this study (circles). Adding 10% of the best canidate (G2) only shifts Ba/La from 45 to 42. The mixing line between G2 (diorite) and GuC1001 has tick marks (small white circles) that indicate 10%, 20%, and 30% mixing. Removing the samples with MgO contents below 5 wt% (open circles) does not greatly alter this correlation.

Table III-3. Results of particle size analysis*.

sample #	cone volume (km^3)	mode (ϕ)	median (ϕ)	mean (ϕ)	dispersion (ϕ)	skewness	kurtosis
GuC1005s	0.0069	-4.5	-3.69	-3.53	1.74	-0.63	1.16
GuC1006s	0.0092	-4.5	-3.57	-3.36	1.54	-0.61	1.18
GuC1004s	0.0589	-3.5	-3.55	-3.56	0.83	-1.64	1.11
GuC1002s	0.0872	-2.5	-2.41	-2.34	1.17	-0.68	1.06
GuC1003s	0.0303	-2.5	-2.39	-2.26	1.38	-0.45	1.27
GuC1007s	0.0455	-2.5	-2.15	-2.02	1.19	-0.51	1.58
GuC1009s	0.0217	-2.5	-2.05	-1.95	1.62	-0.38	0.96
GuC1001s	0.1051	-1.5	-1.75	-1.81	1.19	-0.62	1.21
GuC1008s	0.0337	-1.5	-1.44	-1.43	1.21	-0.47	1.10

* particle sizes are given in ϕ size units for mode, median, mean and dispersion; $\phi=-\log_2(mm)$. Cone volume is in units of km^3; skewness and kurtosis are dimensionless.

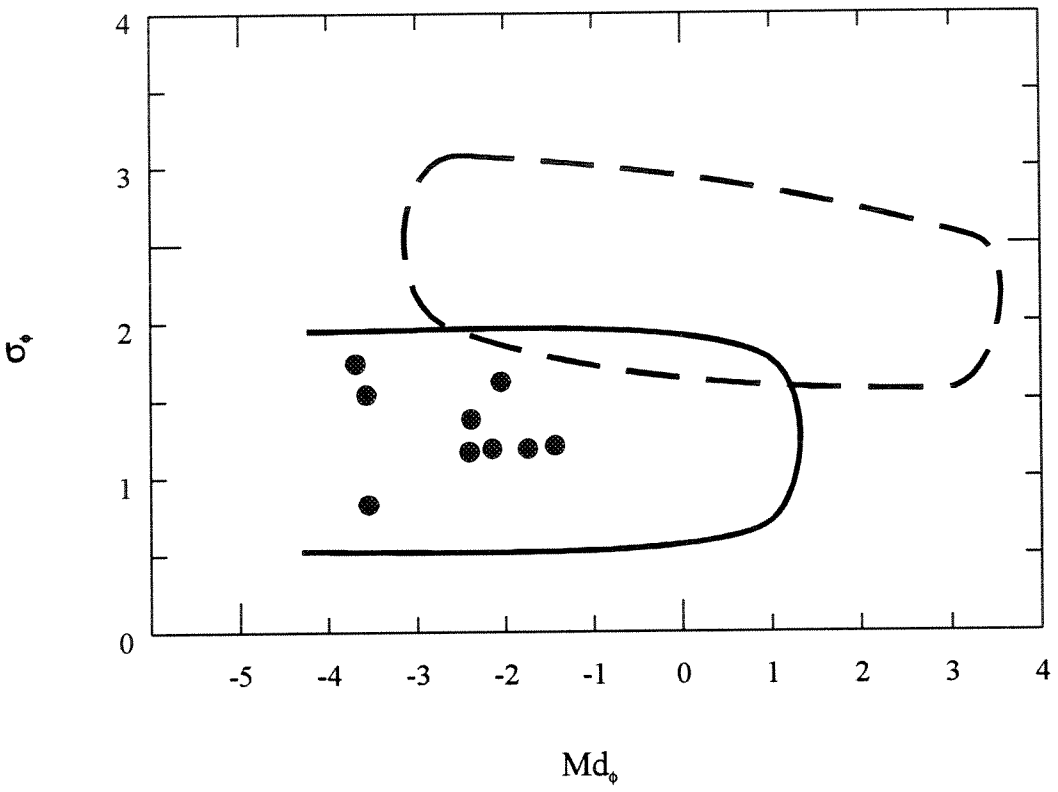


Figure III-5. Md_ϕ vs. σ_ϕ plot after Walker and Croasdale [1972]. In the absence of an isopach map, this is the best way to characterize the strength and explosivity of the eruption forming a cinder cone. Solid line outlines region of strombolian eruptions; dashed line outlines the region of phreatomagmatic eruptions.

The lack of strong correlation in median grain size with cone volume (R=0.56) probably reflects the limited sampling. Grain size distributions in cinder cones have been previously noted to be highly sensitive to location relative to wind direction during the eruption and distance from the vent [Wood, 1980a; McGetchin et al., 1974; Inbar et al., 1994]. In this study, only a single sample was taken from each of nine cones and no effort was made to standardize the position (as noted above sampling was only feasible in quarries). Additionally, many of my samples showed signs of having two populations of grains - or at least a non-log-normal distribution (Figure III-7).

Table III-4. Comparison of grain size data with cone volume and Ba/La ratios.

Correlation		between:	R	t	n	confidence
mode	&	Volume	0.74	2.92	9	95 %
median	&	Volume	0.56	1.77	9	80 %
mean	&	Volume	0.50	1.52	9	80 %
dispersion	&	Volume	-0.81	-3.65	9	99 %
skewness	&	Volume	-0.26	-0.71	9	n.c.
kurtosis	&	Volume	0.09	0.25	9	n.c.
mode	&	Ba/La	0.15	0.41	9	n.c.
median	&	Ba/La	-0.06	-0.18	9	n.c.
mean	&	Ba/La	-0.11	-0.30	9	n.c.
dispersion	&	Ba/La	-0.45	-1.33	9	n.c.
skewness	&	Ba/La	-0.39	-1.13	9	n.c.
kurtosis	&	Ba/La	0.04	0.10	9	n.c.

n.c. = no confidence.

DISCUSSION

Cinder cone volume should depend on the amount of magma present and the proportion of that magma that erupts explosively. Erosion will reduce the volume over time, but the cinder cones studied appear to be at most only slightly degraded. Wood [1980a] has proposed that cinder cone size and lava flow size are related by the following function: $CV = 0.00078 \times FV^{1.26}$, where CV is the cinder cone volume and FV is the lava flow volume. For the size range of the southeast Guatemala cones (10^7 to 10^9 m^3), the cinder cone volume is about 10% of the total volume. The results from Southeast Guatemala suggest that the weak negative correlation of volume with La/Yb (R=-0.55) is consistent with Wood's [1980a] proposal, that is, magmas with high degrees of melting (low La/Yb) give rise to larger batches of magma and larger cones. The positive correlation of Ba/La and cinder cone volume (R=0.56) and the negative correlation between Ba/La and La/Yb (R=-0.48) in southeast Guatemala suggests that the major factor controlling variations in cinder cone volume is increases in the total volume of magma produced due to larger hydrous flux from the subducted slab, as estimated by Ba/La.

The relationship between Ba/La and La/Yb could potentially be caused by assimilation. I argue against assimilation being responsible for the observed correlation. Glazner and Farmer [1992] have shown that isotopic systematics of mafic continental basalts are easily modified and disturbed by cryptic crustal contamination: for example, lavas whose major and trace elements indicate a pristine mantle composition can have their isotopic geochemistry altered by small amounts of crustal assimilation because of the large isotopic contrast between magma and assimilant. Indeed, AFC (assimilation-fractional crystallization) is an important factor in interpreting the isotope geochemistry of these magmas [Walker et al., in press]. However, the assimilation problem is minimized in this study because the Mesozoic plutons that are the best candidates for crustal assimilation,

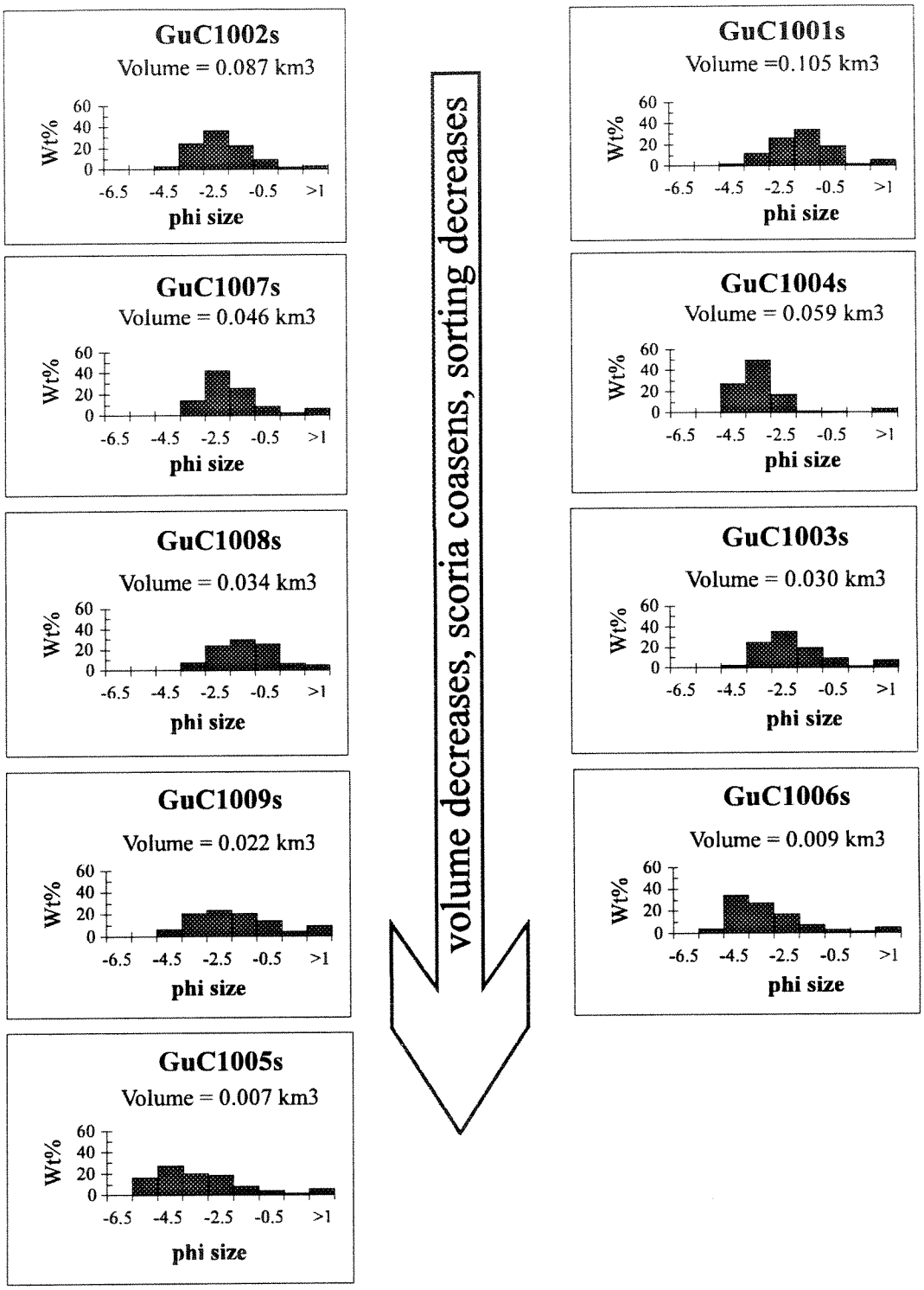


Figure III-6. Histograms of particle size distributions for scoria samples. Volumes of the cones are indicated on each histogram. Note that the smaller cones are coarser grained, but more poorly sorted.

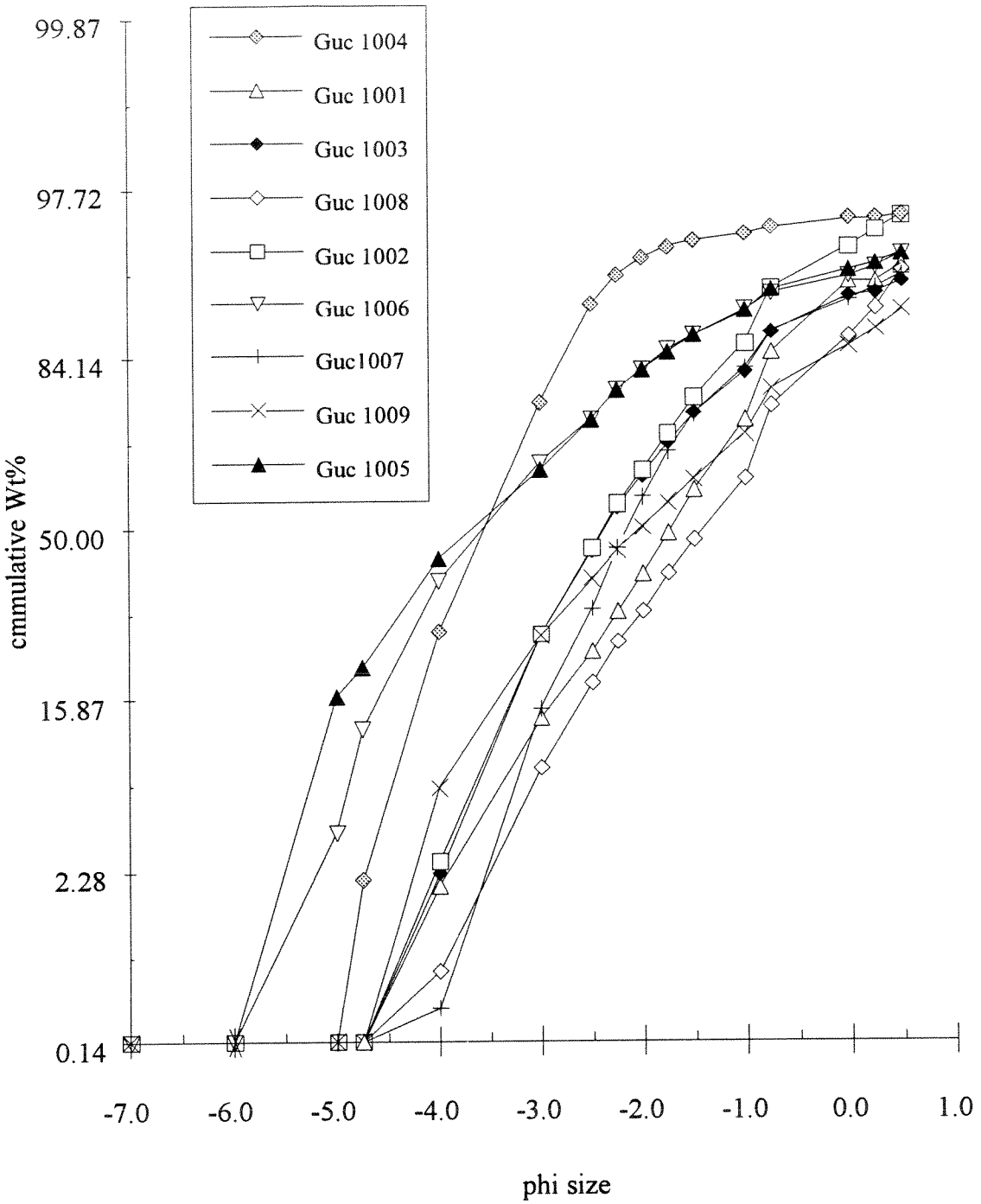


Figure III-7. Probability plot of scoria particle size distribution. Non-straight lines indicate a deviation from a perfectly log-normal distribution. Possible explanations include more than one population being present and a non-log-normal distribution.

based on Sr, Nd, and Pb isotopes [Walker et al., in press], have Ba, La and Ba/La values approximately the same as the basalts being studied (see Table III-1). Therefore, the small amount of assimilation required by the isotope data causes only minor shifts in Ba/La and La/Yb. Furthermore, because assimilation is greatest for the lavas with the lowest MgO, all samples with less than 5 wt % MgO were removed from consideration. The crustal sample (diorite), which is the most appropriate assimilant for explaining the Sr, Nd and Pb isotopic variations has La/Yb and Ba/La values right in the middle of the array of southeast Guatemalan magmas. Adding 10% of this diorite to the most different lava sample causes a small shift in Ba/La from 45 to 42 (see Figure III-4).

I suggest that variation in the amount of subducted slab component is responsible for the variations in Ba/La and La/Yb, as has been proposed for the volcanic front [Carr et al., 1990]. Higher Ba/La indicates a greater amount of slab fluid, which causes higher degrees of melting and therefore lower La/Yb ratios. This conclusion is supported by the results of Stolper and Newman [1994] from the Mariana back-arc. In that region, the volatile content correlates positively with degree of melting.

The spatial distribution of Ba/La and La/Yb ratios was examined carefully to determine if there were any trends relating to distance from the arc front or location within the Ipala Graben relative to the bounding normal faults; I was unable to discern any systematic patterns. The highest and lowest values of Ba/La (in this back-arc region) occur in cinder cones separated by only 5 km. Because there is no spatial variation in Ba/La or La/Yb except for a possibly wider range near the front and a smaller range behind, the slab fluid is apparently randomly distributed in this back arc volcanic field. The data could not be examined for a potential pattern in time as no ages are available.

Hydrous flux, as indicated by Ba/La ratios, may be a primary control on magma volume. However, cinder cone volumes range from about 10% to 30% of a given lava volume [Wood, 1980a] indicating there is considerable variation (in cinder cone volume relative to total erupted volume) that can be attributed to factors other than magma flux.

Grain sizes in pyroclastic deposits are related to the explosive energy of the eruption; higher explosive energies should result in smaller grains (thus larger grain sizes in ϕ units) [Cas and Wright, 1988]. The strong positive correlation between grain size mode (in ϕ) and cinder cone volume, which is observed in southeast Guatemala, suggests that the weaker correlation observed between medium grain size (in ϕ) and cone volume is real. A positive correlation between cinder cone volume and median grain size (in ϕ) would suggest that larger cinder cones are formed by more explosive eruptions, which might be due to higher volatile content. However, a much larger number of samples, than the nine presently existing, is needed to confirm any correlation with median grain size.

Wood [1980a] previously suggested that higher volatile content leads to greater explosivity and larger cinder cones and attributed the variation in volatile content to differences in magma chamber depth. The chemistry of lavas in southeast Guatemala is not consistent with a significant variation in source depth as all lavas appear to have fractionated near the base of the crust [Walker, 1981]. The relationship derived by Wood [1980a] between lava flow volume and cinder cone volume suggests that, as the total volume increases, the proportion of the total magma that is included in the cinder cone volume increases: Wood [1980a] proposes that $CV = 0.00078 \times FV^{1.26}$, where CV is the cinder cone volume and FV is the lava flow volume; the exponent is larger than one, which results in CV increasing faster than FV. This could be explained by an increase in volatile content with magma volume. Stolper and Newman [1994] observed that the volatile content of back-arc lavas increases with increasing slab influence. I observe no correlation between scoria grain size and Ba/La (slab influence), but the values observed do not contradict such a relationship. Additionally, there is no simple relationship between initial volatile content of the magma and the vesicularity of Strombolian pyroclastic deposits [Wilson, 1980]. I cannot confirm or contradict the hypothesis that increasing slab influence results in an increase in magma volatile content.

TECTONIC IMPLICATIONS

The observed random distribution of slab influence in this back arc volcanic field suggests that slab influence is incidental to the tectonic processes that primarily control magma generation (Figure III-8). Furthermore, magma with Ba/La values as low as 18 occur (only slightly higher than values for MORB), suggesting that there is at most a minor slab component and implying that hydrous flux is not the sole cause of volcanism. I agree with Walker et al. [in press] that tectonically generated back arc extension causes asthenospheric decompression along the Ipala Graben, which leads to magma generation. Within the asthenosphere beneath the Ipala Graben, regions metasomatized by hydrous flux have greater degrees of melting, produce larger volumes of magma and lead to eruptions forming larger cinder cones.

RESULTS OF CHAPTER III

The data reported in this paper imply that hydrous flux from the subducted slab is an important factor in determining cinder cone size. The dependence of cinder cone volume in Guatemala on both the degree of partial melting (La/Yb) and the amount of slab influence (Ba/La) suggests that the amount of slab influence is a primary control of the amount of magma generated (even though the trigger for mantle melting is likely to be adiabatic decompression). Larger volumes of magma (corresponding to larger cinder cones) may have higher initial volatile contents, although this still needs to be verified. I note that the use of Ba/La as a proxy for hydrous flux may be strongly dependent on the especially Ba-rich nature of subducted sediments in this region.

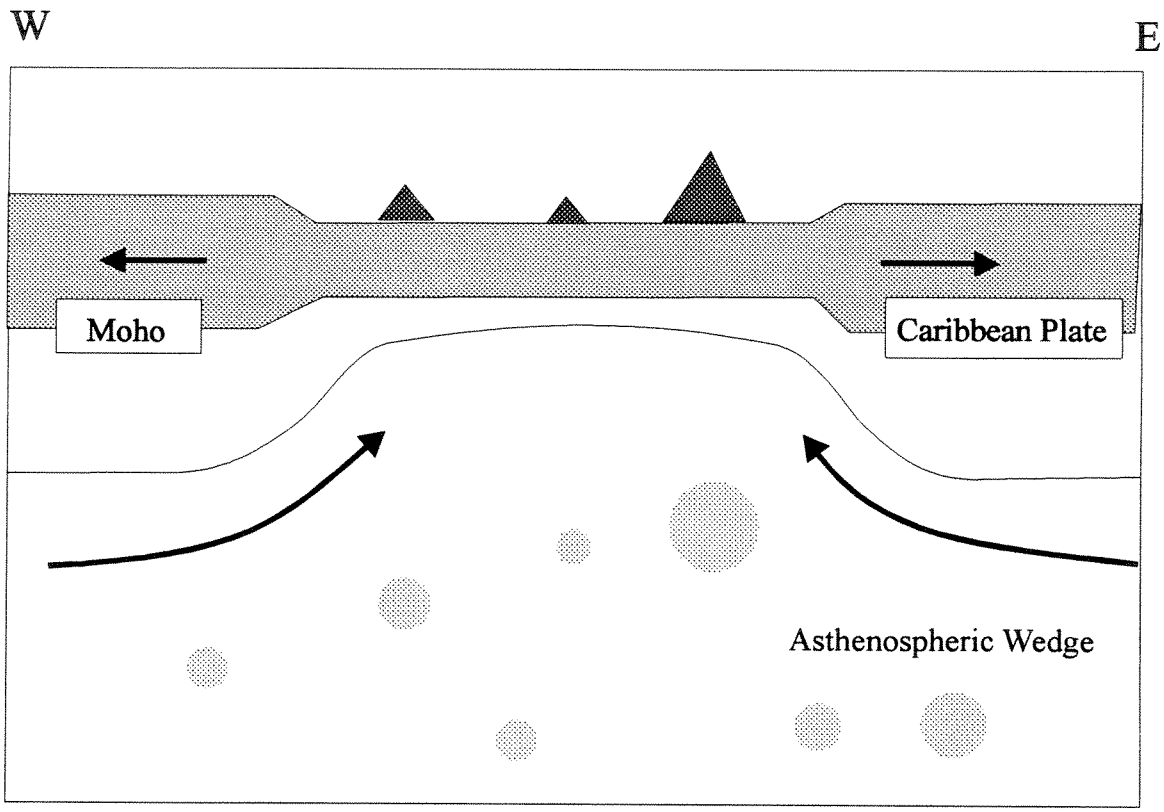


Figure III-8. Schematic longitudinal section, parallel to the volcanic front and about 40 km behind it, illustrates my conception of the tectonic controls on magmatism in southeast Guatemala. The transform interaction of the North American and Caribbean plates causes back-arc extension within the Caribbean plate, which results in asthenospheric decompression. Melt is generated in locations experiencing both decompression (solid arrows) and the randomly distributed hydrous flux from the subducted slab (stipled regions). Larger cinder cones overlie larger fluxes (larger stipled regions) of slab fluid.

REFERENCES CITED

Bemis, K. G., and Carr, M. J. Volcano morphology in Guatemala, *EOS, Trans. AGU*, 74, 333, 1993.

Blackburn, E. A., Wilson, L., and Sparks, R. S. J. Mechanisms and dynamics of strombolian activity, *J. Geol. Soc. London*, 132, 429-440, 1976.

Bohnenberger, O. H. Los focos eruptivos cuaternarios de Guatemala. Trabajos Technicos Presentados en la Segunda Reunion de Geologos de America Central, Publicaciones Geológicas del Institutio Centroamericano de Investigacion y Tecnologia Industrial, Numero II, 1969.

Burkart, B., and Self, S. Extension and rotation of crustal blocks in northern Central America and effect on the volcanic arc, *Geology*, 13, 22-26, 1985.

Carr, M. J., Feigenson, M. D., and Bennett, E. A. Incompatible element and isotopic evidence for tectonic control of source mixing and melt extraction along the Central American Arc, *Contr. Min. Petrol.*, 105, 369-380, 1990.

Carr, M. J. Symmetrical and segmented variation of physical and geochemical characteristics of the Central American front, *J. Vol. Geotherm. Res.*, 20, 231-252, 1984.

Cas, R. A. F., and Wright, J. V. *Volcanic Successions: Modern and Ancient*, London: Chapman and Hall, 1988.

Dehn, J. Model of cinder cone formation, M. S. thesis, Arizona State University, 1987.

Glazner, A. F., and Farmer, G. L. Production of isotopic variability in continental basalts by cryptic contamination, *Science*, 255, 72-74, 1992.

Hasenaka, T., and I. S. E. Carmichael. The cinder cones of Michoacán-Guanajuato, Central Mexico, their age, volume and distribution, and magma discharge rate. *J. Vol. Geotherm. Res.*, 25, 105-124, 1985.

Head, J. W., III, and L. Wilson. Basaltic pyroclastic eruptions, influence of gas-release patterns and volume fluxes on fountain structure, and the formation of cinder cones, spatter cones, rootless flows, lava ponds, and lava flows. *J. Vol. Geotherm. Res.*, 37, 261-271, 1989.

Inbar, M., Hubp, J. L., and Ruiz, L. V. The geomorphological evolution of the Paricutin cone and lava flows, Mexico, 1943-1990, *Geomorphology*, 9, 57-76, 1994.

Leeman, W. P., Carr, M. J., and Morris, J. D. Boron geochemistry of the Central American Volcanic Arc: constraints on the genesis of subduction-related magmas, *Geochim. Cosmochim. Acta*, 58, 149-168, 1994.

McGetchin, T. R., Settle, M., and Chouet, B. A. Cinder cone growth modeled after Northeast Crater, Mount Etna, Sicily, *J. Geophys. Res.*, 79, 3257-3272, 1974.

Morris, J., Leeman, W. P., and Tera, F. The subducted components in island arc lavas: constraints from Be isotopes and B-Be systematics. *Nature*, 344, 31-36, 1990.

Pike, R. J., and Clow, G. D. Revised classification of terrestrial volcanoes and catalog of topographic dimensions, with new results on edifice volume, U. S. Geological Survey Open-File Report 81-1038, 1981a.

Plank, T., and Langmuir, C. H. Tracing trace elements from sediment input to volcanic output at subduction zones, *Nature*, 362, 739-742, 1993.

Plafker, G. Tectonic aspects of the Guatemala earthquake of 4 February 1976, *Science*, 193, 1201-1208, 1976.

Smith, D. K. Shape analysis of Pacific seamounts. *Earth Planet. Sci. Lett.*, 90, 457-466, 1988.

Smith, D. K. and Cann, J. R. The role of seamount volcanism in crustal construction at the Mid-Atlantic Ridge (24°-30°N), *J. Geophys. Res.*, 97 (B2), 1645-1658, 1992.

Stolper, E., and Newman, S. The role of water in the petrogenesis of Mariana trough magmas, *Earth Planet. Sci. Lett.*, 121, 293-325, 1994.

Walker, G. P. L., and Croasdale, R. Characteristics of some basaltic pyroclastics, *Bulletin Volcanologique*, 35 (2), 303-317, 1972.

Walker, J. A. Petrogenesis of lavas from cinder cone fields behind the volcanic front of Central America, *Journal of Geology*, 89, 721-739, 1981.

Walker, J. A., Carr, M. J., Patino, L. C., Johnson, C. M., Feigenson, M. D., and Ward, R. L. Abrupt change in magma generation across the Central American arc in southeastern Guatemala: flux dominated melting near the base of the wedge to decompression melting near the top of the wedge, *Contrib. Mineral. Petrol*, in press.

Williams, H., McBirney, A. R., and Dengo, G. *Geologic reconnaissance in southeastern Guatemala*, Univ. California Publ. Geol. Sci., 50, 1-56, 1964.

Wilson, L. Relationships between pressure, volatile content and ejecta velocity in three types of volcanic explosion, *J. Volc. Geotherm. Res.*, 8, 297-313, 1980.

Wood, C. A. Morphometric evolution of cinder cones, *J. Volc. Geotherm. Res.*, 7, 387-413, 1980a.

Wood, C.A. Morphometric analysis of cinder cone degradation, *J. Volc. Geotherm. Res.*, 8, 137-160, 1980b.

Wood, C. A., and Schuver, H. J., What determines a volcano's form?, *in* Reports of Planetary Geology Program, Wash., D. C., NASA TM-84211, 541-543, 1981.

Chapter IV. Modeling cinder cone growth and degradation

INTRODUCTION

Cinder cone morphology has been extensively documented and related to eruptive processes [McGetchin et al, 1974; Blackburn et al., 1976; Dehn, 1987; Wood, 1980a] and erosion [Wood, 1980b; Dohrenwend et al., 1986]. Most cinder cones are composed of basalt and basaltic andesite and formed by short-lived eruption sequences. Strombolian eruptions, which are typical cinder cone forming eruptions, are generated by degassing and decompression of the volatiles in the magma. The morphology of the cone and the grain size of the scoria should reflect the volatile content of the magma. The volatile content of the magma controls the amount and velocity of ejected material through the processes gas exsolution and expansion. The bulk of the erupted magma emerges passively in the form of lava flows during or after the violent phase of the eruption [Wood, 1980a].

Variations in the size of cinder cones can be attributed to magma supply and eruption duration, but the causes of variations in shape are less clear. Guatemalan cinder cones show a particularly large range in shape compared to cinder cones in previous studies [Wood, 1980a; Porter, 1972]. There are two existing models that might account for variations in the shape of cinder cones. McGetchin et al. [1974] attributes differences in cinder cone shape to variations in the factors that control Strombolian eruptions. Differences in eruption velocity, particle size or density, and vent width result in differences in cinder cone shape [McGetchin et al., 1974; Dehn, 1987]. The second model attributes differences in shape to degradational processes [Wood, 1980b]. Erosion, modeled as material moved from the top of the cone to the base, results in decreased height and increased basal diameter and top diameter, but does not affect volume. Cinder cones may also be affected by burial by lava flows, sediment or ashfalls; this decreases height, basal diameter and volume but leaves top diameter unchanged.

This chapter is intended to determine the variance in shape of Guatemalan cinder cones and the processes (eruptive or erosional) that control the variance in shape. The relative merits of two models of shape variance (McGetchin's growth model and Wood's erosion model) are discussed, with specific application to the cinder cone data from Guatemala. This chapter concludes that the McGetchin growth model best explains the variance in shape observed in Guatemalan cinder cones. Variation in ejection velocity and vent width can account for the total range of morphologies observed in Guatemalan cinder cones; average ejection velocities of 110-190 m/s and vent widths ranging from 40 m to >100 m are interpreted for the Guatemalan cinder cones. However, the morphologic results of erosion and growth are not completely separable.

Geomorphology of Guatemalan cinder cones

The Ipala Graben region in southeast Guatemala is an area of basalt-rhyolite volcanism [Williams, et al., 1964; Bohnenberger, 1969] behind the volcanic front of Central America (Figure IV-1). Quaternary, and earlier, extension has been previously documented along the north trending Ipala Graben, within which most of the volcanism occurs [Plafker, 1976; Burkart and Self, 1985]. More than 95 cinder cones are associated with lava flows and small shield volcanoes (Figure IV-1). Rhyolitic domes occur approximately in the center of the volcanically active region. The cones are estimated to be Holocene or slightly older; some cones and associated flows have little vegetative cover and appear to be comparable in age to the older historic flows along the volcanic front. All of the back-arc volcanism in northern Central America is related to local extensional structures that generally trend N-S, oblique to the volcanic front. Several areas of behind-the-front volcanism occur in Central America; the Ipala Graben is by far the largest of these. The Ipala Graben extends across the Jocotán fault, an E-W striking, left-lateral, strike-slip fault that, together with the similarly oriented Motagua and Polochíc faults to the north, comprise the Caribbean-North American plate boundary [Plafker, 1976]. Thus

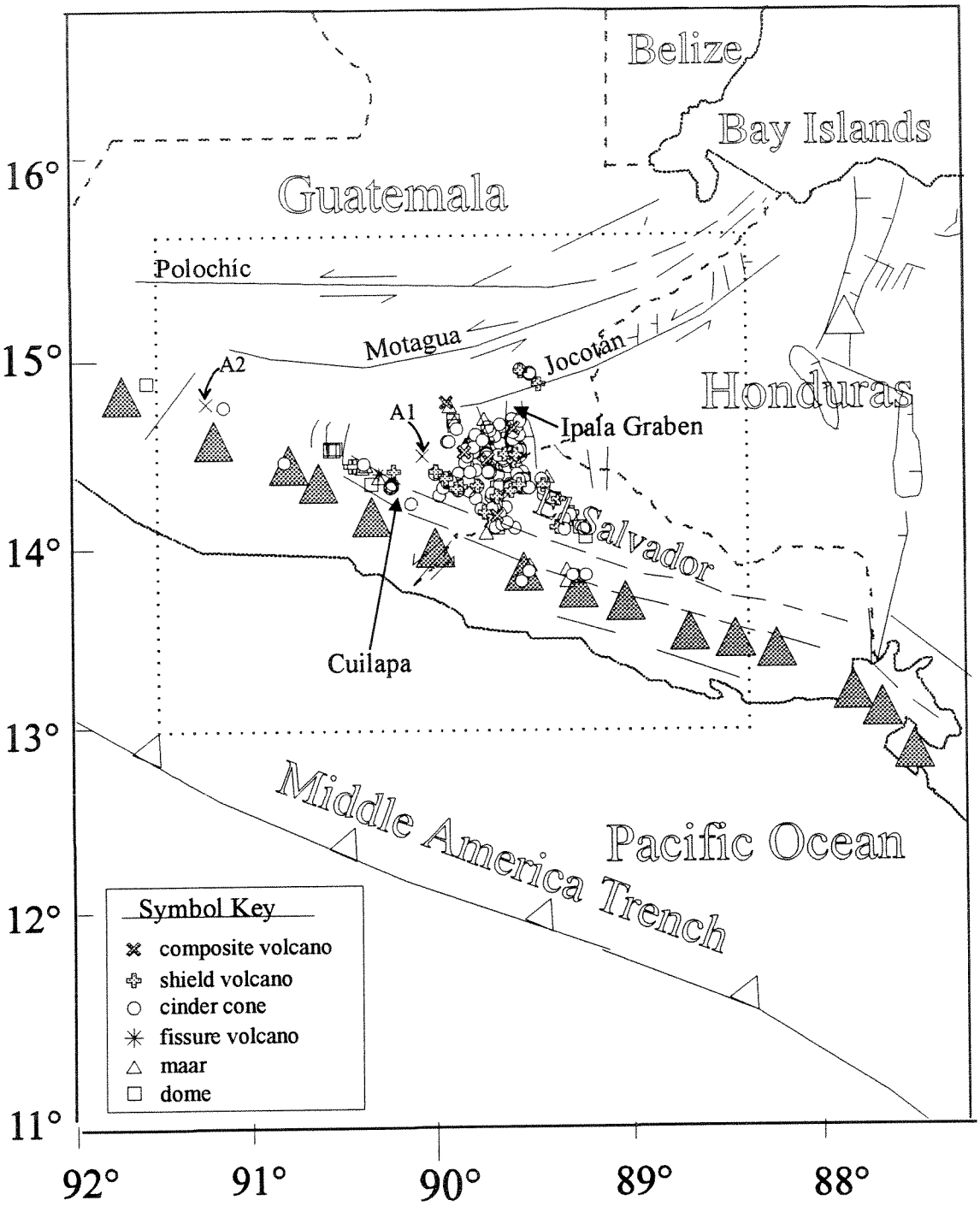


Figure IV-1. (a) Location of the area studied is the Ipala Graben in southeast Guatemala. The large triangles indicate arc front volcanoes. The small symbols indicate volcano type (see inset). Thick lines are coastlines; dashed lines are country boundaries; thin lines are faults. A1 and A2 indicate Ayarza Caldera and Atitlan Caldera, respectively. Box indicates area enlarged in (b).

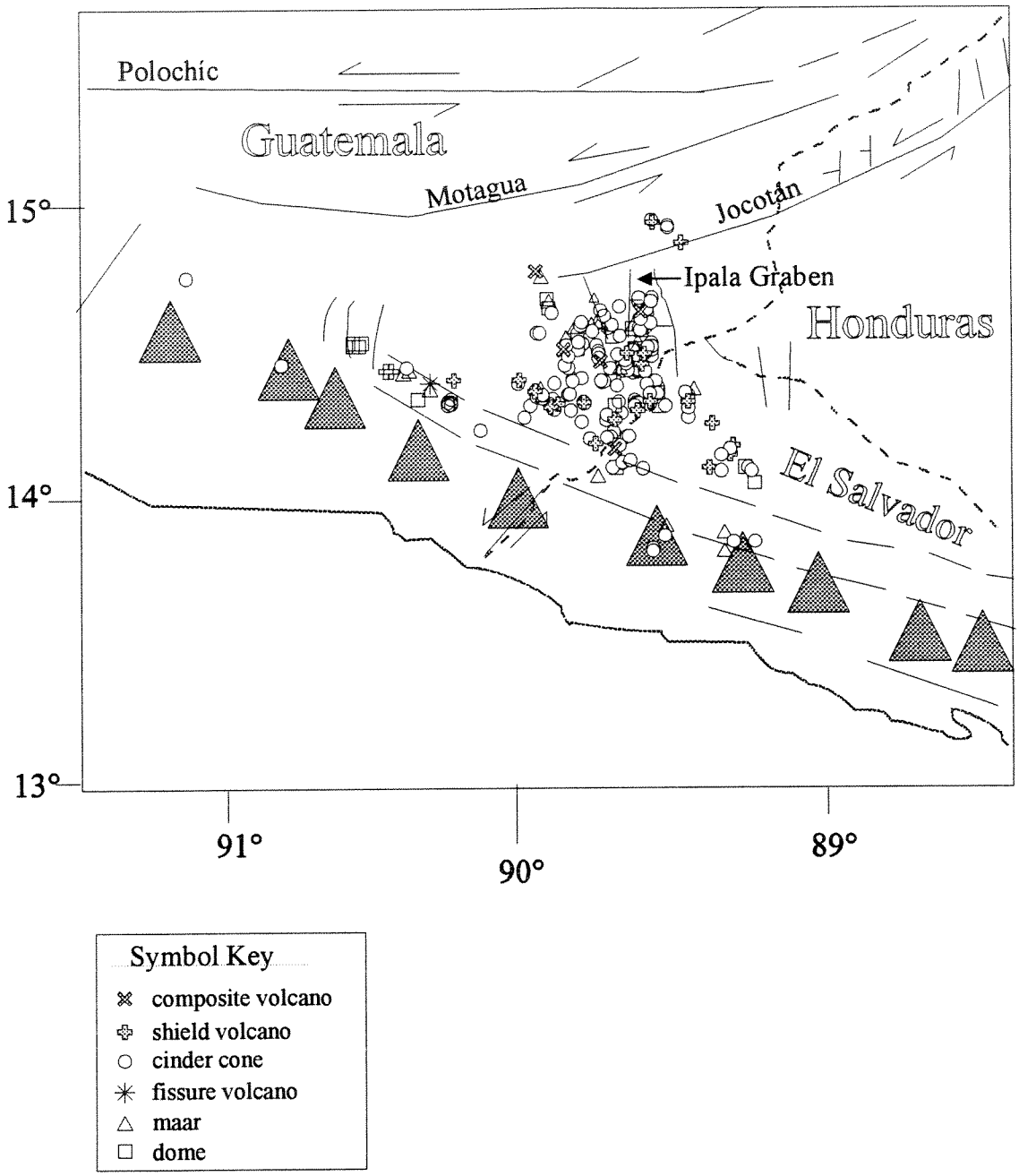


Figure IV-1. (b) Close-up of volcano location in the Ipala Graben, Guatemala and surrounding area.

the tectonic setting of this volcanic region is a composite of back-arc and transform settings [Burkart and Self, 1985].

Air photographs and topographic maps allowed clear determination of volcano morphology, using a modification of criteria developed for submarine volcanoes [Smith 1988; Smith and Cann, 1992; Bemis and Carr, 1993]. Details of the measurements are discussed in Chapter II. For each cinder cone, the height (h), basal diameter (2r), and crater diameter (2t) were measured (Figure IV-2) and the values of h/r, t/r, slope and volume calculated from those measurements (Table IV-1). Note that the crater diameter (2t) is a geomorphic measure determined by the break in slope near the volcano summit and is not determined by the actual placement of any crater rim; for cinder cones, the two measures will generally coincide, but only the first is consistently discernible on topographic maps. Errors in horizontal measurements are around 50-100 m; errors in vertical measurements are 10-20 m. Ratios generally vary less than 10% with the projected errors; volumes are also determined with an error of about 10%.

Scoria was sampled from nine cinder cones in the Ipala Graben and sieved to determine grain size characteristics (details of techniques and results are reported in Chapter 3). The median grain size, Md_ϕ= -2.2 (4.6 mm), and the dispersion (sorting), σ_ϕ= 1.3, indicate that the scoria came from Strombolian-type eruptions based on the Md_ϕ-σ_ϕ plots of Walker and Croasdale [1972]. In general, the smaller cones have less well-sorted, coarser scoria and the larger cones have more well-sorted, finer scoria (see Chapter III).

The observations of this study are mostly consistent with previous studies of cinder cone morphology [Wood, 1980a; Wood, 1980b; Porter, 1972] (compare Table IV-1 and Table IV-2). Height and basal radius increase at about the same rate: Wood [1980a] reports h=0.36r as consistent with relatively uneroded cones in many localities (n=83), while this study finds h=0.35r (n=30) for Guatemalan cinder cones. The average height-to-radius ratios for uneroded cinder cones in the Ipala Graben is h/r=0.35±0.07 (n=30; #gullies>10). All of the cinder cones (n=157) show a large range in both h/r (0.00-0.67)

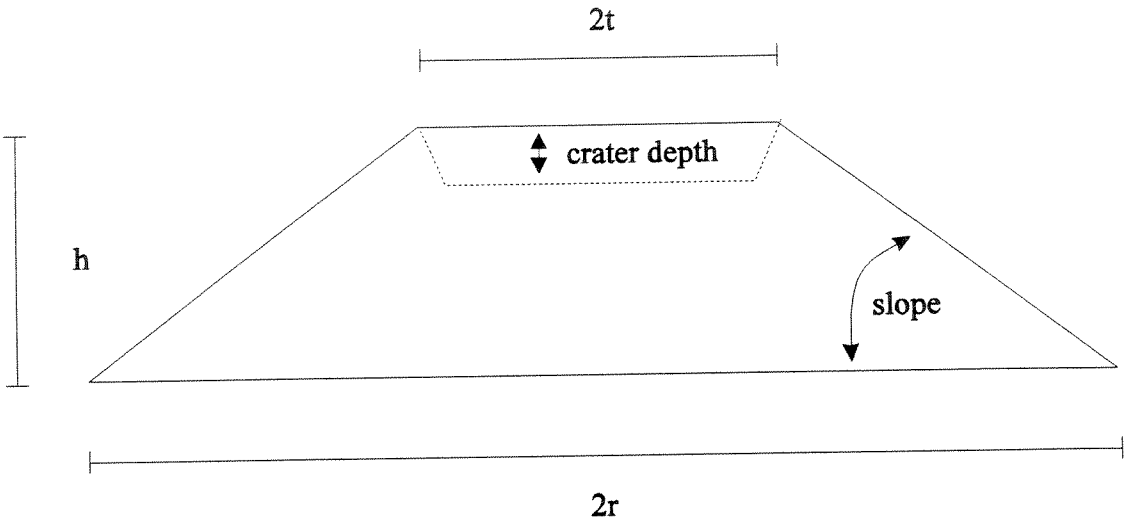


Figure IV-2. Morphometric model of cinder cone indicates the physical dimensions measured to obtain height (h), basal diameter (2r) and top diameter (2t). Physical significance of crater depth and slope are also indicated. Application of model to actual volcanoes is discussed in Chapter II.

and t/r (0.00-0.60). Wood [1980a, 1980b] observed little variation in t/r with degradation and some dependency of t/r on the variability, or lack thereof, in eruption intensity. This study observes that the uneroded cones show a significant variation in t/r (0.16-0.48) with an average (t/r=0.33±0.08) lower than Wood's [1980a,1980b] and Porter's [1972] best fit ratio; this suggests both more variability and a difference in eruption conditions for the cones of this study compared to those studied previously.

Correlations among the observed morphologic parameters are tabulated in Table IV-3 for Guatemalan cinder cones. The h/r ratio increases slightly with increasing h (R=0.72) and appears independent of r (Figure IV-3; Table IV-3). The largest cinder cones exhibit h/r ratios of 0.50-0.60, much larger than any observed in previous studies [Wood, 1980a]. Slope generally reflects h/r (R=0.83), but shows a less definite increase with height (R=0.49). Slope tends to approach but not greatly exceed the theoretical angle of repose (33°); highest slopes are around 35° - with a few exceptions that can be attributed to geometric problems and limited resolution.

The t/r ratio appears independent of h and r (Figure IV-3), but does increase with increasing t (R=0.79). Note that Wood [1980a] and Porter [1972] observed a consistent increase in t with increasing r, implying a constant t/r ratio of 0.40. This study does observe that t increases with r, but with more spread in the actual rate of increase in t relative to r and at a lower average ratio between t and r (0.33).

Based on aerial photographs, the relative amount of vegetation and cultivation and the number of gullies present was recorded for each cinder cone present. Hasenaka and Carmichael [1985] observe that, for cinder cones in Mexico, vegetation and cultivation increase with age while the number of gullies decreases. By combining, these three measures of degradation using a nominal scale (1 = least vegetation/cultivation, most gullies; 2 = moderate; 3 = most vegetation/cultivation, least gullies), some measure of the degree of erosion is obtained for each of 106 cinder cones (some of the 157 cinder cones identified were not imaged on the aerial photographs). None of the morphological

parameters considered in this study (h, r, t, h/r, t/r, slope, volume) vary consistently with the degree of erosion (as given by the erosion # defined above) (Figure IV-4). Hasenaka and Carmichael [1985] also found no change in h/r with age and in slope with age; they concluded that the initial post-eruptive form of cinder cones changes slowly, if at all, over 40 ka. They did find that the number of gullies (the initial stage of erosion) decreases systematically with age from around 30 per 90° at zero age to 10 per 90° at 40 ka. I also compared the morphologic parameters with the number of gullies per 90° and found no correlations (Figure IV-5). This suggests that the overall degree of erosion is small, which is consistent with the young age estimated for the Ipala Graben cinder cones. Tephra from the Atitlan Caldera explosion dated at 84 ka [Drexler et al., 1980] is observed elsewhere in Guatemala but nowhere in the Ipala Graben. In the nearby Cuilapa region, cinder cones are observed to sit on top of tephra that is correlated either with the tephra of the Arayza Caldera dated at 23 ka [Peterson, 1980].

Table IV-1. Summary of morphologic measurements.

Shape	All cones:[1]		Uneroded cones:[2]		
parameter	Range	Average	Range	Average	Regression[3]
h (m)	0-270	110± 50	87-201	140± 30	na
2r (m)	253-1400	670±240	508-1185	790±160	na
2t (m)	0-748	180±150	129-415	260± 80	na
h/r	0.00-0.67	0.33±0.09	0.23-0.50	0.35±0.07	h=0.35r
t/r	0.00-0.60	0.24±0.17	0.16-0.48	0.33±0.08	t=0.32r
slope (°)	0-43	24± 7	20-43	28± 5	na
volume (km^3)	0-0.117	0.025±0.025	0.009-0.105	0.036±0.024	na
d (m)	0-125	23±29	0-125	39±37	d=.14(2t)

[1]n=133.
[2]Uneroded cinder cones were selected for having #gullies/90° >= 10 in this study; n=30.
[3]Constant term forced to zero; n=27. Note d = crater depth.

Table IV-2. Summary of cinder cone morphology reported by previous studies.

Reference:	Wood, 1980b			Wood, 1980a	Porter, 1972
Location	SFVF, Az.				
"Age"	<0.05 My	0.2-0.7 Ma	0.8-6 My	fresh	fresh
h (m)	60-350[1]	40-300[1]	20-60[1]	20-380	10-200
2r (m)	300-1700[1]	250-2500[1]	250-1800[1]	100-1800	100-1250
2t (m)	250-600[1]	50-800[1]	-	130-650	50-650
h/r	0.36 (9)*	0.25 (24)*	0.08 (5)*	~0.36 (83)*	0.36 (31)*
t/r	~0.40	~0.40	~0.40	~0.40 (83)	0.40 (62)*
slope	30.8°±3.9° (7)	23.1°±2.0° (15)	14.1°±4.2° (5)	-	26.5° (28)*
crater depth	-	-	-	-	10-100 m; d=0.14(2t)

Numbers in parenthesis are the number of volcanoes over which average or fit was obtained.
*Value obtained by regression of v1=A v2, where A is the reported value of the ratio v1/v2.
[1]Values read off graph.

Table IV-3. Correlations between morphologic variables.

Correlation	all cones			uneroded cones			
between:	R	t	n	R	t	n	Confidence*
h & 2r	0.73	13.36	155	0.66	4.67	30	>99.8%
h & 2t	0.18	1.87	113	0.30	1.67	30	80%
2t & 2r	0.65	9.15	113	0.63	4.35	30	>99.8%
h/r & h	0.64	10.16	155	0.58	3.78	30	>99.8%
h/r & 2r	0.00	0.05	155	-0.22	-1.20	30	n.c
h/r & 2t	-0.35	-3.94	113	-0.28	-1.55	30	80%
t/r & h	0.30	3.91	155	-0.15	-0.61	30	n.c.
t/r & 2r	0.46	6.50	157	0.04	0.18	30	n.c.
t/r & 2t	0.72	10.96	113	0.79	6.72	30	>99.8%
slope & h	0.67	11.12	155	0.49	2.97	30	99%
slope & 2r	0.26	3.30	155	-0.17	-0.94	30	n.c.
slope & 2t	0.06	0.59	113	0.18	0.99	30	n.c.
h/r & t/r	-0.05	0.61	155	-0.18	-0.96	30	n.c.
slope & h/r	0.73	13.24	155	0.83	7.90	30	>99.8%
slope & t/r	0.62	9.68	155	0.35	2.00	30	90%

* Indicates confidence level at which would accept correlation to be true; >99% is a strong criteria; 90-99% is moderate but may be acceptable given the expected error and no reason for a linear fit; 80-90% is very weak and results in accepting unlikely correlations.

n.c. = no confidence.

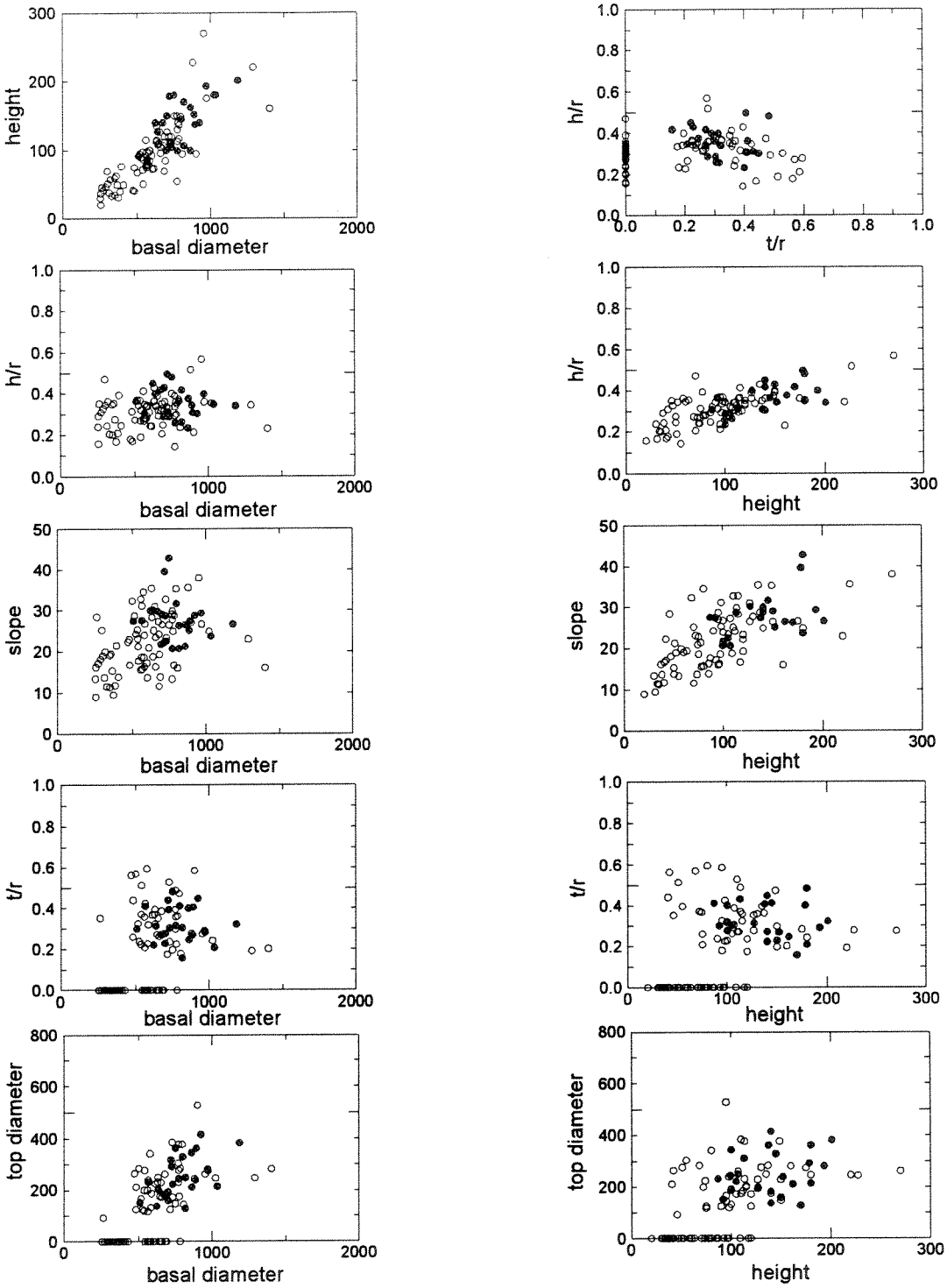


Figure IV-3. Measurements of the basic shape parameters (height, basal diameter and top diameter) are combined to show how the shapes of cinder cones vary. Values are in meters, except for ratios which are non-dimensional. Solid circles are relatively uneroded cones (#gullies /90° >= 10); open circles are relatively more eroded cones (#gullies/90° < 10).

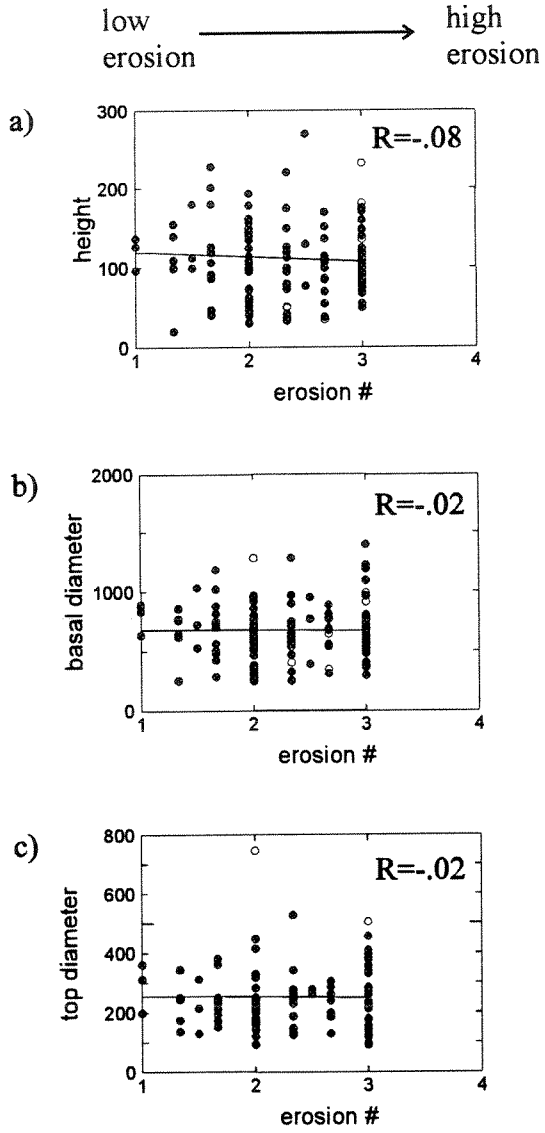


Figure IV-4. Measured shape parameters are compared with the erosion number, which measures the relative amounts of vegetation and cultivation on a cinder cone and the number of gullies per 90°. No significant correlation with erosion number is observed, even though height is predicted to decrease with increasing erosion.

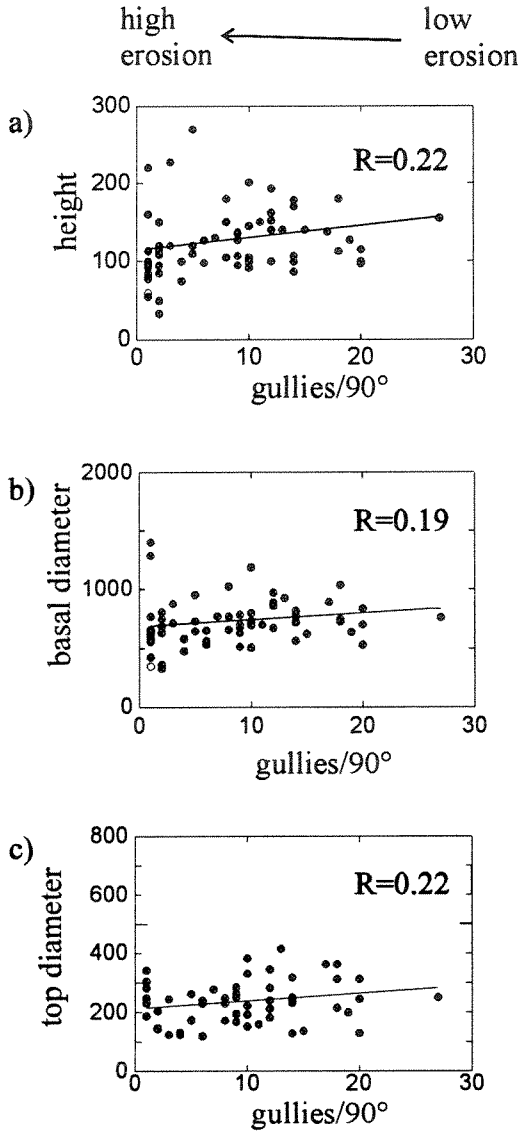


Figure IV-5. Measured shape parameters are plotted against the number of gullies per 90° to indicate the degree of erosion. The number of gullies per 90° has been observed to decrease with increasing age [Hasenaka and Carmichael, 1985]. The slight decrease in height, basal diameter and top diameter with decreasing numbers of gullies is statistically insignificant and visually uncompelling. There does not seem to be any significant erosion of any of the cones included in this study. While the number of gullies generally decreases with erosion, it also decreases with decreasing cone size and increasing dryness of the climate [Hasenaka and Carmichael, 1985].

McGetchin model

The model of cinder cone growth presented by McGetchin et al. [1974] predicts that cinder cones grow through four stages (Figure IV-6). In Stage 1, the distribution of ejected particles (ash, bombs, etc.) is controlled solely by ballistic processes; the shape of the cone is primarily dependent on the volume of erupted particles, the range in ejection angle and the ejection velocity. In Stage 2, the flank slope begins to over-steepen and the formation of talus starts. In Stage 3, the flank slope is controlled by talus formation and the crater rim location begins to shift inward due to talus formation. In Stage 4, talus formation controls the shape of the cone; the flank extends out beyond the ballistic limit and the crater rim is inside the location of the original ballistic rim [McGetchin et al., 1974]. In terms of the morphologic parameters measured in this study, for early stage cones (stages 1-3), the height-to-radius ratio h/r and average flank slope increase as the cone grows taller. Note that the basal diameter is basically constant until stage 3 and the height increases faster than the basal diameter. For later stage cones (stages 3-4), the height-to-radius ratio h/r and average flank slope are constant with growth because the talus slope is maintained at or near the angle of repose (~33°). The flatness (f=t/r) generally decreases with growth in all stages, but the rate of decrease is highest in the transition between ballistic and mass wasting processes controlling slope (stage 2-3).

The McGetchin model is the basis for a computer program modeling the growth of cinder cones [Dehn, 1987]. The original program [Dehn, 1987] calculates the ballistic paths for a group of particles of given size and density with a uniform distribution of ejection angles and velocities and then determines the stability of the landed particles in regards to the angle of repose (~33° for scoria). A copy of this program was modified to run in Qbasic on a Gateway 2000 386 model personal computer. Further modifications were made to the program as follows: (1) unnecessary graphics were eliminated - the original program showed traces of ballistic paths which was not needed for this project, (2) the distribution for ejection angles and velocities was changed from a uniform

distribution to a normal distribution, (3) calculations were rearranged to improve speed, and (4) screen input was reduced as this project did not need to change the atmospheric parameters from Earth normal values.

This program was run for an appropriate range of parameters (see Appendix D for procedure and parameters). Most of the parameters needed to control the computer simulations have little effect on the resultant geometry. Dehn [1987] reported that the five most important factors on cinder cone geometry were the ejection velocity, the ejection angle, gravity, assumed angle of repose and the wind speed and direction. Gravity is constant for this study as all cinder cones studied are on Earth. The angle of repose is assumed to be 33° as in Dehn [1987]. Wind effects are ignored as the morphologic data for Guatemalan cinder cones are obtained assuming axisymmetry. Through several trials, particle size and density were found to have virtually no effect on cone geometry. Ejection angles were assumed to be normally distributed between vertical and 75° from the horizontal based on results reported by Chouet et al. [1974]. Vent width has a major effect and there is very little field evidence as to actual vent widths [Wilson et al. [1980] refer to conduit widths of 5 m to 100 m as reasonable and expect near surface vent widths to be wider than the conduit at depth). Vent widths were chosen such that reasonable top diameters and t/r ratios were observed in the simulations. Ejection velocities were distributed normally over a range of 50 m/s and about a average value that varied between runs. A velocity range of 50 m/s seemed reasonable based on field studies of actual eruptions [Chouet et al., 1974; McGetchin et al., 1974]. The average velocity was varied from McGetchin et al.'s [1974] figure of 50 m/s for Northeast crater, Mt Etna to 170 m/s, which was necessary to reach cone sizes typical of southeast Guatemala before the slope reached 33°.

The computer simulation results confirm the above predictions of the McGetchin model with a few surprises (Figure IV-7). As shown by Dehn [1987], the simulations clearly show a progression through the four growth stages: The initial stage (phase < 3)

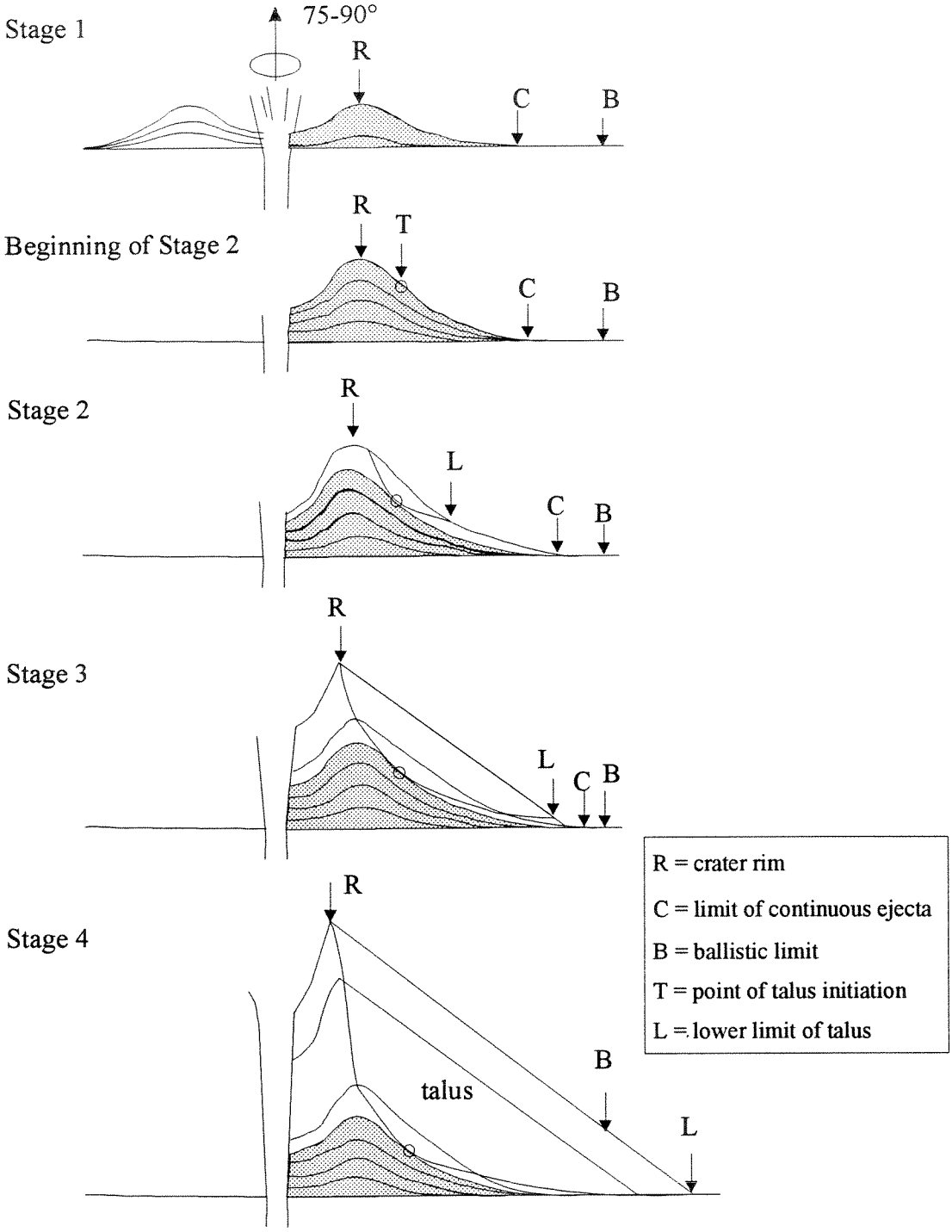


Figure IV-6. Cinder cone growth is modeled in four stages [McGetchin et al., 1974]. Initial growth is due to the buildup of ballistically implaced particles (Stage 1). Eventually, the flanks oversteepen and a talus slope develops (Stages 2-3). In the fully mature cone, landslide processes control slope and cone growth proceedes outwards and upwards at the same rate (Stage 4). After McGetchin et al. [1974].

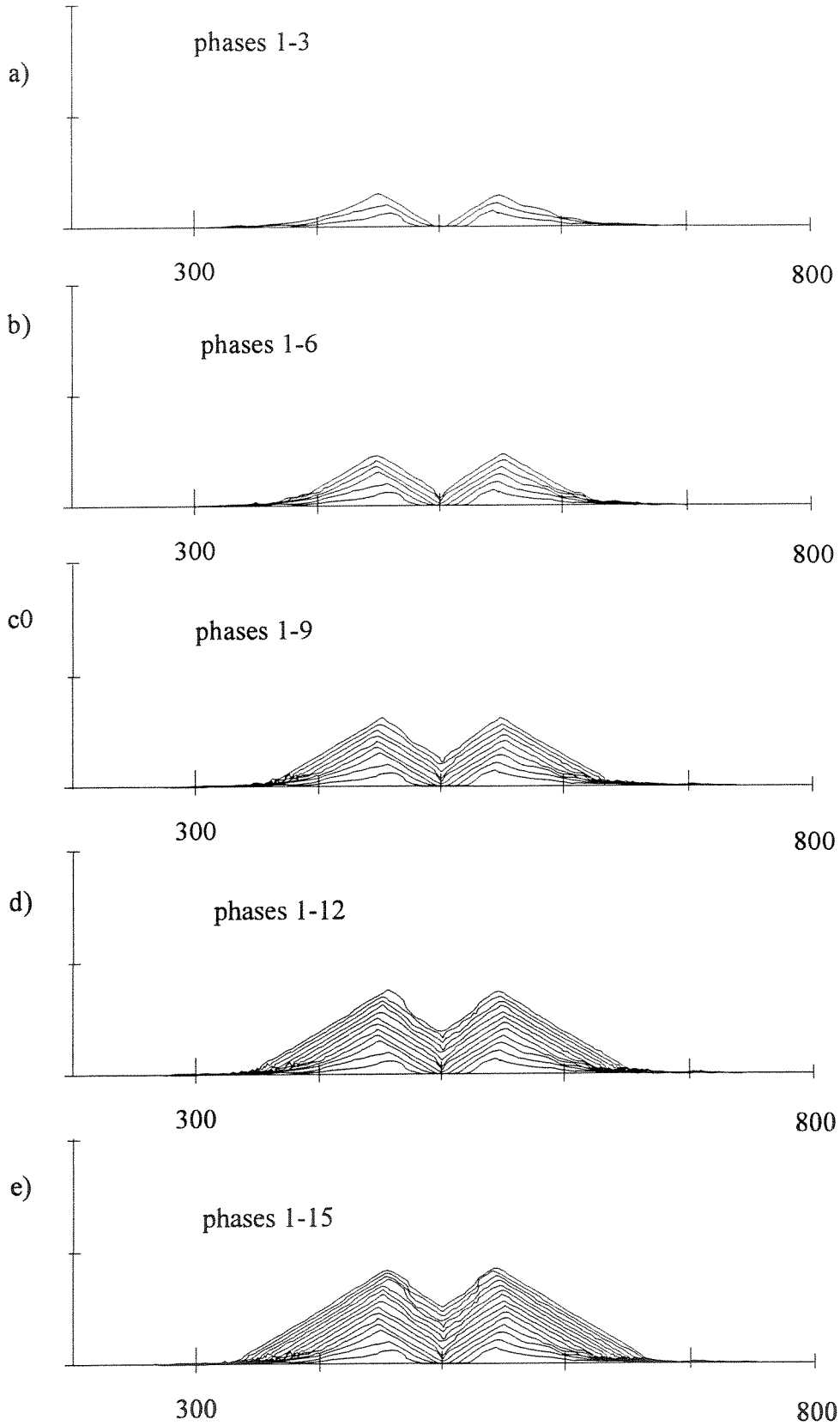


Figure IV-7. Profiles are of cinder cones simulated based on the McGetchin model.

of all simulated cones is characterized by shallow-sloped convex-up flanks (Figure IV-7a). Flanks steepen as growth proceeds (phase increases) (Figure IV-7b), eventually oversteepening and loosing their convex-up character (Figure IV-7c). As growth continues, flanks reach and retain the angle of repose while base widens (Figure IV-7d). Somewhat unexpectedly (as not predicted by the McGetchin model), the visual display indicated (by color coding) that almost all particle blocks moved slightly after ballistic emplacement and, not surprisingly, such movement downslope increased in both magnitude and frequency as flank slopes steepened. Local oversteepening, which is used to calculate the occurrence and magnitude of downslope movement in the simulations, may be more important than implied by McGetchin et al. [1974] for smaller, lower-sloped cones.

Morphological parameters were calculated for each simulated cone at several stages of growth (corresponding to phase = 3, 6, 9, 15); criteria for measurements were based on those developed for characterizing volcanoes on topographic maps. The program yielded, besides a visual display, a final topographic profile for each run (Figure IV-8). Heights correspond to the number of particle blocks deposited in that location times 1 m (the 'size' of the block) and were recorded for each 1 m interval for 500 m to each side of the vent center. The basal diameter is defined as the distance between the innermost uncovered ground (h=0) on each flank of the cone (Figure IV-8). Top diameter, corresponding to a crater diameter, is the distance between the outermost peak on each rim. The height of the cone is defined as the average of the maximum height on each rim. The other morphological parameters are calculated from these.

Figure IV-9 shows the results of simulation runs for an assumed vent width of 40 m and a range of velocities. As expected, h/r and slope increase with h until the slope reaches 33° (Figure IV-9). However, the h/r ratio flattens out at h/r=0.65 instead of the expected value of h/r = 0.36 [from Wood, 1980a]. The basal diameter generally remains constant until h/r and slope approach their asymptotes (it sometimes increases initially for

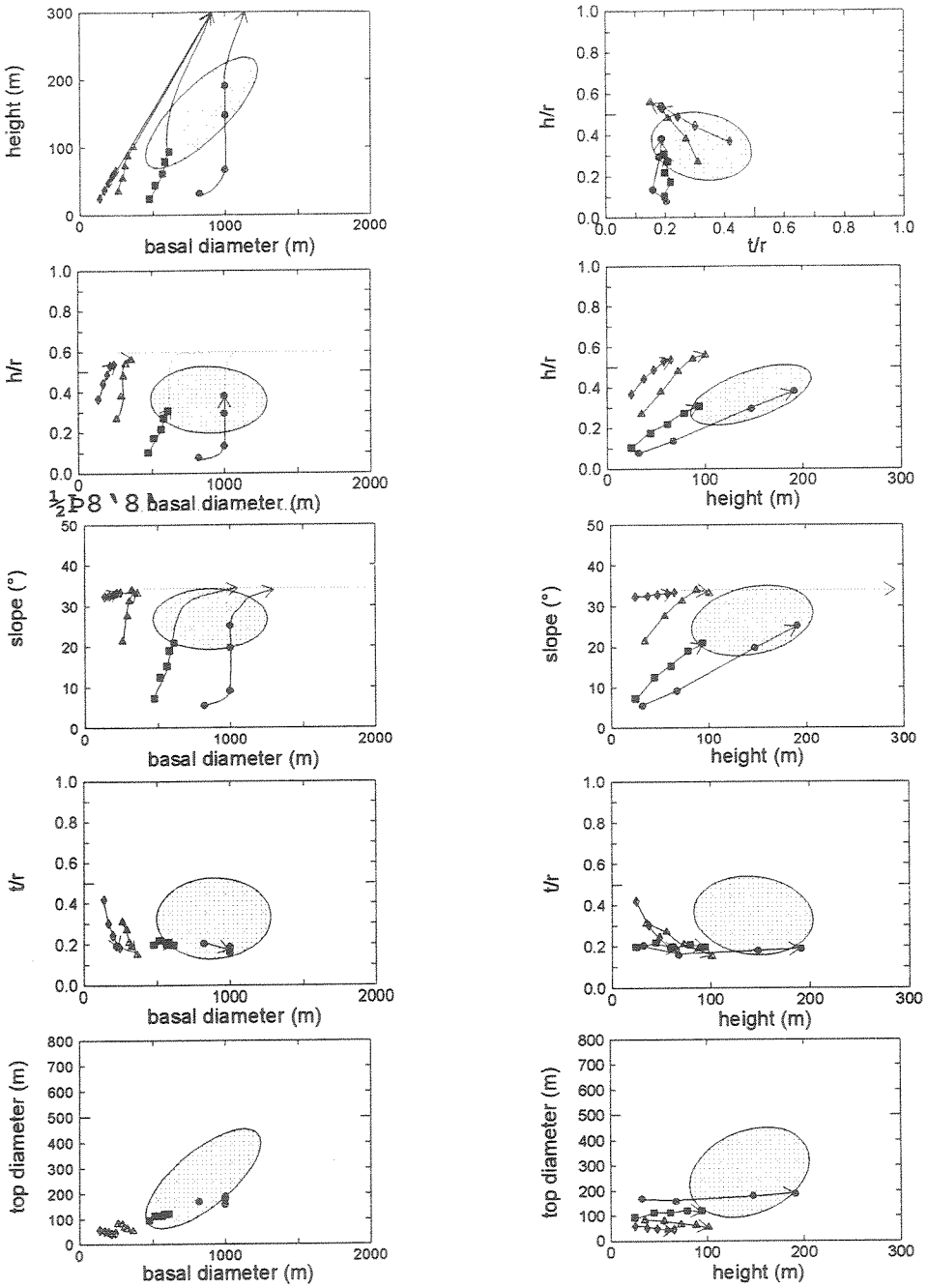


Figure IV-9. Mophologic parameters from cinder cone simulations based on the McGetchin et al. [1974] model are plotted for a vent width of 40 m. Symbols indicate the average ejection velocity for a given run: diamonds are 50 m/s, triangles 90 m/s, squares 130 m/s, and circles 170 m/s. Solid lines indicate growth trajectories and dotted lines indicate projected growth trajectories or asymtotes. Filled large ovals indicate the morphologic fields occupied by uneroded Guatemalan cinder cones (compare with Figure IV-3).

very small flat cones) as expected. The basal diameter is, therefore, a strong indicator of the ejection velocity, although eruptions of long duration could result in unusually high basal diameters (this case is detected by looking for higher h/r and slope than predicted for the basal diameter in a stage 2/3 cone). The top diameter t is highly dependent on vent width, increases consistently with basal diameter (really, velocity), and changes erratically with height if at all. Consequently, there is no clear decrease in t/r as h and volume increase as predicted by the McGetchin model.

The results of these simulations of cinder cone growth can best be summarized by predicting the range of ejection velocities and vent widths that can explain the range of observed morphologies. The average ejection velocity ranges from approximately 110 m/s to just over 170 m/s for Guatemalan cinder cones (the fresh cinder cones of Wood [1980a] would be formed by a similar range of velocities). The vent width needed to produce a given top diameter decreases slightly with increasing velocity (Table IV-4). Vent widths necessary to produce Guatemalan cinder cones range from 40->100 m for a velocity of 130 m/s to 20->100 m for a velocity of 170 m/s.

I also note that ejection velocity needed to produce a given cone of stage 3 or lower (indicated by h/r <0.65 and slope < 33°) is correlated with the size (basal diameter) of the cone. A comparison of Guatemalan cone morphologies and the simulated cones (Figure IV-9) suggests that cone size (as measured by basal diameter or volume) increases with ejection velocity. This is not predicted by the McGetchin model itself because continued eruption can produce larger cones for lower ejection velocities; however, those cones would all have reached stage 4 (and have h/r ~0.65 and slope ~33°). The cinder cones of Guatemala are mostly late stage 2 to stage 3 cones based on the h/r and slope ranges. In general, an average ejection velocity can be interpreted for each cinder cone based on its basal diameter; however, the simulation predictions of such ejection velocities are slightly sensitive to the input ejection velocity range, ejection angles, and vent widths (all of which are unknown in most cases).

Table IV-4. Vent widths to reproduce observed cinder cone top diameters.

Average Ejection Velocity	Vent Width = 20 m Top Diameter: Range	Average	Vent Width = 40 m Top Diameter: Range	Average	Vent Width = 100 m Top Diameter: Range	Average
50 m/s	10 - 23 m	14.4 m	42- 57 m	48.6 m	114 -119 m	116.6 m
90 m/s	21 - 56 m	36.6 m	53- 81 m	68.2 m	131 -147 m	142.2 m
130 m/s	68 - 97 m	83.2 m	94-121 m	111.8 m	143 -186 m	166.2 m
170 m/s	66 -103 m	87.2 m	158-188 m	173.3 m	170 -200 m	183.4 m

All cases are for 2000 traces and phase = {3,6,9,12,15}.

Wood model of cinder cone degradation

Wood [1980b] observes a decrease in h/r with degradation for cinder cones with ages ranging from present to 3 Ma. Significant degradation only occurred after 50 ka to 500 ka in the San Francisco Volcanic Field in Arizona [Wood, 1980b] consistent with Hasenaka and Carmichael's [1985] observations in Mexico. Note that the climate in Mexico is much wetter than it is in Arizona; the southeast Guatemalan climate is both wetter and warmer than the Arizona climate. Wood [1980b] explains the change in h/r with age by two models of degradation - burial and erosion. Burial (by lava flow or sediment) reduces the height of a cone by raising (and shrinking) the basal contour of the topographic feature corresponding to the cone. Burial leaves the remaining profile of the cone unchanged, resulting in (1) a decrease in h, r and h/r, (2) no change in t, and (3) an increase in t/r. Erosion is assumed to occur by removing material from the top of the cone and emplacing it at the base of the cone; consequently, the top diameter grows at the same rate as the base diameter does while the height decreases [Wood, 1980b]. In this case, h and h/r decrease, r and t increase and t/r and volume remain constant. In reality,

the actual effects of erosion on the crater diameter are not so clear and may depend on the degree of breaching; however, Wood [1980b] observed no variation in t/r with age.

Figure IV-10 shows the results of these models of degradation for cones of varying heights that start with h/r=0.36 and t/r=0.38 (chosen to match the average values reported by Wood [1980b] for uneroded (young) cones). Note that in neither case will h/r increase or t/r decrease from the starting values. In general, the erosion and burial models can account for about half the variation observed in Guatemalan cinder cones. To reach the remaining cones (which have higher h/r and lower t/r) would require assuming different starting values of h/r and t/r. The burial model does a reasonable job of explaining ranges and trends in t/r and h/r (especially when a range of starting h/r and t/r pairs is allowed), but cannot explain any variation in slope. Also, note that there is little evidence for extensive burial of many cinder cones in Guatemala. The erosion model can only account for the observed ranges in h/r and t/r if a variety of starting values of h/r and t/r are allowed. It does not account for the observed trends in h/r and t/r.

Dohrenwend et al. [1986] presents a more sophisticated model of erosion based on observed changes in flank slope and debris apron shape in the Cima volcanic field, Mojave desert, California. Unfortunately, the model does not indicate how the top diameter t and basal diameter r should change, making it difficult to compare to the data reported in this study. Dohrenwend et al. [1986] observe that the t/r ratio and flank slope decrease with age (and degradation), that the size of the debris apron increases with age, and drainage networks evolve from scattered rills to evenly spaced gullies to small valleys. Degradation is initially rapid but slows after around 500 ka [Dohrenwend et al., 1986]. These results are somewhat different from those of Hasenaka and Carmichael [1985], but the time scales of the two studies are quite different: Hasenaka and Carmichael [1985] studied 11 cinder cones (in Mexico) whose ages ranged from less than 50 a to 2.8 Ma, with 8 younger than 40 ka. Dohrenwend et al. [1986] studied 11 cinder cones whose ages ranged from 17 ka to 1.09 Ma, with all but the youngest older than 100 ka. The climates of the two regions

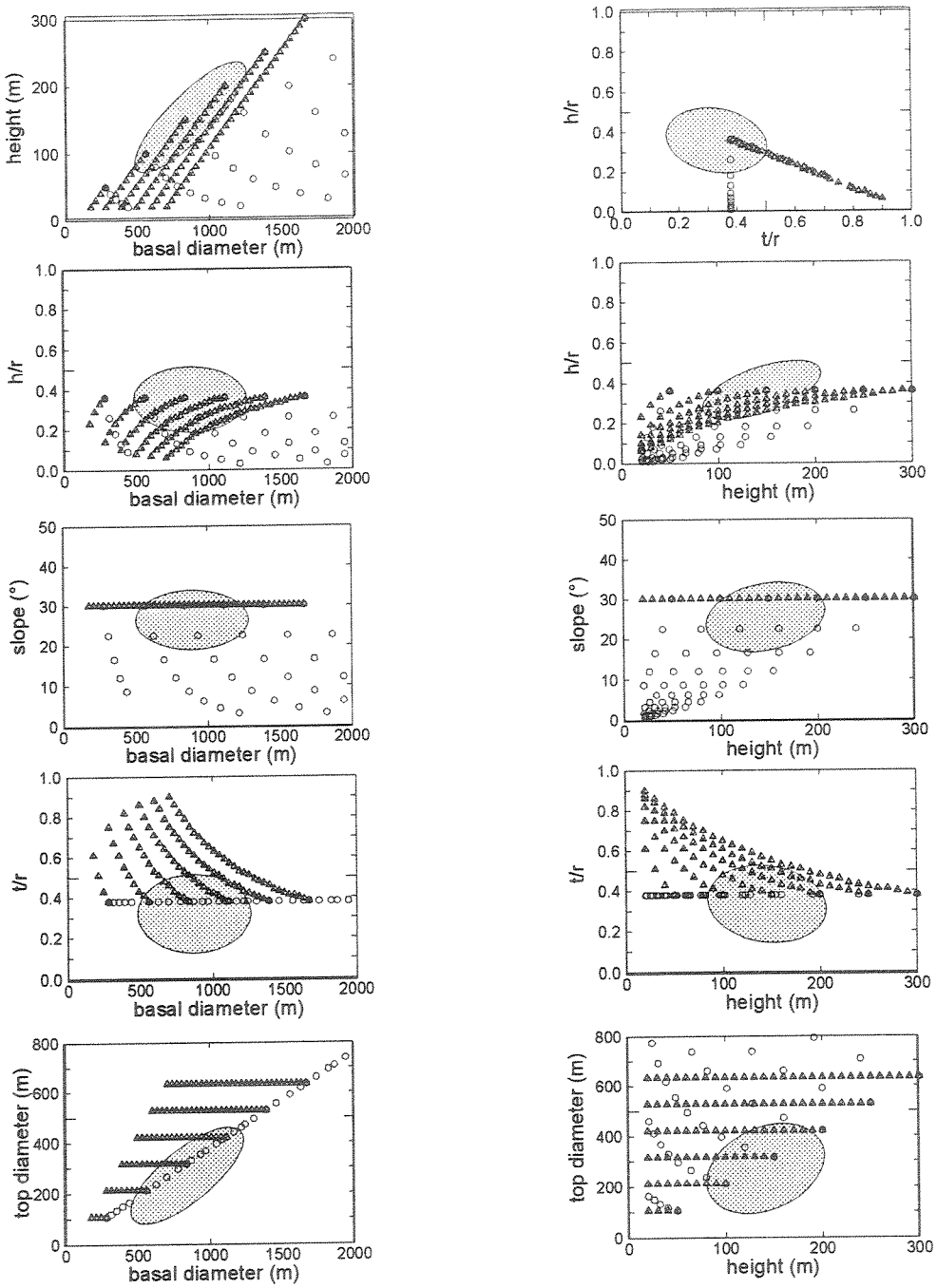


Figure IV-10. Results from applying Wood's [1980b] models of cinder cone degradation to ideal starting cones (h/r=0.36; t/r=0.38) of different heights (h={50, 100, 150, 200, 250, 300}). The filled triangles indicate the results of burying a cone at 10 m intervals. The open circles indicate the results of erosion at intervals of 20% decreases in height. Erosion is assumed to remove material from the top of a cone and place it at the base; volume and t/r are held constant. Filled ovals indicate the range of uneroded Guatemalan cinder cones.

are also very different; the Mojave desert, California, which contains the study area of Dohrenwend et al. [1986], has a semi-arid to arid climate, while the region of central Mexico studied by Hasenaka and Carmichael [1985] has a tropical to temperate climate (the climate of southeast Guatemala is tropical with a pronounced 6 month dry season). Dohrenwend et al.'s [1986] results are also different from those of Wood [1980b]: Dohrenwend et al. [1986] observes a decrease in t/r with age while Wood [1980b] observes no change in t/r with age. The age ranges of the Wood [1980b] study (0-3 Ma) overlap with both Hasenaka and Carmichael [1985] and Dohrenwend et al. [1986]. Wood [1980b] also observes little or no erosion in the first 50 ka.

In regards to the cinder cones in this study, the lack of significant erosion indicated by geomorphic features is consistent with the evidence that the cinder cones are younger that 20-80 ka. I do observe a possible correlation between t/r ratio and slope; this can be explained as indicating a slight progression in erosion or as resulting from the interrelationship between h/r, t/r and slope (see Chapter II). Erosional processes appear unlikely to have significantly effected the morphology of the cinder cones of southeast Guatemala.

DISCUSSION

This observed range of h/r and t/r values is consistent with either the McGetchin model of growth (Figure IV-9) or Wood's [1980b] model of degradation (Figure IV-10) (assuming that a range of initial post-eruptive cone shapes centered on Wood's [1980a] ideal cone is allowed). Thus, some initial difference in cone morphology (due to growth processes) is present in the Guatemalan cinder cone population. Wood [1980a; 1980b] also observed that t/r is generally constant with degradation and during eruption. I observe a much larger range in t/r than is consistent with random scatter or variable eruption rates; the range in t/r most likely reflects variation in the vent widths.

The Wood erosion model cannot explain all of the morphologic relationships observed in Guatemalan cinder cones. In fact, many cones must have started with higher h/r and lower t/r than the ideal cone given in Wood [1980a] (h/r=0.36; t/r=0.38) if the erosion model proposed by Wood is to explain completely the range of observed morphologies. A range of starting h/r and t/r values is needed. But even this does not explain the relationships and ranges of h/r and t/r observed in the least eroded cones. The erosion model proposed by Wood is not contradicted by any data in this study; it is simply insufficient to explain the complete range of morphologies. If the best available measures of erosion (vegetation, cultivation, gullies; Hasenaka and Carmichael [1985]) are considered, some cones (especially those with t/r > 0.5) are clearly affected by erosion. However, there is no clear pattern separating eroded and uneroded cones (Figure IV-11) - the least eroded cones cover most of the range in morphology.

In contrast, the McGetchin model of cinder cone growth easily explains why (1) h increases with r without a constant h/r ratio (h increases throughout growth, but 2r remains constant until maturity (stage 4) is reached) and (2) t increases with r (higher velocities result in both higher r and higher t). It can also be observed that a range of ejection velocities and vent widths is required to fully account for the variation in Guatemalan cinder cone morphology. Ejection velocity can be interpreted to range from 110 m/s to 190 m/s. Vent width is greater than 50 m for 110 m/s and 20 m for 190 m/s. The range in slope, h/r, and r is primarily explained by the variation in velocity. The range in t and t/r is explained by the variation in vent width.

The McGetchin model of cinder cone growth is preferred over the Wood model of cinder cone degradation as an explanation of the observed cinder cone morphologies in Guatemala for the following reasons: (1) No single initial starting morphology can be combined with the Wood model of cinder cone degradation to yield a range of morphologies equivalent to those observed in Guatemala. (2) Many Guatemalan cinder cones show no sign of erosion or burial. (3) No significant difference is observed in the

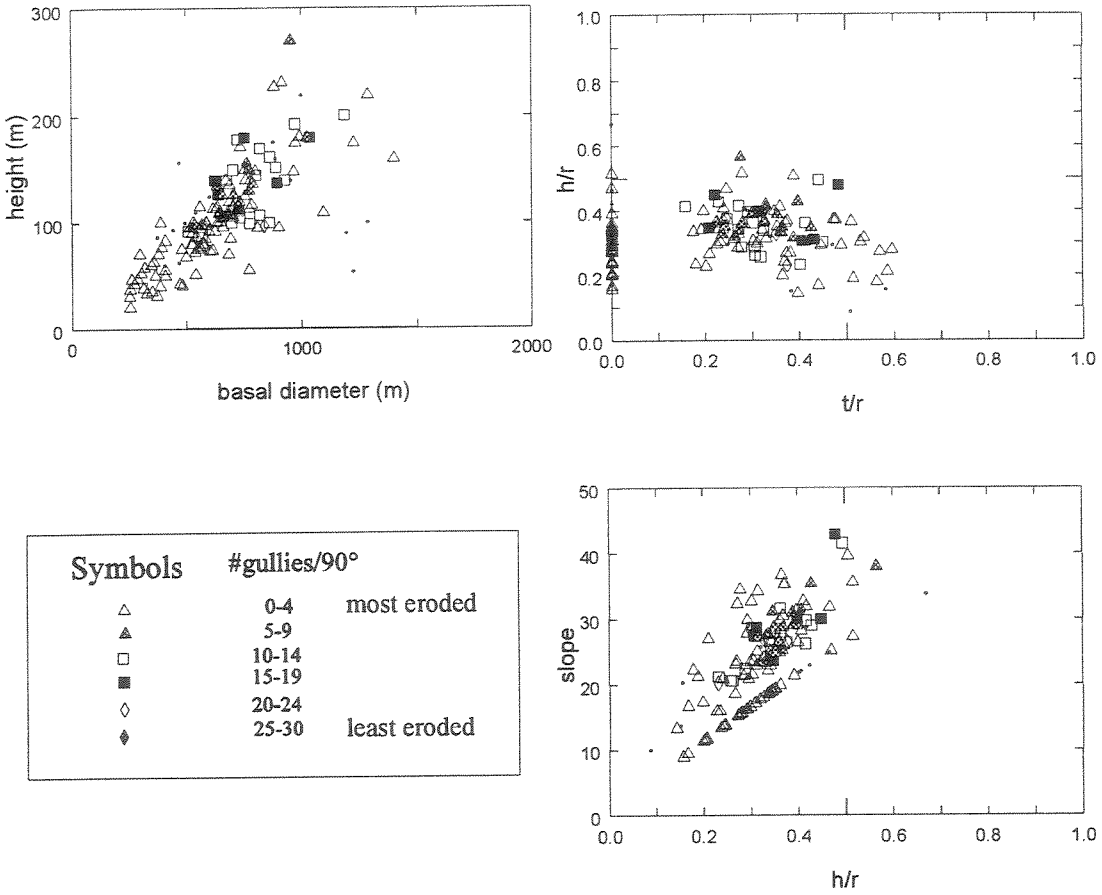


Figure IV-11. Morphologic parameters are plotted in a fashion similar to Figure IV-3, but the symbols indicate the number of gullies per 90°. No consistant pattern is observed, except that the cones with t/r=0 all have less than 5 gullies per 90°.

major morphological patterns between more eroded and less eroded cinder cones. (4) The McGetchin model provides a clear explanation for the major morphological trends observed for Guatemalan cinder cones.

Neither model provides a satisfying explanation of the large (>200 m) top diameters of many cinder cones. In the McGetchin model, lowering the ejection angles (relative to vertical) might result in large top diameters; however, the ejection angles used were based on much lower energy eruptions than interpreted for Guatemalan cinder cones. Erosion can widen the top diameter [Wood, 1980b; Dohrenwend et al., 1986], but it is unclear what effect erosion has on the t/r ratio over the first 50 ka. It is important to note that this study does not invalidate the Wood degradation model; I merely claim that it cannot explain our observations of cinder cone morphology in Guatemala.

The ejection velocities inferred for Guatemalan cinder cones, using the McGetchin model, are relatively high. Ejection velocities, calculated from eruption observations by a variety of methods, include 95 m/s for a large bomb at Paricutin [Fries, 1953], 157 m/s at Heimaey and 31 m/s at Stromboli for gas velocities [Blackburn et al., 1976], 51 m/s at Northeast Crater, Mt. Etna for average particle velocity [McGetchin et al., 1974], 26 m/s and 15 m/s for average particle velocity at Stromboli [Chouet et al., 1974] and 65-165 m/s at Alaid, Klutchevskoy and 90-110 m/s at Mt. Etna for gas velocities [Steinberg and Babenko, 1978]. The velocities suggested here for Guatemalan cinder cones are similar to the ejecta velocities calculated by Wilson [1980] for strombolian eruptions and to those reported for Hole-in-the-Ground Maar, Oregon by Steinberg and Babenko [1978]. It has been previously noted [Walker, 1973] that some cinder cones are formed by sub-plinian eruptions (e.g., Paricutin). The velocities suggested here for Guatemalan cinder cones are intermediate between those expected for strombolian eruptions and those expected for sub-plinian eruptions. The strombolian mechanism of large bursting bubbles seems most appropriate (esp. as Fries [1953] observed bursting bubbles at Paricutin). Direct velocity observations during eruptions are rare. Those by Chouet et al. [1974] at Stromboli, Italy

and McGetchin et al. [1974] at Mt. Etna, Sicily are for weaker eruptions based on qualitative descriptions; I am not aware of any similar measurements for more energetic eruptions.

A relationship between the ejection velocity and the original volatile content of the magma is desirable. However, both theoretical calculations [e.g., Wilson, 1980; Vergniolle and Jaupart, 1986] and observations [e.g., Blackburn et al., 1976] suggest that 10-30% (by mass) of the explosively ejected material is gas. This amount of gas could not possibly be dissolved in the co-ejected lava; so the gas has been concentrated into only part of the total magma supply (the rest is presumably erupted effusively, accounting for the lava flow(s) associated with each cinder cone). Speculation suggests that a larger volume of magma (which in Guatemala can be associated with a larger subduction component: see Chapter III) would result in a higher concentration of volatiles in the explosively erupted phase.

RESULTS OF CHAPTER IV

This chapter concludes that:

(1) **Morphologies produced by growth patterns and those produced by erosion/burial patterns are similar and overlap.** More information than morphology is needed to determine if an individual cone, or even a cinder cone field, is eroded or not. Relevant information includes the number of gullies per 90°, the percentage of vegetative cover, the percentage of cultivated land, and the size and depth of the crater (relative to cone size). All of these factors are measurable on aerial photographs or high resolution satellite images. Additionally, field studies can evaluate the degree of erosion and obtain samples for age dating; however, this is not practical for large numbers of cones.

(2) **The initial starting cone morphology (i.e. morphology immediately after eruption ceases) must vary to account for the range of morphologies observed in the**

Ipala Graben, Guatemala. Erosion and burial processes cannot account for the full range of morphologies if all eruptions result in a cinder cone with Wood's ideal shape (h/r=0.36; t/r=0/38).

(3) **Particle ejection velocities in the range from 110 m/s to 190 m/s are probably typical of the Guatemalan cones**, based on the predictions of the McGetchin model. This is consistent with the relatively fine grain sizes observed in Guatemalan cones (see Chapter III).

(4) **In Guatemala, larger cinder cones are predicted to be produced by eruptions with higher average ejection velocities.** This is consistent with the observation of Chapter III that larger cinder cones tend to be composed of more well-sorted scoria with finer average grain size.

IMPLICATIONS

The first of these conclusions has several implications for remote sensing. It reiterates the caution of Chapter II against interpreting process from morphology alone. Additionally, it implies that in order to interpret the morphology of a cinder cone, aerial photographs or field investigations are necessary in order to determine the degree of erosion or burial.

The second conclusion implies that eruption conditions are not uniform within southeastern Guatemala. This is consistent with the observation of Chapter III that the amount of slab influence is variable within the Ipala Graben, southeastern Guatemala. It further implies that eruption conditions are influenced by magma origin.

The third conclusion infers that Guatemalan cinder cones are formed by vigorous Strombolian to sub-plinian eruptions. It also implies variability of eruption conditions - in particular, it suggests that the volatile contents of the erupting lavas vary. The magma parent bodies may then also vary in volatile content; or the partitioning of volatiles between the explosive and effusive eruption phases may vary.

The fourth conclusion further implies that the volume and the vigor of cinder cone eruptions in Guatemala are correlated. Chapter III concluded that a larger flux from the slab into the source region results in larger degrees of melting and larger volumes of magma. Combining the observations of Chapter III and this chapter suggests either (1) a larger slab flux also results in higher volatiles contents of the magma or (2) as the magma rises, the larger volume of magma allows a higher volatile content to be partitioned into the explosive phase, which is also proportionately larger in volume.

REFERENCES CITED

Bemis, K. G., and Carr, M. J. Volcano morphology in Guatemala, *EOS, Trans. AGU*, 74, 333, 1993.

Blackburn, E. A., L. Wilson, and R. S. J. Sparks. Mechanisms and dynamics of strombolian activity, *J. Geol. Soc. Lond.*, 132, 429-440, 1976.

Bohnenberger, O. H. Los focos eruptivos cuaternarios de Guatemala. Trabajos Technicos Presentados en la Segunda Reunion de Geologos de America Central, Publicaciones Geológicas del Institutio Centroamericano de Investigacion y Tecnologia Industrial, Numero II, 1969.

Burkart, B., and Self, S. Extension and rotation of crustal blocks in northern Central America and effect on the volcanic arc, *Geology*, 13, 22-26, 1985.

Chouet, B., N. Hamisevicz, and T. R. McGetchin. Photoballistics of volcanic jet activity at Stromboli, Italy, *J. Geophys. Res.*, 79, 4961-4976, 1974.

Dehn, J. Model of cinder cone formation. M. S. Thesis, Arizona State University, 1987.

Dohrenwend, J. C., S. G. Wells, and B. D. Turrin. Degradation of Quaternary cinder cones in the Cima volcanic field, Mojave Desert, California, *Geol. Soc. Am. Bull.*, 97, 421-427, 1986.

Drexler, J. W., W. I. Rose, Jr., R. S. J. Sparks, and M. T. Ledbetter, *Quat. Res.*, 13, 373-391, 1980.

Fries, C., Jr. Volumes and weights of pyroclastic material, lava, and water erupted by Paricutin Volcano, Michoacán, Mexico, *Trans., AGU*, 34, 603-616, 1953.

Hasenaka, T., and I. S. E. Carmichael. The cinder cones of Michoacán-Guanajuato, Central Mexico: their age, volume and distribution, and magma discharge rate, *J. Vol. Geotherm. Res.*, 25, 105-124, 1985.

McGetchin, T. R., M. Settle and B. A. Chouet. Cinder cone growth modeled after Northeast Crater, Mount Etna, Sicily, *J. Geophys. Res.*, 79, 3257-3272, 1974.

Peterson, P. S., Tephra of the Laguna de Ayarza calderas of southeastern Guatemala and its correlation to units of the Guatemalan Highlands, M.S. Thesis, Michigan Technological University, 1980.

Plafker, G. Tectonic aspects of the Guatemala earthquake of 4 February 1976, *Science*, 193, 1201-1208, 1976.

Porter, S. C. Distribution, morphology and size frequency of cinder cones on Mauna Kea Volcano, Hawaii, *Geol. Soc. Am. Bull.*, 84, 382-483, 1972.

Smith, D. K. Shape analysis of Pacific seamounts. *Earth Planet. Sci. Lett.*, 90, 457-466, 1988.

Smith, D. K. and J. R. Cann. Hundreds of small volcanoes on the median valley floor of the Mid-Atlantic Ridge at 24°-30°N, *Nature*, 1990.

Smith, D. K. and J. R. Cann, The role of seamount volcanism in crustal construction at the Mid-Atlantic Ridge (24°-30°N), *J. Geophys. Res.*, 97 (B2), 1645-1658, 1992.

Steinberg, G. S., and J. I. Babenko. Experimental velocity and density determination of volcanic gases during eruption, *J. Vol. Geotherm. Res.*, 3, 89-95, 1978.

Vergniolle, S., and C. Jaupart, Separated two-phase flow and basaltic eruptions, *J. Geophys. Res.*, 91, 12842-12860, 1986.

Walker, G. P. L. Explosive volcanic eruptions - a new classification scheme, *Geol. Rundsch.*, 62, 431-446, 1973.

Walker, G. P. L., and R. Croasdale. Characteristic of some basaltic pyroclastics, *Bull. Vol.*, 35, 303-317, 1972.

Williams, H., A. R. McBirney and G. Dengo. *Geologic reconnaissance in southeastern Guatemala*, Univ. California Publ. Geol. Sci., vol. 50, 1964.

Wilson, L. Relationships between pressure, volatile content and ejecta velocity in three types of volcanic eruptions, *J. Vol. Geotherm. Res.*, 8, p. 297-313, 1980.

Wilson, L., R. S. J. Sparks, and G. P. L. Walker. Explosive volcanic eruptions-IV. The control of magma properties and conduit geometry on eruption column behavior, *Geophys. J. R. astr. Soc.*, 63, 117-148, 1980.

Wood, C. A., Morphometric evolution of cinder cones, *J. Vol. Geotherm. Res.*, 7, 387-413, 1980a.

Wood, C.A., Morphometric analysis of cinder cone degradation, *J. Vol. Geotherm. Res.*, 8, 137-160, 1980b.

Chapter V. Growth models for large volcanoes

INTRODUCTION

A number of models of lava flow behavior have been developed which predict the final lengths of lava flows [Hulme, 1974; Borgia and Linneman, 1990; Wadge and Lopes, 1991; Kilburn and Lopes, 1991; Pinkerton and Wilson, 1994], the small-scale morphology of lava flow surfaces [Fink and Griffiths, 1990; Bruno et al., 1994], and the rate at which lava flows cool [Crisp and Baloga, 1990]. These models are very useful for predicting the results of future or current eruptions and for interpreting the emplacement dynamics of past flows. They do not, in general, address how large numbers of lava flows combine to form a volcanic edifice. Individual flow behavior indicates little about how eruption conditions change over time and nothing about the cumulative effects of many eruptions from the same or coincident vents.

There are several models that directly address the question of edifice growth. Borgia and Linneman [1990] infer a topographic profile of an ideal flow field (and thus a lava cone) from a mass conservation model of lava flow dynamics and the assumption that composite flows grow until they attain a constant surface slope. Ben-Avraham and Nur [1980] speculate that the depth of a magma chamber feeding the volcano controls the maximum height of the volcano. The cone deformation model of Shteynberg and Solov'yev [1976] and the hydraulic resistance model of Lacey et al. [1981] also deal with possible limitations on height and how a concave upwards flank is created. Two of these models are based on lava flows piling up to create the edifice, but all of them fit the profile typical of composite volcanoes not that typical of shield volcanoes.

The difference between shield volcanoes and composite volcanoes is generally considered to result from the relative amounts of effusive and pyroclastic activity (ideal shields are nearly 100% effusive and composite volcanoes are usually over 50% pyroclastic) [Cas and Wright, 1988; Pike and Clow, 1981a]. The type shield volcano is in

Iceland and may be monogenetic, but many primarily effusive and shield-shaped volcanoes are known to be polygenetic (e.g. Hawaii). The importance of pyroclastic activity in creating volcanic edifices is unclear and probably varies. Observations of Arenal in Costa Rica suggest most of the pyroclastic material is washed off of the volcanic edifice [Borgia and Linneman, 1990]. In other cases, alternating layers of pyroclastic and effusive material are documented in the central cone [Rose et al., 1977 on Santa Maria]; Grubensky et al. [1993] observed that effusive material dominates the near vent and pyroclastic the far field for a small composite volcano in the central high Cascades. The different shapes and compositions of composite and shield volcanoes form a complex and confusing continuum of volcanic styles that probably varies with tectonic setting.

This chapter is an attempt to understand how the progressive growth of a large edifice, through many eruptions, relates to eruptive processes. In order to do this, I examine the morphology of large volcanoes in more detail; I compare morphologic parameter data collected in Guatemala, Iceland, the Snake River Plain and the South Pacific and topographic profiles of selected volcanoes to existing models of volcanic size and shape. The results consist of two models and several observations: (1) shield volcanoes appear to evolve into composite volcanoes in Guatemala, (2) topographic profiles distinguish between passive effusion, viscous effusion and explosive styles of eruption, (3) composite volcanoes have parabolic flanks, and (4) numerical simulations of lava piles model shield volcanoes as piles of wedge-shaped lava flows of varying length.

PREDICTIONS OF EXISTING MODELS

Limitation of height

Vogt [1974] suggested that the elevation of volcanoes might be controlled by the thickness of the lithosphere. In specific regard to subduction zones, Marsh [1976] related volcano elevation to melting above the subducting slab, with the buoyancy of the melt controlling the maximum elevation of the volcano summit. In this case, the elevation

would be uniform for a given slab. Ben-Avraham and Nur [1980] continued the discussion and observed that whereas the summit elevation above sea level of volcanoes erupted on continental crust is highly variable along volcanic chains, the height of the volcanic edifices is uniform. In contrast, the elevation above sea level of oceanic volcanoes is very uniform but edifice heights vary greatly [Ben-Avraham and Nur, 1980]. Uniform heights for continental volcanoes are used to imply melting occurs at a constant depth below the topographic surface [Ben-Avraham and Nur, 1980]; magma reservoirs are observed at a constant depth of 2-4 km in many regions [Ryan, 1987]. All these buoyancy models predict a height based on hydrostatic balance using a simple equation of the following form:

$$p_l g d = p_m g (h+d), \qquad (1)$$

where d is depth of melt (reservoir) below a reference level, h is elevation of the volcano summit above a reference level, p_m is the melt density, p_l is the lithospheric or crustal density and the reference level is either sea level or the regional topographic surface. These models predict that h will vary with d. If the melt reservoir is a constant depth below sea level, volcano summits will be a constant elevation above sea level. If the melt reservoir is a constant depth below the topographic surface, volcano edifice heights will be uniform. The first case applies to volcanoes on oceanic lithosphere, where lithospheric thickness may control the depth of the magma reservoir. Ben-Avraham and Nur [1980] suggest that the second case applies to continental arcs. Observations of large volcanoes do suggest that many have magma chambers ~2-4 km beneath the summit region [Ryan, 1987; Iyer et al., 1990]. However, Ryan [1987] demonstrates that this is the level of neutral buoyancy for basaltic melt bodies and suggests that it is related to the contraction of pore space and fractures with increasing depth. The hydrostatic balance (equation 1) depends on the level of neutral buoyancy being at or above the volcano summit [Wilson et al., 1992]. Wilson et al. [1992] suggest instead that volcano height is related to total magma supply and the duration of volcano growth. This can explain the uniformity of

height above sea level for intraplate volcanoes on oceanic lithosphere [observations in Vogt, 1974; Eaton and Murata, 1960; Ben-Avraham and Nur, 1980], where the motion of the lithospheric plates limits the duration of magma supply at a given site. It is less clear how it relates to subduction zone volcanoes, where the duration of magma supply to a given segment of the arc is usually longer than the lifetime of an individual volcano. If Wilson et al.'s [1992] model does apply to continental arcs, volcano heights are predicted to be uniform along strike of the arc.

Lava armor

Borgia and Linneman [1990] developed a model of volcano growth based on their interpretation of field observations and measurements of a growing lava field on Arenal, Costa Rica. The model describes a volcano as a hierarchical series of geologic units (Figure V-1): (1) volume-limited uniform flows, (2) composite flows formed by a set of uniform flows emplaced at short time intervals along a channel, (3) lava flow fields consisting of the composite flows of a single eruption, and (4) lava armor which is the volcanic edifice. The lava armor will not be axisymmetric if the vent location changes between eruptions.

A mass conservation model is used to calculate the maximum length of a unit flow for a given set of eruption conditions. Composite flow length is constrained by the observation that the surface of a composite flow tends to attain a constant slope over time. Lava flows are assumed to fill in the topography until the slope increases to 40°. Additionally, for standard assumptions of lava flow behavior (steady-state effusion, plug-flow crust, Bingham rheology, etc.), lava flow length is related to topographic slope by the following relations, which is empirically determined to be linear:

$$L_t = m(\tan a)^{-1} + b, \qquad (2)$$

where L_t is the horizontal component of the final composite flow length, a is the topographic slope, and m and b are coefficients related to parameters of flow behavior that

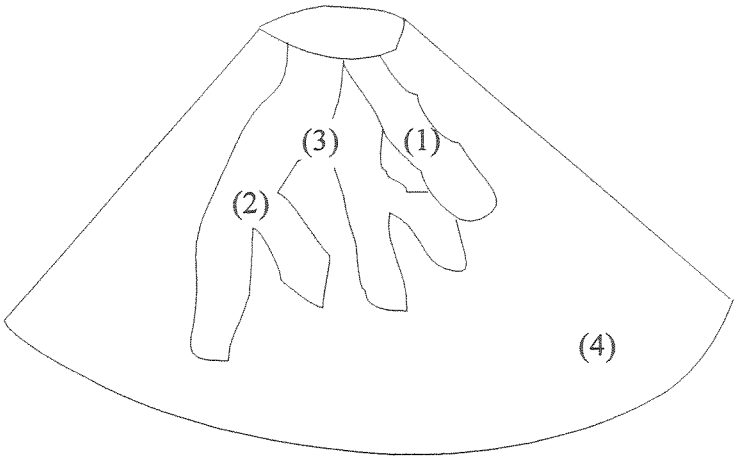


Figure V-1. A volcano can be interpreted as a hierarchical series of geologic units: (1) volume-limited uniform flows, (2) composite flows formed by a set of uniform flows emplaced at short time intervals along a channel, (3) lava flow fields consisting of the composite flows of a single eruption, and (4) lava armor which is the sum of all the lava flow fields, that is, the volcanic edifice. [After Borgia and Linneman, 1990].

have been empirically determined to be constant for a given flow field (or volcano). Based on this relationship and assuming symmetric flow fields, the following equation can be used to generate an idealized model of a volcanic edifice:

$$h(r)=\text{sum}(i=1 \text{ to } I) \text{ of } \{(u_o-u_{L_{ti}})[(m_i L_{ti}/(L_{ti}-b_i))(1-r/L_{ti}) - m_i \ln(L_{ti}-b_i) + C_{3i}] + u_{L_{ti}}[-m_i \ln(r-b_i) + C_{3i}]\}, \quad (3)$$

where $\arctan(m_i/(L_{ti}-b_i))<=38\text{-}40°$, i is the index for lava field, b~1113.8 m and m~261.4 m are from equation (1), r is the horizontal radial coordinate for lava armor, u_o is the step function for r=0, u_{Lt} is the step function for $r = L_t$, t is lava flow thickness, C_{3i} is an integration constant and h is the height (at r) of the lava armor [Borgia and Linneman, 1990].

This model predicts that the basal diameter does not change with growth. It implies that the first layer of composite flows determines the radial extent of the volcanic edifice; the progressive increase in slope results in shorter lava flows over time. The basal diameter 2r is then a function of eruption conditions or lava rheology. This model also predicts that the upper flank has a constant local slope and the lower flank has a steadily decreasing local slope. Figure V-2 shows the predicted topographic and slope profiles (using values of m and b for Volcán Arenal, Costa Rica [Borgia and Linneman, 1990]) for a range of maximum slopes. Notice that the summit height is independent of the initial lava flow length (basal diameter) and depends mainly on the maximum local slope attained and the duration of growth. In general, Borgia and Linneman's [1990] model of lava armour predicts: (1) the h/r ratio and average slope increase with height, but not with basal diameter, (2) lava flow age increases away from the summit, and (3) local flank slope is constant on the upper flank , whereas it increases towards the summit on the lower flank.

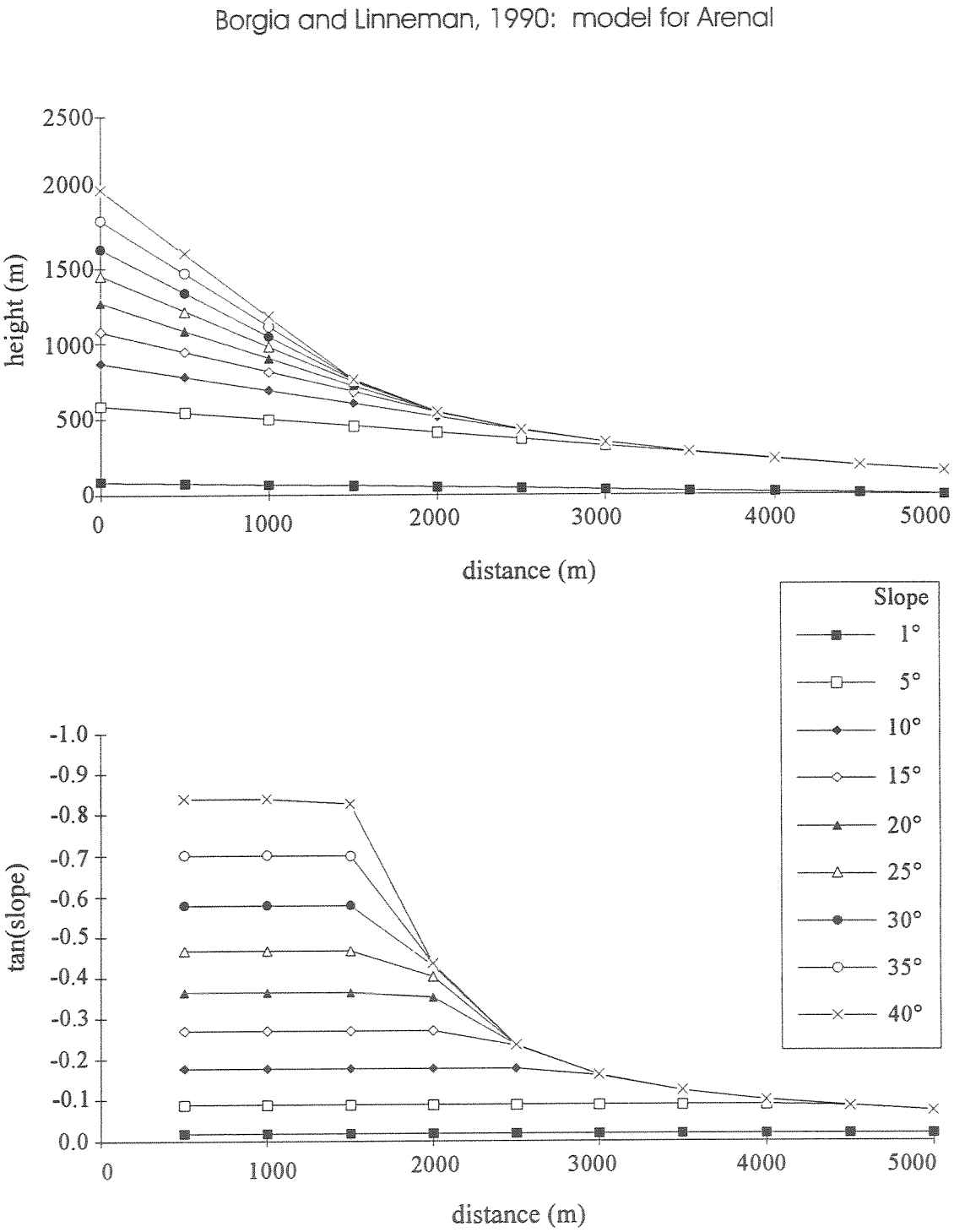


Figure V-2. Profiles of model volcano showing progressive increase in slope and decrease in lava flow length [after Borgia and Linneman, 1990]. (a) Topographic profile. (b) Slope profile.

Hydraulic resistance

Based on the observation of near constant slopes on the lower flanks of many large volcanoes, Lacey et al. [1981] suggest that hydraulic resistance to the flow of magma controls the shape of volcanoes. The volcanic edifice is modeled as a uniform porous material with a surface of constant hydraulic potential [Lacey et al., 1981]. This model assumes that (1) flank eruptions are at least as important as summit eruptions, (2) the elevation and azimuth of flank eruptions is random and (3) for each eruption, magma follows the path of least hydraulic resistance [Lacey et al., 1981]. The steady-state flow equations can be numerically solved for a non dimensional edifice profile, which can be arbitrarily scaled to fit actual volcano profiles [Lacey et al., 1981]; Figure V-3 shows the non-dimensional height (f) and slope (f' = df/de) as a function of non-dimensional distance (e).

Non-dimensional analysis of the flow equations indicates that the edifice radius is a function of time, but that the height is not [Lacey et al., 1981]. The best estimate of the relative growth of the radius and the height is

$$(dh/dr)_0=-0.58(u/kpg)^{3/4}Q_0^{1/4}/t^{1/2}, \quad (4)$$

where h is the height, r is the radius, u is viscosity, k is permeability, p is density, g is gravitational acceleration, Q_0 is flow rate into edifice base, and t is time. The average flank slope should decrease as the volcano grows. The volcano height is proportional to flow rate and viscosity and inversely proportional to permeability and gravity [Lacey et al., 1981]. Volcanoes that grow faster (higher effusion rate) should have generally steeper flanks. Note that all volcanoes are predicted to have flanks that steepen towards the summit.

Several authors argue that the processes this model is based on cannot be realistically claimed to occur in actual volcanoes: magma does not flow on random paths inside the edifice [Wood, 1982], nor is there any reason to believe in a magma equipotential surface [Wadge and Francis, 1982]. Wood [1982] points out that the model fits the shape of

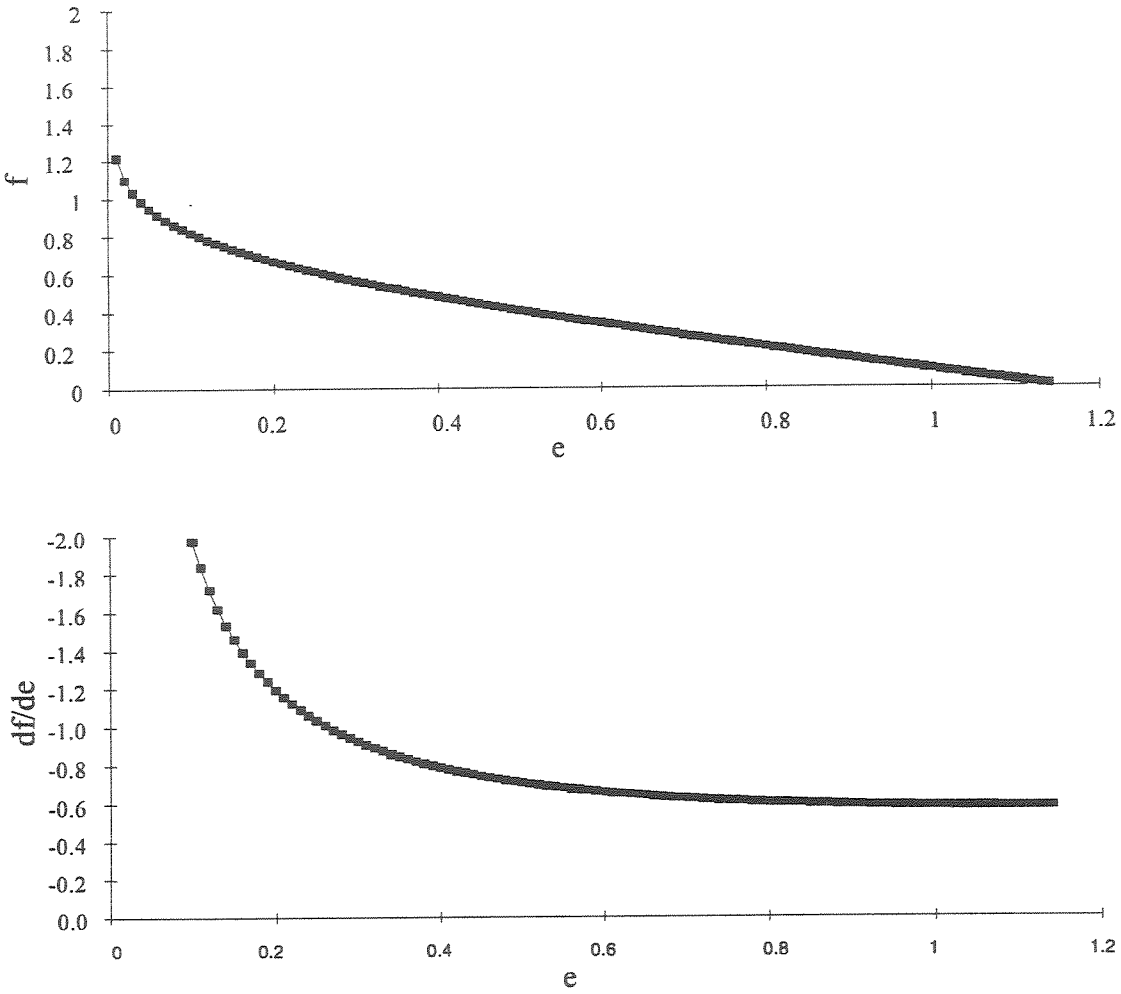


Figure V-3. Profiles of non-dimensional topography from Lacey et al.'s [1981] hydraulic resistance model. (a) Non-dimensional elevation f is shown as a function of non-dimensional distance e. (b) The derivative df/de (f'), which is a measure of tan(slope), is shown as a function of non-dimensional distance e. A scaling factor (which is a function of material properties) is needed to obtain absolute values of tan(slope).

composite volcanoes (in which pyroclastic and erosional processes are important) better than the shape of shield volcanoes. This model is not expected to work well, but is included for completeness.

Basal deformation

Shteynberg and Solov'yev [1976] derive the shape of a volcano assuming that it is a regular, free-flowing cone whose slope angle is the angle of repose and that the base of the cone deforms when the weight of the cone exceeds the yield strength. The limiting height of an undeformed cone is the height where the cone weight and yield strength are exactly balanced. The model divides the volcano into two parts: (1) a free-flowing cone of limiting height forms the top portion and (2) the shape of the base is given by a body of constant strength subject to the weight of the limiting cone and its own weight. The base is effectively squeezed outward; the resulting volcano has concave upward flanks (Figure V-4). The resulting topographic profile can be approximated by the following equation:

$$h(r) = \begin{cases} H_{max} - r\tan(a), & r < R \\ H_{max} - R\tan(a) - (2/3)H_{lim}\ln(r\tan(a)/H_{lim}), & r > R \end{cases} \quad (5)$$

where r is the radial distance from the summit, h(r) is the height of the volcano profile at r, H_{max} is the total volcano height, $H_{lim} = 3o_p/y$ is the limiting height of the undeformed cone, R is the basal radius of the undeformed cone of height H_{lim}, a is the slope of the undeformed cone, y is the specific weight of the undeformed cone and o_p is the tensile strength of volcanic materials.

The main problem with this model is the free-flowing cone is appropriate only for cinder cones. However, the base of shield and composite volcanoes can also be expected to deform due to the weight of the overlying cone. Borgia et al. [1992] recently discussed the deformation due to excess weight for Mt. Etna. Models based purely on deformation of the base of the cone predict nothing about the shape of the upper cone, but predict that the base of the volcano will be anonymously shallow sloped and detached (along a thrust-

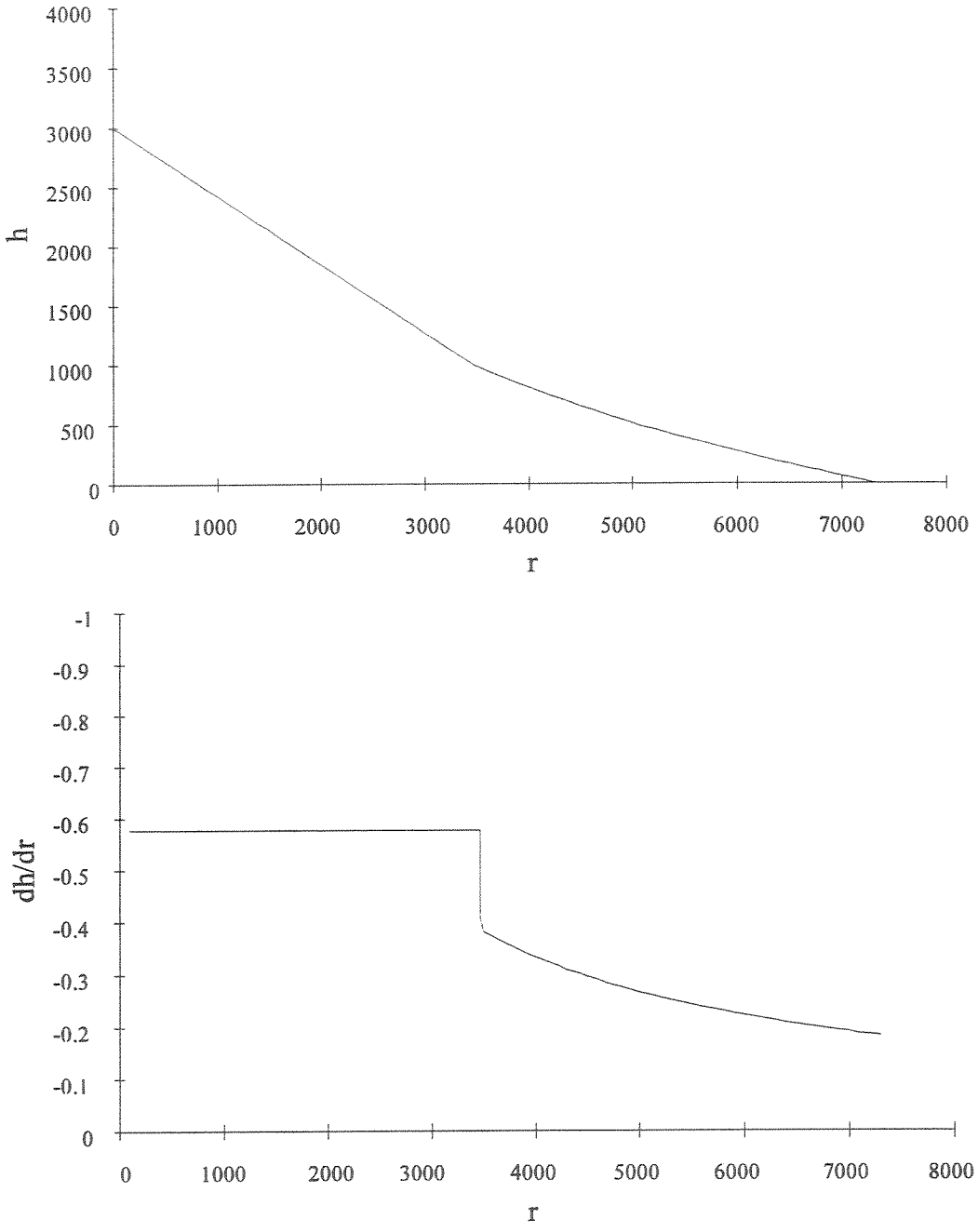


Figure V-4. Profiles of model volcano based on Shteynberg and Solov'yev's [1976] model of cone deformation. (a) The topographic profile shown was estimated for a 3000 m tall volcano with a limiting cone of 2000 m and 30° slope. (b) The slope profile clearly shows the linearity of the upper flank and progressive decrease in slope of the lower flank; the discontinuity is an artifact of the estimating equations.

like fault) from the preexisting basement [Borgia et al., 1992]. The model of Shteynberg and Solov'yev [1976] predicts a constant slope for the upper flank and a shallower slope, which decreases away from the summit, for the lower flank (Figure V-4).

DATA

Morphologic parameters

See Chapter II for a detailed discussion of the morphologic parameters measured and the relationships among them. The following summarizes the pertinent observations for Guatemala, Iceland and the Snake River Plain.

In Guatemala, large volcanoes are found both along the Central American arc and in extensional back-arc grabens. Most shield volcanoes are found in back-arc regions. Shield volcanoes in Guatemala have moderately shallow slopes (slope = 8° ± 3°) and a wide range in flatness (t/r=0.00 to 0.35). The height-to-radius ratio h/r increases with increasing height h (R=0.96) and basal diameter 2r (R=0.55) whereas the flatness (t/r=0.12±0.12) remains constant with increasing h or r (Figure V-5). Flatness is controlled primarily by the top diameter (for t/r vs. 2t, R=0.95), which is apparently independent of volcano size (Figure V-5).

Composite volcanoes in Guatemala are found in both back-arc and arc front regions. Composite volcanoes are steeper than shield volcanoes (slope = 17° ± 6°) with similar flatness (t/r=0.00 to 0.35). The steeper cone probably reflects the addition of pyroclastic material in the near vent region as well as more viscous (so shorter) lava flows. The crater sizes are generally similar. Both slope and height-to-radius ratio h/r are basically constant with increasing height h and basal diameter 2r, although they may decrease slightly in the very largest composite volcanoes (Figure V-5). There does appear to be two separate paths of growth; the shallower set of volcanoes are mostly from southeast Guatemala and El Salvador (the steeper volcanoes are mostly from southwest Guatemala). The h/r ratio correlates negatively with the top diameter 2t (R=-0.72),

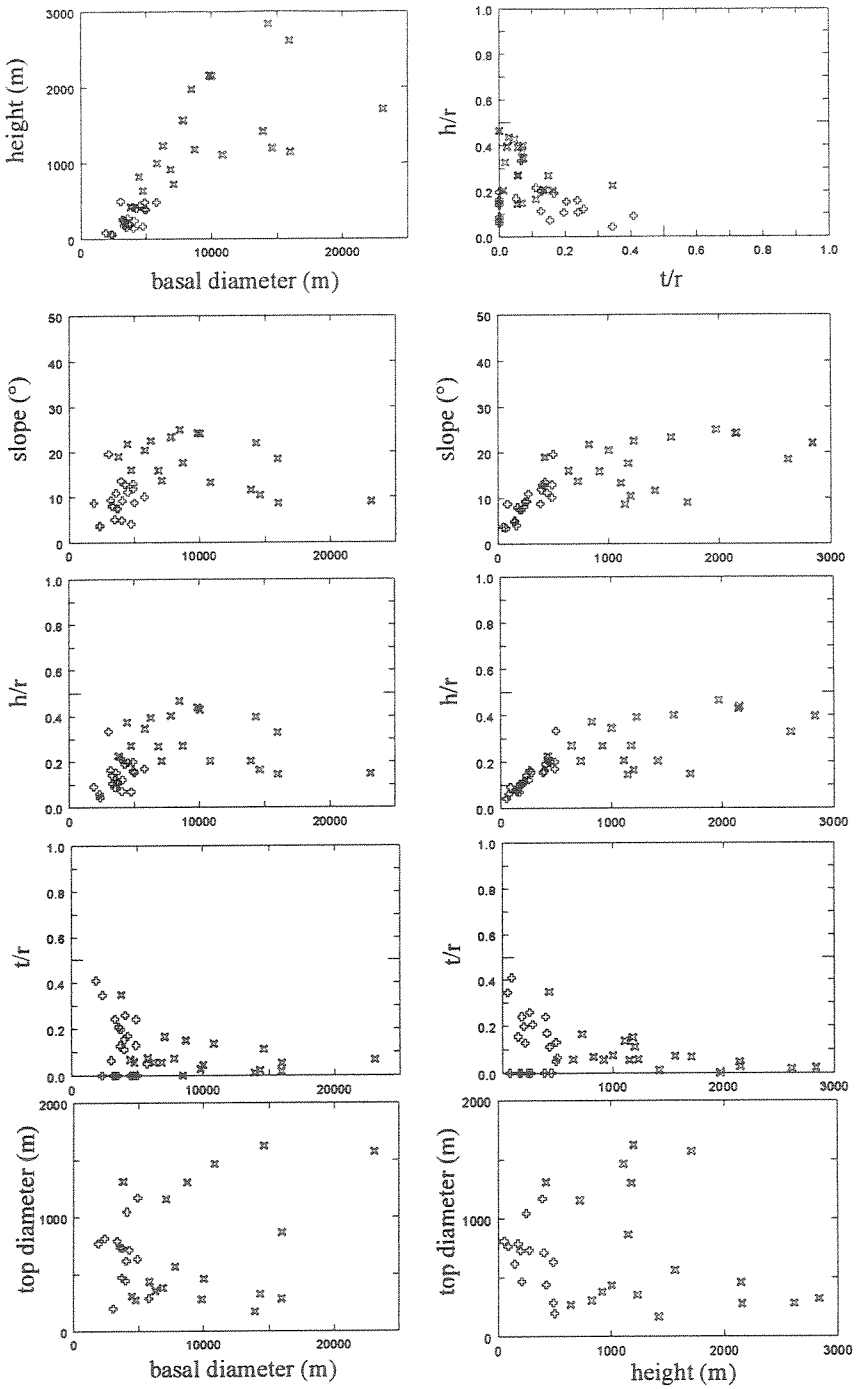


Figure V-5. Morphologic plots for Guatemalan shield (+) and composite (x) volcanoes. The slope and h/r ratio increase with increasing basal diameter 2r for shield volcanoes and decrease slightly with increasing basal diameter 2r for composite volcanoes. The slope and h/r ratio increase with increasing height h for shield volcanoes and remains constant for composite volcanoes. There is an apparent transition between shield volcano shapes and composite volcano shapes.

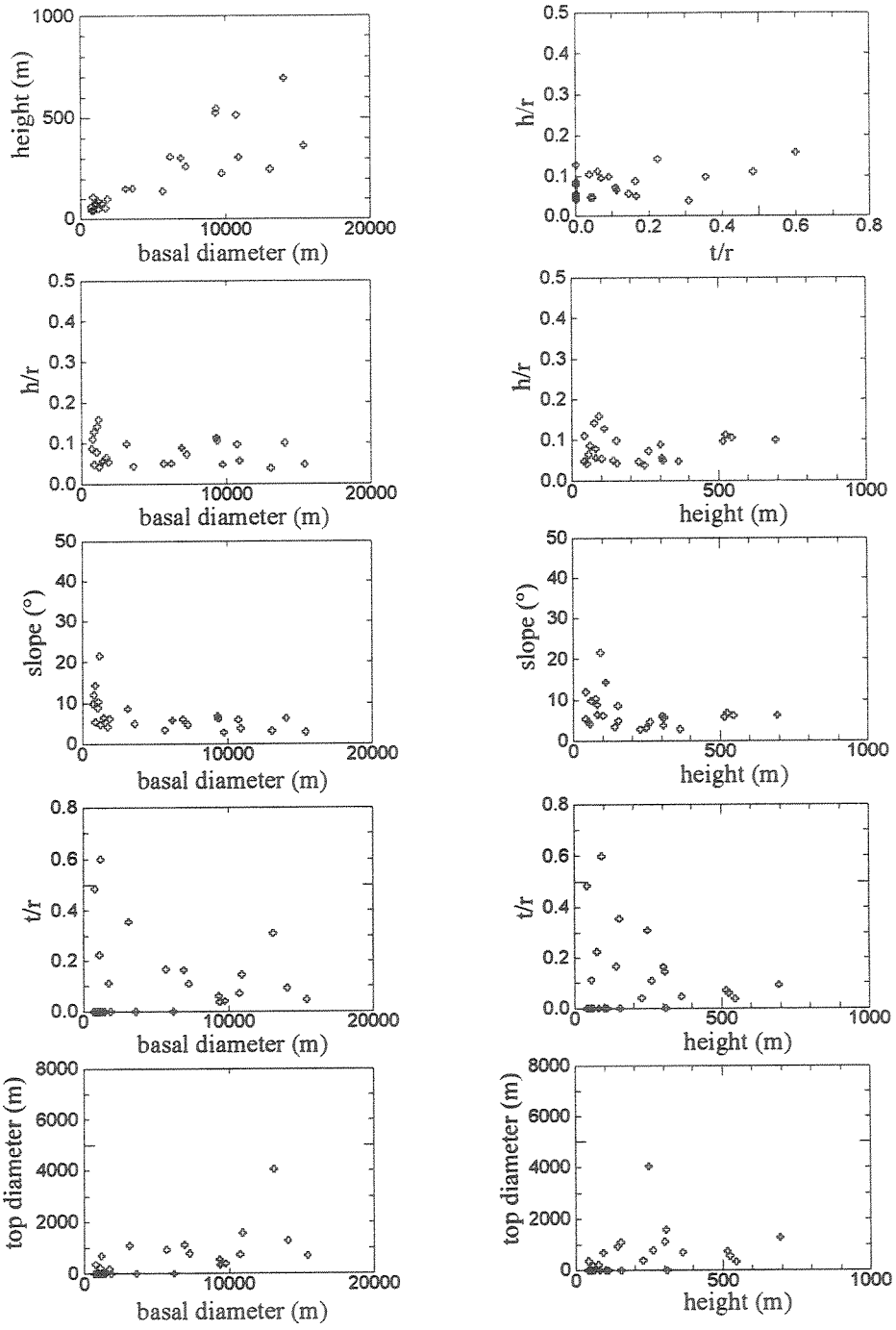


Figure V-6. Morphologic plots for Icelandic shield volcanoes. Note that the morphological parameters vary little with size.

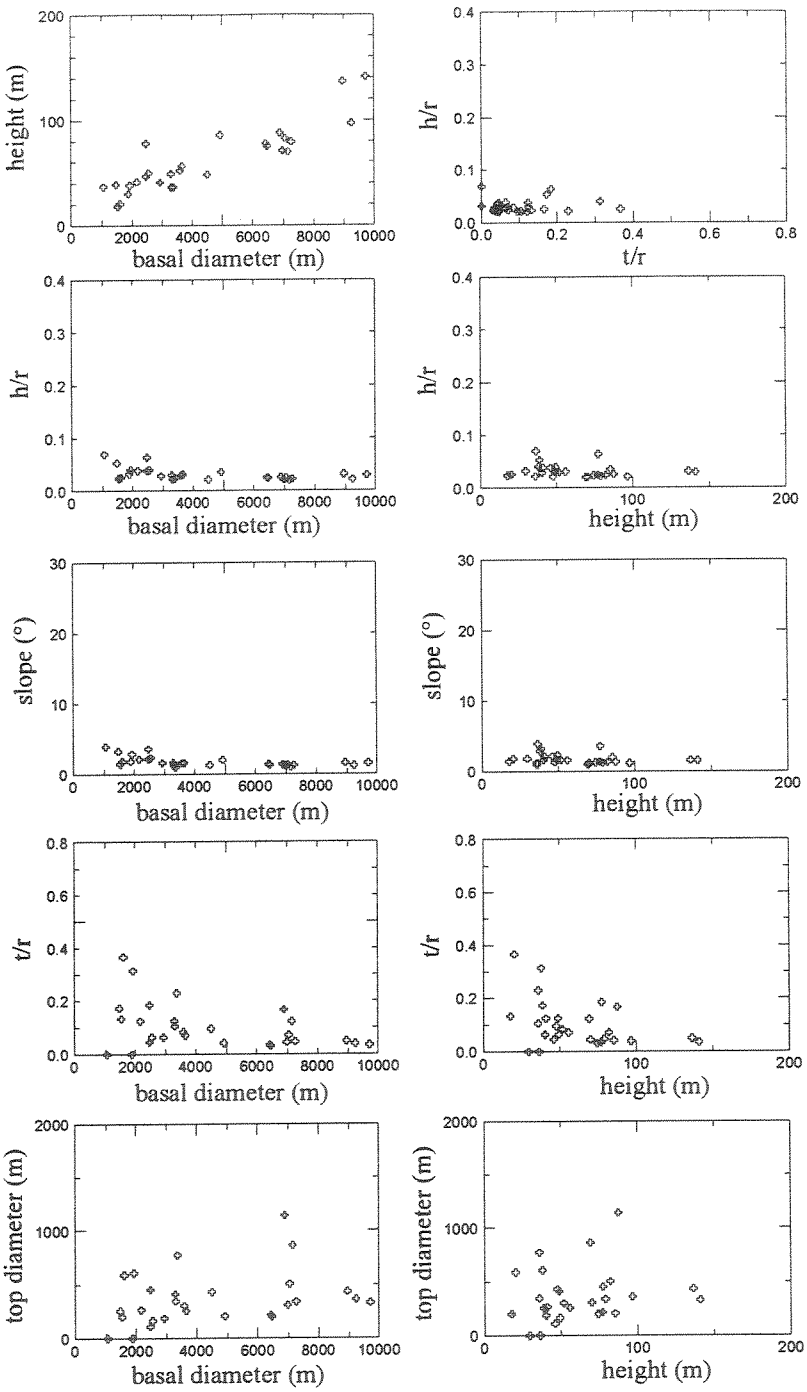


Figure V-7. Morphologic plots for shield volcanoes in the Snake River Plains. Note the slight tendency of the h/r and t/r ratios to decrease with increasing basal diameter.

suggesting that composite volcanoes with exceptionally large calderas appear less steep because the steep summit region has been removed by the caldera forming eruption. Flatness t/r and crater size 2t are independent of volcano size (Figure V-5).

Large central volcanoes are found in the rift zones of Iceland; many of these are shield volcanoes. Icelandic shield volcanoes have low height/radius ratios (h/r=0.08±0.04) which correspond to gentle slopes (slope=6°±5°) and moderately sized summits (t/r=0.16±0.15). The height-to-radius ratio is independent of height and basal diameter, indicating that Icelandic shields maintain a constant slope as they grow (Figure V-6). The t/r ratio and the top diameter change little with volcano size (Figure V-6).

The Snake River Plain is an area of hot spot related volcanism. The shield volcanoes of the eastern Snake River Plain (SRP) are very gently sloped (slope=1.6°±0.7°) with moderately sized summit regions (t/r=0.08±0.05). The height-to-radius ratio h/r may decrease with basal diameter (R=-0.51) suggesting that the shields become more and more like lava flows as they increase in size (Figure V-7). The top diameter 2t (generally a crater diameter) is independent of size, which was also observed in both Guatemala and Iceland (Figure V-7). The t/r ratio decreases with increasing 2r (R=-0.40).

Topographic profiles

Digitized profiles of a variety of volcanic types (e.g. shield, composite, dome, table mountain, cinder cone) in different locations (Iceland, Guatemala, and the South Pacific) were used to determine the local variation in slope for individual volcanoes. Height and radial distance are recorded directly from the topographic maps, generally using the spacing of the contour lines. The resulting digital topographic profile can be analyzed for detailed differences between individual volcanoes of the same type and between volcanic types. A slope profile was calculated from each topographic profile by finite difference:

$$dh/dr = \{h(n)-h(n+2)\}/\{r(n+2)-r(n)\}, \quad (6)$$

a)

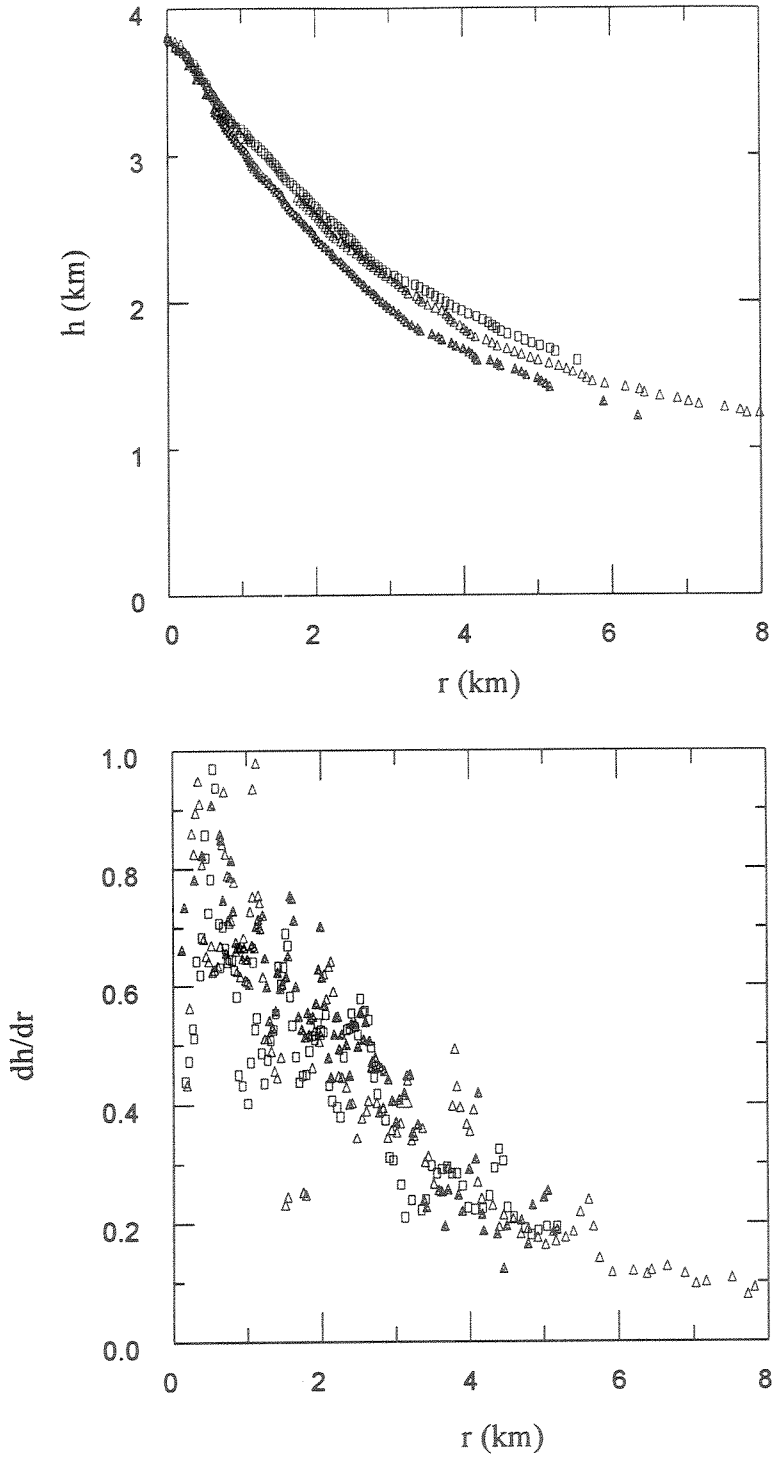


Figure V-8. Topographic and slope profiles for various volcanic types. All scales for h and r are in kilometers. Vertical exaggeration is 2x in each. Symbols indicate profiles with different azimuths. (a) Volcán de Agua is a composite volcano in Guatemala. The three profiles are bearing southeast, southwest and northwest.

b)

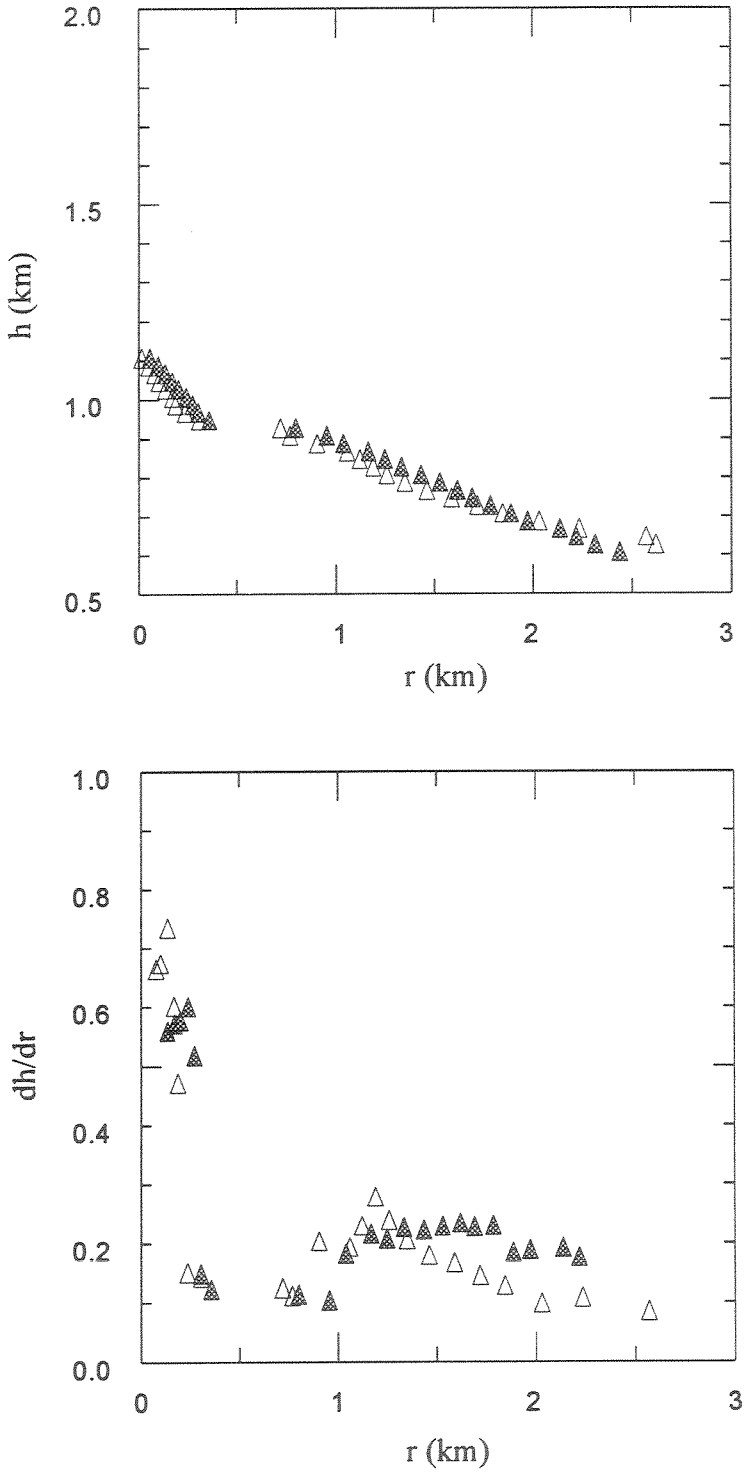


Figure V-8. (b) Volcan las Viboras is a shield volcano in Guatemala.

c)

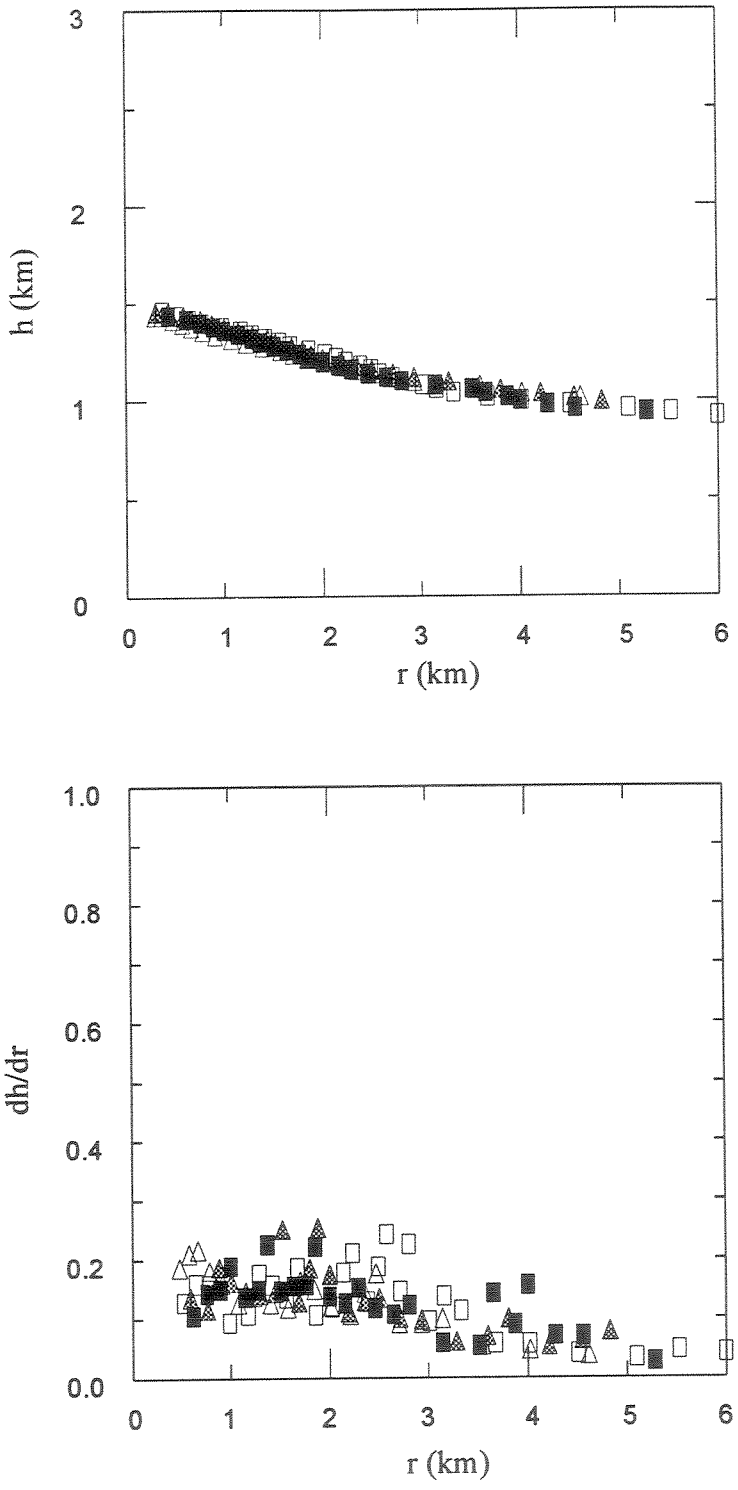


Figure V-8. (c) Trolladyngja is a shield volcano in Iceland.

d)

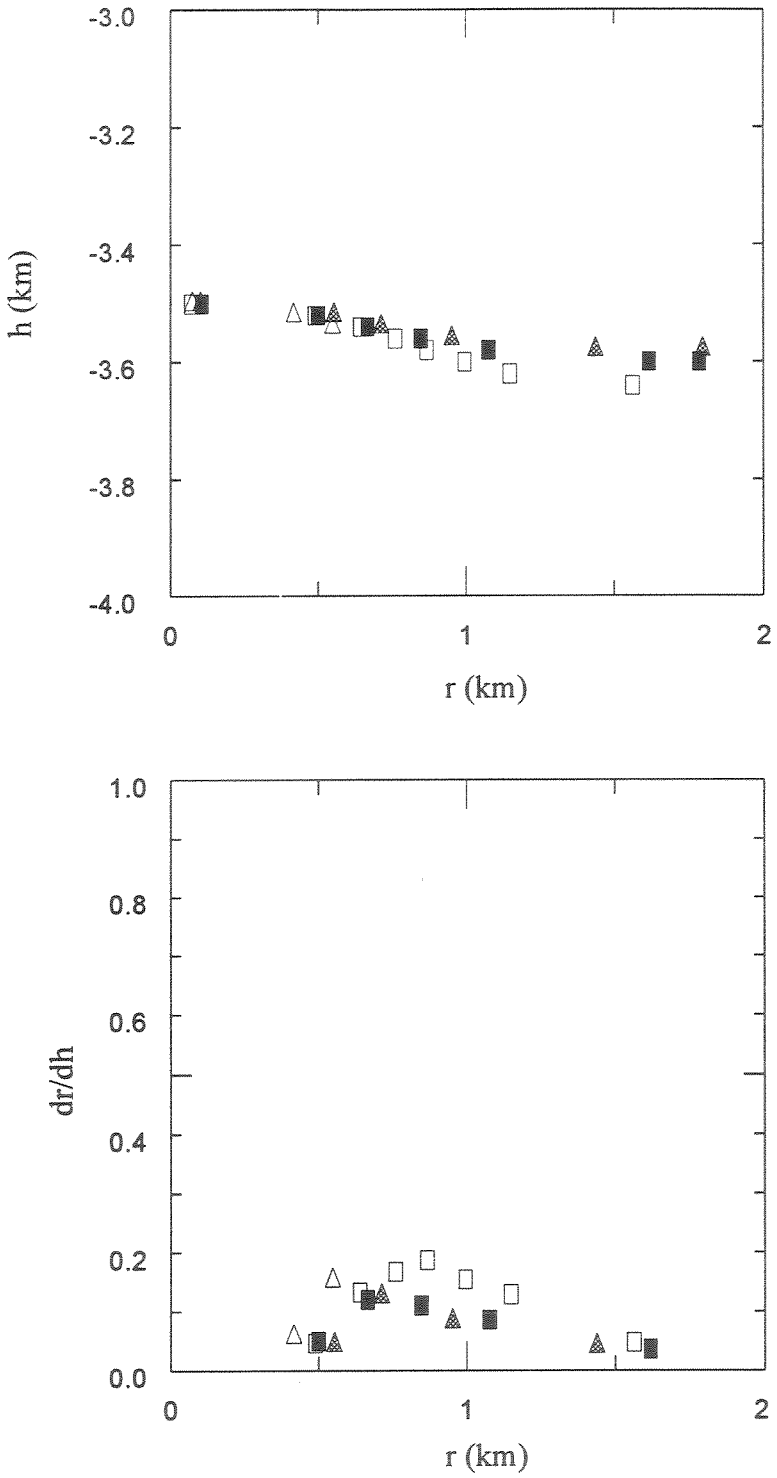


Figure V-8. (d) Seamount 159 is a submarine volcano in the South Pacific.

e)

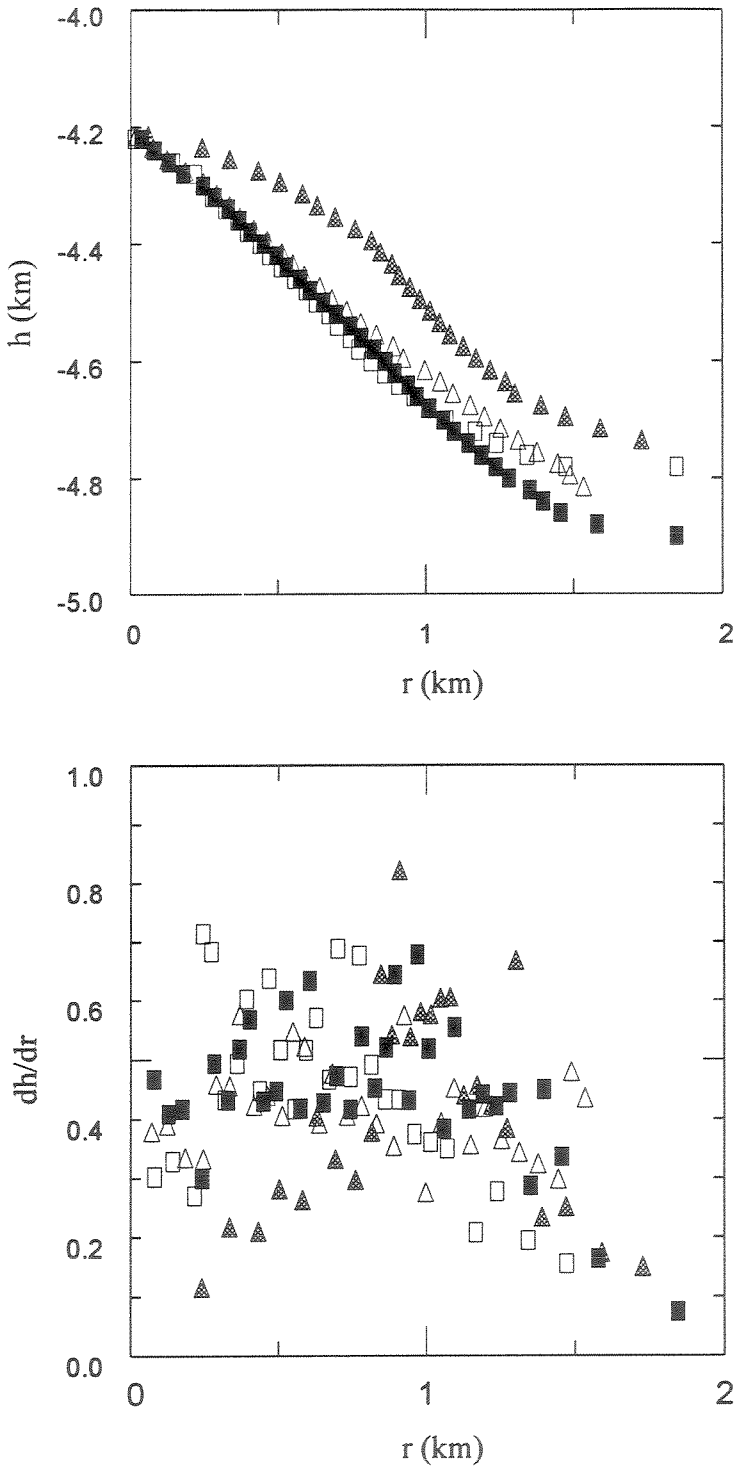


Figure V-8. (e) Seamount 23 is a submarine volcano in the South Pacific.

f)

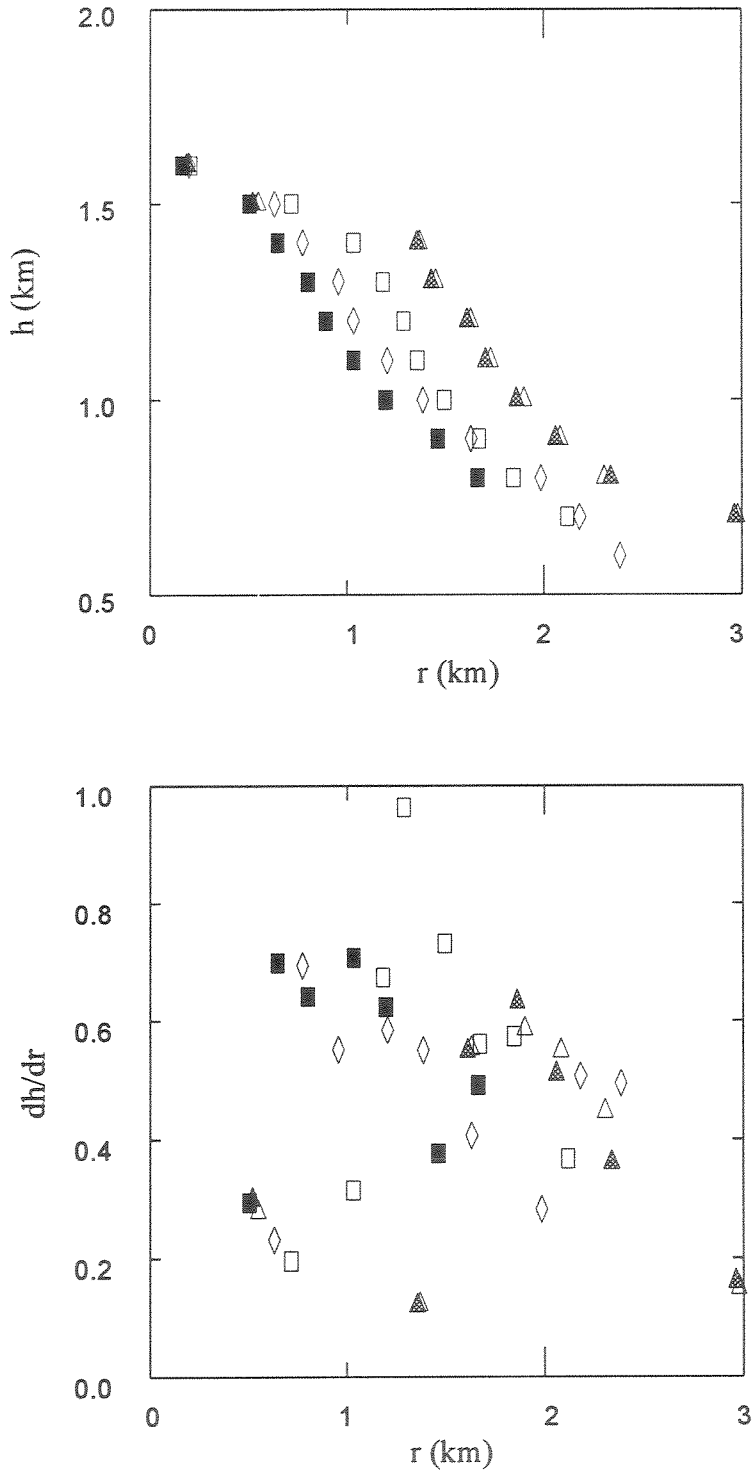


Figure V-8. (f) Herdhubreidh is a table mountain in Iceland.

g)

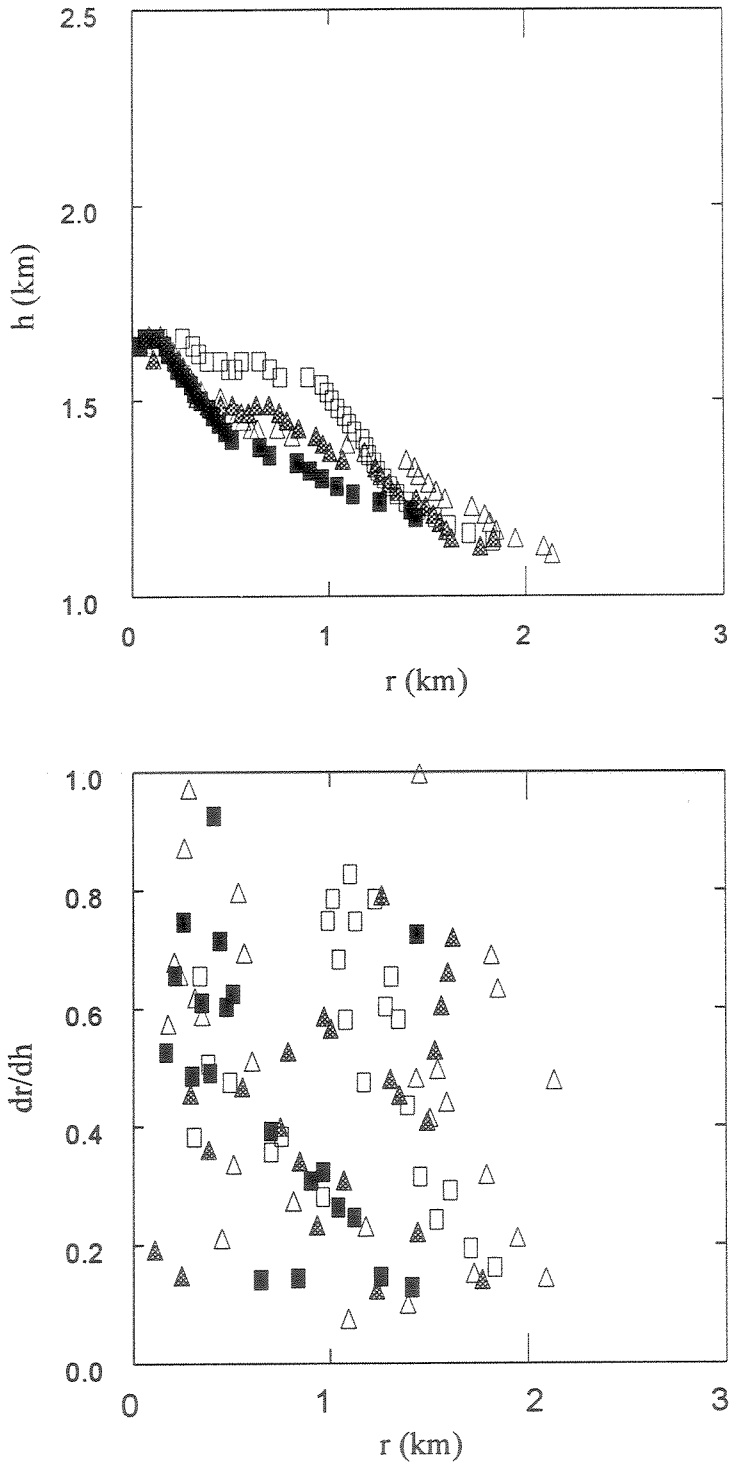


Figure V-8. (g) Volcan Moyuta is a dome in Guatemala (it is also an eruption center along the arc front).

h)

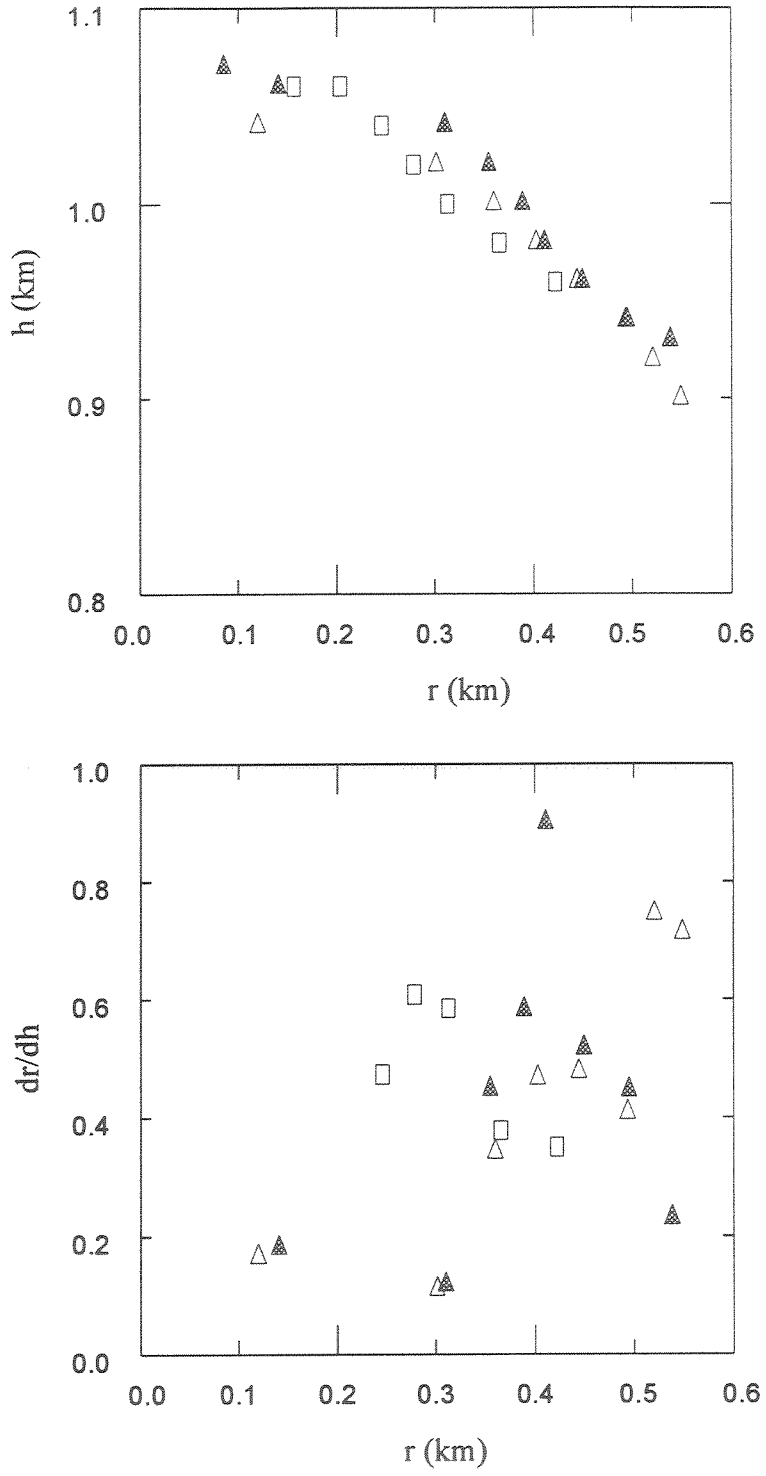


Figure V-8. (h) Cerro Pino Redondo is a dome in Guatemala.

where dh/dr is the tangent of the local slope at r(n+1), r is the radial distance from the summit, and h(n) is the height at r(n). The tangent value, dh/dr, is used instead of the slope as the mathematical analysis of interpreted slope variations is simpler (see sections discussing type differentiation by profile and the quadratic model of composite volcano profiles). Figure V-8 shows the topographic and slope profiles for several different volcanic types. The lengths of the profiles depend on the size of the volcano as the spacing of digitized points depended on the spacing of contour lines (at 20 m intervals).

Notice that the actual dh/dr (and slope) value is highly variable. This is partly a function of the irregularity of volcano surfaces and partly the effect of differentiation, which magnifies small irregularities (integration smoothes). The slope profiles have a larger error than the topographic profiles.

RESULTS OF DATA ANALYSIS

Comparison to existing models

Based on Ben-Avraham and Nur's [1980] observations, volcano height is expected to be uniform and not to correlate with summit elevation in Guatemala, where most of the composite volcanoes lie along the volcanic arc front. Instead, volcano height correlates with summit elevation (Figure V-9). Whereas, shield volcano heights are generally uniform, composite volcano heights are not (Figure V-10). Iceland has oceanic crust, with rift related tectonics instead of intraplate tectonics and the Snake River Plain is continental area with rift or hotspot related tectonics instead of subduction zone tectonics. It is not immediately obvious what trends could be expected. Icelandic shield volcanoes and table mountains increase in height as the summit elevation increases (R=0.70 and R=0.83, respectively) (Figure V-11). No clear trend is observed for the Snake River Plain shield volcanoes (Figure V-12). For the oceanic volcanoes of the South Pacific, I expected to observe that volcano height is inversely correlated with the depth of the seafloor and that the summit elevation is uniform. The volcanoes included in this study are much too small

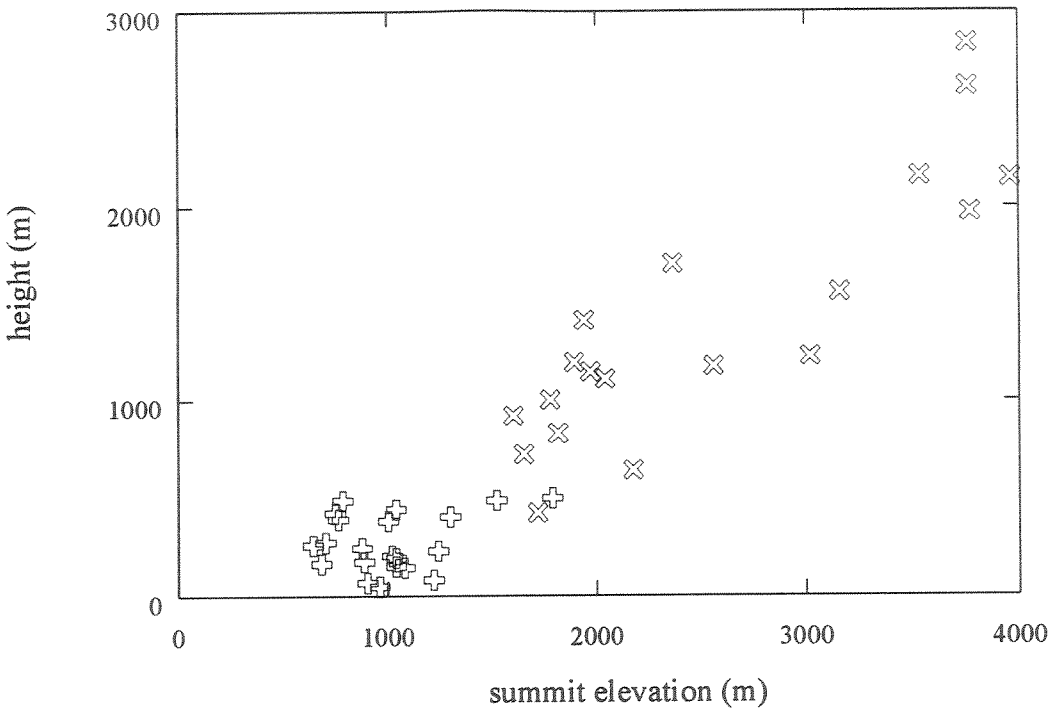


Figure V-9. Volcano height increases with increasing summit elevation for shield volcanoes (open +) and composite volcanoes (open x) along the Central American arc in Guatemala and El Salvador. Composite volcano height is highly correlated with summit elevation (R=0.87), while shield volcano height changes little with summit elevation (R=0.27).

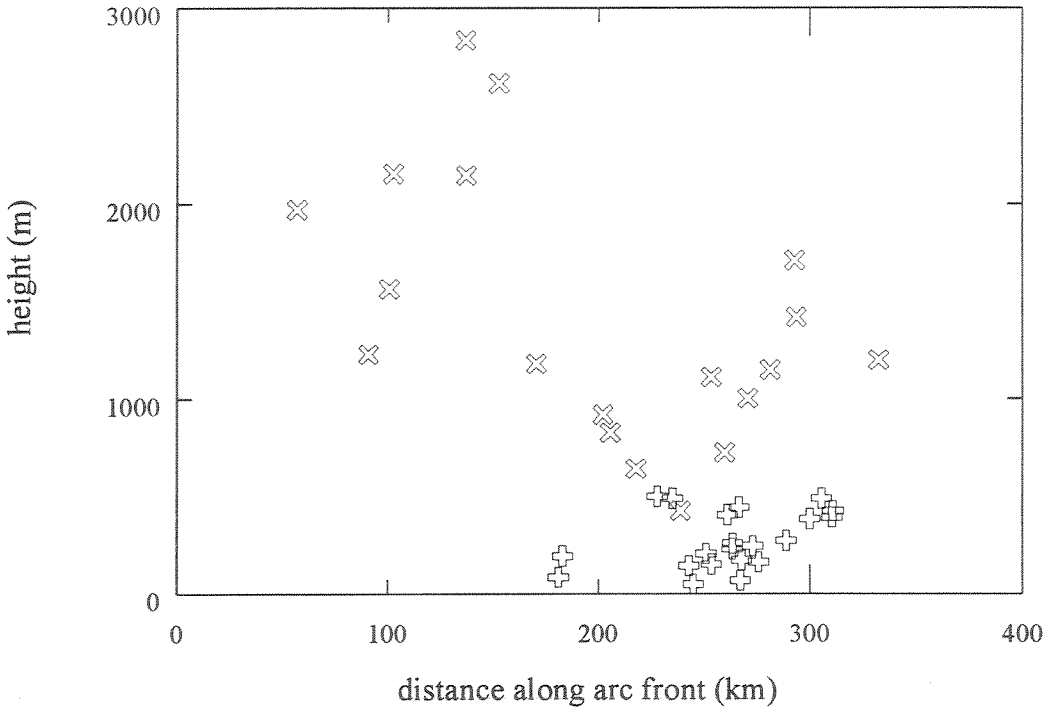


Figure V-10. Volcano height is highly variable along the arc. Shield volcano heights are somewhat more uniform than composite volcano heights. Open crosses are shield volcanoes and open x's are composite volcanoes.

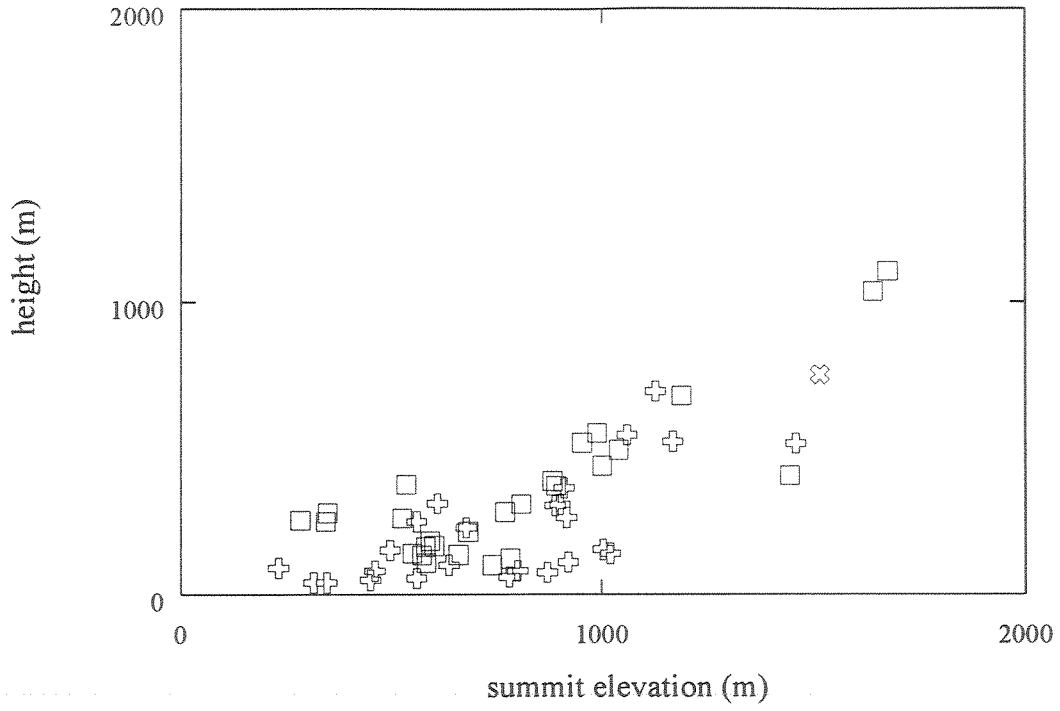


Figure V-11. Volcano height increases with increasing summit elevation for shield volcanoes and table mountains in the rift zone of Iceland. Both table mountain height and shield volcano height are highly correlated with summit elevation (R=0.83 and R=0.70, respectively). Open crosses are shield volcanoes, open x is a composite volcano, and open boxes are table mountains.

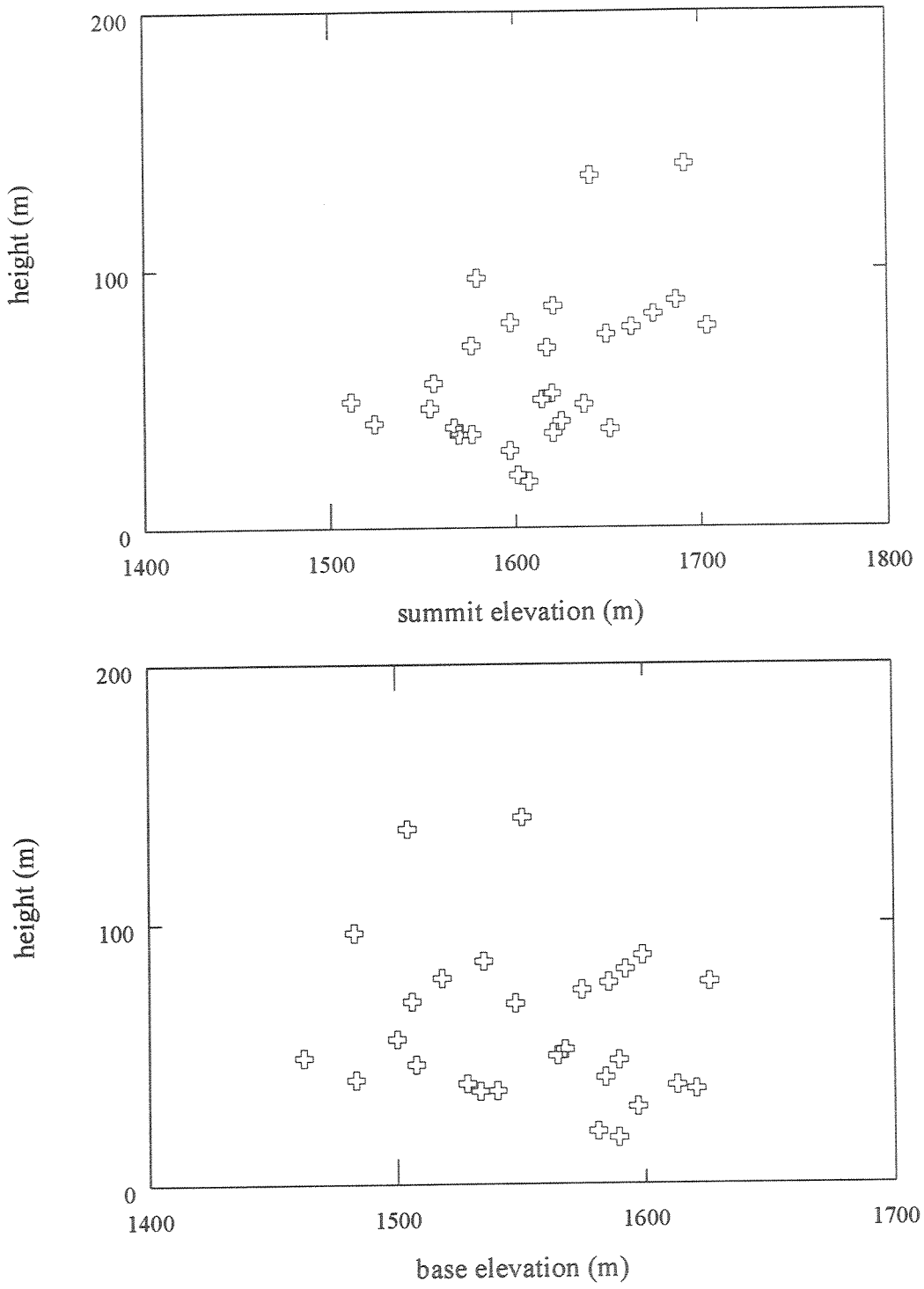


Figure V-12. Height does not change much with either summit elevation or basal elevation for the shield volcanoes of the Snake River Plain. The heights are very low compared to other regions which may account for the lack of correlation between summit elevation and volcano height (R=0.49).

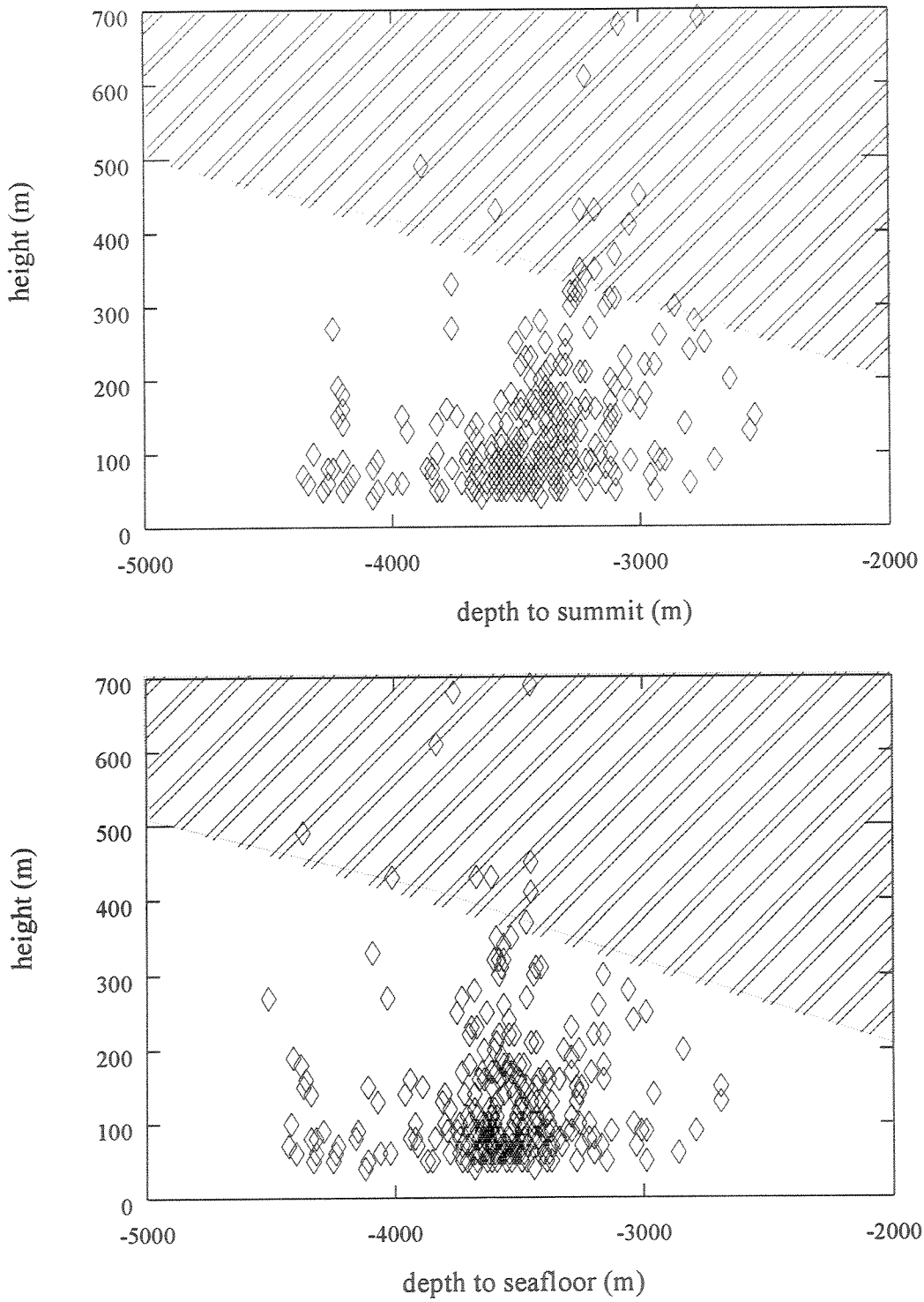


Figure V-13. Relationships between volcano height and summit depth or seafloor depth are difficult to gauge because of the restrictions on sampling large volcanoes by the swath width of SeaBeam data. Shaded region is undersampled because it corresponds to basal diameters significantly wider than the swath width. No correlations can be discerned.

for the summit elevation to mean much (in this model). No obvious correlation is observed between volcano height and the depth of the seafloor (Figure V-13). Clearly, the predictions of Ben-Avraham and Nur [1980] are not borne out.

Borgia and Linneman's [1990] model of lava armor predicts that the h/r ratio and slope increase with height, but not with basal diameter, that lava flow age increases away from the summit, and that local flank slope is constant on the upper flank and increases towards the summit on the lower flank. As their model was developed for a composite volcano, but requires no assumptions that are inappropriate for shield volcanoes, its predictions are compared with observations for both shield and composite volcanoes.

For composite volcanoes (in Guatemala), I observe no change in the h/r ratio or slope with either height or basal diameter (Figure V-5). Rose et al. [1980] present a geologic map of the Lago de Atitlán region that suggests that lava flow age increases away from the summit for Volcán Toliman, Volcán Atitlán, and Volcán San Pedro. Local flank slope increases towards the summit, gradually on the lower flank and rapidly on the upper flank (e.g., Figure V-8a). In Borgia and Linneman's [1990] model, the flank slope increases more slowly as the summit is approached. The Borgia and Linneman [1990] model explains some aspects of composite volcanoes in Guatemala (increase in lava flow age away from the summit; creation of steep upper flanks; rough profile shape), but is inconsistent with the trends observed in their morphological parameters and cannot explain the detailed shape of their slope profiles.

For shield volcanoes in Guatemala, I observe that the h/r ratio and slope increase strongly with height and weakly with basal diameter (Figure V-5). For shield volcanoes in Iceland and Snake River Plain, the h/r ratio and slope show little or no change with height or basal diameter (Figures V-6 and V-7). I have no information on individual lava flow ages for any of the shield volcanoes studied. The slope profiles of shield volcanoes (e.g., Figure V-8b-c) indicate that local flank slope does not vary greatly. However, a comparison of the slope profiles in Figure V-2 and that in Figure V-8c suggests that the

Borgia and Linneman [1990] model for maximum slopes of 5°-10° may explain the detailed structure of the slope profile of Trolladyngja, Iceland.

In summary, Borgia and Linneman's [1990] model provides some understanding about one way lava flows may combine to form an edifice. Their flow field model yields a topographic and slope profile that fits shield volcanoes better than composite volcanoes. In spite of this, the dependence of lava flow length on topographic slope (on which their model is based) is observed in Guatemalan composite volcanoes. The lack of good fit to Guatemalan composite volcano profiles is probably related to the assumption that the upper surface of composite flows tends to attain a constant slope.

Lacey et al.'s [1981] model predicts that average flank slope should decrease as the volcano grows, that volcanoes that grow faster (higher effusion rate) should have generally steeper flanks, and that all volcano flanks should steepen towards the summit. This study observes that the height-to-radius ratio of subduction zone shield volcanoes increases with size (Figure V-5), whereas the height-to-radius ratio of rift or hotspot shields is constant to decreasing with size (Figures V-6-7). Volcanoes expected to have been erupted at higher effusion rates (Iceland, Snake River Plain) are shallower sloped than those expected to have been erupted at slower effusion rates (Guatemala) [Crisp, 1984]. Individual shield volcanoes usually have basically constant flank slopes. Composite volcanoes do have flank slopes that increase towards the summit, but their height-to-radius ratios do not change significantly with size. Lacey et al.'s [1981] model does not explain the shape relationships for either composite or shield volcanoes.

Shteynberg and Solov'yev's [1976] model of basal cone deformation predicts that lower flank slope increases towards summit for larger cones, that circumferential thrust faults will be found around base of flanks, and that the upper flank slope is constant and the same for all volcanoes. Pure deformational models predict only the occurrence of circumferential faults and a low slope for the lower flank. This study observes that flank slope increases towards summit for composite volcanoes (e.g., Figure V-8a), that lower

Table V-1. Analysis of average upper and lower flank slopes of composite volcanoes.

Volcano (Latitude, Longitude)[1]	Upper Flank Average Slope	Lower Flank Average Slope	Full Flank Average Slope[2]
Acatenango (14.5°, 90.9°)	25.7°±0.7°	8.3°±4.7°	24°
Agua (14.5°, 90.7°)	26.8°±0.7°	8.4°±2.4°	18°
Atitlán (14.6°, 91.2°)	25.2°±0.5°	NA	24°
Boqueron (13.7°, 89.3°)	13.8°±0.5°	6.4°±1.0°	10°
Chingo (14.1°, 89.7°)	26.1°±1.1°	NA	21°
Fuego (14.5°, 90.9°)	26.9°±0.6°	6.6°±4.1°	22°
Ipala (14.6°, 89.6°)	14.8°±0.7°	14.8°±6.1°	14°
Izalco (13.8°, 89.6°)	28.1°±0.6°	8.4°±0.4°	12°
Pacaya (14.4°, 90.6°)	27.7°±0.8°	11.6°±0.8°	18°
San Pedro (14.6°, 91.3°)	30.3°±0.3°	NA	23°
Santa Ana (13.8°, 89.6°)	18.6°±0.6°	7.4°±1.1°	9°
Santa Maria (14.8°, 91.6°)	30.1°±0.3°	13.9°±5.0°	25°
Suchitan (14.4°, 89.8°)	19.2°±0.8°	NA	13°
Toliman (14.6°, 91.2°)	28.9°±0.4°	15.7°±6.2°	23°

[1]Figure V-15 is a location map for these volcanoes.

[2]From morphological parameters.

flank slope is constant and upper flank slope increases rapidly towards summit (e.g., Figure V-8a), and that there is significant variation in upper flank slopes (Table V-1). The increase in local flank slope is in the upper flank, not the lower flank as predicted. Also contrary to predictions, the average slope of the upper flank varies from 14° to 30°. Overall, no basal deformation can be inferred for the volcanoes of this study (which are mostly much smaller than those studied by Borgia et al. [1992]). It is not realistic to apply Shteynberg and Solov'yev's [1976] model as composite volcanoes cannot be considered free-flowing cones.

Differentiation of volcanic types using topographic profiles and slope profiles

The topographic profiles of different volcanic types have different shapes and scales (see Chapter II for description of types). Because of differences in the shape of the topographic profile, the slope profiles are also different. Composite volcanoes have flanks that steepen dramatically towards the summit; this is most apparent in the rapid increase of slope towards the summit (e.g., Volcán Agua in Figure V-8a). Shield volcanoes have flatter topographic profiles; their slope profiles indicate virtually constant flank slope (Figures V-8b-c). Icelandic shields have lower average flank slopes than Guatemalan shields; they also show a slight increase and then decrease in the flank slope towards the summit (e.g., Figure V-8c). Submarine volcanoes have a variety of different topographic profiles; they range from flat shield-like profiles (e.g., Figure V-8d) to much steeper profiles (e.g., Figure V-8e). All have reasonably constant flank slopes (Figures V-8d-e). Table mountains are steep flanked features that have a constant flank slope (e.g., Figure V-8f). Guatemalan domes have moderately steep flanks, but widely varying flank slope; average flank slope is probably constant (e.g., Figure V-8g-h).

In summary, topographic and slope profiles come in three classes (Figure V-14). Composite volcanoes have unique slope profiles with slope increasing towards the summit (Type I in Figure V-14). The rest of the volcanic types can be divided into two groups:

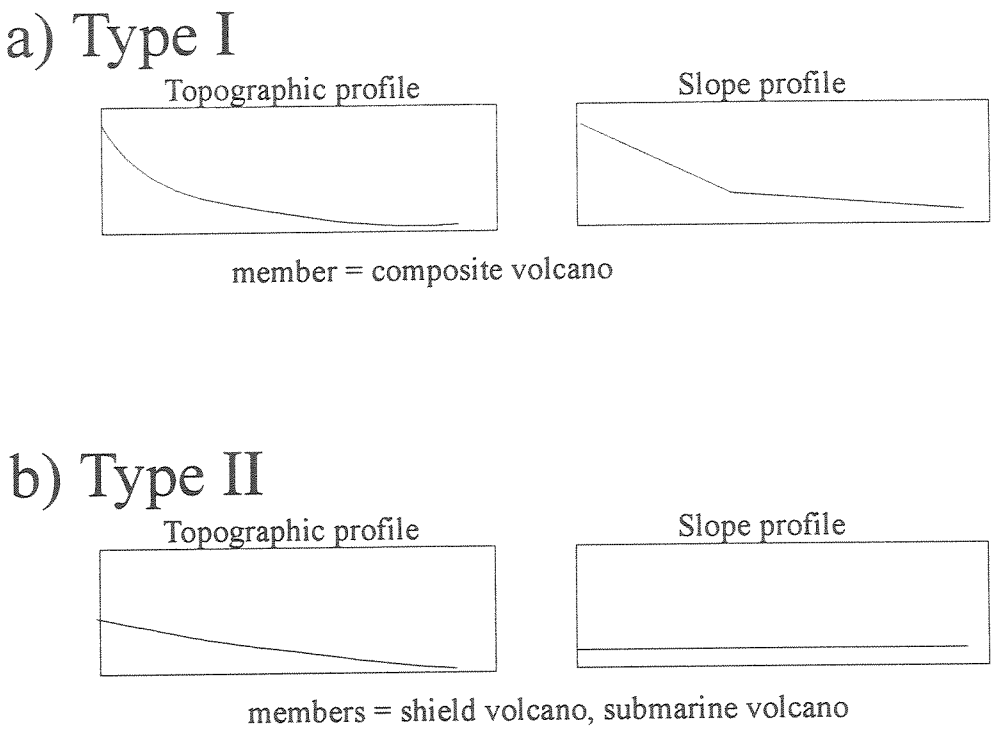


Figure V-14. The three classes of topographic and slope profiles are based on distinctions in the shape of the slope profile and the magnitude of the average flank slope: Type I = slope increases towards summit; moderate average slope; Type II = constant flank slope, low average slope; Type III = constant flank slope; high average slope. Vertical exaggeration on topographic profiles is about 2 times.

Type II with low and constant flank slopes and Type III with steep and constant flank slopes. Slope profiles are primarily useful for distinguishing composite volcanoes. The other volcanic types can be differentiated by a combination of factors (mostly discussed already in Chapter II), including size.

The volcanoes of Types II and III have generally constant flank slopes. In some cases, steeper slopes near the summit are due to the presence of a cinder cone on the summit. Low slopes near the summit are indicative of a wide flat summit region or a crater (which explains negative values near the summit also, which were not shown on Figure V-8). The average flank slope was determined for each slope profile (Table V-2). Regression was performed on both the topographic profile and the slope profile to determine just how little variation in slope could be inferred. The high correlation between height h and radial distance r, the low errors in linear regression of h against r, the low correlation between slope and radial distance r, and the high errors in linear regression of slope against r indicate that for Type II and III volcanoes there is little change in slope with radial distance and the interpretation of constant flank slopes from Figure V-8 is correct (Table V-2). Two of the shield volcanoes in Table V-2 (Las Flores and Trolladyngja) may have a consistent decrease in slope from the summit, but the rate of change is low. Type II volcanoes have consistently lower slopes than type III volcanoes (Table V-2) as observed above.

Composite volcanoes (Type I) have flanks that steepen dramatically towards the summit - the slope increases linearly to exponentially towards the summit. This study observes, however, that the outer flanks have generally a constant slope, rather than gradually increasing as expected with the exponential model (see Milne [1878] and Becker [1885] for an exposition of the exponential model). I interpret this break in slope as an intrinsic morphologic feature and believe its radial location can be used to normalize the profiles of composite volcanoes (Figure V-12). Regression analysis (with height specified as the dependent variable) was used to determine the linearity of slope change on the steep

Table V-2. Analysis of slope profiles for Type II and Type III volcano profiles

Volcano	Volcanic Type[1]	Average Slope	Topographic Profile		Slope Profile		
			Slope	R	Rate	Intercept	R
		(°)	(km/km)		(°/km)	(°)	
Type II:							
Las Viboras	sh (G)	10.3±2.3	-0.176±0.005	-0.98	1.4±1.2	8.4±1.2	0.24
Los Flores	sh (G)	12.5±5.1	-0.169±0.004	-0.99	-0.8±1.3	12.0±1.9	-0.65
Trolladyngja	sh (I)	7.2±0.3	-0.104±0.003	-0.97	-1.5±0.2	10.7±0.1	-0.68
Smt 159	smt (SP)	5.6±0.7	-0.060±0.007	-0.87	-1.7±1.9	7.2±1.1	-0.23
Type III:							
Smt 23	smt (SP)	22.5±0.6	-0.396±0.013	-0.95	-3.4±1.4	25.7±0.3	-0.21
Herdhubreidh	t (I)	28.9±1.9	-0.380±0.025	-0.91	-3.2±3.1	33.2±2.0	-0.15
Moyuta	d (G)	22.8±1.5	-0.263±0.011	-0.92	-7.5±2.3	33.7±0.6	-0.32
Pino Redondo	d (G)	23.1±2.2	-0.344±0.024	-0.95	25±24	14±11	0.25

[1]The first word indicates volcanic type: sh = shield, smt = submarine volcano, t = table mountain, and d = dome. The second word (in parentheses) indicates location: G = Guatemala, I = Iceland, and SP = South Pacific.

Table V-3. Analysis of slope profiles for Type I volcano profiles.

	Upper Flank		
Volcano [1]	Average Slope	Slope of dh/dr vs. r	R
Acatenango	25.7°±0.7°	0.084±0.007	0.58
Agua	26.8°±0.7°	0.128±0.005	0.83
Atitlán	25.2°±0.5°	0.111±0.005	0.76
Boqueron	13.8°±0.5°	0.050±0.008	0.51
Chingo	26.1°±1.1°	0.316±0.022	0.86
Fuego	26.9°±0.6°	0.100±0.005	0.80
Ipala	14.8°±0.7°	NA	NA
Izalco	28.1°±0.6°	0.445±0.029	0.76
Pacaya	27.7°±0.8°	0.255±0.021	0.79
San Pedro	30.3°±0.3°	0.291±0.017	0.91
Santa Ana	18.6°±0.6°	0.123±0.016	0.68
Santa Maria	30.1°±0.3°	0.118±0.006	0.67
Suchitan	19.2°±0.8°	NA	NA
Toliman	28.9°±0.4°	0.148±0.013	0.60

[1]Volcano location is given in Table V-1 and in Figure V-15. All are composite volcanoes in Guatemala.

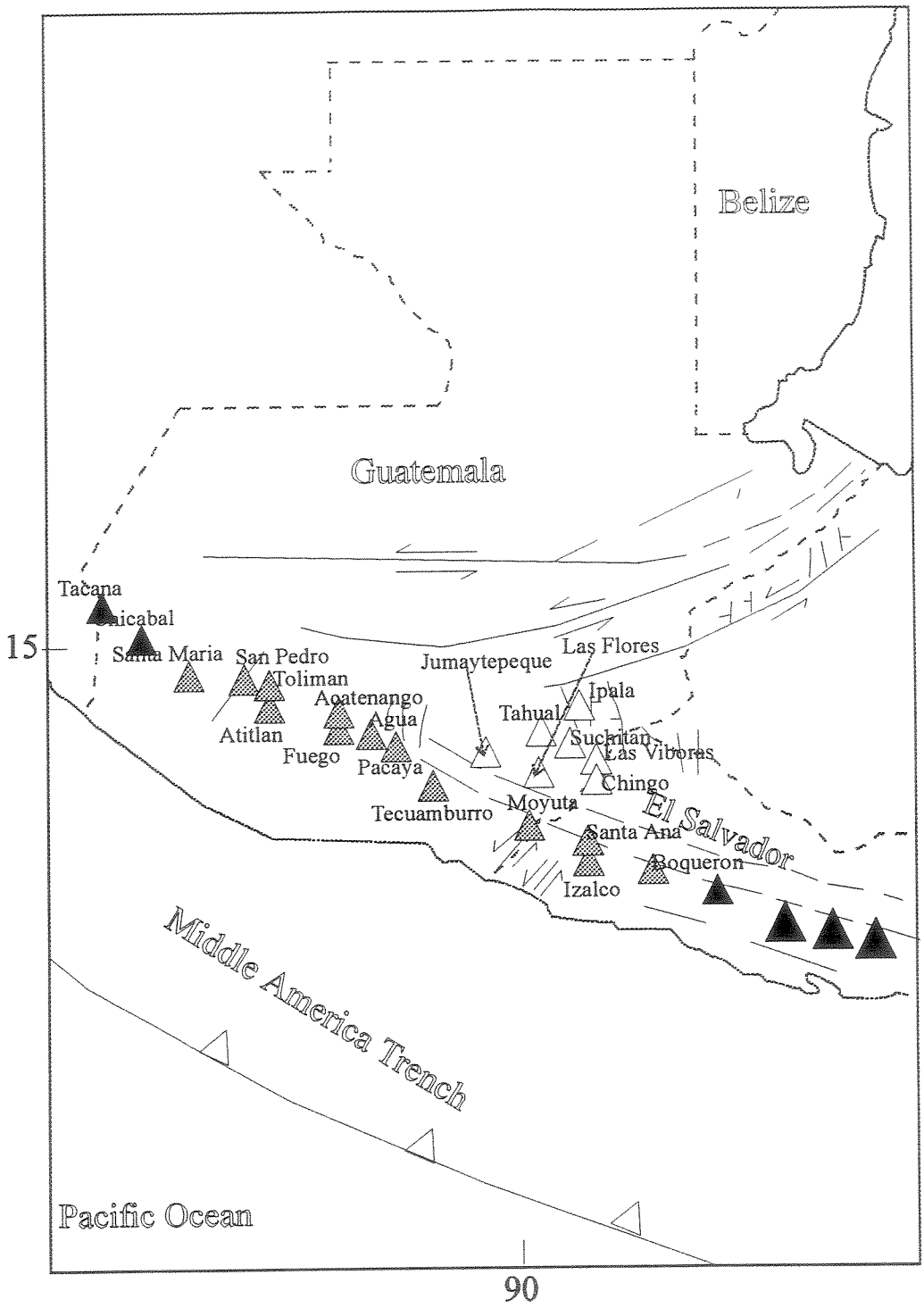


Figure V-15. Location of large volcanoes in Guatemala. Black triangles indicate arc front volcanoes not included in this study. Grey triangles indicate arc front composite volcanoes (except that Moyuta is a dome not a composite volcano). Open triangles indicate behind-the-front volcanoes - which can be either shield or composite volcanoes.

section (r < breakpoint) (Table V-3). The average slope of the lower flanks was also recorded (Table V-1).

Comparison of shield and composite volcanoes

There are many differences in the morphology of shield and composite volcanoes in Guatemala; this section emphasizes the difference in size. The shield volcanoes of Guatemala are uniformly smaller that the composite volcanoes of Guatemala; this holds regardless of size measure. The largest shields and the smallest composite volcanoes have similar shapes. A consistent trend of shape with size can be interpreted from Figure V-5; Figure V-16 shows this trend for the back arc volcanoes. This suggests shield volcanoes may evolve into composite volcanoes. In Guatemala, there are no small composite volcanoes or large shield volcanoes. On the other hand, there are no shields along the arc front and few composite volcanoes in the back arc. Additionally, the petrologic and chemical characteristics of the back-arc composite volcanoes more closely resemble those of the arc front than those of the shield volcanoes [Walker et al., in press]. The small size of the shield volcanoes may represent, not an early stage of evolution, but rather the effect of conduit shifting - the back arc extensional setting may allow magma to rise equally easily anywhere rather than being localized in its initial choice. This would imply that Guatemalan shields are essentially monogenetic (in the sense of being from one batch of magma), whereas composite volcanoes are polygenetic and their large size is due to growth over a longer period of time.

Shield volcanoes in different tectonic settings

This study has considered shield volcanoes from three different tectonic settings: Guatemala (a subduction-related back arc extensional graben), Iceland (a mid-ocean spreading related rift zone with some hot spot influences), and the Snake River Plain (a hot spot trace with possible influences from Basin and Range extension). The shields in all

Table V-6. Multiple regression for the quadratic coefficients of topographic profiles.

Volcano[1]	m/2	a	C	R	r_{int}[2]	h_{int}[3]	p*[4]
Acatenango	0.0432±0.0033	-0.671±0.016	4.01±0.01	0.987	7.77	1.40	2.98
Agua	0.0689±0.0031	-0.786±0.015	3.83±0.01	0.989	5.70	1.60	2.54
Atitlán	0.0536±0.0023	-0.704±0.012	3.61±0.01	0.988	6.57	1.30	2.84
Boqueron	0.0151±0.0053	-0.301±0.031	1.99±0.04	0.969	9.97	0.49	6.64
Chingo	0.1674±0.0246	-0.757±0.046	1.75±0.02	0.970	2.26	0.89	2.64
Fuego	0.0589±0.0011	-0.748±0.006	3.75±0.01	0.998	6.35	1.38	2.67
Izalco	0.1944±0.0253	-0.832±0.045	2.00±0.02	0.975	2.14	1.11	2.40
Pacaya	0.1493±0.0184	-0.783±0.036	2.60±0.01	0.984	2.62	1.57	2.55
San Pedro	0.1399±0.0031	-0.961±0.010	3.24±0.01	0.999	3.43	1.59	2.08
Santa Ana	0.0678±0.0198	-0.679±0.106	2.89±0.13	0.949	5.01	1.19	2.95
Santa Maria	0.0581±0.0021	-0.727±0.008	3.79±0.01	0.995	6.26	1.52	2.75
Toliman	0.0729±0.0107	-0.688±0.035	3.24±0.03	0.971	4.72	1.62	2.91

[1]Volcano location is in Table V-1 and Figure V-15.
[2]$r_{int}=-a/m$.
[3]$h_{int}=C-a^2/2m$.
[4]$p^*=-2/a$.

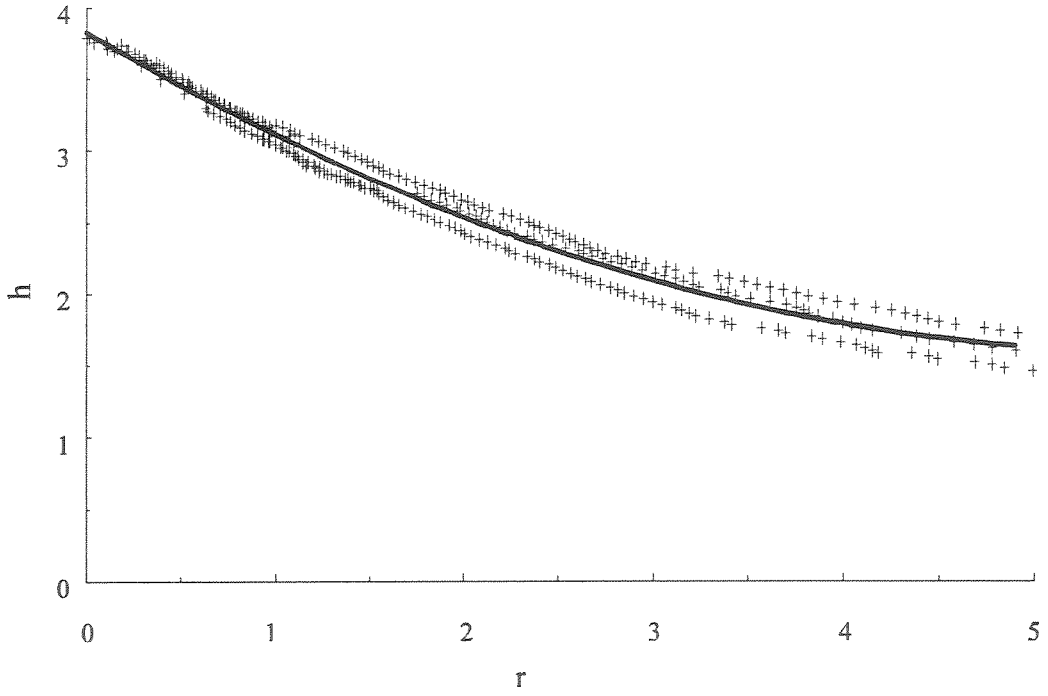


Figure V-21. The three topographic profiles (crosses) for Volcán de Agua, Guatemala are compared to the profile (dark line) predicted by the multiple regression coefficients reported in Table V-6.

Table V-7. Comparison of linear, quadratic and cubic multiple regressions for Agua.

Order	Degrees of Freedom	Variance	Mean Square	F of Regression (Confidence)	F of Improvement (Confidence)[1]
Linear	1	115.312	115.312	5310 (>97.5%)	NA
residual	310	6.731	0.021		
Quadratic	2	119.483	59.7416	7210 (>97.5%)	503 (>97.5%)
residual	309	2.560	0.0083		
Cubic	3	119.513	39.8375	4847 (>97.5%)	3.57 (n.c.)
residual	308	2.531	0.0008		
Total	311	122.043			

[1]Measures the amount of additional variance accounted for by adding a term; F = [{(Variance(higher order) - Variance(lower order)}/{v(higher order) - v(lower order)}]/Residual variance(higher order); v(denominator) = n - order; v(numerator) = 1; v = degrees of freedom; order is order of the polynomial, which is being fit to the data.
n.c. = no confidence.

to have a different geochemical fractionation trend than the others), San Pedro with a steeper profile (a small composite volcano), and Santa Ana with a shallowly sloping summit section, although its lower flanks plot with the majority (the shallow summit is probably the result of a large caldera forming explosion and incomplete recovery of the edifice shape). I conclude that the shapes of most composite volcanoes are similar over a wide range of sizes, but that there are exceptions and in some cases indications of complexity in eruption history.

In the section on along arc variations, this study observed that the slopes of these composite volcanoes varied; different slopes and similar upper flank shapes can be reconciled by considering the variation in the normalized locations of the breakpoints and the basal edge of the volcanic edifice. Differences in breakpoint location affect how far out the profile shape can be expected to be consistent; note that some of the volcanoes in Figure V-22 shallow out faster near the base. The choice of basal edge has a strong effect on the morphologic parameters (e.g., slope), but no effect on the multiple regression of upper flank shape and size normalization. Thus, the average slopes of these composite volcanoes vary, because the width of the lower flank ($r > r_b$) varies. Lower flank width could be related to a variety of factors including initial lava flow length, accumulation of pyroclastic and volcanoclastic material, and regional topography.

The quadratic model of the topographic profile of a composite volcano is empirical; it does not provide an obvious understanding of process. However, its excellent fit to real composite volcano profiles (see Table V-7 for fit analysis) and its usefulness in normalizing profiles for summit location and volcano size justify further investigation of the model's significance. The form of equation (8) is the general form of a parabola whose axis is parallel to the vertical axis (h-axis). The normalization factors r_{int} and h_{int} correspond to the vertex of the parabola. Equation (8) can be rewritten in the form

$$(r-r_{int})^2 = p(h-h_{int}), \tag{14}$$

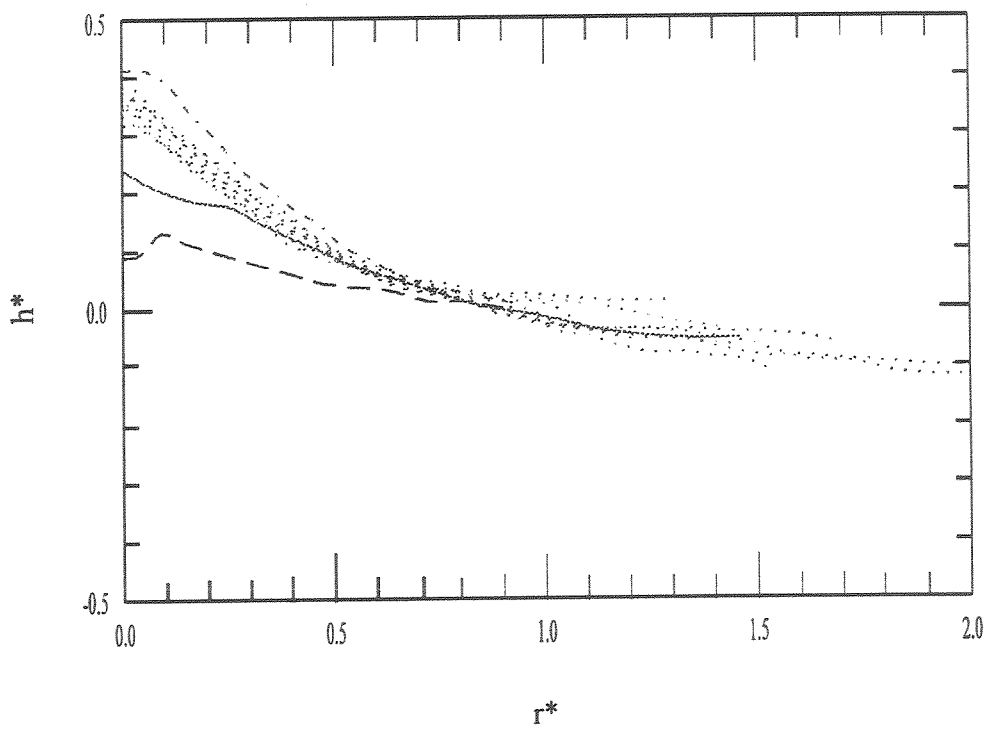


Figure V-22. Normalized topographic profiles for 12 composite volcanoes in Guatemala and El Salvador are plotted together in order to compare their shapes. The normalized height and radius, h* and r*, are defined in the text such that h*=0 when h=hint and r*=1 when r=rint. Notice that most of the profiles form a thin band. The main exceptions are Boqueron with a shallower profile (dashed line), San Pedro with a steeper profile (dash-dot line), and Santa Ana with a shallow summit section, although its lower flanks plot with the majority (solid line). Several volcanoes have profiles that flatten out early and fail to pass through the region of (r*,h*)=(1,0).

where (r_{int},h_{int}) is the vertex of the parabola and p = 2/m is the width of the parabola at the focus, a distance p/4 above the vertex. After normalization, equation (14) becomes

$$(r^*-1)^2 = p^*h^*, \quad (15)$$

where $r^*=r/r_{int}$, $h^*=(h-h_{int})/r_{int}$, and $p^*=p/r_{int}=(-m^2/2a)$. The vertex is now at $(r^*,h^*)=(1,0)$ and all parabolas normalized in this fashion will pass through this point. Notice that in Figure V-22 most of the profiles pass through (1,0); the exceptions are the few that flatten out before r* = 1. The profiles in Figure V-22 that plot together for the whole upper flank correspond to parabolas with the same value of p* (values reported in Table V-6). The parameter p is a measure of the width, or curvature, of the parabola. The parameter r_{int} measures how far the axis of the parabola is shifted from the h-axis. A balance between these parameters (p and r_{int}) indicates that a constant amount of curvature is contained in the distance between r = 0 and r = r_{int} (or the breakpoint of the slope profile for composite volcano profiles). Thus, the shape of the topographic profiles of most of the composite volcanoes in Guatemala is size-independent (i.e. not dependent on the absolute magnitudes of the height and basal diameter).

If the shape of composite volcano profiles is size-independent, it might be expected that the morphological parameters, estimated from the right-circular cone model (rcc), would be independent of size and that slope, in particular, would be constant. All three shape parameters (t/r, h/r and slope) are essentially independent of size (see Figure V-3), but the actual values of the h/r ratio and slope vary significantly. The variation in h/r ratio and slope in the right-circular cone model is a function of the absolute value of the basal diameter not the shape of the upper flank; notice that the average upper flank slopes are generally similar, but the average lower flank slopes and overall slopes vary greatly (Table V-1). I suggest that the processes that determine the basal diameter are independent from the processes that determine the profile (upper flank) shape. One possibility is that the basal diameter is controlled by the formation of a volcaniclastic apron from the cumulative effects of pyroclastic and erosional activity.

The shape of the upper flank may be primarily controlled by the emplacement of lava flows; if so, the lava flows must progressively shorten as the volcano grows. This interpretation is consistent with Borgia and Linneman's [1990] interpretation of Arenal, even though it is not consistent their final model. Borgia and Linneman [1990] assumed that the upper surfaces of composite flows attain a constant slope, implying constant upper flank slopes, whereas the data in this study indicate that upper flank slopes increase progressively towards the summit (compare Figure V-2 (Borgia and Linneman model) with Figure V-8 (data) and Figure V-20 (proposed model)). However, the data of this study are not necessarily inconsistent with Borgia and Linneman's [1990] analysis of lava flow behavior suggesting an inverse relation between lava flow length and the tangent of the topographic slope (equation (2) in the introduction).

The consistency of the fitted parabola shape for most of the composite volcanoes suggests that the shape variations along the arc discussed earlier can be attributed to variations in the lower flank. This study has already observed that the slope (rcc) reflects the extension of the basal diameter beyond the fitted parabola vertex; slope (rcc) is highly, but negatively, correlated with the ratio of the basal diameter (rcc) and r_{int} (R=-0.96). However, this ratio (basal-diameter/r_{int}) does not correlate strongly with crustal thickness (R=-0.39) or along arc distance (R=-0.42) as expected (since slope (rcc) does); the relative importance of Boqueron (which does not fit the same parabola) and Izalco (the youngest composite volcano) to correlations with along arc distance and crustal thickness may explain the lack of a coherent set of correlations (removing Boqueron and Izalco means that only Santa Ana is left with a significantly lower crustal thickness and at that end of the arc). The addition of more composite volcanoes from El Salvador and other parts of the Central American arc might clarify these relationships. On another note, two parameters (C and h_{int}) from the parabola fit do show a consistent increase with crustal thickness and decease southwards along the arc: C is a reasonable measure of summit

elevation and h_{int} is a rough measure of base elevation (although it corresponds with the base of the parabolic portion of the flank).

Model of shield morphology by summing typical lava flow shapes

Shield volcanoes are best defined as piles of lava flows resulting from Hawaiian eruptions [Wood, 1977; Cas and Wright, 1988]. The resulting landform is usually circular to elliptical in plan, convex-up, and gently sloped [Wood, 1977; Wood, 1979; Cas and Wright, 1988]. Minor pyroclastics and breccias may be present (especially as such features as spatter cones, pit craters, etc.). The process that constructs shield edifices is the repeated occurrence of lava flows distributed about a central vent.

A program was written to numerically pile lava flows of a given shape. In most cases, lava flow length was constant for a given run (exceptions are noted below). Several different shapes of lava flows were used: rectangles, wedges and pie sections. Wedges differ from rectangles only in that the thickness increases away from the vent. Varying the lengths of the pie sections was also tried. The ratios of lava flow width to length were based on the reported values for Hawaii, Mt. Etna, and Mt. St. Helens [Posin, 1990]. The thickness of the lava flows was set to 5 m based mainly on the average and maximum thicknesses observed in Hawaii [Posin, 1990]. Input values were weighted highly towards values typical of Hawaii, because they exemplify shield activity and there is a great deal of data for Hawaii. The input parameters for the program include lava flow volume, lava flow length/width ratio, lava flow thickness, and the number of lava flows (see Table V-8 for input values for the reported results). The actual width W and length L are given by

$$W=\mathrm{sqrt}(V/(a*t)) \tag{16}$$

and

$$L=a*W, \tag{17}$$

where a is the length/width ratio, t is the lava flow thickness, and V is the volume of a single lava flow. In order to constrain the size of the data array, all parameters were rescaled inside the calculation such that L = 100 and the other parameters remained in the

same relation to L as they had been; output is rescaled to correct length, etc. The azimuths of the N lava flows are determined by a random number scheme that weights azimuths based on the accumulated thickness of lava flows in order to produce as uniform a distribution of lava as possible.

The output of the program is a 220x220 array of thicknesses that can be contoured, plotted as a mesh, or sliced to get profiles (Figure V-23). For each of four lava flow models, four topographic profiles were obtained (at 90° intervals). Corresponding slope profiles were calculated and analyzed (as discussed for actual profiles for Type II and Type III volcanoes discussed above). The four lava flow models were based on the simplest shapes likely to give interpretable results (Figure V-24): (1) **rectangular box**, (2) **wedge box**, which differs from the rectangular in having increasing thickness away from the vent, (3) **pie section box** and (4) pie section box allowed to vary in length. In the program, lava flow thickness decreases away from the center azimuth of the flow and approaches zero at the flow edges. The profile of each lava flow perpendicular to the azimuth is given by

$$t(y) = 1 - 4y^2/W^2, \qquad (18)$$

where t(y) is the thickness of the lava flow at y, y is the perpendicular distance from the azimuth, and W is the width of the lava flow.

Figure V-25 shows the resulting topographic and slope profiles for each of these models. The profiles vary greatly between the models in variability of slope and shape of the slope profile, although all have extremely low average slopes. Estimates of the morphological parameters (as in Chapter II) are reported in Table V-9. The results of slope analysis are reported in Table V-10.

The rectangular box produces simulated shields whose slope increases rapidly towards the summit (Figure V-25a). The increase in slope towards the vent is not only unshield-like, but unrealistic. It is due to the overlap between rectangles, suggesting that a rectangular box shaped lava flow is too simple to produce realistic volcanoes. Allowing

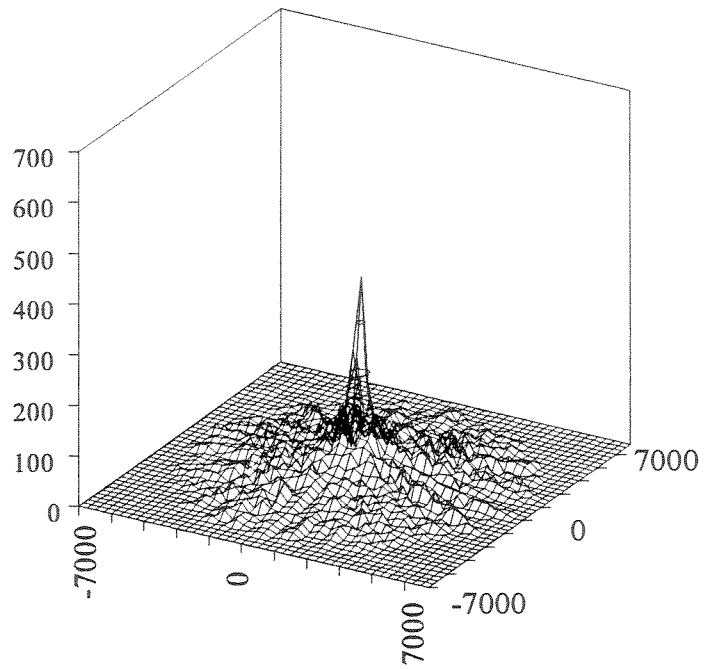


Figure V-23. Example of the output of the lava pile program. (a) Mesh plot of the thickness array. Vertical exaggeration is 20x. This is from a run using the variable pie section box as the lava flow model.

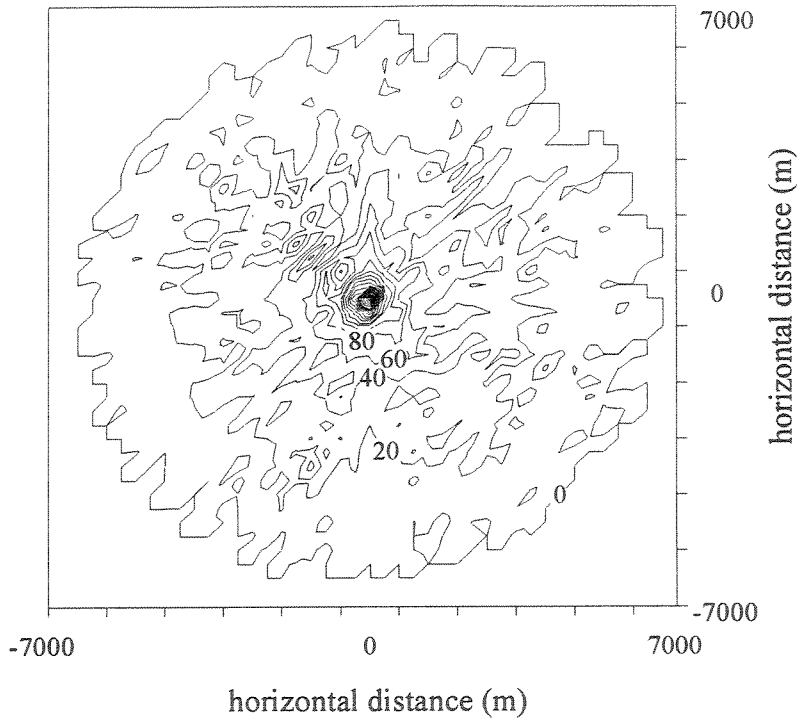


Figure V-23. (b) Contour plot of the thickness array in (a). Contour interval is 20 m; the main contour lines for 0 m to 80 m are labeled. Horizontal units are also in meters.

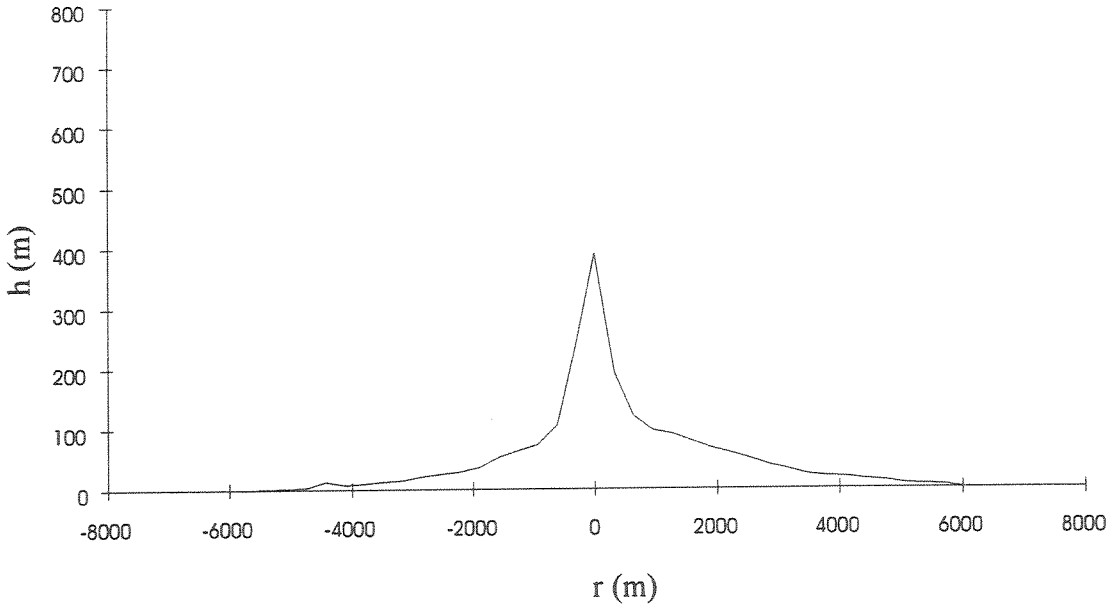
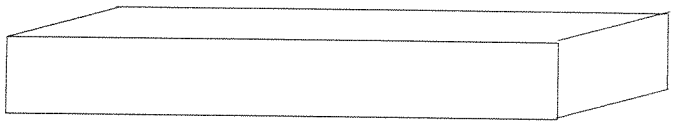


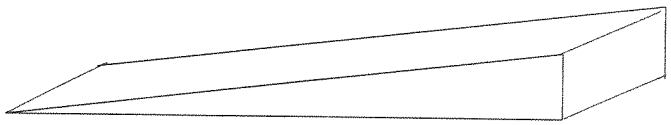
Figure V-23. (c) Profile plot of the thickness array in (a); slice is taken at 90°. Vertical exaggeration is 10x.

LAVA FLOW SHAPE MODELS

a) rectangular box model



b) wedge box model



c) pie section box model

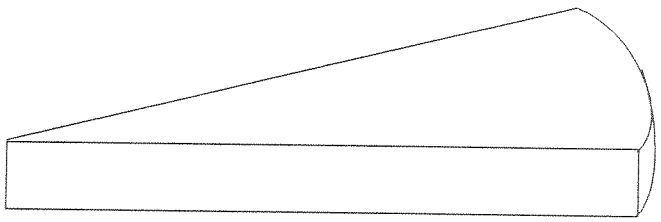


Figure V-24. This study postulates three basic shapes for modeling lava flows: (a) a rectangular box, (b) a rectangular wedge and (c) a pie section box. The fourth lava flow model discussed in the text is formed by varying the length of the pie-shaped box randomly between a minimum and maximum length.

b) wedge box model

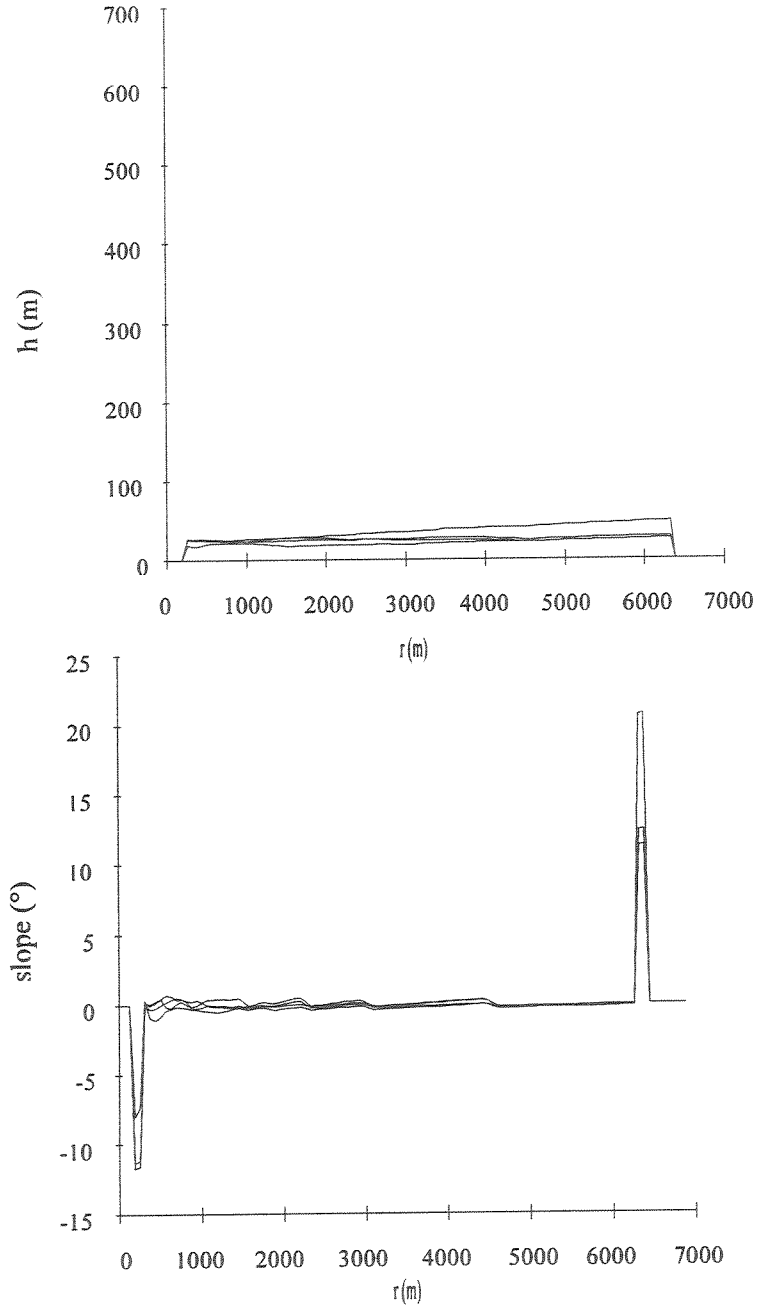


Figure V-25. (b) Increasing the thickness of the rectangular lava flows with distance from the vent produced very flat topographic profiles. Thus, the rectangular shape is necessarily unrealistic. The decrease in thickness towards the summit of the wedge box may be too great as the simulated shield shows a tendency to slope into the vent.

c) pie section box model

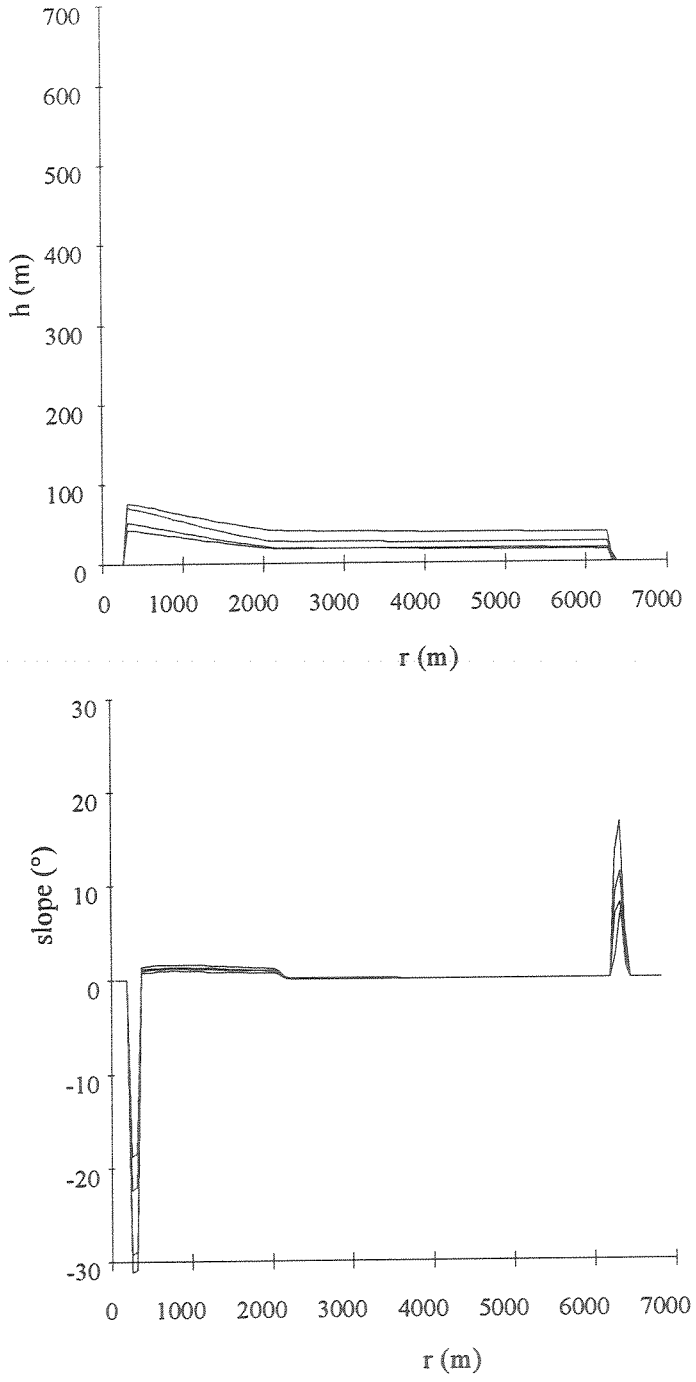


Figure V-25. (c) A pie section box of constant length also produces flat topographic profiles. There is no tendency to slope inward in this case; the flatness is due to lack of overlap between lava flows.

d) variable length pie model

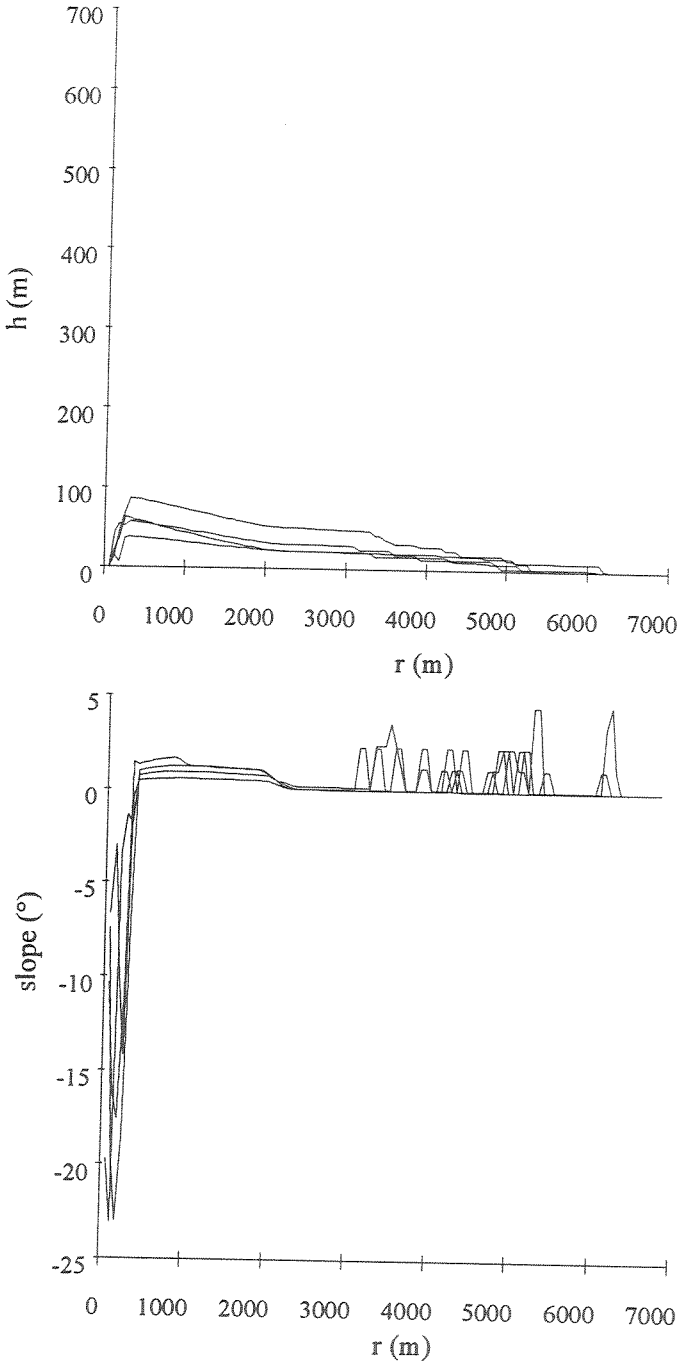


Figure V-25. (d) Varying the length of pie sections produces simulated shields with topographic profiles similar to real shield volcanoes. The slope data (Tables V-9 and V-10) shows these simulated shields have very low average slopes and much higher variation in flank slope than typical for actual shield volcanoes (Tables V-2 and V-4).

A visual comparison of Figure V-8 and Figure V-25 suggests that the simulated topographic profiles are erratic compared to the real ones; both have highly variable slopes, but the simulated slopes flip back and forth between positive and negative. This erraticness of the topography is partly due to the abrupt boundaries of the model lava flows (even though the thickness goes to zero smoothly towards the edge). In addition, each run is composed of only 1000 lava flows, which is near the statistical minimum required for an even distribution of lava. Using more lava flows per run might increase the smoothness of the resulting simulation. A greater number of lava flows will also increase the height of the resulting simulation (without changing the diameter).

RESULTS OF CHAPTER V

Based on the many aspects of the morphology of shield and composite volcanoes discussed in this chapter, there are no existing models that adequately explain the development of either shield or composite morphology or that explain the variations in morphology within and between regions. Borgia and Linneman's [1990] model, in particular, fails to explain the detailed morphology of composite volcanoes. However, it does provide significant insight into the dynamics of edifice building and may be useful, with minor modifications, in modeling shield development.

The morphology of large volcanoes can be classified into three groups. Composite volcanoes (Type I) are characterized by topographic profiles with parabolic (quadratic) upper flanks and nearly linear lower flanks; local flank slope increases rapidly towards the summit. The topographic profiles of other volcanoes are nearly linear and break down into two classes based on average flank slope. Type II volcanoes (which include shield volcanoes and some submarine volcanoes) have low average slopes. Type III volcanoes (which include table mountains, domes and some submarine volcanoes) have high average slopes. Topographic profiles can, thus, be used to identify some aspects of eruption style of large volcanoes; the three classes do correspond to a rough distinction between

explosive processes (Type I), very fluid effusive processes (Type II) and less fluid effusive processes (Type III).

Topographic profiles can also be used to examine in detail the differences between associated volcanoes. Three cases are discussed in the sections above: a detailed examination of Guatemalan composite volcanoes, a comparison across tectonic settings of shield volcanoes and a comparison shield and composite volcanoes in Guatemala.

The characteristic profile of composite volcanoes has been used to formulate a normalizing scheme that allows detailed and quantitative comparisons between individual composite volcanoes and with models of composite volcano growth. The upper flank of a composite volcano is approximately parabolic; multiple regression leads to parameters determining the quadratic equation that characterizes the upper flank shape. These parameters provide a scaling to compare all of the composite volcanoes. Most composite volcano profiles are based on parabolas that differ only in scale not in shape. However, composite volcano steepness varies along the Guatemalan arc front, reflecting differences in the width of the lower flank. Two other parabola parameters (h_{int} and C) vary along the arc, reflecting changes in summit and base elevation; they also correlate with crustal thickness. Neither of the parabola shape coefficients (p and p*) correlate with along arc distance or crustal thickness or, even, volcano volume.

Systematic differences between shield volcanoes of different tectonic settings can be identified based on morphologic parameter relationships. Shield volcanoes in Guatemala and Iceland have similar topographic and slope profiles; they also have similar ranges of morphologic parameters. The shield volcanoes of the Snake River Plain have significantly lower flank slopes than their counterparts in Guatemala and Iceland. The trends of morphologic parameters with size are different in each of the three regions: Guatemalan shield volcanoes increase in steepness as they increase in size. The steepness of Icelandic shield volcanoes changes little, or not at all, with size. Snake River Plains shield volcanoes decrease in steepness as they increase in size. These differences in

morphologic trends are probably related to changes in the factors controlling lava flow length; overall magma supply (to an individual volcano) cannot be a factor as the ranges in edifice volume are identical in Guatemala and the Snake River Plain (Icelandic shield volcanoes have a wider, but overlapping, range of volume).

Based on a comparison of shield and composite characteristics, the Guatemalan shield volcanoes may be monogenetic. The largest shield volcanoes in Guatemala approach the size and shape of the smallest composite volcanoes; however, they are still very different in geochemistry (and presumably eruption style). Duration of magma supply in a single location (conduit) may control the range of shapes displayed in volcanic edifices (as well as their final size).

Simple piles of lava flows (of simple shapes) can produce shield shapes, although not all the details have yet been worked out. So far, numerical simulations of lava flow accumulation have produced topographic profiles that resemble Snake River Plains shield volcanoes. Simulations using larger numbers of lava flows may be able to produce steeper edifice forms. Further experimentation with variations in the number of lava flows and variations in lava flow length (in a single simulation) are needed to define the flexibility and utility of this numerical simulation of lava flow accumulation.

REFERENCES CITED

Becker, G. F. The geometrical form of volcanic cones and the elastic limit of lava. *American Journal of Science*, 30, 283-293, 1885.

Ben-Avraham, Z., and A. Nur. The elevation of volcanoes and their edifice heights at subduction zones, J. Geophys. Res., 85, 4325-4335, 1980.

Borgia, A. and S. R. Linneman, On the mechanisms of lava flow emplacement and volcano growth: Arenal, Costa Rica, in *Lava flows and domes*, edited by J. H. Fink, International Association of Volcanology and Chemistry of the Earth's Interior Proc. Volcanol., 2, 208-243, 1990.

Borgia, A., L. Ferrai, G. Pasquare, Importance of gravitational spreading in the tectonic and volcanic evolution of Mount Etna, *Nature*, 357, 231-235, 1992.

Bruno, B. C., G. J. Taylor, S. K. Rowland, and S. M. Baloga, Quantifying the effect of rheology on lava-flow margins using fractal geometry, Bull. Volcanol., 56, 193-206, 1994.

Cas, R. A. F., and J. V. Wright, *Volcanic Successions: Modern and Ancient*, London: Chapman and Hall, 1988.

Carr, M. J., Symmetrical and segmented variation of physical and geochemical characteristics of the Central American volcanic front, J. Vol. Geotherm. Res., 20, 231-252, 1984.

Carr, M. J., and R. E. Stoiber, Volcanism: in Dengo, G., and Case, J. E., eds., The Caribbean Region: Boulder, Colorado, Geol. Soc. America, *The Geology of North America, Volume H*, Chapter 14, 375-391, 1990.

Crisp, J. A. Rates of magma emplacement and volcanic output, J. Vol. Geotherm. Res., 20, 177-211, 1984.

Crisp, J. A., and S. Baloga, A model for lava flows with two thermal components, J. Geophys. Res., 95, 1255-1270, 1990.

Eaton, J. P., and K. J. Murata. How volcanoes grow, Science, 132, 925-938, 1960.

Fink, J. H., and R. W. Griffiths, Radial spreading of viscous gravity currents with solidifying crust, J. Fluid. Mech., 221, 485-509, 1990.

Grubensky, M. J., G. A. Smith, and J. W. Geissman. Textural analysis and temperature of emplacement of near-vent, cone-forming breccias at Broken Top Crater, Central Oregon, GSA Annual Meeting Abstracts with Programs, 1993.

Hulme, G., The interpretation of lava flow morphology, Geophys, J. R. astr. Soc., 39, 361-383, 1974.

Iyer, H. M., J. R. Evans, P. B. Dawson, D. A. Stauber and U. Achauer, Differences in magma storage in different volcanic environments as revealed by seismic tomography: silicic volcanic centers and subduction-related volcanoes, in Magma Transport and Storage, (ed.) M. P. Ryan, 293-316, 1990.

Kilburn, C. R. J., and R. M. C. Lopes, General patterns of flow field growth: aa and blocky lavas, J. Geophys. Res., 96, 19721-10732, 1991.

Lacey, A., J. R. Ockendon, and D. L. Turcotte. On the geometrical form of volcanoes, Earth Planet. Sci. Lett., 54, 139-143, 1981.

Marsh, B. D., Mechanics of Benioff zone magmatism, in The Geophysics of the Pacific Ocean Basin and its Margin, Geophys. Monogr. Ser., 19, (eds.) G. H. Sutton, M. H. Manghnani, and R. Moberly, 337-350, AGU, Washington, D. C., 1976.

Milne, J. On the form of volcanos. The Geological Magazine, 5, 337-345, 1878.

Pike, R. J. and G. D. Clow. Revised classification of terrestrial volcanoes and catalog of topographic dimensions, with new results on edifice volume. *U. S. Geological Survey Open-File Report* 81-1038, 1981a.

Pinkerton, H., and L. Wilson, Factors controlling the lengths of channel-fed lava flows, Bull. Volcanol., 56, 108-120, 1994.

Posin, S. B. Eruptive conditions and volcano morphology, M.S. Thesis, Arizona State University, 1990.

Rose, W. I., Jr., and six others. The evolution of Santa Maria volcano, Guatemala. *Journal of Geology*, 85, 63-87, 1977.

Rose, W. I., Jr., G. T. Penfield, J. W. Drexler, and P. B. Larson. Geochemistry of the andesite flank lavas of three composite cones within the Atitlán Cauldron, Guatemala. Bull. Volcanol., 43, 131-153, 1980.

Ryan, M. P. Neutral buoyancy and the mechanical evolution of magmatic systems, in Magmatic Processes: Physiochemical Principles, (ed) B. O. Mysen, The Geochemical Society, Special Publication No. 1, 1987.

Shteynberg, G. S. and TS. V. Solov'yev, The shape of volcanoes and the position of subordinate vents, *Bull. (Izv.) Acad. Sci. USSR Earth Physics*, 12(5), 83-84, 1976.

Vogt, P. R., Volcano height and plate thickness, Earth Planet. Sci. Lett., 23, 337-348, 1974.

Wadge, G., and P. Francis. A porous flow model for the geometrical form of volcanoes - critical comments, Earth Planet. Sci. Lett., 57, 453-455, 1982.

Wadge, G., and R. M. C. Lopes, The lobes of lava flows on Earth and Olympus Mons, Mars, Bull. Volcanol., 54, 10-24, 1991.

Walker, J. A., Carr, M. J., Patino, L. C., Johnson, C. M., Feigenson, M. D., and Ward, R. L. Abrupt change in magma generation across the Central American arc in southeastern Guatemala: flux dominated melting near the base of the wedge to decompression melting near the top of the wedge, *Contrib. Mineral. Petrol*, in press.

Wilson, L., J. W. Head, III, and E. A. Parfitt. The relationship between the height of a volcano and the depth to its magma source zone: a critical reexamination, Geophysical Research Letters, 19, 1395-1398, 1992.

Wood, C. A. Cinder cones on Earth, Moon and Mars, *EOS, Trans. AGU*, 58, 425, 1977.

Wood, C. A., Monogenetic volcanoes of the terrestrial planets, *Proc. Lunar Sci. Conf.* 10th, 2815-2840,1979.

Wood, C. A. On the geometric form of volcanoes - comment, Earth Planet. Sci. Lett., 57, 451-452, 1982.

Chapter VI. Conclusions

This dissertation attempted to develop a model relating volcanic type (eruption style) to volcanic morphology; in particular, the verification and quantification of conventional hypotheses (based on field experience) about the shapes and types of volcanoes required a uniform description of volcanic shape. This dissertation acquired a database of geomorphic measurements of volcanoes from volcanic fields in four tectonically distinct regions. The identification and measurement criteria are based on a right-circular model of volcanic shape.

This dissertation demonstrates: (1) The right circular cone model can be used to acquire a consistent database of volcano morphologic measurements. The right circular cone model is consistent in its reflection of shape. (2) The database acquired can be used to quantify comparisons of volcanic shape within and between regions. Variations in process produce consistent variations in shape. Shape variations in a single region for a single type can be related quantitatively to variations in process. (3) The conventional hypotheses concerning volcanic shape are accurate, although not all information relevant to them is acquired using the right-circular cone model of volcanic shape. (4) The right circular cone model cannot consistently distinguish between all volcanic types, especially if volcanoes from more than a single region are compared. (5) A model based on topographic profiles provides more information about the shape of large volcanoes.

Chapter II concludes that the right-circular cone model, used in this and previous studies, has significant limitations. Common morphological features of many volcanoes are ignored by the model; including the curved flanks of composite volcanoes, the breached craters of some cinder cones, and the elongation possible in many types of volcanoes. Additionally, the basic model uses only three measurements (height, basal diameter and top diameter) so that size-independent morphology is

described by only two parameters. Morphological separation of volcanic types is not fully achieved in this study. The most obvious additional measurements (crater depth and cone circularity) do not improve the separation. Geologic equivalence is based on more than simple shape characteristics; it includes both smaller-scale (e.g., flow features) and non-morphologic (e.g., petrology) information.

In spite of the above limitations, Chapter II demonstrates two additional conclusions; both of which suggest that there is not a one-to-one correspondence between volcano shape and eruption process. First, different volcanic processes can produce similar volcano morphologies. The morphologic spaces of cinder cones and domes overlap almost completely. Varying degrees of overlap are observed amongst other combinations of volcanic types. However, in a given region, the shapes of most volcanic types can be distinguished based on visual (or statistical) analysis of the measured shape parameters; the main exception is the coincidence of the shapes of cinder cones and domes. Second, volcanoes with the same type labels, based on geologic classification, have distinct morphologies and different developmental trends in different regions. The volcanoes of the Snake River Plain (especially cinder cones and shield volcanoes) are shallower sloped than their geologic counterparts in Guatemala and Iceland. The shield volcanoes appear to evolve into composite volcanoes in Guatemala, but not in Iceland or the Snake River Plain.

Chapter III shows that in Guatemala cinder cone volume is correlated with the Ba/La ratios, a tracer of subduction influence, of associated lava flows. This implies that hydrous flux from the subducted slab is an important factor in determining cinder cone size. The dependence of cinder cone volume in Guatemala on both the degree of partial melting (La/Yb) and the amount of slab influence (Ba/La) suggests that the amount of slab influence is a primary control of the amount of magma generated (although the trigger for mantle melting is likely to be adiabatic decompression).

Larger volumes of magma (corresponding to larger cinder cones) may have higher initial volatile contents, although this still needs to be verified.

Chapter IV concludes that cinder cone shape is determined by the dependence of basal diameter on eruption energetics. A numerical simulation of cinder cone eruptions was used to create model cinder cones whose morphologies could be compared with the morphologic data for Guatemalan cinder cones and with the morphologic predictions of erosion models. The comparison showed that: (1) Morphologies produced by growth patterns and those produced by erosion/burial patterns are similar and overlap. (2) The initial starting cone morphology (i.e. morphology immediately after eruption ceases) must vary to account for the range of morphologies observed in the Ipala Graben, Guatemala. (3) Particle ejection velocities in the range from 110 m/s to 190 m/s are probably typical of the Guatemalan cones, based on the predictions of the McGetchin model. (4) In Guatemala, larger cinder cones are predicted to be produced by eruptions with higher average ejection velocities.

Chapter V shows that large volcanoes can be modeled using topographic profiles such that morphologic separation of types is achieved: shield volcanoes have shallow, linear flanks; table mountains and domes have steep, linear flanks; and composite volcanoes have parabolic flanks. The generic form (of the parabola) is consistent for most composite volcanoes in Central America. Variations in generic form appear to relate to lava type, pre-existing topography, and maturity (lack) of cone development.

Most composite volcano profiles are based on parabolas that differ only in scale not in shape. However, composite volcano steepness varies along the Guatemalan arc front, reflecting differences in the width of the lower flank. Two other parabola parameters (h_{int} and C) vary along the arc, reflecting changes in summit and base elevation; they also correlate with crustal thickness. Neither of the parabola shape coefficients (p and p*) correlate with along arc distance or crustal thickness or, even, volcano volume.

Numerical simulations of lava piles suggest that shield volcanoes may be piles of wedge-shaped lava flows of varying length. So far, the numerical simulations of lava flow accumulation have produced topographic profiles that resemble Snake River Plains shield volcanoes. Simulations using larger numbers of lava flows may be able to produce steeper edifice forms.

This dissertation has shown that shape is not uniquely determined by the eruption style, although it clearly is affected by eruption style. In large part, this is the result of the broadness of the classification corresponding to each eruption style. Within each eruption style, smaller morphological variations occur that relate to variations in effusion rate, eruption temperature, magma volatile content, and crustal thickness among other factors. This dissertation cannot distinguish amongst many of these factors as they cannot be interpolated from purely morphological data. The lack of a unique relationship between shape and eruption style has two other causes. First, volcano shape can change progressively as an eruption proceeds, or as the results of numerous eruptions accumulate. Relationships between size and shape can indicate that shape depends on total eruption volume, effusion rate, or eruption duration; these factors cannot be distinguished unless the duration and effusion rate of the forming eruptions is known. Second, very different eruption styles can include sub-processes, that seem volcanologically insignificant but are extremely important in determining volcano shape. In particular, cinder cones and domes may have similar shapes because, although the eruption style is different, the flank slope is controlled by debris flow and corresponds to the angle of repose for scoria in cinder cones and for blocky lava talus in domes. In summary, this morphometric study has shown that a broad range of volcano shapes corresponds to each eruption style and demonstrated a number of relationships between size and shape for individual volcanic types; however, it cannot distinguish between the many tectonic and magmatic factors controlling subtle variations in eruption style, nor can it distinguish between the effects of volume and duration. A detailed model of how shape varies with the known factors controlling the

detailed eruption processes can help distinguish between possible effects. Detailed geochemical and tectonic data can also help distinguish between possible effects.

SUGGESTIONS FOR FUTURE RESEARCH

Both the morphologic parameters and the normalized topographic profiles allow composite volcanoes of different sizes to be compared for shape; composite volcano shape can be interpreted as reflecting eruption processes and compared to tectonic and geochemical variations. Composite volcano slope and crustal thickness correlate in Guatemala and western El Salvador - predicting that slope and crustal thickness should correlate over the rest of the Central American arc. If the similarity of most composite volcano profiles in Guatemala signifies the style of eruption, I would expect a correspondence between normalized profile shape and geochemical trends. A detailed study of the relationships between volcano shape, eruptive products (pyroclastic vs. effusive material) and geochemistry along the entire Central American arc is desirable.

The differences in the trend of shape with size for the shield volcano populations in different tectonic settings predicts that the relative importance of the factors controlling lava flow shape and size also varies with tectonic setting. There are two obvious lines of approach to investigation into this prediction. First, one path is to study the shapes of volcanoes with historical eruptions for which many of the factors known to control lava flow behavior can be estimated. Posin [1990] and Pinkerton and Wilson [1994] have documented a great variability in lava flow behavior. A second approach is to document in more detail the differences in lava chemistry, effusion rate, crustal thickness, etc. between the regions of this study. Comparison of the variations in these parameters within and between volcanic populations with the morphologic variations in the same populations has the potential to demonstrate how volcanic edifice shape depends on the geologic forces resulting in an eruption.

The lava flow pile program is still in its earliest stages of development. Further runs are needed to elucidate how the resultant shapes vary with the input parameters for each of the four lava flow models. Additional complexity may also be added to the models. For example, the length/width ratio can be allowed to vary within a run.

This study has clarified the most useful directions to pursue for further understanding of the growth of volcanic edifices. It has shown that topographic profiles (and slope profiles) are extremely useful in distinguishing volcanic types. It has shown that considering a population of volcanoes as a whole can provide much useful insight. it has suggested that there may be tectonic controls on volcano shapes.

Appendix A. Morphologic plots

The set of morphologic plots on which the qualitative morphologic analyses were based are found on the following pages. There are other plots that could be made, but this set provides a compact picture of the total variation observed.

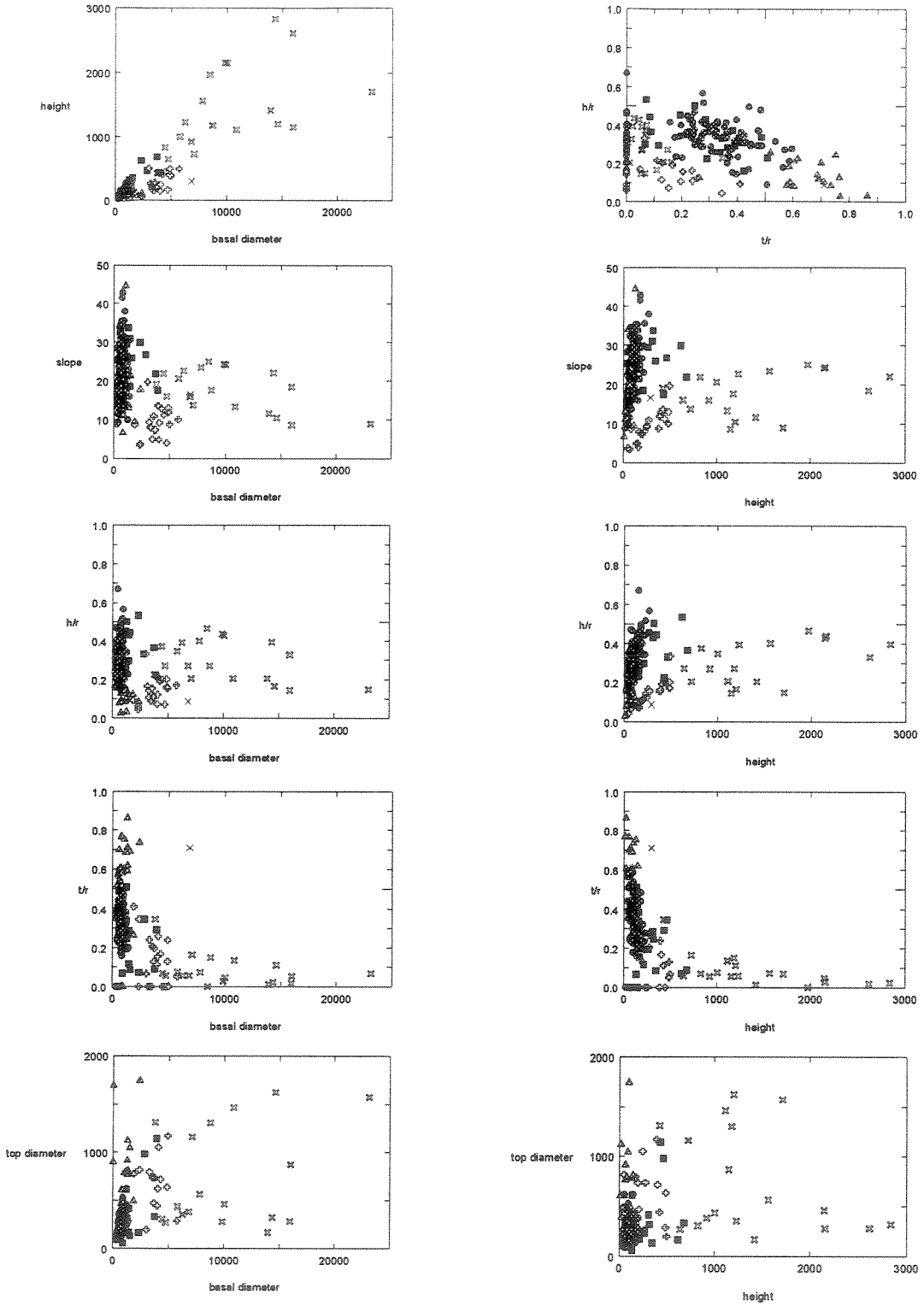


Figure A-1. Morphologic plots of Guatemalan volcanoes. Small dots indicate volcanoes whose types could not be identified. Other symbols are as in Figure II-4.

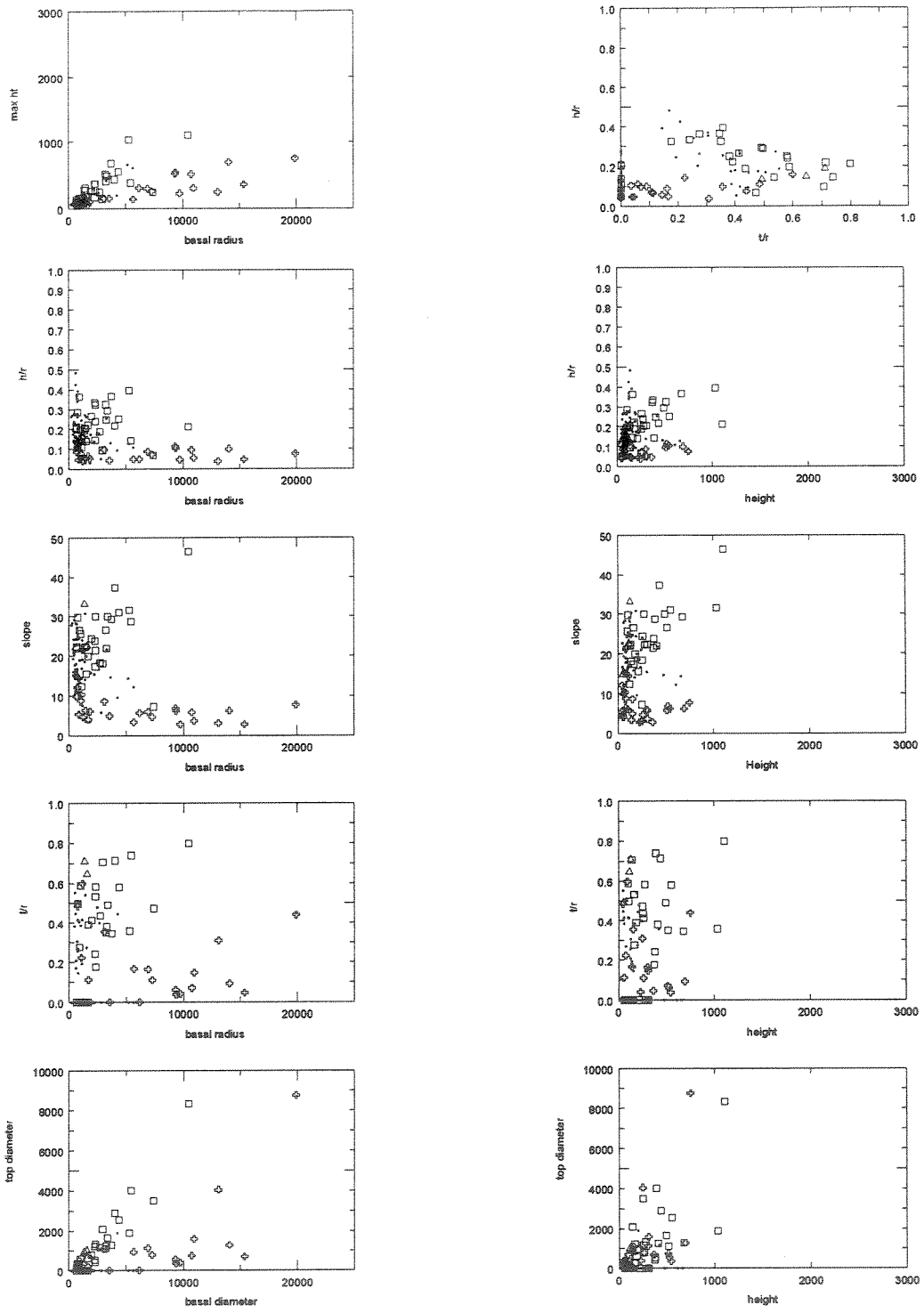


Figure A-2. Morphologic plots of Icelandic volcanoes. Small dots indiacte volcanoes whose type could not be identified. Other symbols are as in Figure II-6.

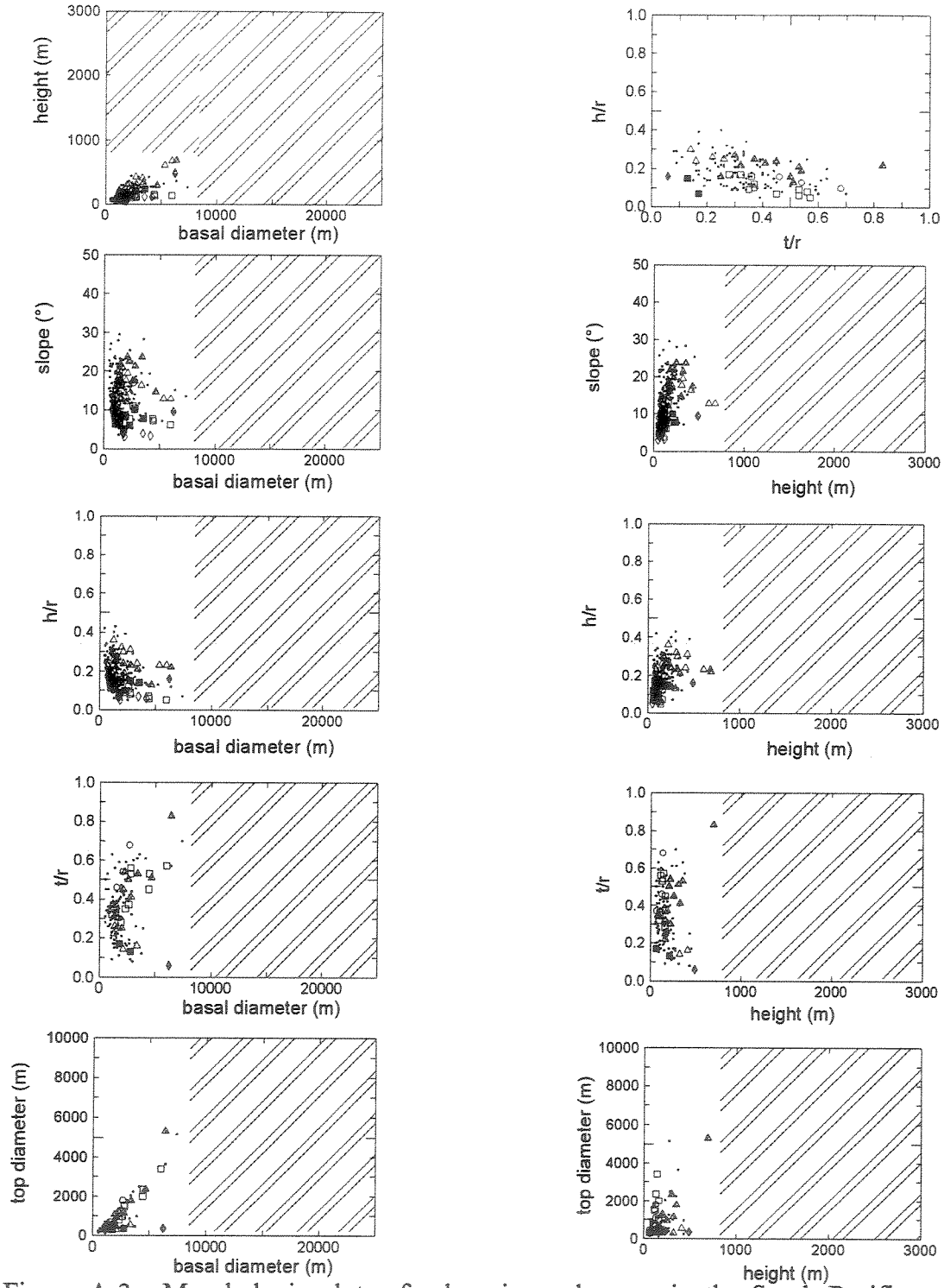


Figure A-3. Morphologic plots of submarine volcanoes in the South Pacific. Small dots indicate volcanoes whose type could not be identified. Other symbols are as given in Table II-6. Shaded areas delineate the regions of morphospace within which no volcanoes could be measured because of the spatial restictions of SeaBeam swaths.

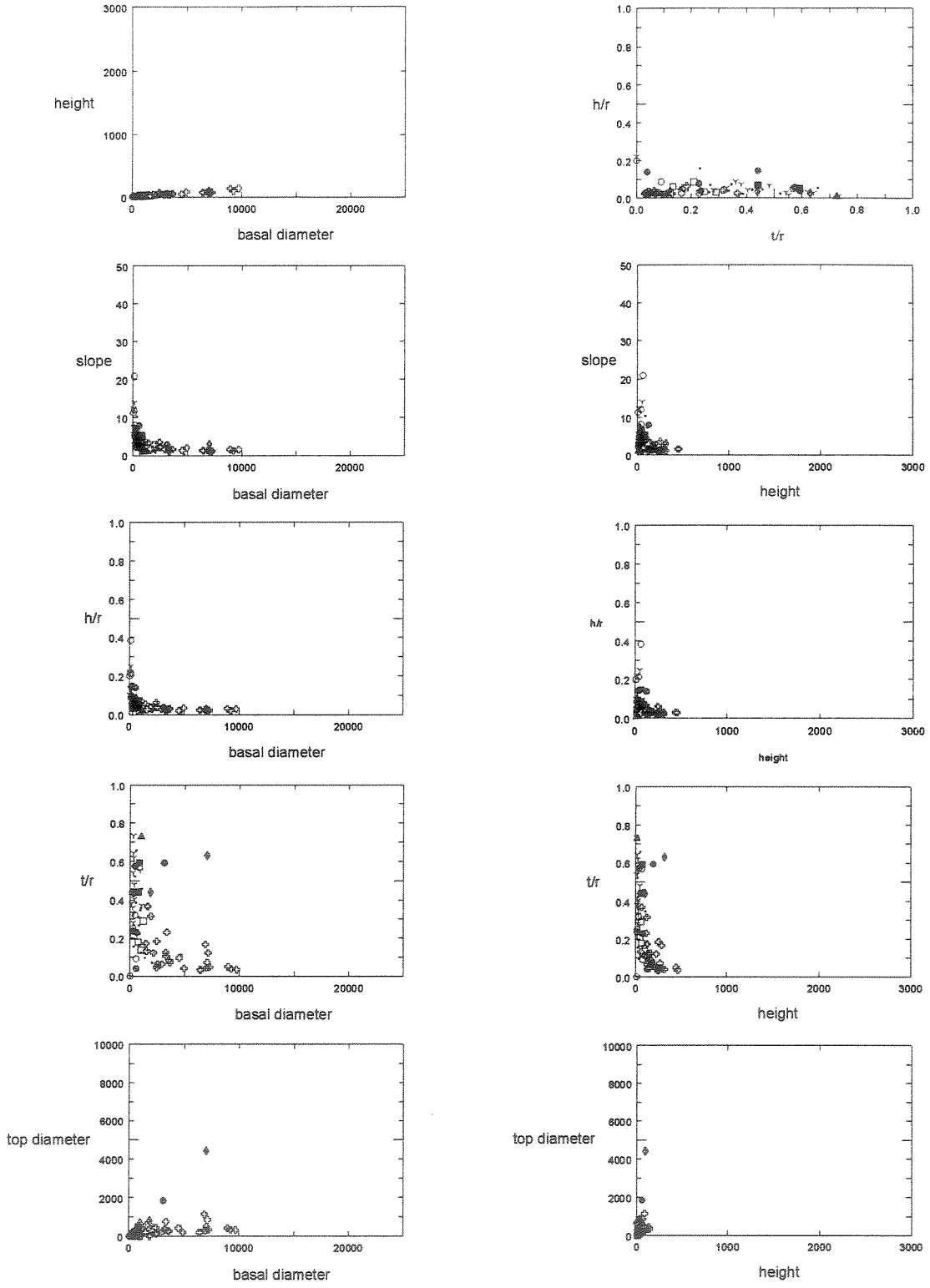


Figure A-4. Morphologic plots of Snake River Plains volcanoes. Small dots indicate volcanoes whose type could not be identified. Other symbols are as in Figure II-12.

Appendix B. Grain size analysis

Scoria samples (~1-2 lb) were obtained from nine cinder cones in southeast Guatemala for dry sieving. Sieves at 1/4 to 1 ϕ intervals were used to obtain size fractions; results are reported in Table B-1 as weight percent. Grain size distributions were characterized by interpolating graphically for the ϕ size at which specified cumulative fractions were obtained (Table B-2). These values were used to calculate the properties of the distributions (Table III-3) based on the Folk and Ward [1957] formulas (the Inman [1952] formulas are more commonly used for pyroclastic fall deposits, but the Folk and Ward formulas use more information about the distribution).

Table B-1. Particle size distribution (as wt %) for basaltic scoria in selected cinder cones of southeastern Guatemala.

phi size	-6.00	-5.0	-4.75	-4.00	-3.00	-2.5	-2.25	-2.00	-1.75	-1.5	-1.00	-0.75	0	0.25	0.5	Pan	Total
dia.(mm)	64	32	26.9	16	8	5.66	4.76	4	3.36	2.83	2	1.68	1	0.84	0.71	0	
GuC1004s	0	0	2.04	25.57	49.57	13.34	2.71	1.19	0.77	0.29	0.41	0.33	0.36	0.01	0.14	3.14	97.82
GuC1001s	0	0	0	1.92	11.47	10.33	8.14	8.11	9.55	9.76	14.50	11.29	7.59	0	1.3	5.52	99.48
GuC1003s	0	0	0	2.24	24.97	18.15	9.54	7.49	7.07	5.51	7.05	5.39	3.92	0.30	1.06	6.94	99.64
GuC1008s	0	0	0	0.50	7.59	10.32	7.23	6.19	8.10	7.82	13.81	14.63	10.87	3.26	3.35	5.21	98.87
GuC1002s	0	0	0	2.68	24.55	18.48	9.96	7.85	7.63	6.50	8.55	5.93	3.12	0.79	0.74	3.11	99.88
GuC1006s	0	3.91	8.38	26.07	26.91	8.87	4.80	3.38	2.84	2.05	2.79	1.69	1.49	0.71	0.81	5.17	99.87
GuC1005s	42.89	9.44	2.62	12.77	11.52	5.88	2.80	1.91	1.62	1.25	1.56	1.19	0.92	0.29	0.38	2.92	99.94
GuC1007s	0	0	0	0.26	14.50	17.59	13.45	11.43	10.48	7.32	7.48	5.14	3.46	1.03	1.14	6.54	99.81
GuC1009s	0	0	0	6.65	20.24	11.95	6.76	5.17	5.57	5.14	9.63	8.18	6.38	2.11	2.26	9.74	99.80

Table B-2. Standard values picked for statistical calculations.

expected phi	5	16	25	50	75	84	95
actual phi	5.15	16.07	25.46	50.1	74.99	84.14	95.31
GuC1005s*	-5.72	-5.05	-4.63	-3.69	-2.45	-1.85	0.45
GuC1006s	-4.98	-4.67	-4.39	-3.57	-2.48	-1.85	0.50
GuC1004s	-4.67	-4.37	-4.09	-3.55	-3.05	-2.76	-1.85
GuC1009s	-4.21	-3.57	-3.11	-2.05	-0.90	-0.23	0.98
GuC1002s	-3.91	-3.48	-3.11	-2.41	-1.63	-1.12	-0.10
GuC1003s	-3.91	-3.46	-3.11	-2.39	-1.53	-0.92	0.98
GuC1001s	-3.75	-2.88	-2.47	-1.75	-0.97	-0.80	0.65
GuC1007s	-3.70	-2.97	-2.70	-2.15	-1.53	-0.95	0.83
GuC1008s	-3.42	-2.64	-2.27	-1.44	-0.80	-0.21	0.55

* largest clast (>10 cm) not included; interpreted as bomb.

Appendix C. Field notes, southeast Guatemala, November 1993.

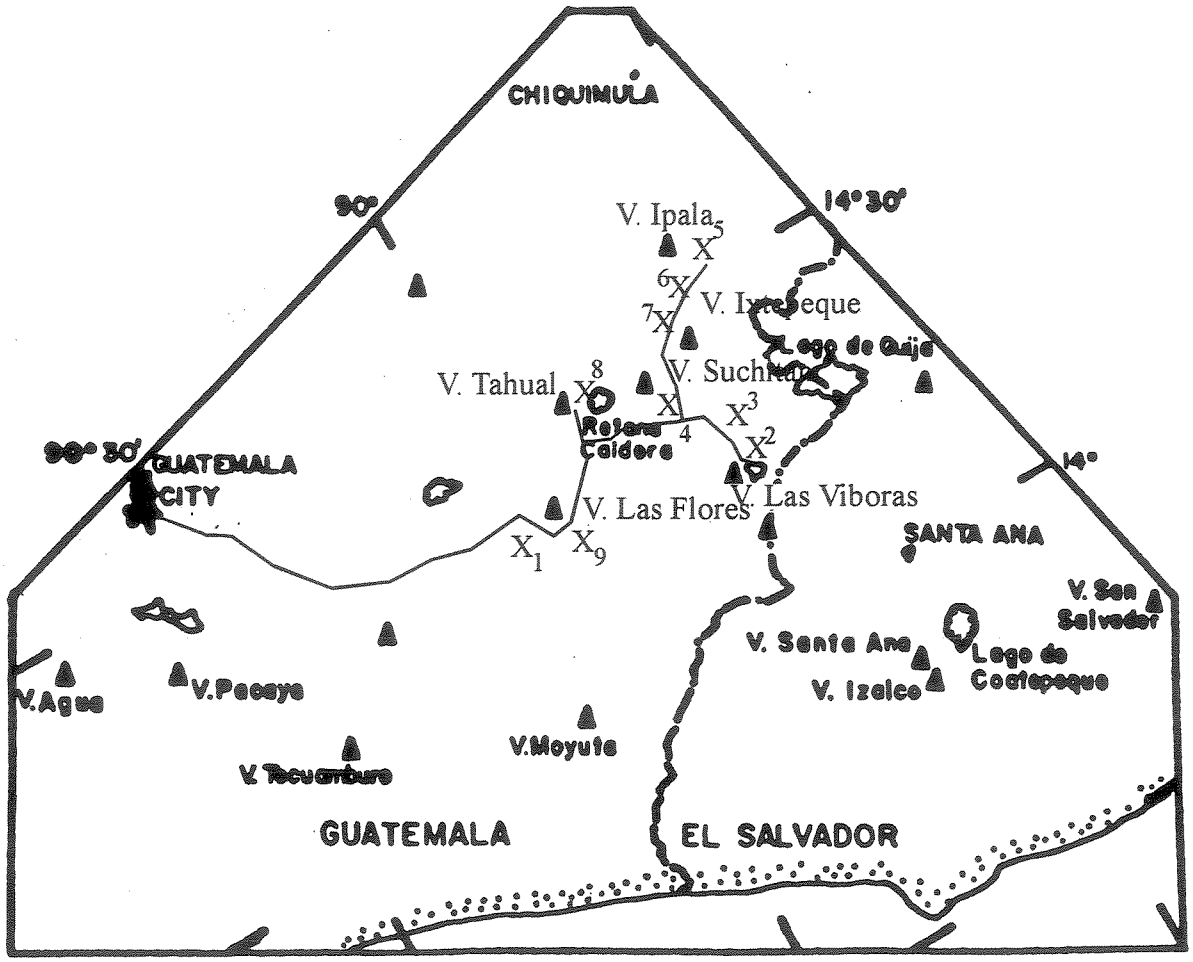
Table C-1 summarizes my observations in the field and from aerial photographs of the nine cinder cones whose scoria was sampled. Overall, all nine cones are composed almost entirely of highly vesicular scoria with minor silicic pumice present in one case (these pumices are probably lithic inclusions). Large bombs are present in about half the cones; plastic deformation features are clearly visible on bombs. However, the small clasts composing the bulk of the cone are never observed to be plastically deformed, indicating a low pyroclast temperature on landing [Head and Wilson, 1989]. No obvious variation of pyroclast nature or size over cone history was observed in any of the quarries. Visual observation of the sections suggest that most beds have similar clast size and distribution and reverse grading (related to grain flows occurring during active growth). No observations are available on the stratigraphic relationships of these cinder cones and their associated flows (the base of the cones was generally not exposed).

Table C-1. Characteristics of cinder cones sampled for scoria.

Cone ID	Sample #'s	Aerial Photo Observations.	Field Observations.	Photo?	Name
75.04	GuC1001s GuC1001 GuC704	large crater maybe cult.?; no vegetation gullies (5/45° on SW side)	fine layering loose clasts	y	C. Buena Vista
92.17	GuC1002s GuC201	cone backed against preexisting topo. two craters? vegetated 18 gullies/360°	some pumice layers; rare pumice in scoria layers; fairly indurated	y?	C. Mongoy
92.18	GuC1003s GuC309	crater 14 gullies/180° N side cultivated	no pumice very indurated		C. San Jeronimo
91.05	GuC1004s GuC1004a GuC1004b	visible crater, breached variable gullying (~25/360°) variable vegetation lower slopes cultivated	very coarse reverse grading loose clasts	y	C. El Reparo
91.50	GuC1005s GuC1005	baby cone	very coarse; bombs looks better in person than on map		C. Colorado
90.24	GuC1006s GuC1006	too highly eroded to tell what is - could be maar?	coarse scoria; bombs alternating coarse and fine layers looks better in person than on map		La Cieba
91.20	GuC1007s GuC403	gullies (17/90° to 20/360°) elongate cone and crater	finer scoria not very indurated		El Tablon

Table C-1 continued. Characteristics of cinder cones sampled for scoria.

Cone ID	Sample #'s	Aerial Photo Observations.	Field Observations.	Photo?	Name
83.40	GuC1008s GuC714	crater w/ ridge off breach little vegetation cultivated at base gullies (9/30° & 18/90°) on two sides	very fine scoria loose clasts on upper levels; very indurated on lower levels near river	y	El Overjero
84.14	GuC1009s GuC702	NE side of crater breached gullies (10/360° - 5/90°) some vegetation; no cultivation large debris? apron surrounds odd looking crater?	-	y	C. Gordo



1 = Cerro Buena Vista	5 = Cerro Colorado	9 = Cerro Gordo
2 = Cerro Mongoy	6 = La Ceiba	
3 = San Jeronemo	7 = El Tablon	
4 = El Reparo	8 = El Ovejero	

Figure C-1. The scoria samples are located at the nine X's.

Appendix D Computer simulation based on the McGetchin model

Procedure for Computer Simulation of Cinder Cones

1) Run program for given set of parameters (cinderj.exe or cinvent.exe)

input parameters for each run:

random number seed

number of eruptive phases

number of traces (particle groups per phase)

minimum exit velocity

(vent width)

2) Combine output files for each set of runs (a set has the same parameters except for different numbers of eruptive phases). Output consists of the height of the volcano at each profile point from x=1m to x=1000m (vent center is at x=500 m).

3) Find flank edges and crater rims. Flank edge is defined in two ways: 1) as the first occurrence of cinder deposit (first height>0 from each end) and 2) the last occurrence of original ground(last height=0 from each end). The second definition is used for the morphologies reported in the text. The distance between the two flank edges is the basal diameter of the cone; in most cases, it is probably overestimated relative to what would be discernible on a topographic map. Crater rim is defined as the maximum height reached on each side of the vent. The height of the cone is the average of the two crater rim heights. The top diameter of the cone is distance between the two crater rims.

4) Insert values for flank edge locations, crater rim locations, and crater rim heights in excel worksheet. The worksheet calculates the morphologic parameters of interest from these values.

Table D-1. Input parameters.

PARAMETER	VALUES USED	SOURCE OR SIGNIFICANCE
Number of eruptive phases	3,6,9,12,15,...	essentially is increment of growth (can use as time or volume proxy)
Number of traces	500-3000	Volume per eruptive phase
Minimum exit velocity	25 m/s, 65 m/s, 105 m/s, 145 m/s	lowest value from McGetchin et al., 1974; higher values needed to get to morphologic space occupied by real cinder cones
Velocity range	50 m/s (also 25 m/s and 100 m/s)	McGetchin et al., 1974 Chouet et al., 1974
Particle density	1.5 g/cc (also 2.0 g/cc)	Dehn, 1987
Particle size	20 cm (also 5 cm)	Dehn, 1987
Vent width	0 m, 20 m, 40 m, 60 m, 80 m, 100 m	Wilson et al., 1980
Ejection angles	70°-90° (normal distribution)	McGetchin et al., 1974

Example Worksheet

cinder cone experiment			zg					
#traces =	2000		minimum velocity =		25	m/s		
vent width	40	m	velocity range =		50	m/s		
			particle size =		20	cm		
			particle density =		1.5	g/cc		
			detectable edge		highest point			crater
phase	first 1	last 1	left	right	left	right	height	bottom
3	424	585	430	566	472	529	25	2
6	416	585	415	584	476	527	37.5	20
9	403	598	402	599	476	524	48	30
12	391	608	390	609	479	521	58	41
15	378	620	377	621	477	522	65.5	49
30	332	669	331	670	481	519	97	80
					using min dia			crater
phase	max dia	min dia	top width	height	h/r	t/r	slope	depth
3	161	136	57	25	0.37	0.42	32.33	23
6	169	169	51	37.5	0.44	0.30	32.44	17.5
9	195	197	48	48	0.49	0.24	32.79	18
12	217	219	42	58	0.53	0.19	33.24	17
15	242	244	45	65.5	0.54	0.18	33.36	16.5
30	337	339	38	97	0.57	0.11	32.80	17
					using max dia			
phase	max dia	min dia	top width	height	h/r	t/r	slope	
3	161	136	57	25	0.31	0.35	25.68	
6	169	169	51	37.5	0.44	0.30	32.44	
9	195	197	48	48	0.49	0.25	33.15	
12	217	219	42	58	0.53	0.19	33.54	
15	242	244	45	65.5	0.54	0.19	33.62	
30	337	339	38	97	0.58	0.11	32.98	

Cinder Cone Growth Simulation Program

```
10 '   Cinder Cone Model      June 21, 1987
20 '   Jonathan Dehn   Arizona State University
30 '                Smithsonian Institution
35 '
40 '   modified by Karen G. Bemis (June 1993) Rutgers, New Jersey
45 '
'*************************************************************
50 '   Parametric, internal morphology model
60 '
90 '   Variable set-up
100 '  VX = initial x; VY = initial y velocities
110    DIM VX(2500), VY(2500), PC(2500), VPOS(2500): 'PC = particle count
120 '   Topography array 0= pre-topo, 1= surface, 2= K.E.
130    DIM T(1000, 3)
140    MB = 0
150 '
160 '
170 '  Prompts for variables needed
180    COLOR 2: CLS
190    RANDOMIZE
200    INPUT "How many eruptive phases"; ER
210    INPUT "Choose the number of representative traces"; PP
220 '   INPUT "Continuous or Phase eruption (C/P) "; Q0$
       Q0$ = "c"
230    GRAV = 9.8: ' assumes earth gravity
240 '
250 '   INPUT "Is there a wind(Y/N)"; Q2$
260 '      IF Q2$ = "Y" OR Q2$ = "y" THEN GOSUB 30000
265    WVX = 0: 'sets wind velocity to zero
270 '   INPUT "(W)ide vent or (P)oint source vent"; Q3$
280 '      IF Q3$ = "P" OR Q3$ = "p" THEN GOTO 290
285          INPUT " How wide is the vent (m)"; WDTH
290    INPUT "What is the minimum exit velocity (m/sec)"; VMIN
300 '   INPUT "What is the maximum exit velocity (m/sec)"; VMAX
       VMAX = VMIN + 50: ' fixed range
310 '   INPUT "What is the lowest ejection angle (degrees)";
       AVGANGLE = 80:  ' changed to generate guassian dist. of angles
       MINANGLE = -90 + 2 * AVGANGLE
320    RHO = .00129 / 1000: 'air density (kg/m) assumed
330    ETA = .00017: 'air viscosity (1 kg/m/s = 10 poise) assumed
340 '  INPUT "What is the mean diameter of the particles (mm)";
       DIAM = .2:   ' particle dia 20 cm
```

```
350 '   INPUT "What is the density of the particles (g/cc)";
      SIGMA = .0015:  ' particle density 1.5 g/cc
360 '   INPUT "Would you like a pre-existing topography(Y/N)"; Q3$
370 '   IF Q3$ = "Y" OR Q3$ = "y" THEN GOSUB 40000
400 '
410 '   Assumed variables;
420     KMU = .05: ' Coefficient of Kinetic Friction
430     SMU = .5:  ' Coefficient of Static Friction
435     TIME = CINT((2 * VMAX) / GRAV): ' Max travel time estimation
      MINTIME = INT((.68404 * VMIN) / GRAV): ' Min travel time estimate
436 '   Drag factors for velocity
437         DX = (.2222 * (DIAM / 2) ^ 2 * WVX) / ETA: ' X drag
438         DY = (.2222 * (DIAM / 2) ^ 2 * (SIGMA - RH0) * GRAV) / ETA
439 '       Stokes Law for Y drag
440 '
450 '   Calculation of density factor (DF), MASS and BETA for ballistic equations
460     DF = ((SIGMA - RHO) / SIGMA) * (GRAV)
470     MASS = SIGMA * 8: ' 2 * 2 * 2 meters for array block.
480     BETA = .01745 * MINANGLE
490 '
500 '
510 '   Screen setup for graphics
520     SCREEN 9, , 1, 1: KEY OFF: 'EGA
530 '
540     WINDOW (-500, -50)-(500, 700)
550     LOCATE 1, 65: PRINT "Cycles/": 'EGA screen only  through line 650
555     LOCATE 2, 65: PRINT "Phases"
560     FOR G1 = 1 TO 7: 'EGA loop for phase color identification
570       GP = ((G1 - 1) * 40) + (G1 * 5): GC = G1 + 8
580       LINE (450, 375 + GP)-(500, 375 + GP), G1: LINE -(500, 395 + GP), G1
590       LINE -(450, 395 + GP), G1: LINE -(450, 375 + GP), G1:
           PAINT (485, 380 + GP), G1
600       LINE (450, 395 + GP)-(500, 395 + GP), GC:
           LINE -(500, 415 + GP), GC
610       LINE -(450, 415 + GP), GC: LINE -(450, 395 + GP), GC:
           PAINT (485, 400 + GP), GC
615     NEXT G1
620     LOCATE 11, 75: PRINT "1": LOCATE 9, 75: PRINT "2"
621     LOCATE 7, 75: PRINT "3": LOCATE 6, 75: PRINT "4"
622     LOCATE 5, 75: PRINT "5": LOCATE 3, 75: PRINT "6"
630     LOCATE 1, 75: PRINT "7"
631     LOCATE 9, 65: PRINT "dark =":   LOCATE 10, 65: PRINT " blstc "
632     LOCATE 6, 65: PRINT "light=":   LOCATE 7, 65:   PRINT " mrph"
633     LINE (-500, 650)-(290, 650), 7: LINE (-500, 640)-(290, 640), 7
634     LINE (-500, 650)-(-500, 475), 7: LINE -(-350, 475), 7:  LINE -(-350, 640), 7
```

```
635   LINE (290, 700)-(290, 370), 7: LINE -(500, 370), 7
636   LINE (410, 700)-(410, 370), 7
640 '
650 '
660 ' Set up the base ground line, topography, vent, and scale
670   FOR T1 = 1 TO 1000
680     LINE (T1 - 500, 0)-(T1 - 500, T(T1, 0)), 8: 'EGA
700   NEXT T1
705 '
710   LINE (-500, 0)-(500, 0), 6: 'EGA
730   LINE (0, 0)-(0, -20), 2
731   IF WDTH = 0 THEN GOTO 735
732      LINE (-WDTH / 2, -15)-(-WDTH / 2, -20), 2: LINE -(WDTH / 2, -20), 2
733      LINE -(WDTH / 2, -15), 2
735      LOCATE 25, 43: PRINT "vent";
740   LINE (-350, -5)-(-350, -15), 3: LINE -(-250, -15): LINE -(-250, -5)
750   LOCATE 25, 1: PRINT "100 meters";
755   LOCATE 25, 60: PRINT "(no gas thrust)"; : 'EGA only
760   LOCATE 1, 1: PRINT "Cinder Cone Model 38; 21.6.87 J.DEHN; "
770 '
780 '
790 ' Loop through eruptive phases
800   FOR W = 1 TO ER
810 '
820 '       Particle velocity generation
830         GOSUB 10000
840 '
850 '         Save vent for accurate erasure of material
860   VENT = T(500, 1)
870 '
880 ' Creation of the eruptive cloud
890 ' Loop through time (g determines length of time, .5 sec. inc.)
900 '  FOR PASS = 1 TO 2: ' (color animation)
910 '
920   FOR T = .5 TO TIME STEP .5
930 '
940           LOCATE 4, 2: PRINT "ph "; W
945           LOCATE 5, 2: PRINT "t "; T; " "
950 '
960 '         Loop for individual particle path
970           FOR I = 1 TO PP
980 '
1030 ' Ballistic equations
1040   X = INT((VX(I) - WVX - DX) * T + VPOS(I))
1050   Y1 = (VY(I) - DY) * T
```

```
1060   Y2 = (DF * (T ^ 2))
1070   Y = INT(VENT + Y1 - Y2)
1080 '
1090 '
1100 ' Skip the plotting routine if point is outside
1110 '        of the window, or is on the surface
1120 ' Set XI as the integer value for position
1130    XI = X + 500: IF XI > 1000 THEN GOTO 1450
1135    IF XI <= 1 THEN GOTO 1450
1140 '
1220 '
1230 ' Check to see if the particle is on the surface
1240   IF Y > T(XI, 1) THEN GOTO 1450
1250 ' Check to see if the particle has been counted
1260   IF PC(I) >= W THEN GOTO 1450
1270     PC(I) = PC(I) + 1
1280 ' Check to see if particle is in blast path
1290   IF XI < (500 - (WDTH / 2)) THEN GOTO 1350
1300   IF XI < (500 + (WDTH / 2)) THEN GOTO 1450
1310        DIST = ABS(XI - 500)
1320        HMAX = VENT + (DIST * TAN(BETA))
1330        IF T(XI, 1) >= HMAX THEN GOTO 1450
1340 '
1350 '  Loading of the topography array and plotting
1360 '        each eruptive pixel represents 1 surface pt.
1370        T(XI, 1) = T(XI, 1) + 1
1380        E1 = W MOD 8
1420        PSET (X, T(XI, 1)), E1: '    EGA, color EC passes
1430 '
1450   NEXT I
1460 '
1470 ' Continuous or phase, phase allows settling time.
1480 '      IF PASS = 1 THEN GOTO 1500
1490 '      IF Q0$ = "C" OR Q0$ = "c" THEN GOTO 2110
     IF T < MINTIME THEN GOTO 2110
1500 '     Morph length determination loop
1510       FOR L1 = 1 TO 1000: ' Find left limit
1520            DIFF1 = T(L1, 1) - T(L1, 0)
1530            IF DIFF1 > 0 THEN
1540             MA = T(L1, 1): SA = L1
1550              L1 = 1000
1560            END IF
1570       NEXT L1
1580       IF SA = 0 THEN GOTO 2110
1590       FOR L2 = 1 TO 1000: ' Find right limit
```

```
1600            DIFF2 = T(1000 - L2, 1) - T(1000 - L2, 0)
1610            IF DIFF2 > 0 THEN
1620              SB = 1000 - L2
1630              L2 = 1000
1640            END IF
1650        NEXT L2
1660    FOR L3 = SA TO SB: 'Find highest point in cone
1670      MBT = T(L3, 1)
1680      IF MBT > MB THEN MB = MBT
1690    NEXT L3
1700    MB = MB / 2
1710 '
1720 '
1730    FOR m = MA TO MB
1740 '      LOCATE 6, 2: PRINT "hgt "; INT(M * 2); " "
1750        FOR s = SA TO SB: ' From left to right edge of cone
1755            IF s <= 10 THEN GOTO 2090
1756            IF s >= 990 THEN GOTO 2090
1760 '          LOCATE 7, 2: PRINT "pos "; S - 500; " "
1770            KE = T(s, 2): T(s, 2) = 0
1780            VM = SQR((2 * KE) / MASS)
1790 '
1800 '          Check for 'surface' particle
1810            IF T(s, 1) - T(s - 1, 1) > 0 THEN GOTO 1830
1820            IF T(s, 1) - T(s + 1, 1) <= 0 THEN GOTO 2090
1830            HL = T(s, 1) - T(s - 3, 1)
1840    HR = T(s, 1) - T(s + 3, 1)
1850    IF HL < 0 AND HR < 0 THEN GOTO 2090
1860    IF HL < HR THEN H = HR ELSE H = HL
1870    ALPHA = ATN(H / 5)
1880 '
1890    PARNO = T(s, 1) - m + 1
1900    NF = PARNO * MASS * (GRAV) * COS(ALPHA)
1910    PF = PARNO * MASS * (GRAV) * SIN(ALPHA)
1920 '
1930    KFF = NF * KMU
1940    SFF = NF * SMU
1950    IF KFF + SFF > PF + (VM * MASS) THEN GOTO 2090
1960 '
1970    VM = VM + SQR((2 * SIGMA * GRAV * H) / MASS)
1980    VL = KMU * (GRAV) * COS(ALPHA) * VM
1990    VM = VM - VL
2000 '
2010              XPOS = VM * .5 * SIN(ALPHA)
2020              IF HL > HR THEN XPOS = -XPOS
```

```
2030            T(s + XPOS, 2) = (MASS * (VM ^ 2)) / 2
2040            PRESET (s - 500, T(s, 1))
2050            T(s, 1) = T(s, 1) - 1
2060            PSET (s + XPOS - 500, T(s + XPOS, 1) + 1), E1 + 8: ' EGA
2070 '
2080            T(s + XPOS, 1) = T(s + XPOS, 1) + 1
2090          NEXT
2100          NEXT
2110          NEXT
2120 '        NEXT
2130    NEXT
2140
2150    LOCATE 9, 2: INPUT "Store surface data in a file"; Q4$
2160    IF Q4$ = "N" OR Q4$ = "n" THEN GOTO 2240
2170     INPUT "What is the name of the file"; N1$
2180     OPEN N1$ FOR OUTPUT AS #1
2190     FOR F = 1 TO 1000
2200        P1 = F * COS(WA): P2 = F * SIN(WA)
2210        PRINT #1, P1; CHR$(44); P2; CHR$(44); T(F, 1)
2220     NEXT F
2230     CLOSE #1
2240    END
10000 ' Subroutine for determination of velocities and angles******************
10010 '
10020 ' Loop for particle velocity generation
10030    FOR L = 1 TO PP
10040 '     Width routine, determination of velocity position
10050       IF WDTH = 0 THEN GOTO 10080
10060          TEMPPOS = RND(1) * WDTH
10070          VPOS(L) = -(WDTH / 2) + TEMPPOS
10080 '        Generation of parametric values;
10090          SX = RND(1)
             Y = ABS(SQR(-2 * LOG(RND(1))) * COS(6.283185 * RND(1))) / 3
10100          VANGLE = 90 - (Y * (90 - AVGANGLE))
10110          VANGLE = .01745 * VANGLE
             Y = SQR(-2 * LOG(RND(1))) * COS(6.283185 * RND(1)) / 6
10120          VELOC = (Y + .5) * (VMAX - VMIN) + VMIN
10130          VXT = VELOC * COS(VANGLE)
10140          VYT = VELOC * SIN(VANGLE)
10150 '
10160 '        Setting up arrays with computed values
10170          IF SX < .5 THEN VXT = -VXT
10180          VX(L) = VXT
10190          VY(L) = VYT
10200    NEXT L
```

```
10210   RETURN
20000 ' Gravity input subroutine ELIMINATED*****************
20040 '
30000 ' Wind direction subroutine COMMENTED OUT*******************
30010 '
30020 'PRINT " What is the wind velocity in the X direction (m/s)?"
30030 'INPUT " A negative values blows to the right"; WVX
30040 'INPUT " What is the inclination of this section to the wind"; WA
30050 '  WA = .01745 * WA
30060 '  WVX = WVX * COS(WA)
30070 '  RETURN
40000 ' Pre-existing topography subroutine COMMENTED OUT***************
40010 '
40020 'PRINT " Prexisting topography may be chosen as a user defined slope"
40030 'PRINT " or a given irregular topography."
40040 'INPUT " (S)lope or (I)rregular"; QSS
40050 '    IF QS$ = "I" OR QS$ = "i" THEN GOTO 40110
40060 '      INPUT " What is the slope in degrees"; SLP: SLP = .01745 * SLP
40070 '    FOR S1 = 1 TO 1000
40080 '        T(S1, 0) = INT(S1 * TAN(SLP))
40090 '    NEXT S1
40100 '  GOTO 40190
40110 '    T(0, 0) = RND(1) * 25
40120 '  FOR S2 = 1 TO 1000
40130 '         SLP1 = RND(1)
40140 '         SLP2 = RND(1)
40150 '         IF SLP1 < .5 THEN SLP2 = -SLP2
40160 '        T(S2, 0) = T(S2 - 1, 0) + SLP2
40170 '     IF T(S2, 0) < 0 THEN T(S2, 0) = 0
40180 '  NEXT S2
40190 '  FOR S3 = 1 TO 1000
40200 '     T(S3, 1) = T(S3, 0)
40210 '  NEXT S3
40220 '   RETURN
50000 ' Unit normalization subroutine ELIMINATED*************
50010 '
```

Appendix E. Morphological descriptions of individual volcanoes.

The morphological descriptions of various volcanoes used as examples in Chapter V are reported in Tables V-11 and V-12. The morphologic parameters were obtained as described in Chapter II and are included in the databases. These are included here to supplement the visual presentation, where even the slight vertical exaggerations of most figures can fool the eyes.

Table E-1. Morphologic parameter descriptions of the example volcanoes in Figure V-8.

Volcano	h	2r	2t	summit elevation	h/r	t/r	slope
Agua	2615 m	15955 m	280 m	3760 m	0.33	0.02	18°
Las Viboras	440 m	4470 m	0 m	1040 m	0.20	0.00	11°
Trolladyngja	514 m	10718 m	745 m	1459 m	0.10	0.07	6°
Smt 159	100 m	2100 m	800 m	-3500 m	0.10	0.38	9°
Smt 23	580 m	3100 m	0 m	-4220 m	0.19	0.00	11°
Herdhubreidh	1035 m	5258 m	1885 m	1640 m	0.39	0.36	32°
Moyuta	467 m	2833 m	978 m	1662 m	0.33	0.35	23°
Pino Redondo	127 m	865 m	415 m	1070 m	0.29	0.48	29°

Table E-2. Morphologic parameter descriptions of the composite volcanoes.

Volcano	h	2r	2t	summit elevation	h/r	t/r	slope
Acatenango	2147 m	10040 m	458 m	3960 m	0.43	0.05	24°
Agua	2615 m	15955 m	280 m	3760 m	0.33	0.02	18°
Atitlán	2155 m	9855 m	278 m	3535 m	0.44	0.03	24°
Boqueron	1200 m	14610 m	1623 m	1893 m	0.16	0.11	10°
Chingo	1004 m	5803 m	433 m	1777 m	0.35	0.07	21°
Fuego	2835 m	14345 m	320 m	3760 m	0.40	0.02	22°
Ipala	725 m	7090 m	1158 m	1650 m	0.20	0.16	14°
Izalco	1420 m	13940 m	168 m	1940 m	0.20	0.01	12°
Jumay	643 m	4743 m	270 m	2176 m	0.27	0.06	16°
Jumaytepeque	828 m	4445 m	305 m	1815 m	0.37	0.07	22°
La Rama	1150 m	15990 m	865 m	1970 m	0.14	0.05	9°
Pacaya	1180 m	8738 m	1303 m	2560 m	0.27	0.15	18°
Santa Ana	1712 m	23120 m	1570 m	2365 m	0.15	0.07	9°
Santa Maria	1972 m	8480 m	0 m	3772 m	0.47	0.00	25°
San Pedro	1230 m	6275 m	353 m	3020 m	0.39	0.06	23°
Suchitan	1112 m	10850 m	1463 m	2042 m	0.20	0.13	13°
Tecuamburo	920 m	6835 m	380 m	1600 m	0.27	0.06	16°
Tahual	426 m	3778 m	1310 m	1716 m	0.23	0.35	19°
Toliman	1565 m	7813 m	563 m	3158 m	0.40	0.07	23°

Appendix F. Program listing for shield simulation

pile.m is a MATLAB script.

```
function        [topo]=pile(stuff,numflows,ventdia,filename,surface)
% The function pile([t,volume,a],numflows,ventdia,filename,surface)
% calculates lava flow shapes based on t and volume
% and builds an edifice of numflows number of flows.
%       ventdia controls size of crater and azimuthal spacing of
% flows.
%       filename is not currently used.
%       surface indicates whether there is any original topography.
%       The vector "stuff" is specified in the MATLAB function "shape.m".

t1=clock;
ARRAYSIZE=100;
q=ARRAYSIZE+10;

%************************************************************
% call shape.m to determine the shape of the lava flows
[L,W,t]=shape(stuff);
%************************************************************
% mesh spacing:  dx=dy=1;  assumes L=ARRAYSIZE
% real vs mesh length:  determine scaling factors
        z=L/ARRAYSIZE;
        dx=z;
        dy=dx;
        zw=W/z;
        zvr=ventdia/2/z;
        zL=ARRAYSIZE;
fprintf('z=%6.3f ',z)
fprintf('zL=%6.2f  zw=%6.2f  zvr=%6.3f \n',zL,zw,zvr)
fprintf ('\n')

% mesh length&width = ARRAYSIZE
% note topo=topo(x,y)
%       [x,y]=meshdom(-1000:1:1000,-1000:1:1000);
%   [nx,ny]=size(x)=2000;
        topo=zeros(2*q);
        A=zeros(360,1);
        B=zeros(360,1);
```

```
%   surface can contain a pre-existing surface
if surface~=0
        topo=surface;
end



% ************************************************************
% build pile
%
count=0;
rand('uniform')
k=rand(1)*360;
hw=fix(180*atan(zw/zvr/2)/pi);
for m=1:numflows
% ******************************************************
        if (k>45&k<135)
                phi=(90-k)*pi/180;
                x1=fix(zvr*cos(phi)-sign(phi)*0.5*zw*sin(phi));
                x2=fix(zvr*cos(phi)+sign(phi)*0.5*zw*sin(phi));
                x3=fix((zL)*cos(phi)-sign(phi)*0.5*zw*sin(phi));
                x4=fix((zL)*cos(phi)+sign(phi)*0.5*zw*sin(phi));
                for x=x1:1:x2
                        py=ceil(x*tan(phi));
                        zigy=ceil(0.5*zw/cos(phi))+1;
                        for y=(py-zigy):1:(py+zigy)
                                r=sqrt(x.^2 + y.^2);
                                theta=atan2(y,x);
                                hwtheta=atan2(zw,2*r);
                                if (r>zvr&r<=zL)
                                 if (theta>=(phi-hwtheta)&theta<=(phi+hwtheta))
                        th=t*(1-(4/(zw.^2))*((tan(phi-theta).*r).^2));
                        topo(x+q,y+q)=th + topo(x+q,y+q);
                                 end
                                end
                        end
                end
                for x=(x2+1):1:(x3-1)
                        py=x*tan(phi);
                        zigy=0.5*zw/cos(phi);
% first part of next line rounds away from zero
%
y=(fix(py-zigy+0.999*sign(phi))):1:(py+zigy);
[m,n]=size(y);
                        qo=q.*ones(m,n);
```

```
                    r=sqrt(ones(m,n).*x.^2 + y.^2);
                    theta=atan2(y,x.*ones(m,n));
th=t.*(1-(4/(zw.^2)).*((r.*tan(phi.*ones(m,n)-theta)).^2));
                    topo(x+q,y+qo)=th + topo(x+q,y+qo);
                end
                for x=x3:1:x4
                    py=ceil(x*tan(phi));
                    zigy=ceil(0.5*zw/cos(phi))+1;
                    for y=(py-zigy):1:(py+zigy)
                        r=sqrt(x.^2 + y.^2);
                        theta=atan2(y,x);
                        hwtheta=atan2(zw,2*r);
                        if (r>zvr&r<=zL)
                         if (theta>=(phi-hwtheta)&theta<=(phi+hwtheta))
                    th=t*(1-(4/(zw.^2))*((tan(phi-theta)*r).^2));
                    topo(x+q,y+q)=th + topo(x+q,y+q);
                        end
                        end
                    end
                end
% ***************************************************
        elseif(k>135&k<225)
                phi=(180-k)*pi/180;
                y1=fix(zvr*cos(phi)-sign(phi)*0.5*zw*sin(phi));
                y2=fix(zvr*cos(phi)+sign(phi)*0.5*zw*sin(phi));
                y3=fix((zL)*cos(phi)-sign(phi)*0.5*zw*sin(phi));
                y4=fix((zL)*cos(phi)+sign(phi)*0.5*zw*sin(phi));
                for y=y1:1:y2
                    px=ceil(y*tan(phi));
                    zigx=ceil(0.5*zw/cos(phi))+1;
                    for x=(px-zigx):1:(px+zigx)
                        r=sqrt(x.^2 + y.^2);
                        theta=atan2(x,y);
                        hwtheta=atan2(zw,2*r);
                        if(r>zvr&r<=zL)
                         if (theta>=(phi-hwtheta)&theta<=(phi+hwtheta))
                th=t*(1-(4/(zw.^2))*((tan(phi-theta)*r).^2));
                topo(x+q,-y+q)=th + topo(x+q,-y+q);
                        end
                        end
                    end
                end
                for y=(y2+1):1:(y3-1)
                    px=y.*tan(phi);
                    zigx=0.5.*zw/cos(phi);
```

```
% first part of next line rounds away from zero
%
x=(fix(px-zigx+0.999*sign(phi))):1:(px+zigx);
[m,n]=size(x);
                        qo=q.*ones(m,n);
                        r=sqrt(ones(m,n).*y.^2 + x.^2);
                        theta=atan2(x,y.*ones(m,n));
th=t.*(1-(4/(zw.^2)).*((r.*tan(phi.*ones(m,n)-theta)).^2));
                        topo(x+qo,-y+q)=th' + topo(x+qo,-y+q);
                end
                for y=y3:1:y4
                        px=ceil(y*tan(phi));
                        zigx=ceil(0.5*zw/cos(phi))+1;
                        for x=(px-zigx):1:(px+zigx)
                                r=sqrt(x.^2 + y.^2);
                                theta=atan2(x,y);
                                hwtheta=atan2(zw,2*r);
                                if(r>zvr&r<=zL)
                                 if (theta>=(phi-hwtheta)&theta<=(phi+hwtheta))
                th=t*(1-(4/(zw.^2))*((tan(phi-theta)*r).^2));
                topo(x+q,-y+q)=th + topo(x+q,-y+q);
                                 end
                                end
                        end
                end
% ************************************************************
        elseif(k>225&k<315)
                phi=(270-k)*pi/180;
                x1=fix(zvr*cos(phi)-sign(phi)*0.5*zw*sin(phi));
                x2=fix(zvr*cos(phi)+sign(phi)*0.5*zw*sin(phi));
                x3=fix((zL)*cos(phi)-sign(phi)*0.5*zw*sin(phi));
                x4=fix((zL)*cos(phi)+sign(phi)*0.5*zw*sin(phi));
                for x=x1:1:x2
                        py=ceil(x*tan(phi));
                        zigy=ceil(0.5*zw/cos(phi))+1;
                        for y=(py-zigy):1:(py+zigy)
                                r=sqrt(x.^2 + y.^2);
                                theta=atan2(y,x);
                                hwtheta=atan2(zw,2*r);
                                if (r>zvr&r<=zL)
                                 if(theta>=(phi-hwtheta)&theta<=(phi+hwtheta))
                        th=t*(1-(4/(zw.^2))*((tan(phi-theta)*r).^2));
                        topo(-x+q,-y+q)=th + topo(-x+q,-y+q);
                                 end
                                end
```

```
                    end
                end
                for x=(x2+1):1:(x3-1)
                    py=x*tan(phi);
                    zigy=0.5*zw/cos(phi);
% first part of next line rounds away from zero
%
y=(fix(py-zigy+0.999*sign(phi))):1:(py+zigy);
[m,n]=size(y);
                    qo=q.*ones(m,n);
                    r=sqrt(ones(m,n).*x.^2 + y.^2);
                    theta=atan2(y,x.*ones(m,n));
th=t.*(1-(4/(zw.^2)).*((r.*tan(phi.*ones(y)-theta)).^2));
                    topo(-x+q,-y+qo)=th + topo(-x+q,-y+qo);
                end
                for x=x3:1:x4
                    py=ceil(x*tan(phi));
                    zigy=ceil(0.5*zw/cos(phi))+1;
                    for y=(py-zigy):1:(py+zigy)
                        r=sqrt(x.^2 + y.^2);
                        theta=atan2(y,x);
                        hwtheta=atan2(zw,2*r);
                        if (r>zvr&r<=zL)
                         if(theta>=(phi-hwtheta)&theta<=(phi+hwtheta))
                    th=t*(1-(4/(zw.^2))*((tan(phi-theta)*r).^2));
                    topo(-x+q,-y+q)=th + topo(-x+q,-y+q);
                         end
                        end
                    end
                end
% ************************************************************
        else  %  for 315<k<=360 & 0<=k<45
                if k>45
                    phi=(360-k)*pi/180;
                else
                    phi=-k*pi/180;
                end
                y1=fix(zvr*cos(phi)-sign(phi)*0.5*zw*sin(phi));
                y2=fix(zvr*cos(phi)+sign(phi)*0.5*zw*sin(phi));
                y3=fix((zL)*cos(phi)-sign(phi)*0.5*zw*sin(phi));
                y4=fix((zL)*cos(phi)+sign(phi)*0.5*zw*sin(phi));
                for y=y1:1:y2
                    px=ceil(y*tan(phi));
                    zigx=ceil(0.5*zw/cos(phi))+1;
                    for x=(px-zigx):1:(px+zigx)
```

```
                                r=sqrt(x.^2 + y.^2);
                                theta=atan2(x,y);
                                hwtheta=atan2(zw,2*r);
                                if (r>zvr&r<=zL)
                                 if (theta>=(phi-hwtheta)&theta<=(phi+hwtheta))
                th=t*(1-(4/(zw.^2))*((tan(phi-theta)*r).^2));
                topo(-x+q,y+q)=th + topo(-x+q,y+q);
                                 end
                                end
                        end
                end
                for y=(y2+1):1:(y3-1)
                        px=y.*tan(phi);
                        zigx=0.5.*zw/cos(phi);
% first part of next line rounds away from zero
%
x=(fix(px-zigx+0.999*sign(phi))):1:(px+zigx);
[m,n]=size(x);
                        qo=q.*ones(m,n);
                        r=sqrt(ones(m,n).*y.^2 + x.^2);
                        theta=atan2(x,y.*ones(m,n));
th=t.*(1-(4/(zw.^2)).*((r.*tan(phi.*ones(m,n)-theta)).^2));
                        topo(-x+qo,y+q)=th' + topo(-x+qo,y+q);
                end
                for y=y3:1:y4
                        px=ceil(y*tan(phi));
                        zigx=ceil(0.5*zw/cos(phi))+1;
                        for x=(px-zigx):1:(px+zigx)
                                r=sqrt(x.^2 + y.^2);
                                theta=atan2(x,y);
                                hwtheta=atan2(zw,2*r);
                                if (r>zvr&r<=zL)
                                 if (theta>=(phi-hwtheta)&theta<=(phi+hwtheta))
                th=t*(1-(4/(zw.^2))*((tan(phi-theta)*r).^2));
                topo(-x+q,y+q)=th + topo(-x+q,y+q);
                                 end
                                end
                        end
                end
        end
        for bys=-hw:1:hw,
                ang=k+bys;
                if(ang<1),ang=ang+360;end
                if(ang>360),ang=ang-360;end
                B(ang)=B(ang)+t*(1-(bys/hw).^2);
```

```
        end
        b0=max(B);
        A=b0*ones(B)-B;
        T=sum(A);
        T=rand(1)*(T-1)+1;
        k=0;
        while T>0
                k=k+1;
                T=T-A(k);
        end
        % k now contains correct new angle
%fprintf('k = %5f \n',k)
        count=count+1;
end
fprintf('numflows=%5.0f \n',count)
fprintf('elapsed time = %5.2f min\n',etime(clock,t1)./60)
topo(1,1)=1000;
```

Appendix G. Data disk

A computer disk (IBM format) is enclosed. It contains the data files of measured and tabulated morphological information for the four regions studied. Also included are files containing the digitized topographic files. All data files are in ASCII text format.

Bibliography

Basaltic Volcanism Study Project. *Basaltic Volcanism on the Terrestrial Planets*, Pergamon Press, Inc., New York, 1981.

Batiza, R. Abundances, distribution and sizes of volcanoes in the Pacific Ocean and implications for the origin of non-hotspot volcanoes. *Earth Planet. Sci. Lett.*, 60, 195-206, 1982.

Becker, G. F. The geometrical form of volcanic cones and the elastic limit of lava. *American Journal of Science*, 30, 283-293, 1885.

Bemis, K. G., and Carr, M. J. Volcano morphology in Guatemala, *EOS, Trans. AGU*, 74, 333, 1993.

Bemis, K. G. and D. K. Smith. Production of small volcanoes in the Superswell Region of the South Pacific. *Earth Planet. Sci. Lett.*, 118, 251-262, 1993.

Ben-Avraham, Z., and A. Nur. The elevation of volcanoes and their edifice heights at subduction zones, *J. Geophys. Res.*, 85, 4325-4335, 1980.

Blackburn, E. A., Wilson, L., and Sparks, R. S. J. Mechanisms and dynamics of strombolian activity, *J. Geol. Soc. London*, 132, 429-440, 1976.

Bohnenberger, O. H. Los focos eruptivos cuaternarios de Guatemala. Trabajos Technicos Presentados en la Segunda Reunion de Geologos de America Central, Publicaciones Geológicas del Institutio Centroamericano de Investigacion y Tecnologia Industrial, Numero II, 1969.

Borgia, A., L. Ferrai, G. Pasquare, Importance of gravitational spreading in the tectonic and volcanic evolution of Mount Etna, *Nature*, 357, 231-235, 1992.

Borgia, A. and S. R. Linneman, On the mechanisms of lava flow emplacement and volcano growth: Arenal, Costa Rica, in *Lava flows and domes*, edited by J. H. Fink, International Association of Volcanology and Chemistry of the Earth's Interior Proc. Volcanol., 2, 208-243, 1990.

Borgia, A., S. Linneman, D. Spencer, L. D. Morales, and J. B. Andre, Dynamics of lava flow fronts, Arenal Volcano, Costa Rica, *J. Volc. Geotherm. Res.*, 19, 303-329, 1983.

Bruno, B. C., G. J. Taylor, S. K. Rowland, and S. M. Baloga, Quantifying the effect of rheology on lava-flow margins using fractal geometry, *Bull. Volcanol.*, 56, 193-206, 1994.

Burkart, B., and S. Self. Extension and rotation of crustal blocks in northern Central America and effect on the volcanic arc, *Geology*, 13, 22-26, 1985.

Calmant, S., and A. Caznave, Anomalous elastic thickness of the oceanic lithosphere in the south-central Pacific, *Nature*, 328, 236-238, 1987.

Carr, M. J. Symmetrical and segmented variation of physical and geochemical characteristics of the Central American front, *J. Volc. Geotherm. Res.*, 20, 231-252, 1984.

Carr, M. J., and R. E. Stoiber, Volcanism, in *The Caribbean Region*, edited by G. Dengo and J. E. Case, Boulder, Colorado, Geol. Soc. America, The Geology of North America, v. H, 1990.

Carr, M. J., M. D. Feigenson, and E. A. Bennet, Incompatible element and isotopic evidence for tectonic control of source mixing and melt extraction along the Central American Arc, *Contr. Min. Petrol.*, 105, 369-380, 1990.

Cas, R. A. F., and J. V. Wright, *Volcanic Successions: Modern and Ancient*, London: Chapman and Hall, 1988.

Chouet, B., N. Hamisevicz, and T. R. McGetchin. Photoballistics of volcanic jet activity at Stromboli, Italy. *J. Geophys. Res.*, 79, p.4961-4976, 1974.

Cipolletti, D. L. Morphometry of Central American composite cones. MS Thesis, Rutgers University, 1988.

Cochran, J. R., Variations in subsidence rates along intermediate and fast spreading mid-ocean ridges, *Geophys. J. R. Astron. Soc.*, 87, 421-454, 1986.

Crisp, J. A. Rates of magma emplacement and volcanic output, *J. Volc. Geotherm. Res.*, 20, 177-211, 1984.

Crisp, J. A., and S. Baloga, A model for lava flows with two thermal components, *J. Geophys. Res.*, 95, 1255-1270, 1990.

Dehn, J. Model of cinder cone formation, M. S. thesis, Arizona State University, 1987.

Dohrenwend, J. C., S. G. Wells, and B. D. Turrin. Degradation of Quaternary cinder cones in the Cima volcanic field, Mojave Desert, California. *Geol. Soc. Am. Bull.*, 97, 421-427, 1986.

Dragoni, M., S. Pondrelli, and A. Tallarico, Longitudinal deformation of a lava flow: the influence of Bingham rheology, *J. Volc. Geotherm. Res.*, 52, 247-254, 1992.

Drexler, J. W., W. I. Rose, Jr., R. S. J. Sparks, and M. T. Ledbetter, *Quat. Res.*, 13, 373-391, 1980.

Eaton, J. P., and K. J. Murata. How volcanoes grow, *Science*, 132, 925-938, 1960.

Fink, J. H., and R. W. Griffiths, Radial spreading of viscous gravity currents with solidifying crust, *J. Fluid. Mech.*, 221, 485-509, 1990.

Folk, R. L., and Ward, W. C. Brazos River Bar: a study in the significance of grain size parameters, *Jour. Sed. Petrology*, 27, 3-27, 1957.

Francis, P. W., and B. M. Abbot. Sizes of conical volcanoes, *Nature*, 244, 22-23, 1973.

Fries, C., Jr. Volumes and weights of pyroclastic material, lava, and water erupted by Paricutin Volcano, Michoacán, Mexico. *Trans., AGU*, 34, p.603-616, 1953.

Furman, T., P. S. Meyer, and F. Frey, Evolution of Icelandic central volcanoes: evidence from the Austurhorn intrusion, southeastern Iceland. *Bull. Volcanol.*, 55, 45-62, 1992.

Geist, D., and M. Richards. Origin of the Columbia Plateau and Snake River plain: deflection of the Yellowstone plume, *Geology*, 789-792, 1993.

Glazner, A. F., and Farmer, G. L. Production of isotopic variability in continental basalts by cryptic contamination, *Science*, 255, 72-74, 1992.

Greeley, R., The Snake River Plain, Idaho: Representative of a new category of volcanism, *J. Geophys. Res.*, 87, 2705-2712, 1982.

Grubensky, M. J., G. A. Smith, and J. W. Geissman. Textural analysis and temperature of emplacement of near-vent, cone-forming breccias at Broken Top Crater, Central Oregon, *GSA Annual Meeting Abstracts with Programs*, 1993.

Gutman, J. T. Structure and eruptive cycle of cinder cones in the Pincate volcanic field and the controls of Strombolian activity. *J. Geol.*, 87, p. 448-454, 1978.

Hasenaka, T., and I. S. E. Carmichael. The cinder cones of Michoacán-Guanajuato, Central Mexico, their age, volume and distribution, and magma discharge rate. *J. Volc. Geotherm. Res.*, 25, 105-124, 1985.

Head, J. W., III, and L. Wilson. Basaltic pyroclastic eruptions, influence of gas-release patterns and volume fluxes on fountain structure, and the formation of cinder cones, spatter cones, rootless flows, lava ponds, and lava flows. *J. Volc. Geotherm. Res.*, 37, 261-271, 1989.

Head, J. W., III, and L. Wilson. Lava fountain heights at Pu'u' O'o', Kilauea, Hawaii: indicators of amount and variations of exsolved magma volatiles., *J. Geophys. Res.*, 92, p. 13715-13719, 1987.

Houghton, B. F., and H.-U. Schmincke. Mixed deposits of simultaneous strombolian and phreatomagmatic volcanism: Rothenberg Volcano, East Eifel Volcanic Field, *J. Volc. Geotherm. Res.*, 30, 117-140, 1986.

Hulme, G., The interpretation of lava flow morphology, Geophys, J. R. astr. Soc., 39, 361-383, 1974.

Inbar, M., Hubp, J. L., and Ruiz, L. V. The geomorphological evolution of the Paricutin cone and lava flows, Mexico, 1943-1990, *Geomorphology*, 9, 57-76, 1994.

Inman, D. L. Measures for describing the size distribution of sediments, *Jour. Sed. Petrology*, 22, 125-145, 1952.

Iyer, H. M., J. R. Evans, P. B. Dawson, D. A. Stauber and U. Achauer, Differences in magma storage in different volcanic environments as revealed by seismic tomography: silicic volcanic centers and subduction-related volcanoes, in *Magma Transport and Storage*, edited by M. P. Ryan, 293-316, 1990.

Jakobsson, S. P. Chemistry and distribution patterns of Recent basaltic rocks in Iceland. *Lithos*, 5, 365-86, 1972.

Jordan, T. H., H. W. Menard, and D. K. Smith. Density and size distribution of seamounts in the eastern Pacific inferred from wide-beam sounding data, *J. Geophys. Res.*, 88, 10508-10518, 1983.

Kear, D., Erosional stages of volcanic cones as indicators of age. *New Zealand Journal of Science and Technology*, 38, 671-682, 1957.

Kilburn, C. R. J., and R. M. C. Lopes, General patterns of flow field growth: aa and blocky lavas, *J. Geophys. Res.*, 96, 19721-10732, 1991.

Kuntz, M. A., B. Skipp, M. A. Lanphere, W. E. Scott, K. L. Pierce, G. E. Dalrymple, L. A. Morgan, D. E. Champion, G. F. Embree, R. P. Smith, W. R. Hackett, D. W. Rodgers. Revised geologic map of the Idaho National Engineering Laboratory and adjoining areas, eastern Idaho. U.S.G.S. Open-file report 90-333, 1990.

Lacey, A., J. R. Ockendon, and D. L. Turcotte. On the geometrical form of volcanoes, *Earth Planet. Sci. Lett.*, 54, 139-143, 1981.

Leeman, W. P., Carr, M. J., and Morris, J. D. Boron geochemistry of the Central American Volcanic Arc: constraints on the genesis of subduction-related magmas, *Geochim. Cosmochim. Acta*, 58, 149-168, 1994.

Loewenherz, D., Stability and the initiation of channelized surface drainage: a reassessment of the short wavelength limit. *J. Geophys. Res.*, 96, 8453-8464, 1991.

Marsh, B. D., Mechanics of Benioff zone magmatism, in *The Geophysics of the Pacific Ocean Basin and its Margin*, Geophys. Monogr. Ser., 19, (eds.) G. H. Sutton, M. H. Manghnani, and R. Moberly, 337-350, AGU, Washington, D. C., 1976.

McClelland, L., Simkin, T., Summers, M., Nielsen, E., and Stein, T. C., (eds.) *Global Volcanism 1975-1985: The first decade reports from the Smithsonian Institution's Scientific Event Alert Network (SEAN)*, New Jersey: Prentice Hall, Inc., 1989.

McGetchin, T. R., M. Settle and B. A. Chouet. Cinder cone growth modeled after Northeast Crater, Mount Etna, Sicily. *J. Geophys. Res.*, 79, p.3257-3272, 1974.

McNutt, M. K., and K. M. Fischer, The South Pacific Superswell. in *Seamounts, Islands and Atolls*, AGU Geophys. Monogr. 43, 25-34, 1987.

McNutt, M. K., and A. V. Judge, The Superswell and mantle dynamics beneath the South Pacific, *Science*, 248, 969-975, 1990.

Milne, J. On the form of volcanos. The Geological Magazine, 5, 337-345, 1878.

Morris, J., Leeman, W. P., and Tera, F. The subducted components in island arc lavas: constraints from Be isotopes and B-Be systematics. *Nature*, 344, 31-36, 1990.

Parsons, B., and J. G. Sclater, An analysis of the variation of ocean floor bathymetry and heat flow with age, *J. Geophys. Res.*, 82, 803-827, 1977.

Peterson, P. S., Tephra of the Laguna de Ayarza calderas of southeastern Guatemala and its correlation to units of the Guatemalan Highlands, M.S. Thesis, Michigan Technological University, 1980.

Pieri, D. C., and S. M. Baloga, Eruption rate, area and length relationships for some Hawaiian lava flows. *J. Volc. Geotherm. Res.*, 30, 29-45, 1986.

Pike, R. J. and G. D. Clow. Revised classification of terrestrial volcanoes and catalog of topographic dimensions, with new results on edifice volume. U.S. Geological Survey Open-File Report 81-1038, 1981a.

Pike, R. J. and G. D. Clow, Numerical taxometry of central volcanoes on the planets, in NASA Tech. Memo. 84211, Reports of Planetary Geology Program - 1981, compiled by H. E. Holt, 138-140, 1981b.

Pinkerton, H., and L. Wilson, Factors controlling the lengths of channel-fed lava flows, *Bull. Volcanol.*, 56, 108-120, 1994.

Plafker, G. Tectonic aspects of the Guatemala earthquake of 4 February 1976, *Science*, 193, 1201-1208, 1976.

Plank, T., and Langmuir, C. H. An evaluation of the global variations in the major element chemistry of arc basalts, *Earth Planet. Sci. Lett.*, 90, 349-370, 1988.

Porter, S. C. Distribution, morphology and size frequency of cinder cones on Mauna Kea Volcano, Hawaii. *Geol. Soc. Am. Bull.*, 84, p.382-483, 1972.

Posin, S. B. Eruptive conditions and volcano morphology, M.S. Thesis, Arizona State University, 1990.

Rose, W. I., Jr., and six others. The evolution of Santa Maria volcano, Guatemala. *J. Geol.*, 85, 63-87, 1977.

Rose, W. I., Jr., G. A. Hahn, J. W. Drexler, M. L. Malinconico, P. S. Peterson, and R. L. Wunderman, Quaternary tephra of northern Central America, in S. Self and R. S. J. Sparks (eds.), *Tephra Studies*, 193-211, D. Reidel Publishing Company, 1981.

Rose, W. I., Jr., G. T. Penfield, J. W. Drexler, and P. B. Larson. Geochemistry of the andesite flank lavas of three composite cones within the Atitlán Cauldron, Guatemala. *Bull. Volcanol.*, 43, 131-153, 1980.

Ryan, M. P. Neutral buoyancy and the mechanical evolution of magmatic systems, in *Magmatic Processes: Physiochemical Principles*, (ed) B. O. Mysen, The Geochemical Society, Special Publication No. 1, 1987.

Sæmundsson, K., Outline of the geology of Iceland, *Jökull*, spec. issue, 29, 7-28, 1979.

Schilling, J.-G., Iceland mantle plume: geochemical evidence along Reykjanes Ridge, *Nature*, 242, 656-571, 1973.

Self, S., R. S. J. Sparks, B. Booth, and G. P. L. Walker. The 1973 Heimaey strombolian scoria deposit, Iceland. *Geol. Mag.*, 111, p. 539-548, 1974.

Shteynberg, G. S. and TS. V. Solov'yev, The shape of volcanoes and the position of subordinate vents, *Bull. (Izv.) Acad. Sci. USSR Earth Physics*, 12(5), 83-84, 1976.

Smith, D. K. Shape analysis of Pacific seamounts. *Earth Planet. Sci. Lett.*, 90, 457-466, 1988.

Smith, D. K. and J. R. Cann, The role of seamount volcanism in crustal construction at the Mid-Atlantic Ridge (24°-30°N), *J. Geophys. Res.*, 97 (B2), 1645-1658, 1992.

Smith, D. K. and J. R. Cann. Hundreds of small volcanoes on the median valley floor of the Mid-Atlantic Ridge at 24°-30°N. *Nature*, 1990.

Smith, D. K. and T. H. Jordan. Seamount Statistics in the Pacific Ocean, *J. Geophys. Res.*, 93, 2899-2918, 1988.

Steinberg, G. S., and J. I. Babenko. Experimental velocity and density determination of volcanic gases during eruption. *J. Volc. Geotherm. Res.*, 3, p.89-95, 1978.

Stolper, E., and Newman, S. The role of water in the petrogenesis of Mariana trough magmas, *Earth Planet. Sci. Lett.*, 121, 293-325, 1994.

Thorarinsson, S., and K. Saemundsson, Volcanic activity in historic time. *Jökull*, 29, 29-32, 1979.

Vergniolle, S., and C. Jaupart, Separated two-phase flow and basaltic eruptions, *J. Geophys. Res.*, 91, 12842-12860, 1986.

Vessel, R. K., and D. K. Davies, Non-marine sedimentation in an active fore-arc basin, In *Recent and ancient non-marine depositional environments: models for exploration,* F. G. Ethridge and R. M. Flores (eds), 31-45, SEPM Spec. Publn 31, 1981.

Vogt, P. R., Volcano height and plate thickness, *Earth Planet. Sci. Lett.*, 23, 337-348, 1974.

Wadge, G., and P. Francis. A porous flow model for the geometrical form of volcanoes - critical comments, *Earth Planet. Sci. Lett.*, 57, 453-455, 1982.

Wadge, G., and R. M. C. Lopes, The lobes of lava flows on Earth and Olympus Mons, Mars, *Bull. Volcanol.*, 54, 10-24, 1991.

Walker, G. P. L. Explosive volcanic eruptions - a new classification scheme. *Geol. Rundsch.*, 62, p.431-446, 1973.

Walker, G. P. L., and R. Croasdale. Characteristic of some basaltic pyroclastics. *Bull. Volc.*, 35, p. 303-317, 1972.

Walker, J. A. Petrogenesis of lavas from cinder cone fields behind the volcanic front of Central America, *J. Geol.*, 89, 721-739, 1981.

Walker, J. A., Carr, M. J., Patino, L. C., Johnson, C. M., Feigenson, M. D., and Ward, R. L. Abrupt change in magma generation across the Central American arc in southeastern Guatemala: flux dominated melting near the base of the wedge to decompression melting near the top of the wedge, *Contrib. Mineral. Petrol*, in press.

Weill, A., G. Brandeis, S. Vergniolle, F. Baudin, J. Bilbille, J.-F. Fèvre, B. Piron, and X. Hill. Acoustic sounder measurements of the vertical velocity of volcanic jets at Stromboli Volcano. *Geophys. Res. Lett.*, 19, p. 2357-2360, 1992.

Whitford-Stark, J. L., Shield volcanoes, in *Volcanoes of the Earth, Moon and Mars*, eds. G. Fielder and L. Wilson, London: Paul Elek Ltd., 1975.

Williams, H., McBirney, A. R., and Dengo, G. *Geologic reconnaissance in southeastern Guatemala*, Univ. California Publ. Geol. Sci., 50, 1-56, 1964.

Williams, H., *The history and character of volcanic domes*, Univ. Calif. Publn Bull Dept. Geol. Sci., 21, 51-146, 1932.

Williams, R. S., S. Porarinsson, and E. C. Morris, Geomorphic classification of Icelandic volcanoes. *Jökull*, 33, 19-24, 1983.

Wilson, L. Relationships between pressure, volatile content and ejecta velocity in three types of volcanic eruptions. *J. Volc. Geotherm. Res.*, 8, p. 297-313, 1980.

Wilson, L., and J. W. Head, III. Mars: review and analysis of volcanic eruption theory and relationships to observed landforms, *Rev. Geophys.*, 32, 221-263, 1994.

Wilson, L., J. W. Head, III, and E. A. Parfitt. The relationship between the height of a volcano and the depth to its magma source zone: a critical reexamination, *Geophysical Research Letters*, 19, 1395-1398, 1992.

Wilson, L., R. S. J. Sparks, and G. P. L. Walker. Explosive volcanic eruptions-IV. The control of magma properties and conduit geometry on eruption column behavior. *Geophys. J. R. astr. Soc.*, 63, p.117-148, 1980.

Wood, C. A. Cinder cones on Earth, Moon and Mars, EOS, Trans. AGU, 58, 425, 1977.

Wood, C. A., Morphometric evolution of composite volcanoes, *Geophysical Research Letters*, 5 (6), 437-439, 1978.

Wood, C. A., Monogenetic volcanoes of the terrestrial planets, *Proc. Lunar Sci. Conf. 10th*, 2815-2840,1979.

Wood, C. A. Morphometric evolution of cinder cones, *J. Volc. Geotherm. Res.*, 7, 387-413, 1980a.

Wood, C.A. Morphometric analysis of cinder cone degradation, *J. Volc. Geotherm. Res.*, 8, 137-160, 1980b.

Wood, C. A. On the geometric form of volcanoes - comment, *Earth Planet. Sci. Lett.*, 57, 451-452, 1982.

Wood, C. A., and Schuver, H. J., What determines a volcano's form?, in *Reports of Planetary Geology Program*, Wash., D. C., NASA TM-84211, 541-543, 1981.

Wright, J. V., A. L. Smith, and S. Self. A working terminology of pyroclastic eruptions. *J. Volc. Geotherm. Res.*, 8, p.315-336, 1980.

Vita

Karen G. Bemis

1988	B.A. in Geophysics, magna cum laude, Rice University, Houston, Texas.
1988-1991	Graduate Research Assistant, Department of Geology and Geophysics, WHOI.
1991	M.S. in Oceanography, WHOI/MIT Joint Program in Oceanography, Woods Hole, Massachusetts.
1991-1993	Excellence Fellow, Rutgers, The State University of New Jersey. New Brunswick, New Jersey.
1993	K. G. Bemis and D. K. Smith. Volcanism in the South Pacific. *Earth and Planetary Science Letters.* 118: 251-262.
1993	K. G. Bemis, R. P. Von Herzen, and M. J. Mottl. Geothermal heat flux from hydrothermal plumes on the Juan de Fuca Ridge, *Journal Geophysical Research.* 98: 6351-6365.
1993-1994	Teaching Assistant, Department of Geological Sciences, Rutgers, The State University of New Jersey. New Brunswick, New Jersey.
1994-1995	Graduate Research Assistant, Department of Geological Sciences, Rutgers, The State University of New Jersey. New Brunswick, New Jersey.
1995	Ph.D. in Geological Sciences

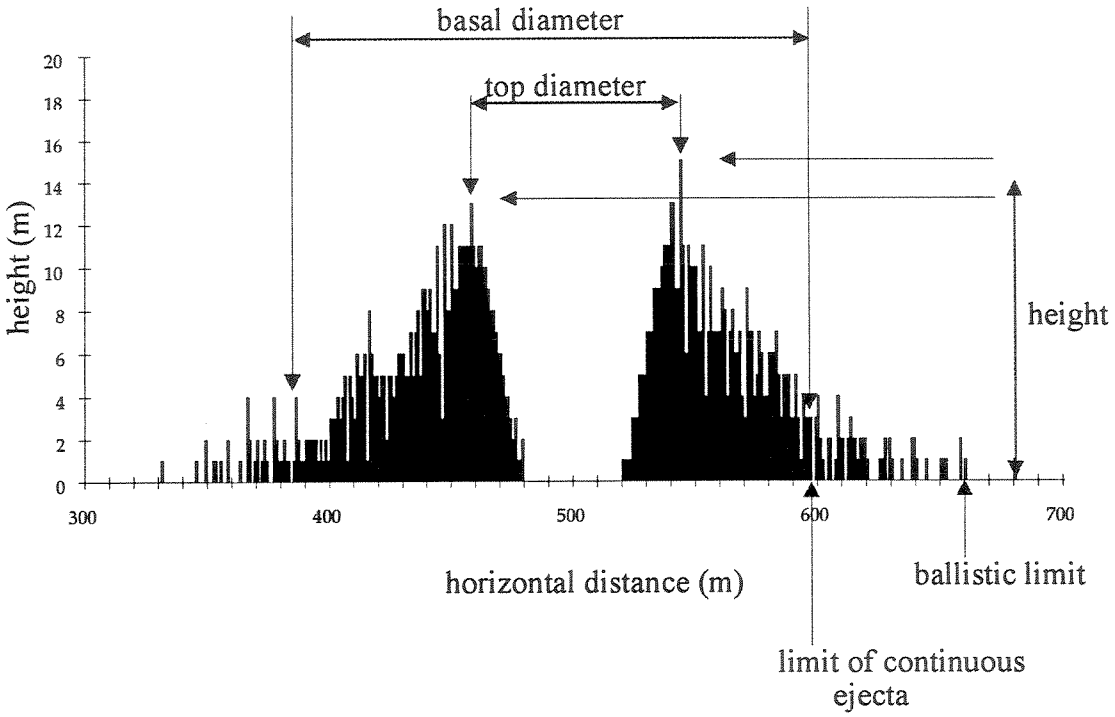


Figure IV-8. McGetchin model program yields a column of numbers equal the height a successive points along a profile. Here, the output is presented in histogram form and the various measured quantities are indicated. Vertical exaggeration is approximently 10x.